THE UNIVERSITY OF ASTON IN BIRMINGHAM

A STUDY OF ELECTROSTATIC ION SOURCES

Thesis submitted for the degree of

DOCTOR OF PHILOSOPHY

by

Ahmed Mohamed Ahmed Ghander (B.Sc., M.Sc.).

Department of Physics

October 1974

ABSTRACT

Ion sources have important applications in metallurgy, solid state physics and biology, where the controlled removal of materials is required. The present thesis is aimed at increasing the understanding of "saddle-field" electrostatic ion sources in which an oscillating electron beam produces a narrow beam of ions without the aid of a magnetic field.

The characteristics of the cylindrical source, incorporating a cylindrical cathode and two anode rods, have been investigated. The main objectives were the improvement of the intensity and focussing of the emerging ion beam so as to increase the ion etching rate.

The characteristics of a new source, which incorporates an annular anode instead of the two anode rods and two hemispherical cathodes instead of a cylindrical cathode, have also been investigated. It was found that this source produces an intense narrow central beam which is very suitable for ion-thinning of small specimens.

The energy of the emerging ions have been measured for both sources. It was found that the energy distribution for both sources is broad but exhibits a number of peaks at different energies. The shape of the energy spectrum depends upon the gas pressure, the nature of the gas, the discharge conditions and the size of the ion exit aperture.

The charge state of the ions is important for nuclear applications. A magnetic analyzer has been used

to determine the charge states of ions produced by the cylindrical source. Using the appropriate gas, the predominant ions were found to be H_2^+, He^+, N^+ and A^{2+}. Higher charge states such as N^{3+} and A^{3+} were also observed at lower abundance. However, the relative abundance of these states increases as the input power to the source is increased.

It would appear that practical forms of "saddle-field" electrostatic ion sources described above can find wide application in materials analysis and nuclear physics.

PREFACE

In this thesis a study of the saddle-field electrostatic ion sources is reported. Efforts have been made to improve the performance of the sources as well as the quantity and quality of the emerging ion beam. In Chapter 1, the general theory of plasma ion sources is discussed together with the discharge processes; ionization, recombination and surface phenomena. In Chapter 2, existing theories of the glow discharge and in particular the theories concerning the positive column are summarized. The theory of the saddle-field charged particle oscillator is dealt with in Chapter 3. The electrostatic field, mechanism of the discharge and the plasma ion density are discussed and reviewed.

Chapter 4 is devoted to the formation of ion beams from plasma ion sources. Principles of extraction of a plasma, different extraction systems and the mechanism of ion extraction from the electrostatic ion source are discussed.

Experimental investigations of the characteristics of the twin-anode electrostatic ion source are reported in Chapter 5. The effect of gas pressure on the oscillator characteristics and the ion output current are investigated. The operational modes of the oscillator and the change in the efficiency have been investigated and are discussed. The characteristics of newly developed double-beam ion source is also reported.

Chapter 6 is concerned with means by which the field distortion due to the ion exit aperture can be

corrected and also with the production of focused high-current ion beams. The effects of two focused-electrode systems on the source performance have been investigated.

The characteristics of an electrostatic source with spherical symmetry are given in Chapter 7. The investigations of the effect of the source geometry on the source efficiency, the current density of the emergent ion beam, the current density distribution, production of neutral ions and the ion beam profile are reported.

Investigations of the two important parameters of the ion source, the ion energy distribution and the magnetic analysis of the ions, are reported in Chapter 8. A retarding field electrostatic analyser was used to measure the ion energy distribution of different gases under different experimental conditions. A water-cooled source was used with a magnetic analyser to determine the ion charge state for different gases.

The work reported in this thesis has been mainly carried out at the Physics Department, University of Aston in Birmingham. The work on the spherical source was carried out at Ion Tech. Ltd., Teddington, and investigations with the aid of a magnetic spectrometer was carried out at the Linear Accelerator Laboratory of the Department of Physics, University of Manchester.

I am very grateful to Dr. R.K. Fitch and Professor T. Mulvey for their help and discussions, and Professor S.E. Hunt for his encouragement. I am also grateful to Dr. J. Franks of Ion Tech. Ltd., for his

discussions and financial support during the course of work on the spherical source.

Thanks are due to Professor Phillips of the Department of Physics, the University of Manchester for his financial help and to Messrs. B. Clark, A.G. Smith and R. King for their help during the course of magnetic analysis.

Acknowledgments are also due to Mr. F. Lane and the staff of the Physics Department Workshop for their assistance in the construction of many of the devices described in this thesis.

My thanks are also due to the Egyptian Atomic Energy Establishment Authority for granting me a study leave to do this work.

Last and not least I express my greatest appreciation to my wife, Wafdia and my children, Mohamed, Noha and Kamal for their patience and suffering for being away from them during my period of study.

CONTENTS

LIST OF FIGURES

5.9 The relation between the discharge input power and the output ion current with ion exit aperture of 3.2 x 10 mm.

5.10 Schematic diagram of the double-beam ion source.

5.11 The electrical circuit of the double-beam ion source.

5.12 A photograph showing two beams of the double-beam ion source.

5.13 The relation between the discharge input power and the ion beam current of the double-beam ion source.

5.14 The relation between the pressure, the ion beam current and the tube voltage for an ion exit aperture of 5 mm. diameter and a tube current of 4 mA.

5.15) 5.16) 5.17) The relation between the pressure, the ion beam current and the tube voltage of an ion exit aperture of 3.2 x 10 mm.

5.18 Diagramatic representation of a copper film etched by ions for different operational modes of the oscillator.

5.19 The relation between the ion beam current and the tube current at different pressures showing the tube-current dependent modes.

5.20 Schematic representation showing the confinement of the discharge for a smaller diameter cathode tube.

5.21 The shape of the discharge in various operational modes.

8.1 The energy analyzer.

8.2)
8.3)
8.4) Energy distribution for nitrogen.
8.5)
8.6)

8.7 Energy distribution for helium.

8.8 Energy distribution for ions emerging from apertures in different position of the ion source.

8.9) Energy distribution of ions from the spherical
8.10) source.

8.11 Energy distribution for the ions from the cylindrical source with a focus electrode.

8.12 Energy distribution for the ions from the spherical source with a focus electrode.

8.13 Water-cooled source.

8.14 Photographs of the water-cooled source.

8.15 Experimental arrangement for the mass analysis.

8.16)
8.17) The magnet calibration.

8.18)
8.19) Mass spectrum for nitrogen.

8.20 Mass spectrum for argon.

8.21 Mass spectrum for helium.

8.22 Mass spectrum for hydrogen.

8.23 Mass spectrum calibration.

LIST OF SYMBOLS

A, B, C	Neutral atoms.
A^+, B^+, C^+	Positive ions.
A^-, B^-, C^-	Negative ions.
A_2	Molecule.
A_2^+	Molecular positive ion.
A^*	Excited atom.
A_2^*	Excited molecule.
a	Position of anode rod from centre.
b, C_g	Constants, characteristics of each gas.
C_{oe}	Most probable velocity of the electrons.
D	The focus for points for which the electric field component, E_x is zero.
D_a	Ambipolar diffusion coefficient.
D^+	Ion normal diffusion coefficient.
D^-	Electron normal diffusion coefficient.
d	spacing between the focus electrode and the cathode (cm)
E	Electric field strength inside the cathode (V/ cm).
E_1	Electric field strength outside the cathode (V/cm).
E_e	Electron energy (eV)
E_{ex}	Excitation energy (eV)
E_i	Ionization energy (eV)
E_r	Radial space charge field (V/cm).

E_x, E_y	Electric field components (V/cm).
e	Electric charge unit.
e^-	Symbol for an electron.
F_x, F_y	Force components on the electron.
g	Cathode - plasma boundary spacing.
H	Magnetic field.
h	Planck's constant.
I_B, I_{B1}, I_{B2}	Ion beam current.
I_d	Discharge current.
I_{ep}	Secondary electron current due to primary ions.
I_{es}	Secondary electron current due to secondary ions.
I_f	Focus electrode current.
I_i	Ion current due to ions hitting the cathode.
I_{ip}	Primary ion current.
I_{is}	Secondary ion current.
I_o	Primary electron current.
I_T	Tube current.
I_e	Electron current to the anode.
I_{es}	Secondary electron current from the anode.
J_{ic}	Ion current density near the cathode.
J_{ip}	Plasma ion density.
J_+	Ion beam current density.
K_e	Secondary electrons energy (eV).
k	Boltzman's constant.
k_n	Concentration of the n^{th} type of ions.
L	Cathode tube length.

m	Mass of the neutral.
m_e	Electron mass.
m_i	Ion mass
M_{ip}	Mass number of the n^{th} type of ions.
n	Neutrals concentration.
n_e	Number of electrons passing through any cross-section of the positive column.
n_{ic}	Ion density at the cathode.
n_{is}	Number of ions produced by secondary electrons.
n_o	Ion density at the centre of the positive column.
n_R	Ion density at the discharge wall.
n_r	Ion density at r.
n^+	Positive charges concentration.
n^-	Negative charges concentration.
P	Pressure.
(r,θ)	Polar coordinate.
q	Charge per unit length.
R	Tube radius.
R_c	Radius of curvature.
S	Area of the two etched regions in the cathode.
S_1	Plasma boundary.
S_2	Electrode in contact with the plasma.
S_3	Extractor.
T_e	Electron temperature.
U	Internal energy of the atom or molecule (eV).
V_a	Anode fall in potential.

V_b	The potential difference between the axis and the boundary of the discharge.
V_c	Cathode fall in potential.
V_d	Discharge voltage (potential difference between the cathode and the anode).
V_{ex}	Extraction voltage (potential difference between the extraction electrode and the cathode).
V_f	Focus electrode voltage (potential difference between the focus electrode and the cathode.
V_i	Ionization potential (eV).
eV_l	Ion energy after leaving the ion source.
V_p	Anode fall in potential
V_R	Potential difference between the retarding grid and the cathode.
V_r	Radial potential.
eV_{sa}	Ion energy after acceleration.
V_{sl}	Plasma boundary potential.
V_T	Tube voltage.
v	Velocity of the neutrals.
v_d	Drift velocity of the electrons.
v_i	Ion velocity in the beam.
v_{ic}	Ion velocity near the cathode.
v_{ip}	Plasma ion velocity.
$\bar{v}$	Average drift velocity of the ions and the electrons.
Z	Charge number.
Z	Charge number of the n^{th} type of ions.
β	Number of ionizing collisions per second per each electron.

γ	Secondary electron coefficient.
ν	Frequency of radiation.
$\nu_{diff.}$	Rate of diffusion.
$\nu_{ioniz.}$	Rate of ionization.
μ^+	Positive ion mobility.
μ^-	Electron mobility.
λ_e	Electron mean free path.
$\bar{\lambda}$	Average mean free path for the ions and the electrons.
ϕ	Focus electrode diameter.
φ	Work function of the cathode material.
η	The angle with which the ions leave the source.

1. INTRODUCTION

1.1. General Theory of Ion Sources.

Ion sources are one of the important components of accelerators for studying various nuclear reactions and are an essential part of all mass spectrometers. They are also useful tools in vacuum technology, ion etching, ion beam machining, sputtering and ion implantation.

In plasma ion sources an ion current is extracted from, or diffuses out of, a region where there is a high degree of gas ionization. Therefore they generally consist of a region of a highly ionized gas and a mechanism for the extraction of the ions.

In order to design a plasma ion source, or to improve its performance, two main problems have to be considered. The first is to produce a plasma having the required ion concentration with the maximum degree of ionization, and the second is to make the best use of the ions in the form of a beam of given energy and having the highest ratio of ion density to neutral density. The first problem can be solved by the design of the ion source geometry and the use of some mechanism for plasma intensification, and the second by the proper extraction of the ions from the plasma and their subsequent focusing.

The mechanism for producing and for concentrating the plasma varies from one ion source to another. To intensify the plasma, the electrons must have long path lengths and this can be achieved by allowing the electrons to have an oscillatory motion and thus prevent them from

being collected quickly by the anode. In R.F. ion sources electrons are allowed to oscillate under the influence of an R.F. field. A radial magnetic field could also be used to prevent loss of charged particles to the wall of the discharge (Thoneman and Harrison, 1953 and 1955). The discharge of Penning ion sources depends on the oscillatory motion between two cathodes separated by a cylindrical anode using a combined electric and magnetic field (Penning and Moubis, 1937). In the duoplasmatron ion source, magnetic confinement as well as mechanical confinement are both used to produce a plasma with high ion density (von Ardenne, 1956).

In the electrostatic charged particle oscillator ion source, which is the subject of this thesis, electrons are allowed to oscillate between two anodes placed symmetrically on the axis of a cylindrical cathode as described by McIlraith (1966) and will be discussed later in Chapter 3.

The performance of the twin anode electrostatic charged particle oscillator has been studied by Rushton and Fitch (1971). They reported the discharge characteristics for a tube of 2" diameter and 8" long without using direct gas injection. It was found that the tube current is maximum at an optimum anode separation of about 6 mm. and no discharge was obtained using an anode separation less than about 4mm. Also, it was found that serious deterioration in the performance of the oscillator will result under the influence of an external magnetic field greater than the earth field.

Initially, McIlraith predicted that the anode diameter should be as small as possible, but Rushton and Fitch found that this was not necessary. In fact anodes of 2mm. in diameter were used without a significant drop in the oscillator efficiency.

Recently Fitch et al (1970) used the electrostatic charged particle oscillator as an ion source which produces an ion current density of 100 $\mu A/cm^2$ at a pressure of about 5×10^{-4} torr. This was done by milling an ion exit aperture in the cathode.

Fitch and Rushton (1970) showed that using thermionic electron injection into the oscillator, there are two operational modes, namely, an orbiting mode where the electrons orbit around the anode and a normal oscillating mode. However, with either of these modes of operation long electron path lengths are achieved giving efficient gas ionization.

Fitch et al (1972) showed from the rubber model experiments that the cylindrical cathode can be replaced by a cathode of square or rectangular cross section. In this type of the ion source the beam was more divergent and a wide ion beam was obtained. Also, Fitch et al (1972) showed that a multiple ion beam gun can also be produced using any even number of electrodes.

Rushton et al (1973) used a definition of the ion source efficiency as the ion beam current divided by the tube current and reported three modes of operation of the electrostatic charged particle oscillator as the operating pressure changes. These modes were called the

oscillating mode, the transition mode and the glow discharge mode respectively. However, no quantitative attempt was made to explain how these modes change with the source efficiency and source pressure.

Some other requirements are also necessary for most ion sources such as a source of electrons (for a hot cathode discharge) for low discharge voltage and high plasma density and a relatively small ion exit aperture separating the plasma region from the high vacuum region to produce the necessary pressure differential.

The adjustable parameters of an ion source are:- electron emission (hot cathode discharge), voltage across the discharge, magnetic field (if it is used), gas pressure, general shape and dimensions of the discharge container, and geometry and surface properties of the electrodes.

1.2. Discharge Processes.

1.2.1. Ionization.

When an atom (or molecule) has absorbed a sufficient amount of energy for one of its electrons to escape to infinity, it is said to have been ionized and its internal energy is increased by the ionization energy

$$U = eV_i \qquad \ldots. 1.2.1.$$

where V_i is the ionization potential of the atom or molecule. When sufficient ionization takes place a plasma is produced which is a conducting medium and is

characterized by having a small potential drop such that the number of ions is almost equal to the number of electrons.

When an incident particle (ionization agent) has sufficient energy to collide with an atom, it can eject an electron from the inner shell of the atom. During the subsequent rearrangement of the atom, the last electron is replaced by an electron from a higher level. This transition is accompanied by the emission of a high energy photon which may in turn ionize the same atom. Furthermore, the electrons ejected from the inner shells of the atom often have a considerable energy and can themselves become effective ionization agents. In fact they are more effective than the initial photon radiation (Papoular, 1968).

Ionization by electrons and photons are represented by:-

$$e^- + A \longrightarrow A^+ + 2e^- \quad \text{(Ionization by electrons)} \quad .. \ 1.2.2.$$

$$h\nu + A \longrightarrow A^+ + e^- \quad \text{(Ionization by photons)} \quad .. \ 1.2.3.$$

Where, e^-, A, A^+ represent an electron, neutral atom and positive ion respectively.

In addition to ionization, excitation can take place when the ionizing agent has not enough energy to ionize the atom. When an atom has absorbed a sufficient amount of energy for one of its electrons (generally that farthest from the nucleus) to pass to higher energy level, the atom is said to have been excited, its internal energy

has been increased by the difference between the energies of the final and initial states.

$$\Delta U = eV^{*} \quad \text{.... 1.2.4.}$$

Where V^{*} is the excitation potential.

Excitation can take place by electrons or photons. The respective reactions are represented by:-

$$e^{-} + A \longrightarrow A^{*} + e^{-} \quad \text{... (Excitation by electrons).. 1.2.5.}$$

$$h\nu + A \longrightarrow A^{*} \quad \text{... (Excitation by photons) 1.2.6.}$$

where, A^{*} represents an excited atom. The inverse to reaction (1.2.6) is possible and the result is the emission of a photon by an atom:-

$$A^{*} \longrightarrow A + h\nu \quad \text{.... 1.2.7.}$$

Ions, atoms, or molecules can be ionizing agents when they have enough energy, for example:-

$$A^{+} + B \longrightarrow B^{+} + A^{+} + e^{-} \quad \text{.. (Ionization by ions).. 1.2.8.}$$

$$A + B \longrightarrow B^{+} + A + e^{-} \quad \text{.. (Ionization by atoms). 1.2.9.}$$

Where, B represents another atom. In practice, electrons are the most efficient ionizing agents, followed by ions and lastly, photons.

Excitation by ions or atoms may also take place. These may be represented by:-

$$A^{+} + B \longrightarrow B^{*} + A^{+} \quad \text{.. (Excitation by ions) .... 1.2.10.}$$

$$A + B \longrightarrow B^{*} + A \quad \text{.. (Excitation by atoms) .... 1.2.11.}$$

1.2.2. Recombination.

Recombination is the attachment of particles in the course of an encounter between a positive ion and an electron or between a positive ion and a negative ion. The ions can be atomic or molecular.

Four types of ion-electron recombination are known. These are: recombination with double excitation, recombination in the presence of a charged particle and dissociative recombination.

Ion-electron recombination may be represented by:-

$$e^- + A^+ \rightarrow \begin{matrix} A + h\nu \\ * \\ A + h\nu \end{matrix} \qquad \ldots\ 1.2.12$$

The first reaction leads to an electron being taken into the ground level and the emission of a photon of energy:

$$h\nu = E_e + E_i \qquad \ldots\ 1.2.13$$

where,

E_e = kinetic energy of electron

E_i = ionization energy of target

The second reaction gives rise to a particle which is in an excited state and a photon is emitted with an energy,

$$h\nu = E_e + E_i - E_{ex} \qquad \ldots\ 1.2.14$$

where $E_{ex.}$ = excitation energy.

The direct attachment of electrons to neutral atoms is a particular case of recombination. This is shown as:-

$$e^- + A \longrightarrow A^- + h\nu \qquad \ldots. 1.2.15$$

Ion-electron recombination with double excitation may be represented by:

$$e^- + A \longrightarrow A^* \begin{cases} \nearrow A^* + e^- \\ \searrow A + h\nu + h\nu' \end{cases} \qquad \ldots. 1.2.16$$

During the first stage, the incident electron is drawn into an excited state of the atom and the energy available raises another electron of the same atom to another excited level. After a certain time one of two possible processes can take place - either one of the electrons can be ejected leaving the ion in its initial state, or the two electrons fall to the ground state emitting two photons.

Ion-electron recombination in the presence of a third particle is represented by:

$$e^- + A^+ + X \longrightarrow A + C + X \qquad \ldots. 1.2.17$$

When an electron encounters a particle X in the neighbourhood of an ion A^+, it may communicate its energy to this particle and slow down sufficiently to recombine with A^+. Instead of being emitted in the form of photons, the recombination energy, $E_k + E_i$, of this is used to accelerate the third particle X. The probability of this reaction depends on the nature and density of the X particles.

Ion-electron dissociative recombination can take place in the course of a collision between an electron and molecule ion:

$$e^- + A_2^+ \longrightarrow A + A \qquad \ldots. 1.2.18$$

The two resultant atoms can be excited or non-excited.

Three types of ion - ion recombination are known:-

(a) Recombination with associated radiation (radiative recombination)

$$A^+ + B^- \longrightarrow AB + h\nu \qquad \ldots. 1.2.19$$

(b) Mutual neutralization (exchange of charge without forming a molecule)

$$A^+ + B^- \longrightarrow A + B \qquad \ldots. 1.2.20$$

(c) Three body recombination

$$A^+ + B^- + C \longrightarrow AB + C \qquad \ldots. 1.2.21$$

Reactions (1.2.19) and (1.2.21) are binary and take place at low pressure ($\sim$ 1 torr).

The negative ions are generally formed in one of two ways.

(a) by an electron becoming attached to an atom or molecule

$$e^- + A_2 \longrightarrow A + A^- \qquad \ldots. 1.2.22$$

(b) by dissociation of a molecule

$$e^- + A_2 \longrightarrow A^+ + A^- + e^- \qquad \ldots. 1.2.23$$

1.2.3. Surface Phenomena.

The surfaces of solid bodies act in various ways on the gas and ions with which they are in contact. The

important processes are:-

(a) Primary of spontaneous emission. This results in emission of neutral particles and charged particles due to the effect of heat.

(b) Reflection of photons and neutral or charged particles.

Certain charged and uncharged particles of matter incident on the surface of a solid, or walls of an enclosure, undergo reflection, analogous to an elastic collision. In the same way, photons are partly reflected or scattered by the walls. Moreover, certain ions are able to capture electrons and to re-emerge in the form of neutral particles in either the ground or the excited states.

(c) Secondary emission:

Ions, like electrons, may cause secondary emission from surfaces upon bombardment. However, they differ primarily in that the threshold is double that of electrons. This is due to the fact that besides the secondary electron which is liberated, the ion itself leaves the surface taking with it a second electron which neutralises the ion. The number of secondary electrons per incident ion is generally smaller than unity. When the incident particles possesses sufficient energy, they may eject atoms or molecules. This is known as sputtering.

(d) Absorption and adsorption.

Some of the photons, charged or uncharged particles of matter bombarding a material surface will be absorbed. Part of the energy carried by the incident

particles is expended in heating this surface, the other part being removed by secondary particles or radiation.

Neutral atoms or molecules may become adsorped to the surface of a solid. The actual process may be one of physical adsorption due to Van der Waals forces or may be electrostatic due to the induced or permanent dipole moment of the atom or molecule. Alternatively, the atom or molecule may become chemisorped on the surface due to the chemical reaction between the atom or molecule and the surface.

2. THE GLOW DISCHARGE

2.1. Introduction.

Since the electrostatic particle oscillator produces a glow discharge, it is useful to summarize the existing theories of the glow discharge and in particular the theories concerning the positive column which is the most important part of the discharge. These theories were based on experiments carried out for a sealed cylindrical glass tube containing two plane parallel electrodes, one at each end of the tube. To simplify the theoretical analysis, it is assumed that the electrodes are infinite and the following analysis is done with the above conditions in mind.

When the current in a Townsend discharge increases, the voltage between the electrodes diminishes and a new type of discharge is eventually established. This is the glow discharge, characterized by the appearance of several diffuse luminous zones. These zones are from the cathode to the anode: Aston dark space, cathode sheath, cathode dark place, negative glow, Faraday dark space, Positive column, anode dark place and anode fall.

The relative size of the different zones varies with the pressure and the distance between the electrodes. As the pressure decreases, the negative glow and the Faraday dark space expand at the expense of the positive column. At the same time, if the distance between the electrodes decreases, the positive column diminishes in

the same ratio, without any change in the size of the other zones.

The potential V_b, at the boundaries of the discharge tube is made up of:

V_c = cathode fall in potential

V_{pc} = fall over the positive column

V_a = anode fall in potential

i.e. V_b is given by:

$$V_b = V_c + V_{pc} + V_a \qquad \ldots\ (2.1.1)$$

It should be noticed that;

$$V_c \gg V_p + V_a$$

2.2. The Positive Column.

The positive column is the most luminous part of the discharge after the negative glow. The electrons are slow because the electric field is very small. The positive column is a form of plasma where the ion and the electron concentration are equal.

2.2.1. The radial distribution of charge.

When the mean free path of the electrons, λ_e, is smaller than the tube radius, R, (i.e. $\lambda_e \leq R$), the diffusion laws are applicable and we have:

$$n^+ \simeq n^- = n \qquad \ldots\ (2.2.1)$$

and

$$\frac{dn^+}{dr} \simeq \frac{dn^-}{dr} = \frac{dn}{dr} \qquad \ldots\ (2.2.2)$$

Where,

n^+ = the positive charge concentration

n^- = the negative charge concentration

n = the neutral concentration

By following the anlysis of V. Engel and Steenbeck (1932), the rate at which ions are moving by diffusion (see Fig.(2.1)) at the radius r is;

$$\left(\frac{dn}{dt}\right)_r = -2\pi r D_a \left(\frac{dn}{dr}\right)_r \quad \ldots\ (2.2.3)$$

where D_a is the ambipolar diffusion coefficient. The rate of diffusion out of the shell of thickness dr and unit length is:

$$\left(\frac{dn}{dt}\right)_{r+dr} = -2\pi(r + dr)\ D_a\left(\frac{dn}{dr}\right)_{r+dr} \quad \ldots\ (2.2.4)$$

The difference between the rates at which the ion concentrations are changing at the two boundaries is the net loss by diffusion, of ions from the shell per second, i.e.:

$$d\nu_{diff.} = 2\pi r D_a\left(\frac{dn}{dr}\right)_r - 2\pi(r + dr)\ D_a\left(\frac{dn}{dr}\right)_{r+dr} \quad \ldots\ (2.2.5)$$

By expansion, neglecting higher order terms, Eq. (2.2.5) reduces to:

$$d\nu_{diff.} = -2\pi D_a\left[r\frac{d^2n}{dr^2} + \frac{dn}{dr}\right]dr \quad \ldots\ (2.2.6)$$

This number loss has to be balanced by ionization in the same element dr, i.e. ions must be produced in this region at the same rate, or,

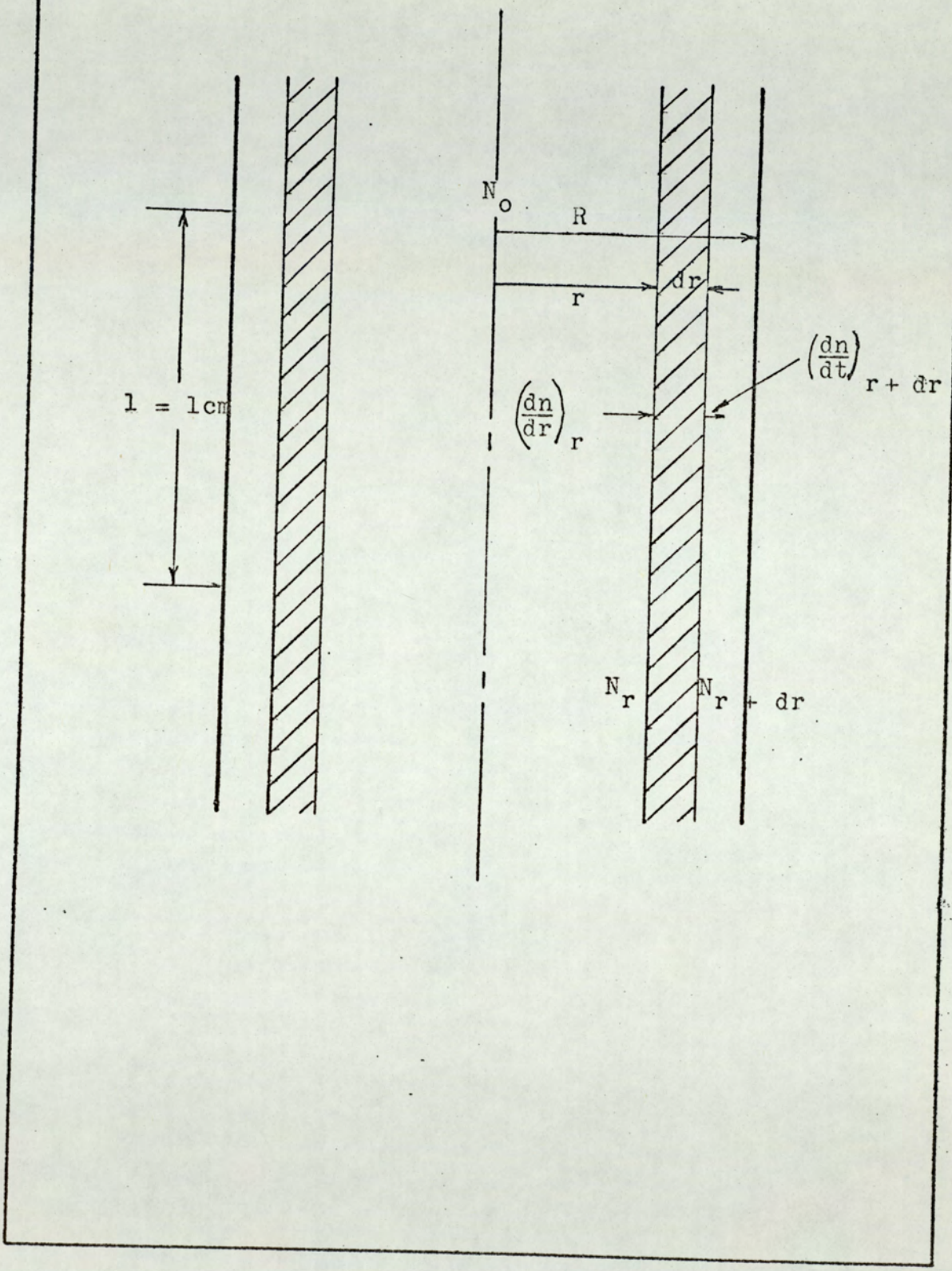

Figure 2.1 Section of positive column of glow discharge.

$$d\nu_{ioniz.} = \beta\, n 2\pi r\, dr \qquad \ldots\ (2.2.7)$$

Where β is the number of ionizing collision per second made per each electron. Equating eqs. (2.2.6) and (2.2.7), we find

$$\frac{d^2n}{dr^2} + \frac{1}{r}\frac{dn}{dr} + \frac{\beta}{D_a}\, n = o \qquad \ldots\ (2.2.8)$$

Making the substitution:

$$r = \sqrt{\frac{D_a}{\beta}}\ X \qquad \ldots\ (2.2.8^1)$$

in Eq. (2.2.8)

$$\frac{d^2n}{dX^2} + \frac{1}{X}\frac{dn}{dX} + n = 0 \qquad \ldots\ (2.2.9)$$

The solution of this equation is a Bessel function of zero order, i.e.

$$n_r = n_o J_o(X) = n_o J_o\left(r\sqrt{\frac{\beta}{D_a}}\right) \qquad \ldots\ (2.2.10)$$

which is an oscillatory function with a variable period (Bessel function properties (Byerly 1893).

n_o is the concentration of ions along the axis of the column ($r = o$), and $J_o(X)$ is a Bessel function of zero order. The greatest value X can have is 2.0405 which correspond to $r = R$. The concentration at the Walls, n_R, is adjusted for each discharge condition so that the diffusion of ions from the concentration n_o at the centre is just equal to the rate of ion production per unit length (neglecting column recombination). Taking the

value of X for r = R as:

$$X_R = R \sqrt{\frac{\beta}{D_a}} = 2.405 \qquad \ldots. (2.2.11)$$

gives the necessary relation between the production of ions, β and the diffusion coefficient D_a. Substituting this relation in Eq. (2.2.10),

$$n_r = n_o J_o (2.45\ r/R) \qquad \ldots. (2.2.12)$$

2.2.2. Ambipolar Diffusion.

When ions and electrons are present in equal concentrations at a point, they each tend to diffuse with their respective diffusion velocity. Since electrons diffuse more rapidly than ions, the latter tend to remain behind, thus creating a positive space charge and a field which tends to retain electrons. Thus, the electrons decelerate and eventually particles of both signs diffuse with the same velocity. This type of diffusion is illustrated in Fig. (2.2). This diffusion can be discussed in terms of the space charge field, E_r, created by charge separation. The particle flow equation for positive ions can be written as:

$$\phi^+ = n^+ v^+ = -D^+ \nabla n^+ + n^+ \mu^+ E_r \qquad \ldots. (2.2.13)$$

Which gives the positive ion velocity as:

$$v^+ = -\frac{D^+}{n^+} \nabla n^+ + \mu^+ E_r \qquad \ldots. (2.2.14)$$

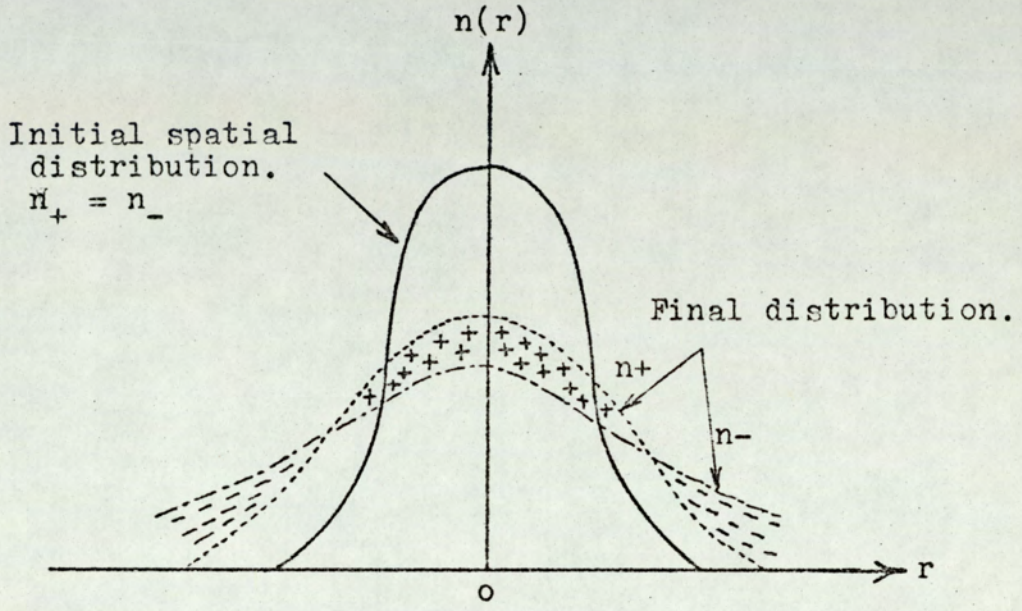

Figure 2.2 Represention of ambipolar diffusion.

and similarly for electrons:

$$v^- = -\frac{D^-}{n^-} \nabla n^- - \mu^- E_r \qquad \ldots\ldots (2.2.15)$$

Where D^+ and D^- are the ion and electron normal diffusion coefficient respectively. μ^+ and μ^- are the ion and the electron mobility respectively and v^+ and v^- are the ion and the electron drift velocity respectively.

Eliminating E_r and making the assumption that

$n^+ = n^- = n$, $\nabla n^+ = \nabla n^- = \nabla n$ and $v^+ = v^- = v$,

therefore,

$$v = -\left(\frac{D^+\mu^- + D^-\mu^+}{\mu^+ + \mu^-}\right) \cdot \frac{\nabla n}{n}$$

$$= -D_a \frac{\nabla n}{n} \qquad \ldots\ldots (2.2.16)$$

Where

$$D_a = \frac{D^-\mu^+ + D^+\mu^-}{\mu^+ + \mu^-} \qquad \ldots\ldots (2.2.17)$$

D_a is called the ambipolar diffusion coefficient. Eq. (2.2.16) is only valid if n^+ and n^- are sufficiently high for the space to be charged significantly.

The magnitude of the ambipolar coefficient in terms of free diffusion may be determined approximately, since:

$$\frac{D^+}{\mu^+} = \frac{D^-}{\mu^-} \qquad \ldots\ldots (2.2.18)$$

if $\mu^- \gg \mu^+$,

$$D_a = \frac{2D^+\mu^-}{\mu^+ + \mu^-} \approx 2D^+ \qquad \ldots\ (2.2.19)$$

on terms of temperature, T_e,

$$\frac{D_a}{2\mu^+} = \frac{kT_e}{e} \qquad \ldots\ (2.2.20)$$

or

$$\mu^+ = \frac{eD_a}{2kT_e} = 5.9 \times 10^3 \frac{D_a}{T_e} \qquad \ldots\ (2.2.21)$$

Where D_a is in units of $cm^2\ sec^{-1}$ and μ^+ in units of $cm^2\ volt^{-1}\ sec^{-1}$ and k is Boltzman's constant.

Loeb (1937) derived an expression for D_a as,

$$D_a = \frac{\lambda \bar{v}}{3} \qquad \ldots\ (2.2.22)$$

Where λ is the mean free path and $\bar{v}$ is the average velocity. For constant energy,

$$D_a P = \text{Constant} \qquad \ldots\ (2.2.23)$$

Where P is the pressure, Eq. (2.2.23) has been demonstrated experimentally (Biondi and Brown, 1949).

2.2.3. The electron temperature.

A useful relation for the number of ions β produced per second per electron has been derived by V. Engel and Steenbeck (1932) as,

$$\beta = \frac{600\, m_e\, Pb}{e\sqrt{\pi}}\, C^3_{oe}\, e^{-eV_i/kT_e}\left(1 + \frac{eV_i}{2kT_e}\right) \quad \ldots\ (2.2.24)$$

Where T_e is the electron temperature. C_{oe} is the most probable velocity of the electrons, b is a constant and V_i is the ionization potential of the gas. Since the electron temperature T_e is high compared with that of the positive ions T_i, the ambipolar diffusion coefficient of Eq. (2.2.19) and using Eq. (2.2.20) reduced to:

$$D_a = \mu^+ \frac{kT_e}{e} \quad \ldots\ (2.2.25)$$

Substituting the values of D_a and Z from Eqs. (2.2.25) and (2.2.24) into Eq. (2.2.11) and put

$$y = eV_i/kT_e \quad \ldots\ (2.2.26)$$

we get:

$$\frac{e^y}{\sqrt{y}} = 1.2\ (10)^7\ C_g^2 P^2 R^2 \quad \ldots\ (2.2.27)$$

The constant C_g is a characteristic of the gas, it is $3.5\ (10)^{-2}$ and $5.3\ (10)^{-2}$ for nitrogen and argon respectively (Cobine, 1958). It should be noted that T_e depends only on PR. The theory fails at very low values of PR.

2.2.4. <u>The Radial Potential Distribution</u>.

From the equation of ambipolar flow which were derived previously in (2.2.2), the radial field is:

$$E_r = \frac{1}{n}\frac{dn}{dr}\frac{D^- - D^+}{\mu^+ + \mu^-} \approx \frac{D^-}{\mu^-}\frac{1}{n}\frac{dn}{dr}$$

$$\approx \frac{1}{n}\frac{dn}{dr}\frac{kT_e}{e} \qquad \ldots\ldots (2.2.28)$$

By integrating Eq. (2.2.28), the potential V_r is found at a point r from the axis,

$$-V_r = \frac{kT_e}{e} \ln \frac{n_o}{n_r} \qquad \ldots\ldots (2.2.29)$$

Where, $n_r = n_o$ and $V_r = o$ at $r = o$. Eq. (2.2.29) can be written as:

$$\frac{n_r}{n_o} = \exp\left(-\frac{eV_r}{kT_e}\right) \qquad \ldots\ldots (2.2.30)$$

which shows that the concentration of charges follows the Boltzman distribution.

2.2.5. Determination of n_r/n_o.

For a current I, the number of electrons n_e passing through any cross-section of the column in one second is $n_e = I/e$. If v_d is the drift velocity of electrons along the column, each electron produces Z/v_d ion pairs per centimeter. Therefore, the number of new ions produced per second is:

$$n_{is} = \frac{I\beta}{ev_d} \qquad \ldots\ldots (2.2.31)$$

This must be equal to the rate at which ions are diffusing to the cathode wall per centimeter length. If n_i is the ion concentration with an average random

velocity $\bar{v}$, the number of ions crossing unit area of any surface in one second is $n_i \bar{v}/4$. It is assumed that an ion reaching the cathode wall is permanently lost from the column, the number of ions lost per unit length of the column per second is:

$$n_{il} = \frac{n_R \bar{v}}{4} \, 2\pi R \qquad \ldots\ldots (2.2.32)$$

From Eqs. (2.2.31) and (2.2.32):

$$n_R = \frac{2I\beta}{e\pi} \, \frac{1}{Rv_d \bar{v}} \qquad \ldots\ldots (2.2.33)$$

$\bar{v}$ is the average diffusing velocity of the ions and electrons which can be found from Eq. (2.2.22) by using an average mean free path for the ions and electrons, therefore Eq. (2.2.22) can be written as:

$$D_a = \frac{\bar{v}\bar{\lambda}}{3} \qquad \ldots\ldots (2.2.34)$$

Eliminating $\bar{v}$ from Eqs. (2.2.33) and (2.2.34),

$$n_R = \frac{2I\beta\bar{\lambda}}{3e\pi D_a v_d} \qquad \ldots\ldots (2.2.35)$$

Now, the current carried by the column is:

$$I = \int_o^R en_r v_d 2\pi r dr \qquad \ldots\ldots (2.2.36)$$

Substituting for n_r from Eq. (2.2.12)

$$I = 2\pi e v_d n_o \int_o^R J_o\left(\frac{2.4r}{R}\right) r dr \qquad \ldots\ldots (2.2.37)$$

By making the change variable, $X = 2.4\ r/R$

$$I = \frac{2\pi e v_d\ n_o\ R^2}{(2.4)^2} \int_{X=o}^{X=2.4} X\ J_o(X)\ dX \quad .... (2.2.38)$$

The definite integral of Eq. (2.2.38) has the value of 1.25, therefore,

$$I = 1.36\ e v_d\ n_o R^2 \quad .... (2.2.39)$$

From eqs. (2.2.39) and 2.2.33)

$$\frac{n_R}{n_o} = \frac{2.72\ R\ \beta\bar{\lambda}}{3\pi D_a} \quad .... (2.2.40)$$

And by using Eq. (2.2.11),

$$\frac{n_R}{n_o} = \frac{1.66}{R}\ \bar{\lambda} \quad .... (2.2.41)$$

The potential difference between the axis and the boundary, Eq. (2.2.30) can be written as a function of the tube radius:

$$-V_R = \frac{kT_e}{e}\ \ln\left(\frac{1.66}{R}\right) \quad .... (2.2.42)$$

2.3. Extension of the Theory of the Positive Column.

At low pressure, $\lambda_e \gg R$, ions and electrons, whenever produced, move to the cathode, colliding rarely with gas molecules. A strong negative charge builds up on the wall. The larger part of the electrons are deflected back into the gas by this charge and the positive ions follow. Although collisions between

electrons and gas molecules are rare, there are many of them to provide the necessary number of ionizations which is equal to the number of charges lost to the wall (Maxwellian energy distribution of electrons assumed to exist at low pressure). Von Angel (1965) gave the following relation between the electron temperature and the other discharge parameters:

$$\frac{kT_e}{eV_i} \approx 1 \Big/ \ln \left[bV_i PR \sqrt{m_i/m} \right]^{\frac{1}{2}} \qquad \ldots\ldots (2.3.1)$$

Where b is a constant and is a characteristic of each gas.

3. THEORY OF THE CHARGED PARTICLE OSCILLATOR

3.1. Theory of the oscillator.

This theory which was developed by McIlraith (1966), depends on the fact that electrons near two positively charged anode rods will follow an oscillatory motion and stay in this state for an appreciable length of time.

McIlraith proved the above theory by considering the field shown in Figure (3.1.a). The electrostatic field (Francken, 1967) and the equipotentials of two equal charges of the same sign are also shown in Figure (3.1.b). The field has a saddle point at the origin O.

In the vicinity of the origin the lines of force are strongly curved as shown in the two figures but elsewhere they are essentially straight and radiate from O. D is the focus for points for which the electric component, E_x, is zero. Outside D, E_x is directed away from the Y-axis while inside D it is directed towards the Y-axis. D always passes through the poles, a and a and for a pair of parallel rods it is a circle.

Let an electron be released from rest at a point Q (r, θ). Initially the electron follows a line of force but owing to its momentum, it fails to follow the sharp bend to 'a' and so its trajectory crosses the x-axis at an angle α. Then owing to the symmetry of the field about the X-axis, the trajectory of the particle about this axis is always symmetrical and is therefore

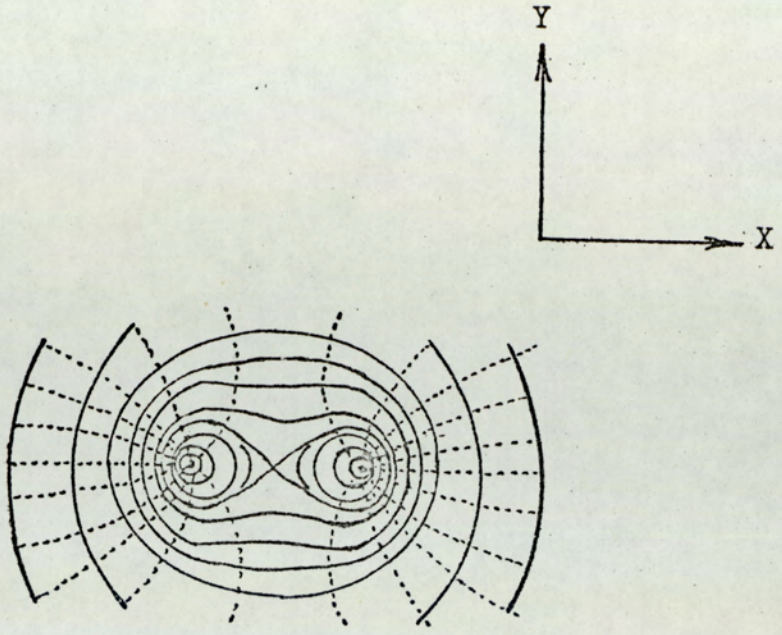

(b) The electrostatic field of two equal charges.

——— Equipotentials.

..... Field lines.

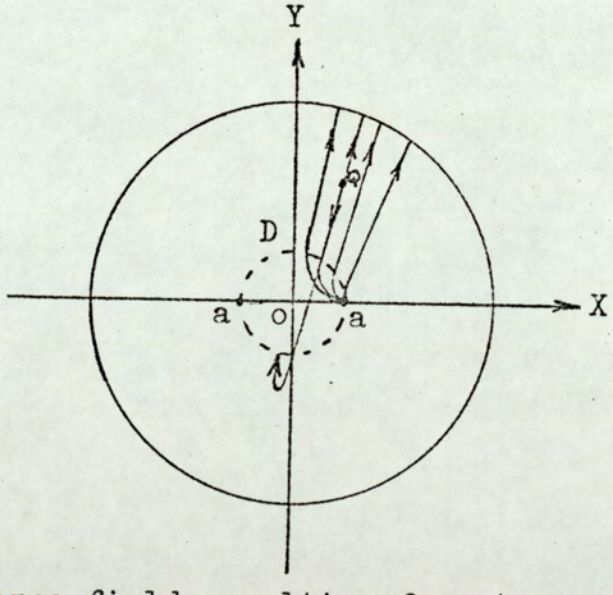

(a) Force field resulting from two equal charges.

Figure 3.1

stationary, (assuming that the electron does not suffer collision with other particles).

3.2. The field in the oscillator.

Consider an oscillator of infinite length and let the charge of each pole be $\pm q$ per unit length. Suppose that the two charges are equally placed from the origin O with a distance $\pm$ a as shown in Figure (3.2). The potential at a point Q (r, θ) is:

$$= -2q \ln r_1 - 2q \ln r_2 \quad \ldots\ldots (3.1)$$

Therefore, the potential at the origin O is,

$$= -4q \ln a \quad \ldots\ldots (3.2)$$

and hence the potential at Q relative to O is,

$$= 4q \ln a - 2q (\ln r_1 + \ln r_2) \quad \ldots\ldots (3.3)$$

$$= q \ln \frac{a^4}{r_1^2 + r_2^2}$$

$$= q \ln \frac{a^4}{(y^2 + (x^2 - a)^2)^2 (y^2 + (x + a)^2)^2} \quad \ldots\ldots (3.4)$$

The electric field along the X-axis, E_x and that along the Y-axis, E_y, are found by differentiating Eq. (3.4) with respect to x and y respectively,

$$E_x = \frac{4q\, x\, (x^2 + y^2 - a^2)}{(y^2 + (x + a)^2)\, (y^2 + (x - a)^2)} \quad \ldots\ldots (3.5)$$

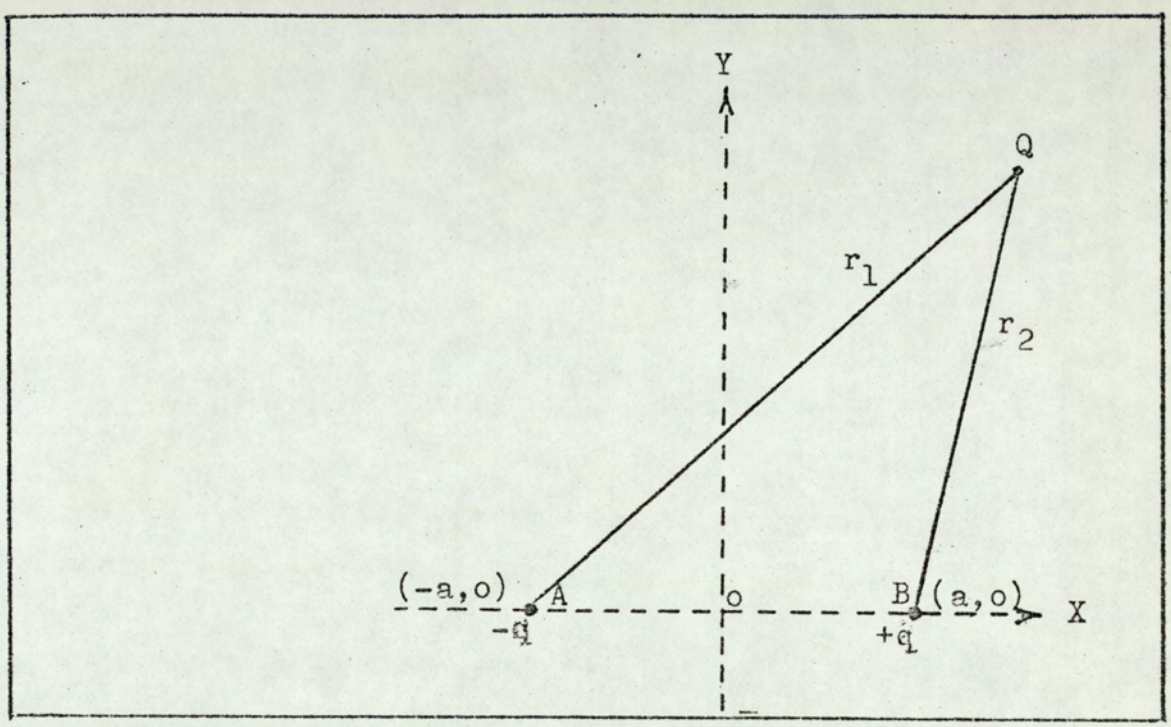

Figure 3.2 Calculating the field in the oscillator.

$$E_y = \frac{4qy\,(x^2 + y^2 + a^2)}{(y^2 + (x + a)^2)\,(y^2 + (x - a)^2)} \quad \ldots\ldots (3.6)$$

Therefore, it can be seen that $E_x = 0$ for $x^2 + y^2 = a^2$, i.e. E_x is zero on the Y-axis and on a circle with AB as diameter. Inside this circle the force, F_x, on an electron is away from the Y-axis, while outside this circle, F_x, is towards the Y-axis. The force, F_y, on an electron is always towards the X-axis (McIlraith, 1967).

The origin is a saddle point in the potential field,

$$E_y/E_x = \frac{y}{x} \cdot \frac{x^2 + y^2 + a^2}{x^2 + y^2 - a^2} \rightarrow \frac{y}{x} \text{ for } x^2 + y^2 \gg a^2$$

$$\ldots\ldots (3.7)$$

Although the saddle-point is a point of unstable equilibrium, electrons can oscillate through it in stable trajectories along the general direction of the Y-axis of the oscillator. Oscillatory trajectories of this type have been demonstrated on a rubber analogue of the twin wire oscillator by McIlraith (1967).

When using a pair of equally charged cylindrical rods of finite length as poles surrounded by an oppositely charged cylinder of the same length, the force, F_z, on electrons is away from the centre of the cylinder and no stable trajectories are obtained. Therefore, the cylinder must be fitted by end plates to prevent particles from escaping from the device and reflect them in such a way that they continue to follow

stable trajectories.

3.3. Mechanism of the oscillator discharge.

It has been shown that electrons oscillate between the twin anode several times before they are captured by the anode. If the electrons do not suffer collision with other particles, they are able to oscillate indefinitely. When the device has enough neutral particles and as a result of oscillating electrons, they make elastic or non-elastic collisions with these neutrals. If the electron energy, E_e, is higher than the ionization potential of the atom (or molecule), i.e.,

$$E_e \geqslant eV_i$$

the result is that the atom (or molecule) is ionized. Where V_i is the ionization potential of the atom (or molecule). Since the electrons are used efficiently due to their long path length, a high density plasma can be produced at low operating gas pressures.

In the following, an attempt is made to deduce the discharge equation of this device. Let, I_o, be the primary electron current for electrons which are able to start oscillating. Each electron giving B_p ion pairs along its path across the gas, $(B_p + 1)$ electrons will go to the anode, and B_p ions bombard the cathode. As a result of ions bombarding the cathode, (γB_p) secondary electrons will be emitted by the cathode, where γ is the secondary electron coefficient for ions falling on the cathode. γ depends upon the type of positive ions, the

energy of positive ions and the nature and state of the cathode material. Also, as a result of the ions falling on the cathode, neutral particles and sputtered ions are emitted from the cathode surface. It is well known that metals are a good catalyst for electron-ion recombination to form neutral particles, so when positive ions impinge on the cathode they become neutralized by extracting electrons from the cathode surface. Sometimes these neutrals are metastable atoms.

From the conservation of energy and the fact that for each ejected electron from the cathode surface, another electron has to escape to neutralize the positive ion which is left behind, the condition for the emission of secondary electrons from the cathode surface upon bombardment with positive ions is,

$$K_e + eV_i \geqslant 2e\varphi \qquad \ldots\ (3.8)$$

where, K_e is the energy of secondary electrons and φ is the work function of the cathode material. As a result of the electron transition from higher energy levels to lower ones to neutralize cathode ions, photons will be also emitted in the process.

Now, on the next oscillation between the two anodes $B_p(B_p + 1)$ electrons will arrive at the anode and $(B_p\gamma B_p)$ ions will return to the cathode. The next journey will involve $(B_p\gamma)^2 B_p$ ions and so on. The multiplication factor is equal to the sum of all electrons reaching the anode for one primary electron.

$$\frac{I_d}{I_o} = (B_p + 1) + B_p\gamma(B_p + 1) + B\gamma^2 (B + 1) + ...$$

$$= (B_p + 1)\,(1 + \gamma B_p + B_p\gamma^2 + ...) \quad .... (3.9)$$

From $(B\gamma)^2 < 1$, the multiplication factor is,

$$\frac{I_d}{I_o} = \frac{B_p + 1}{1 - B_p\gamma} \quad .... (3.10)$$

Where, I_o is the primary electron current and I_d is the discharge current. From Townsend's theory, the breakdown condition is,

$$1 - B_p\gamma = \text{zero}$$

$$\text{or} \quad B_p\gamma = 1 \quad .... (3.11)$$

The above analysis was carried out ignoring the effect of secondary electrons on the anodes since they have no role in the ionization. This is because they are enhanced by the negative space-charge sheath surrounding the anode. Possible electron and ion currents in the discharge are shown in Figure (3.3).

Since B_p depends on the electron energy, the gas pressure and the type of the gas used and that γ depends on the cathode material as well as the kind of positive ions, therefore, I_d, will depend on these parameters too as it is expected. Rushton (1972) used aluminium and stainless steel cathode and obtained different oscillator characteristics. The tube current was higher for

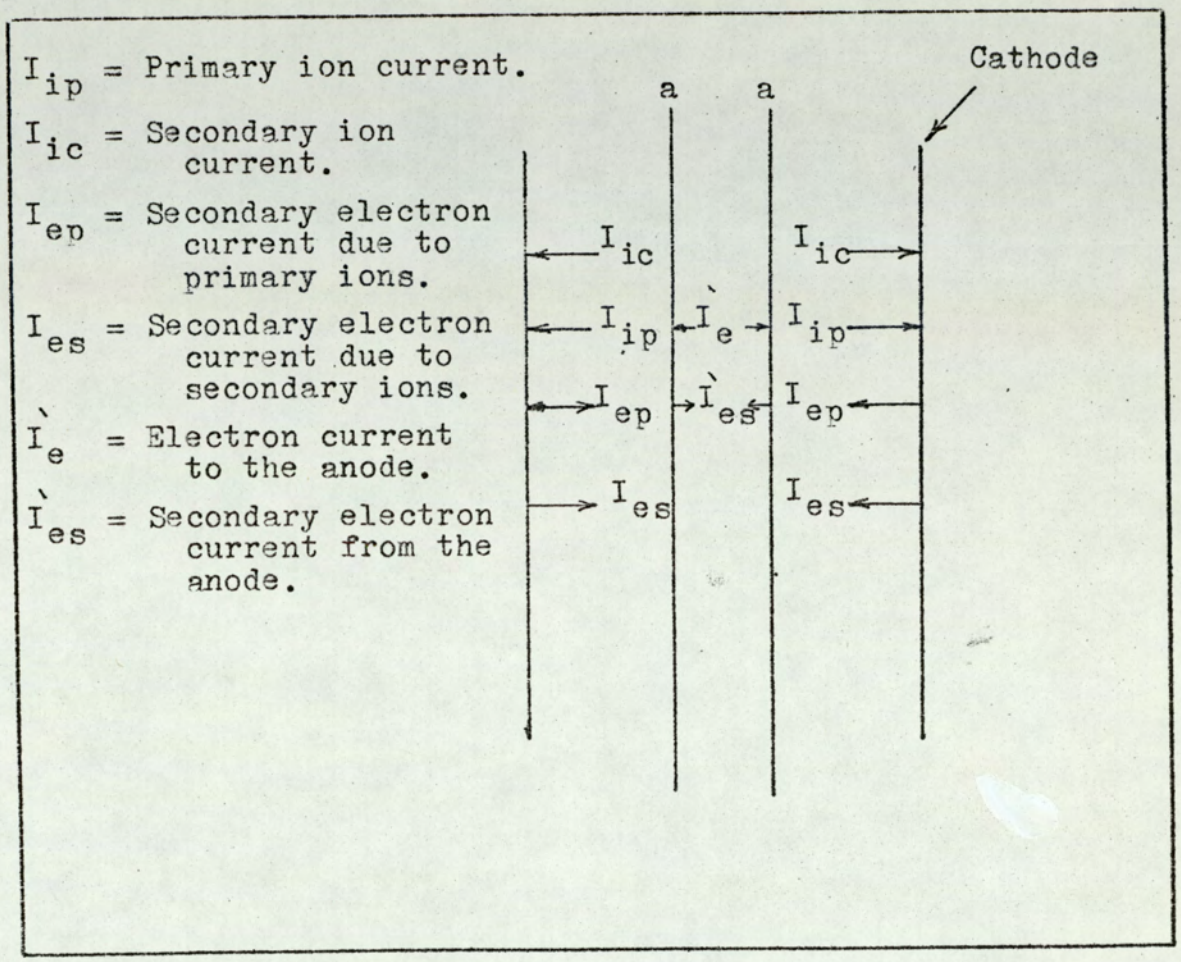

Figure 3.3 Ion and electron currents in the discharge.

aluminium which agrees with the above analysis.

3.4. Ion density of the plasma.

It was found that the discharge produced two ion etched regions on the inside surface of the cathode as shown in Figure (3.4). Therefore, the average positive ion current density at the cathode will be equal to the ion current hitting the cathode divided by the area of the two etched regions.

The plasma ion density (number of ions/c.c.) can be calculated if the ion current density is known. When an ion current, I_i, hits the cathode, the latter will emit γI_i secondary electrons. Where γ is the secondary electron coefficient of the cathode material when it is bombarded by ions of energy approximately equivalent to the discharge voltage, V_d, so the discharge current is given by,

$$I_d = I_i + \gamma I_i \qquad \ldots. (3.12)$$

The ion current density, J_{ic} near the cathode is equal to,

$$J_{ic} = \frac{I_i}{S} = n_{ic}\, e v_{ic} \qquad \ldots. (3.13)$$

Where S is the area of the two ion etched regions in the cathode, n_{ic} is the ion density at the cathode and v_{ic} is the ion velocity which is given by:

$$e\, V_d = \frac{1}{2} m_i\, v_{ic}^2 \qquad \ldots. (3.14)$$

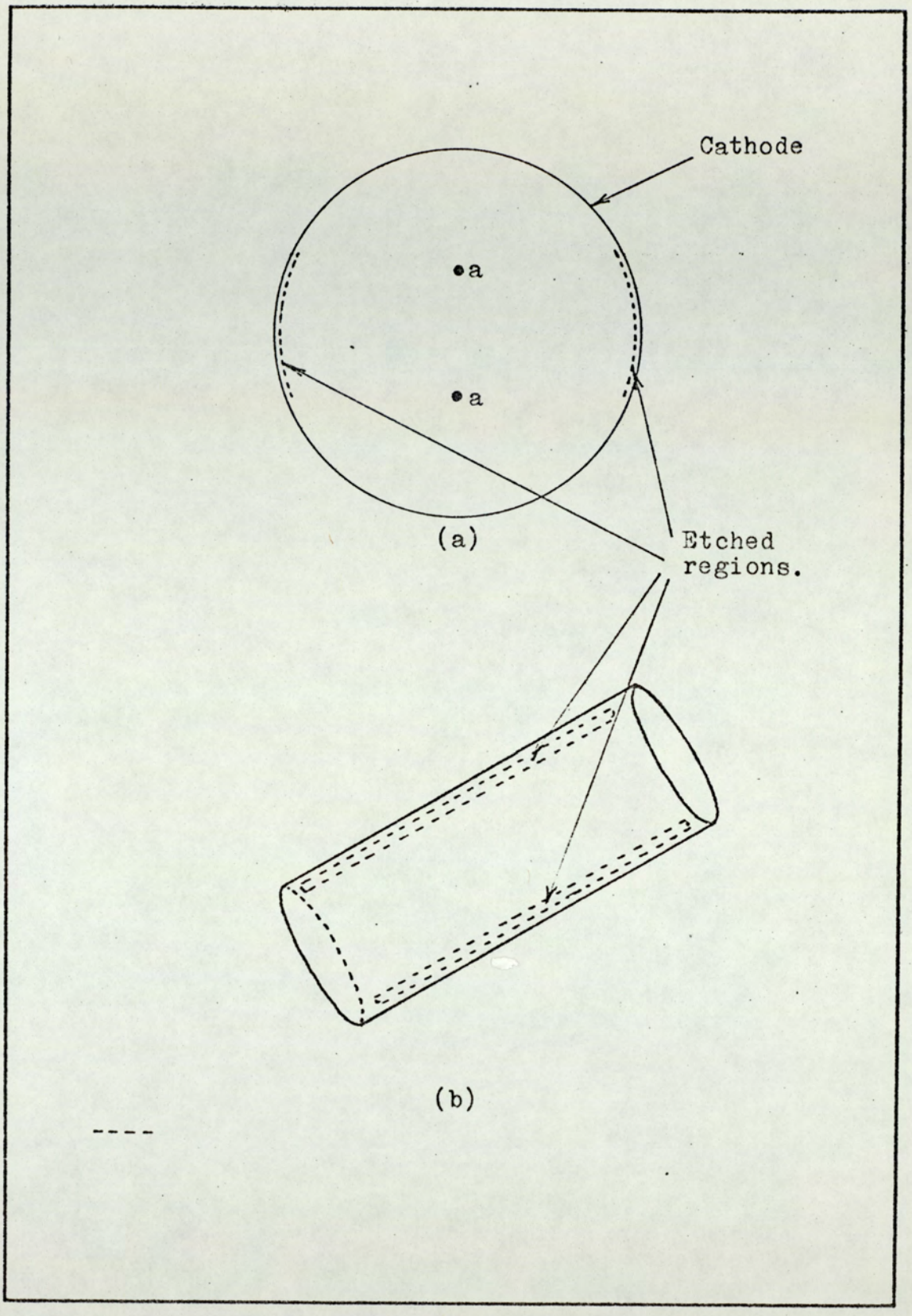

Figure 3.4 The cathode ion etched regions.

Therefore,

$$n_{ic} = \frac{J_{ic}}{e}\left[\frac{m_i}{2eV_d}\right]^{\frac{1}{2}} \quad \ldots\ldots (3.15)$$

By assuming that the ion current density in the plasma is equal to the ion current density near the cathode (Bohm 1949), therefore,

$$n_{ic}\, eV_{ic} = n_{ip}\, eV_{ip} \quad \ldots\ldots (3.16)$$

Where, n_{ip} is the plasma ion density and V_{ip} is the ion velocity in the plasma and V_{ip} is equal to a few volts. Bohm (1949) assumed it is equal to 1 volt. Eqs. (3.15) and (3.16) give the ion density at the cathode as well as the plasma ion density.

4. ION BEAM FORMATION

4.1. Principles of ion extraction from Plasma.

The second important step in ion sources after the production of high density plasma, is to extract the plasma ions in the form of beam of given energy. This can be done by an electrode that is held at a negative potential with respect to that of the plasma. The basic problem is to find an optimum geometry for this electrode (extraction electrode) which possessthe following requirements.

(a) It must yield as an intense ion beam as possible, with minimum divergence and to be free of aberrations as possible. This requires using high extraction voltages.

(b) Neutral atoms, which have escaped ionization in the source, must be prevented as far as possible from leaking to the vacuum system, while the maximum number of ions must be allowed to be extracted in order to increase the efficiency of the source.

4.2. Classical extraction systems.

An ideal plasma is, by definition, an equi-potential region without intense electric field. When a plasma comes in contact with an electrode S_2 (Fig. 4.1.a) held at a negative potential, a positive ion sheath is formed and the whole potential difference between the

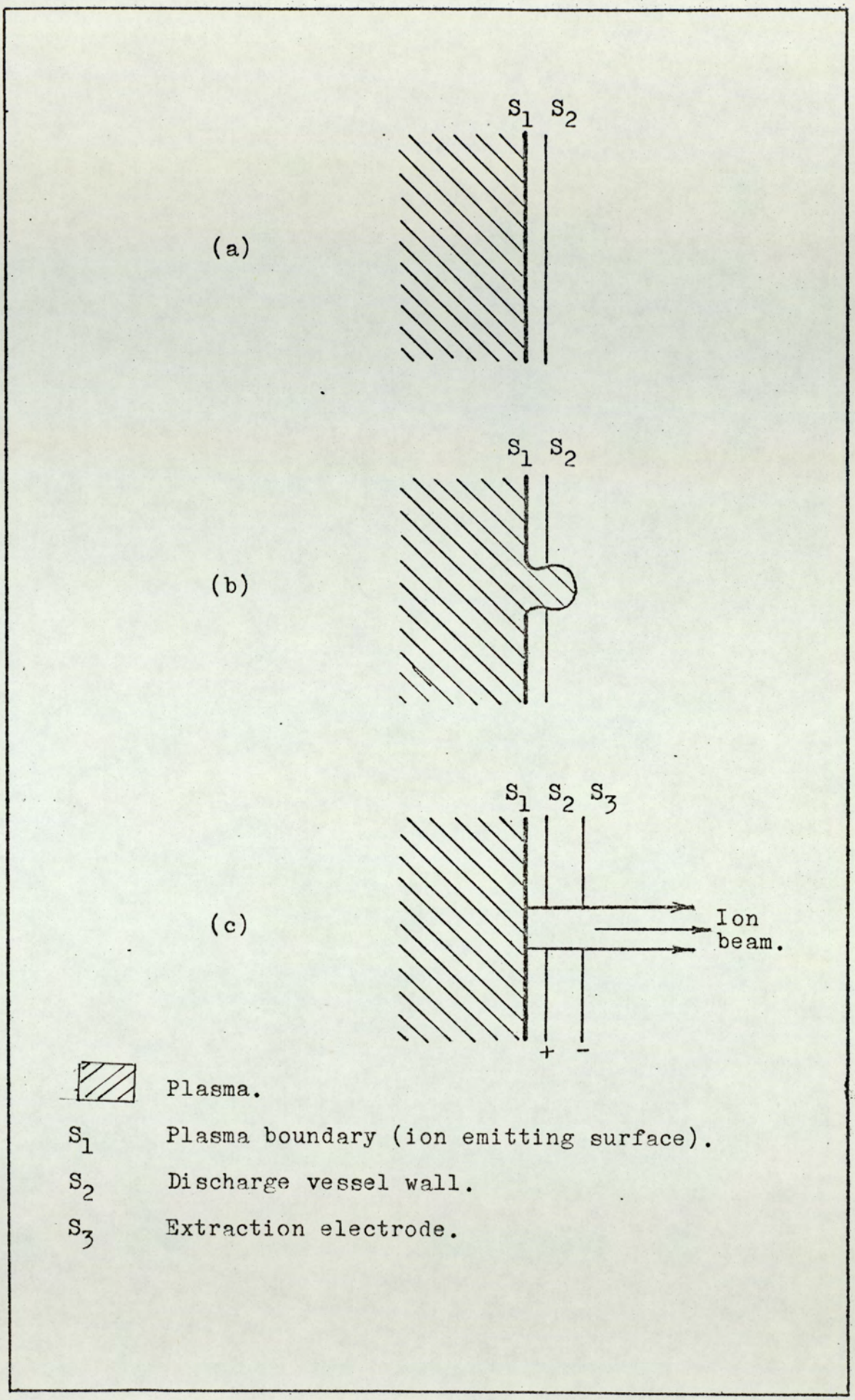

Figure 4.1 Schematic diagrams of ion beam formation.

plasma and this electrode is localized within the sheath. Such a sheath can be formed between the plasma boundary S_1, and any surface near the plasma boundary S_2, e.g. the wall of the discharge vessel or any electrode carrying a negative potential. Under this condition the wall of the discharge vessel becomes charged negatively and the plasma assumes a positive potential with respect to the wall.

As the potential difference between the plasma and the electrode S_2 changes, the thickness of the ion sheath alters, in such a way that the surface S_1 remains in equilibrium. S_1 is an equipotential surface, $V_{s1} = V_p$ where V_p is the plasma potential. Since the electric field in the plasma is very small, no electric force draws S_1 towards the interior of the plasma; the same must therefore be true of the side S_1 facing the electrode S_2.

When a hole is cut in S_2 (the wall of the discharge vessel in this case) the plasma expands and gives a concave plasma boundary outside the discharge as shown in Fig. (4.1.b)(Thoneman and Harrison, 1955). This plasma boundary is the ion emitting surface and ions can be extracted from it by applying a negative potential to an electrode S_3 (extractor) nearest to it as shown in Fig. (4.1.c).

The plasma boundary is an elastic electrode, its shape and position is affected by the electric field between it and the extractor electrode, the shape of this electrode and the discharge parameters. The plasma

boundary in Fig. (4.1.b) can be pushed back to its original position and a parallel ion beam flows from a flat plasma boundary by applying the proper potential between the extraction electrode S_3 and S_2 as shown in Fig. (4.1.c).

The value of the ion current density from the plasma boundary is space-charge limited and is given by Langmuir (1923, 1924) for parallel plane electrodes.

$$J_+ = \frac{(2Ze)^{\frac{1}{2}} \; V_{ex.}^{3/2}}{9\pi m_i^{\frac{1}{2}} L^2} \qquad A/Cm^2 \qquad \ldots\ldots (4.1.1)$$

Where,

$V_{ex.}$ = extraction voltage in volts

L = the distance between S_1 and S_3 in cm

Z = charge number of the ion

e = electron charge

m_i = the mass of the ion

The total theoretical ion current which can be extracted from the plasma is equal to the ion current density, J_+, multiplied by the area of the plasma boundary.

It should be noted that equation (4.1.1) was derived for ions of one kind, but in practice ion beams usually contain more than one kind of ion, so this equation is modified to:

$$J_+ = \frac{1}{9}\left[\frac{(2e)^{\frac{1}{2}}}{\pi m^{\frac{1}{2}}}\left(\frac{Z_1K_1}{m_{i1}^{\frac{1}{2}}} + \frac{Z_2K_2}{m_{i2}^{\frac{1}{2}}} + \ldots\ldots\right)\right]\frac{V_{ex.}^{3/2}}{d^2} \qquad A/cm^2$$

$\ldots\ldots (4.1.2)$

Where,

$$(K_1 + K_2 + \ldots\ldots\ldots) = 1$$

m_{in} = mass value of n^{th} type of ion

Z_n = charge number of the n^{th} type of ion in the plasma

K_n = the concentration of the n^{th} type of ion in the plasma.

4.3. Other extraction systems.

When a high ion current is required, the holes in the discharge vessel and in the extraction electrode can be increased, also higher extraction voltages may be used to form a concave plasma boundary which results in producing a focused beam of higher intensity as shown in Fig. (4.2.a). However, increasing the area of the holes cannot be done indefinitely because of gas loading and using high extraction voltage may be accompanied with high voltage breakdown. Therefore, the advantages of plasma diffusing outside the source through a small aperture which restricts the gas flow from the source to the extraction region can be used. This depends upon plasma penetration through a small hole outside the source. This principle is well known and was first used in ion sources by Gabovich et al. The plasma passes through a small aperture to the extraction region and leads to a bigger plasma boundary which results in a large ion current. The ions can be extracted from the expanded plasma by applying a negative potential to electrode S_3 as in Fig. (4.2.b). This electrode may be a cylinder or grid

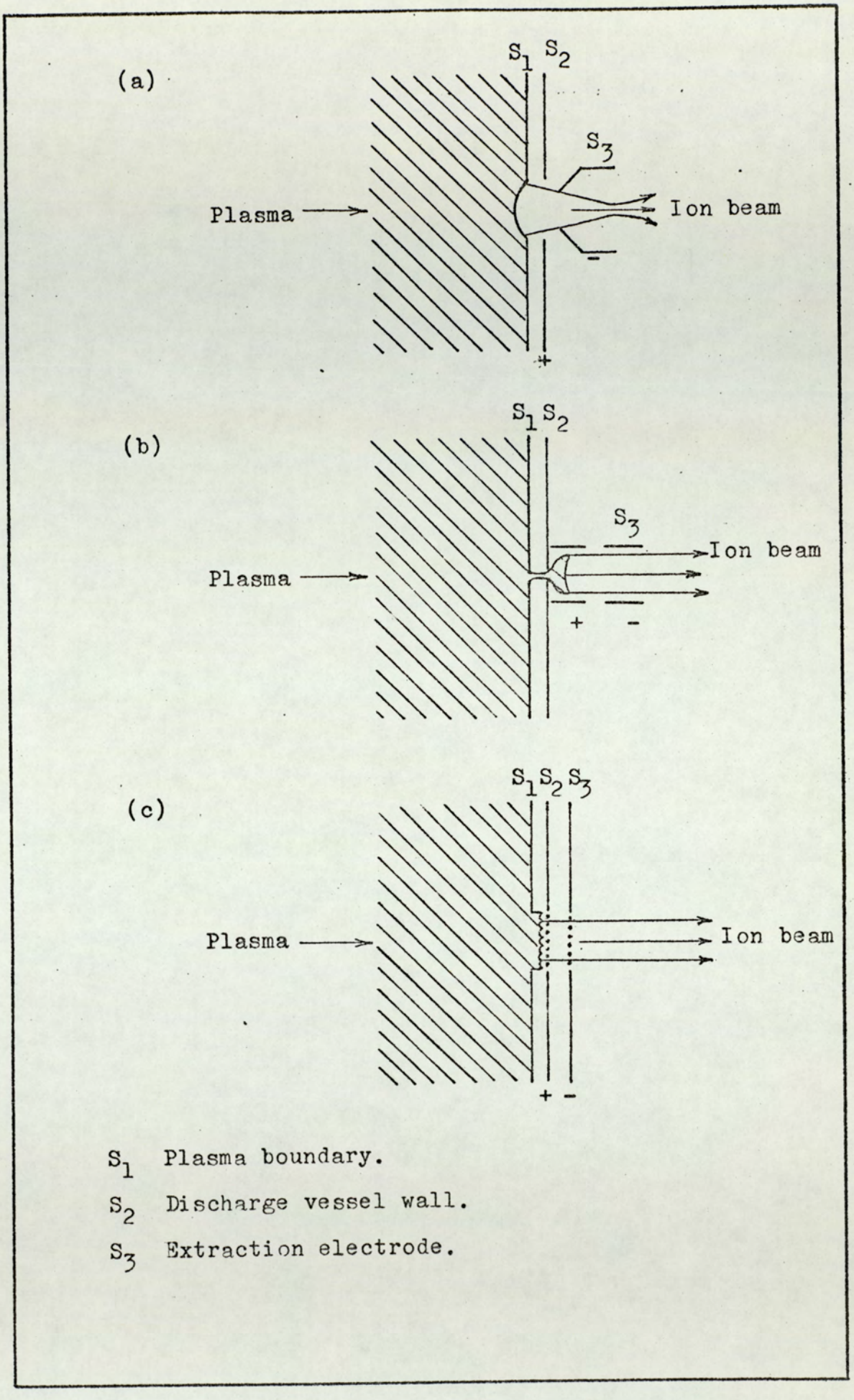

Figure 4.2 Schematic diagrams of ion beam formation.

(Solnyshkov, 1963). This method has the advantage of producing ion beams with low divergence (Collins and Strouds, 1964).

Another way for ion extraction is shown in Fig. (4.2.c). It depends on fixing a grid in the hole of S_2 electrode and using an extraction grid. This gives a well defined extraction geometry and the plasma boundary in this case will be wavy (Rose, 1964).

4.4. Ion extraction from the electrostatic charged particle oscillator.

The manner in which the ions emerge out from the source was described by Ghander and Fitch (1973). Fig. (4.3) shows the shape of the discharge. Since the plasma is in contact with the cathode in two parts, a plasma ion sheath is formed close to each side of the cathode. McIlraith (1971) showed that the discharge voltage is confined mainly in the Y-axis, and since the plasma is a conducting medium, the plasma ion sheath will carry most of the discharge voltage except small drop due to the cathode fall and the plasma drop. This means that a diode will be formed between the ion sheath and the cathode in the Y-axis and ions will be moving towards the Y-axis giving two etched regions in the cathode. Therefore, one or more holes in either side of the cathode will allow some of the ions to escape out of the source in the form of energetic ion beams without using an extraction system (self extraction). The ion beam current at a particular pressure will be space-charge limited according to Eq. (4.1.1).

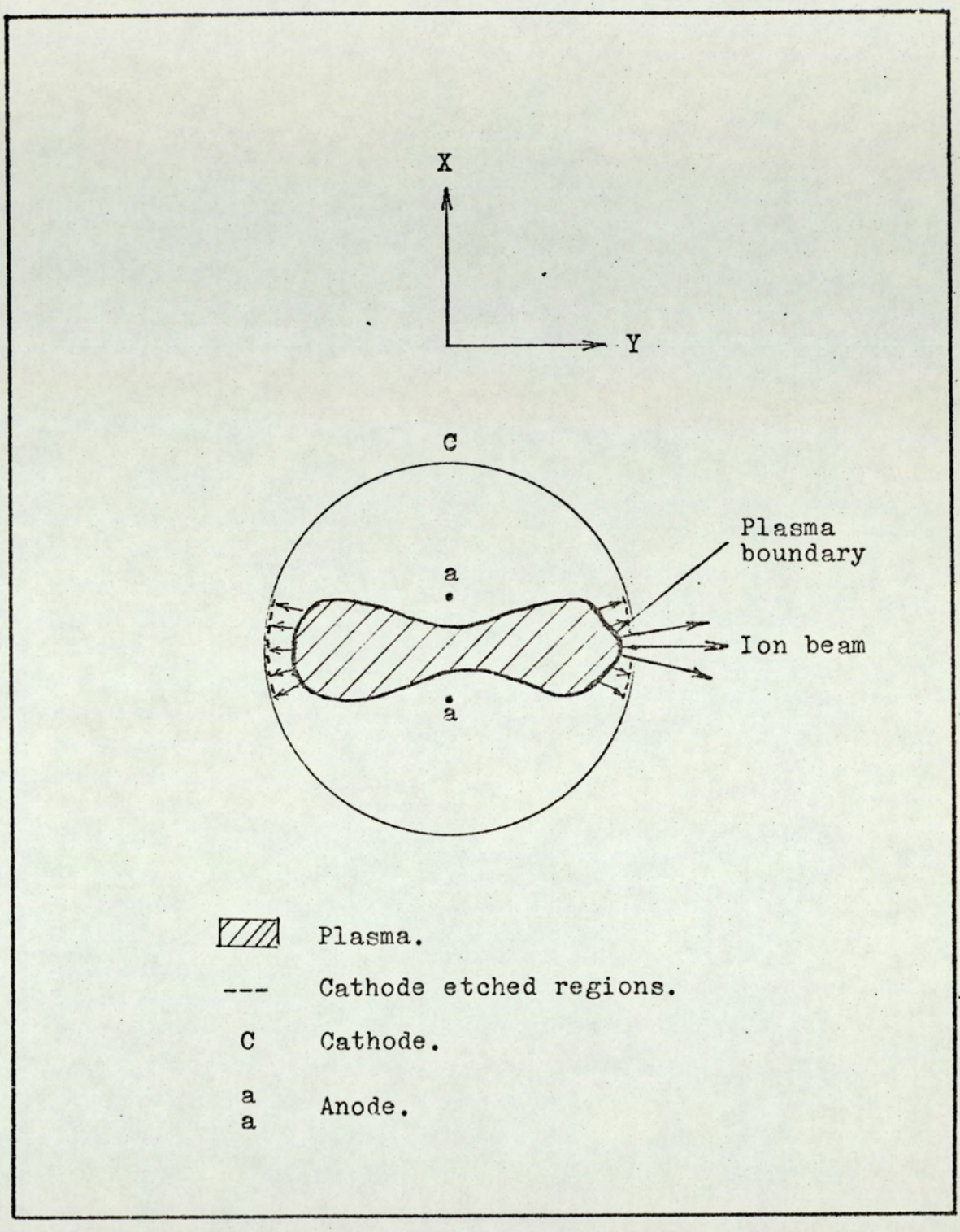

Figure 4.3 Schematic diagram of self extraction of ions from the charged particle oscillator ion source.

5. THE CONVENTIONAL TWIN ANODE ELECTROSTATIC ION SOURCE.

5.1. Introduction.

Investigations of the characteristics of the twin anode electrostatic ion source are described in this Chapter. The discharge voltage-current characteristics are examined as a first step. The effect of gas pressure on the source characteristics and the ion beam current are described. The operational modes of the source and the change in the ion current efficiency of the oscillator when it is used as an ion source are described and explained.

5.2. Design of the twin anode electrostatic ion source.

A schematic diagram of the twin anode electrostatic ion source is shown in Figure (5.1). The source consists essentially of a cylindrical stainless steel cathode, length 7.5 cm. and diameter 2.5 cm. and two tungsten anode rods of diameter 1.5 mm. The separation of the anode rods was fixed at 5 mm. throughout these investigations. Two stainless steel plates were positioned at the end of the cathode tube. The anode rods were positioned and electrically insulated from the end plates by two ceramtec bushes, in such a way that they are able to expand freely when they get hot. The anode rods were aligned by means of four screws fixing the ceramtec bushes into the end plates and four other screws were used to fix the end plates into the cathode

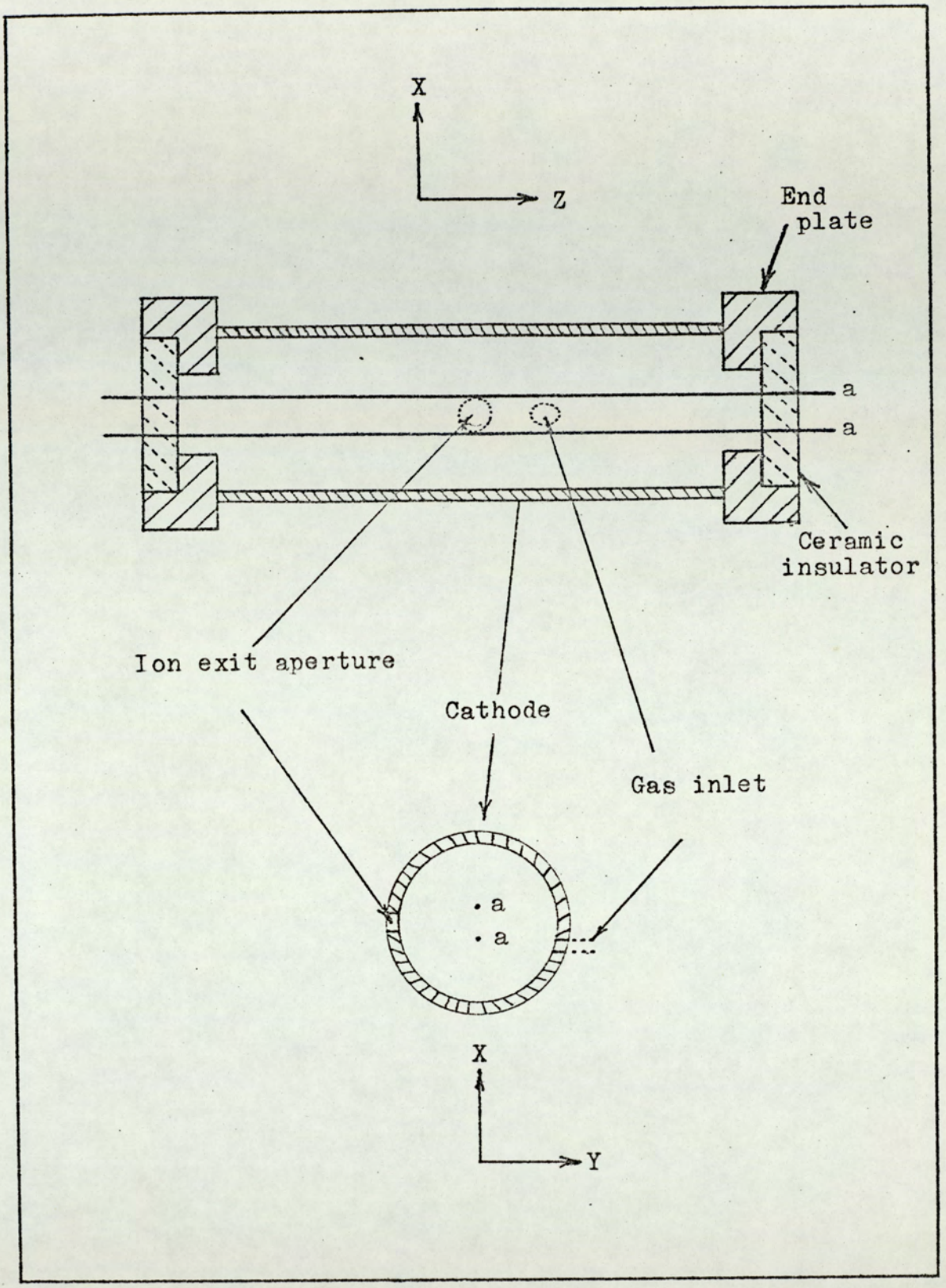

Figure 5.1 Drawing of the twin-anode ion source.

tube to ensure that the anode rods were placed symmetrically about the axis of the cathode. Gas was admitted directly into the source through a small stainless steel tube welded into the cathode tube as first described by Franks (1972).

5.3. The ion source rig.

In order to have the ion source in a fixed position inside the vacuum chamber, a rig to carry the source, ion beam diagnostic systems and other additional parts to the ion source was designed. A drawing of this experimental stand is shown in Figure (5.2). The ion source sits on two pins in two metal flanges fixed at one end of the top part of the stand and then locked into position by two metal strips. This ensures that the centre of the ion exit hole is horizontal which is necessary for ion beam diagnostic measurements. The top part of the stand has a slit designed so that different parts of the diagnostics part can be fixed facing the ion exit hole and that relative distances between them can be changed.

The top part is carried by four aluminium rods which are fixed in a lower metal frame. These rods are isolated from the lower metal frame by teflon insulators. The whole system is placed inside the vacuum chamber.

5.4. The high vacuum system.

Experimental investigations using different versions of ion sources were carried out using a high vacuum system of the standard type. It consists of a

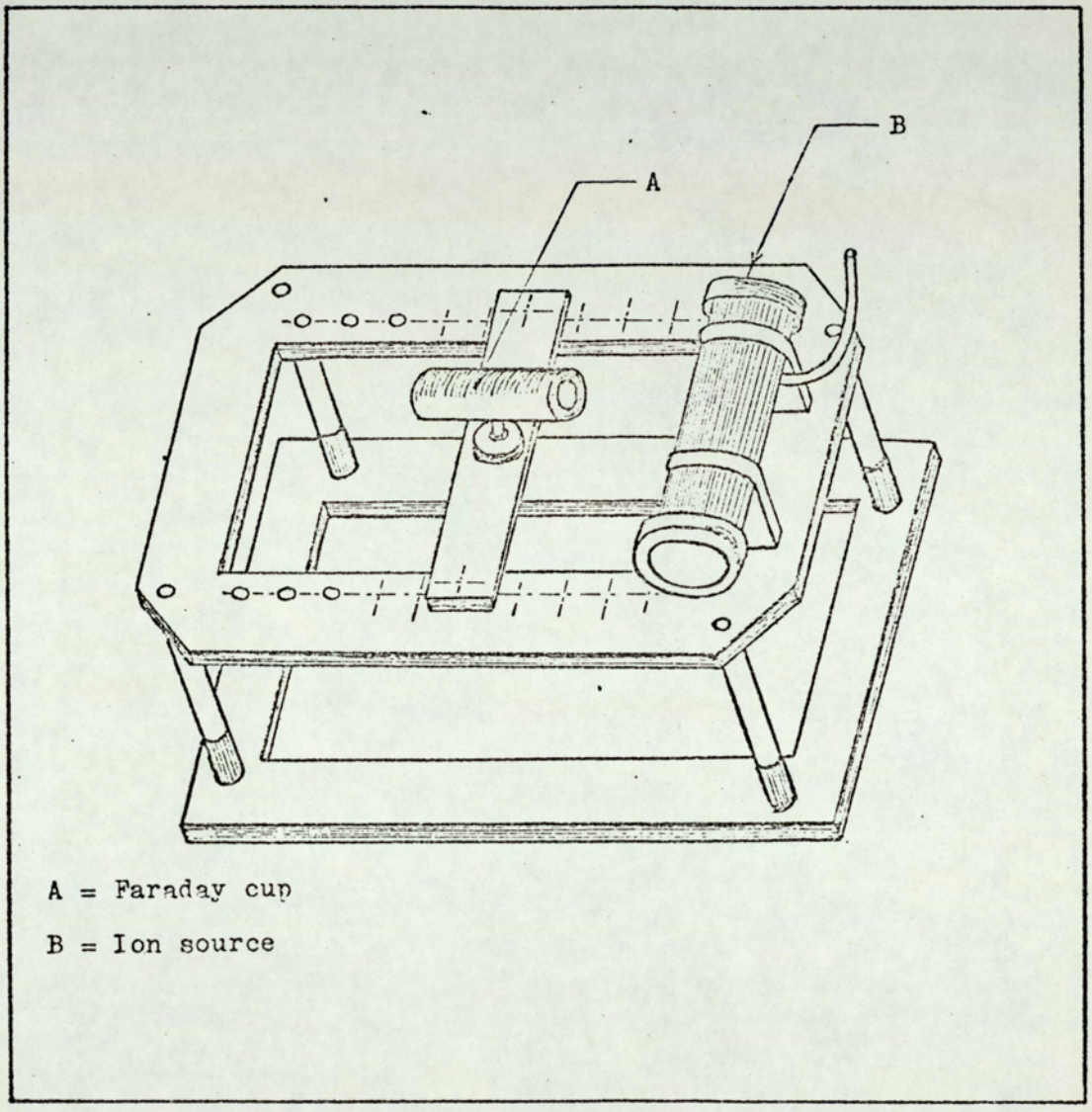

Figure 5.2 The ion source rig.

'Santovac 5' oil diffusion pump (effective speed is 100 litre/sec.) and a rotary pump. The vacuum chamber is stainless steel type of 12" in diameter which contains two flanges carrying 8 high voltage electrical feedthrough and 3 glass viewing ports. The gas (nitrogen, argon or helium) is admitted to the ion source through a needle valve.

The system was capable of achieving pressures down to 10^{-6} torr which were measured by a Penning gauge mounted just above the baffle valve.

5.5. The electrical circuit.

A schematic diagram of the conventional twin anode ion source and its associated electrical circuit is shown in Figure (5.3). The stabilised power supply for the discharge was capable of providing 50 mA at 15 kV. The twin anodes are connected to the positive output via a current limiting resistor which is built in the supply itself, whilst the cathode and end-plates are maintained at earth potential.

The tube current, I_T, and the tube voltage V_T, were measured by means of meters built in the high voltage power supply. V_T is the actual voltage between the anode and the cathode. The ion beam current, I_B, was measured by a conical Faraday cup and a microameter.

5.6. The Discharge characteristics.

The discharge characteristic is the variation of the tube current, I_T, with tube voltage, V_T, at different gas pressures in the chamber. In order to

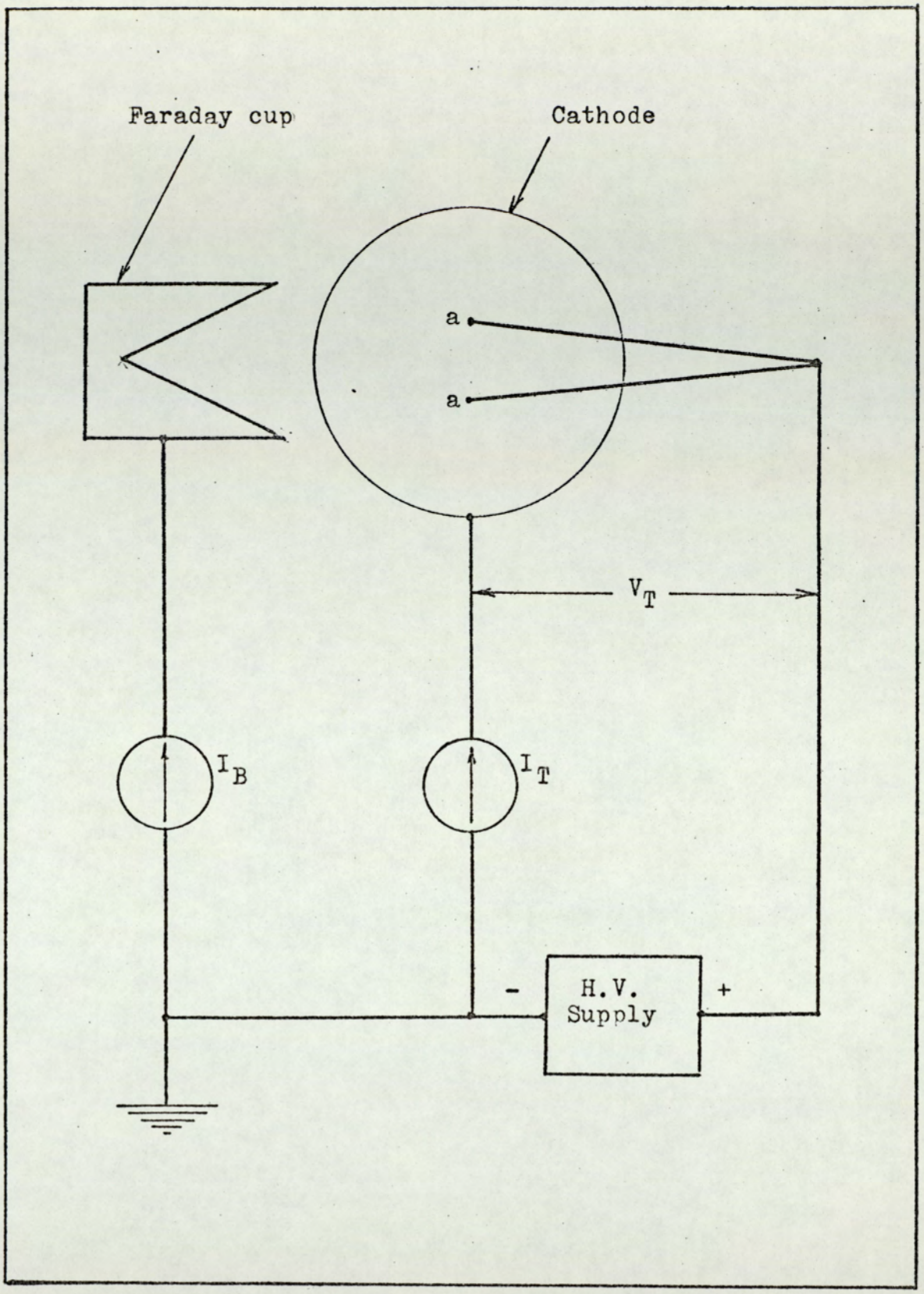

Figure 5.3 The electrical circuit.

obtain reproducible results, the source was operated for a period of time in order to outgas the different parts before any measurements were made.

The characteristics for argon gas are given in Figure (5.4) at different gas pressures. The shape of these characteristic curves are similar to those obtained by Thatcher (1971) and Rushton (1972), except the tube voltages are much lower and the tube currents are much higher in spite of using a relatively bigger ion exit hole. The tube currents at low pressures are as expected lower than those at high pressures. The current-voltage characteristics were obtained down to pressures of 5×10^{-5} torr.

It was noticed that after a long period of operation, the source performance deteriorated and the voltage-current characteristics were not reproducible. In other words, the tube voltage must be increased to get the same tube currents as shown in Figure (5.5). However, if the anode and the cathode were carefully cleaned, the voltage-current characteristics could be reproduced again. It was found also that another cause of the deterioration was due to the fact that the anode rods became distorted and not parallel due to thermal expansion.

The current-voltage characteristics could be obtained at pressures less than 5×10^{-5} torr if higher values of V_T were used, however this was found to be extremely difficult due to high voltage breakdown. In addition the discharge was unstable at lower pressure

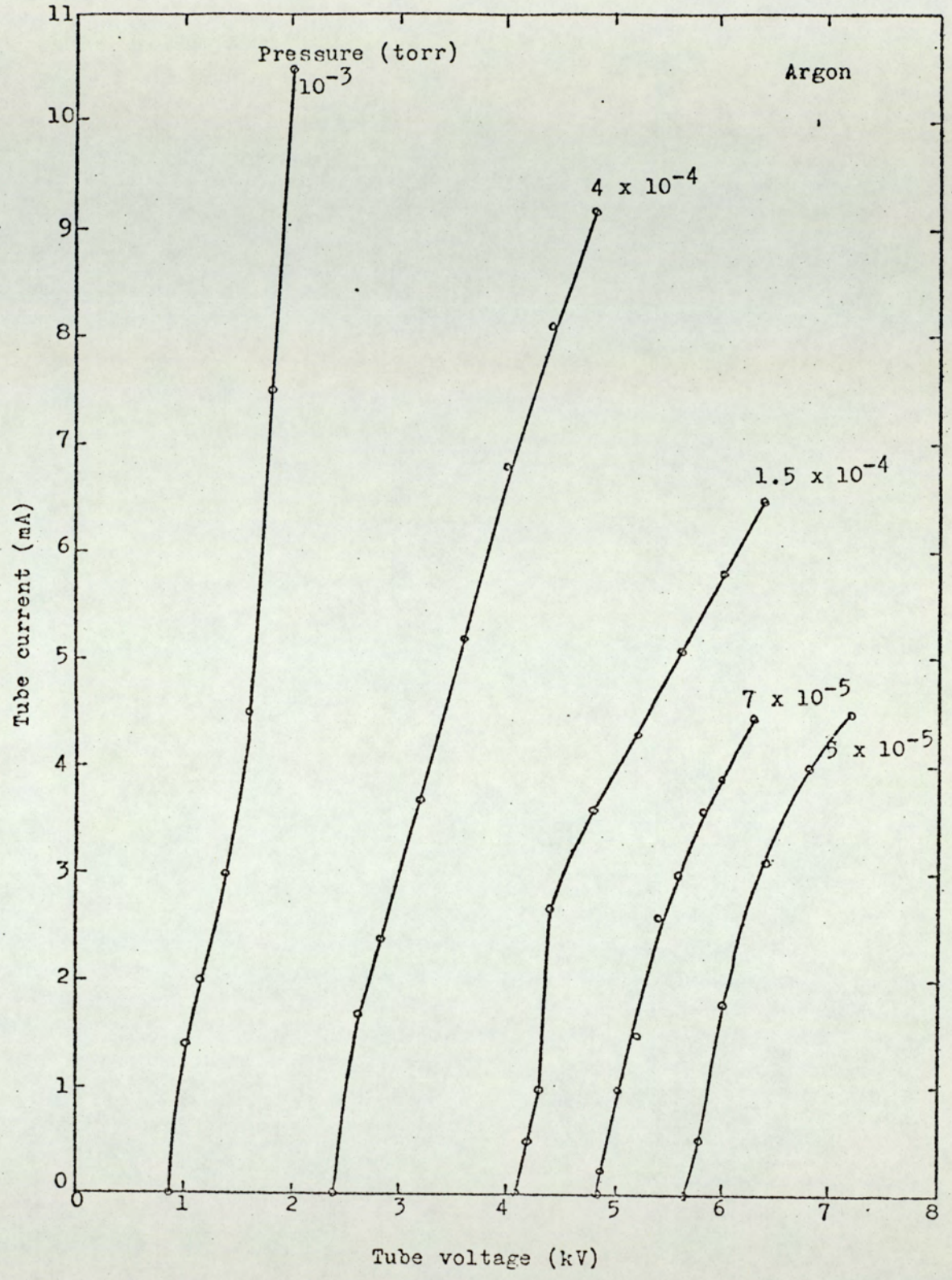

Figure 5.4 The discharge characteristics at the beginning of operation for an ion exit aperture of 5 mm diameter.

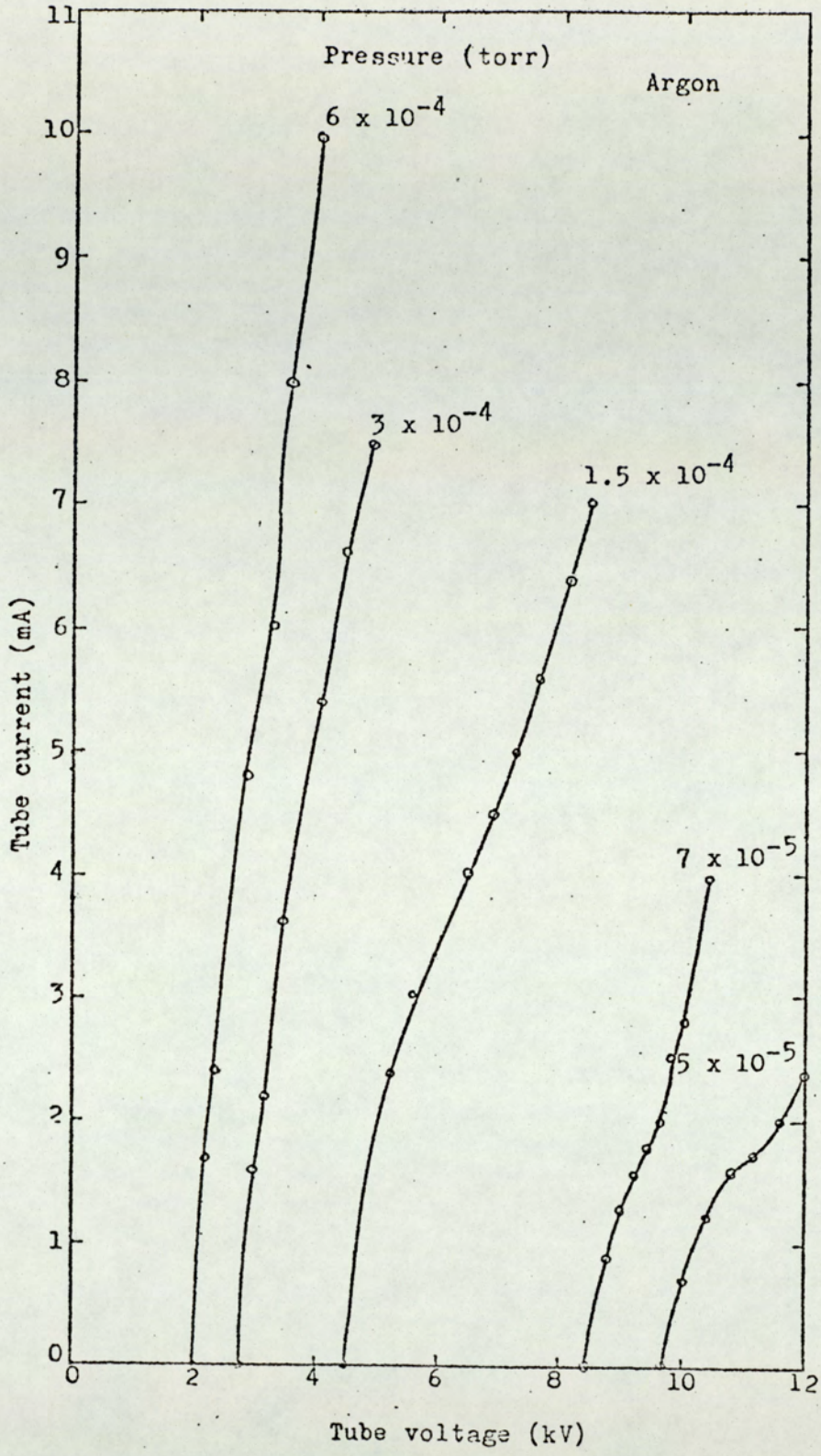

Figure 5.5 The discharge characteristics with a long period of operation for an ion exit aperture of 5 mm diameter.

and low tube currents were obtained.

The characteristics of another source having the same dimensions as mentioned before but with a 3.2 x 10 mm. rectangular ion exit aperture were also investigated. The V_T - I_T characteristic curves are shown in Fig. (5.6), their shapes are similar to those of Fig. (5.4). In order to compare these curves with those of the previous source of 5 mm. circular aperture in diameter, the pressure has to be divided by 1.6 approximately due to the difference in the conductance of the apertures. It can be seen from Fig. (5.6) that a higher tube voltage was needed to get the same tube current when a 5 mm. aperture was used, or expressed in another way, the discharge starts at a higher tube voltage.

The characteristics of a source modified to produce two ion beams have also been investigated, where two rectangular slots, 3.2 x 10 mm., milled in the cathode were used as ion beam apertures. The V_T - I_T characteristic curves of this source are shown in Fig. (5.7). The pressure in this case has to be divided by 2 in order to make it possible to draw a comparison between these curves and those of a single aperture source shown in Fig. (5.6). Again the shape of these curves are similar to the previous ones, but the discharge starts at higher tube voltages than when one slot was used and even more higher tube voltages were needed than when the 5 mm. circular aperture was used.

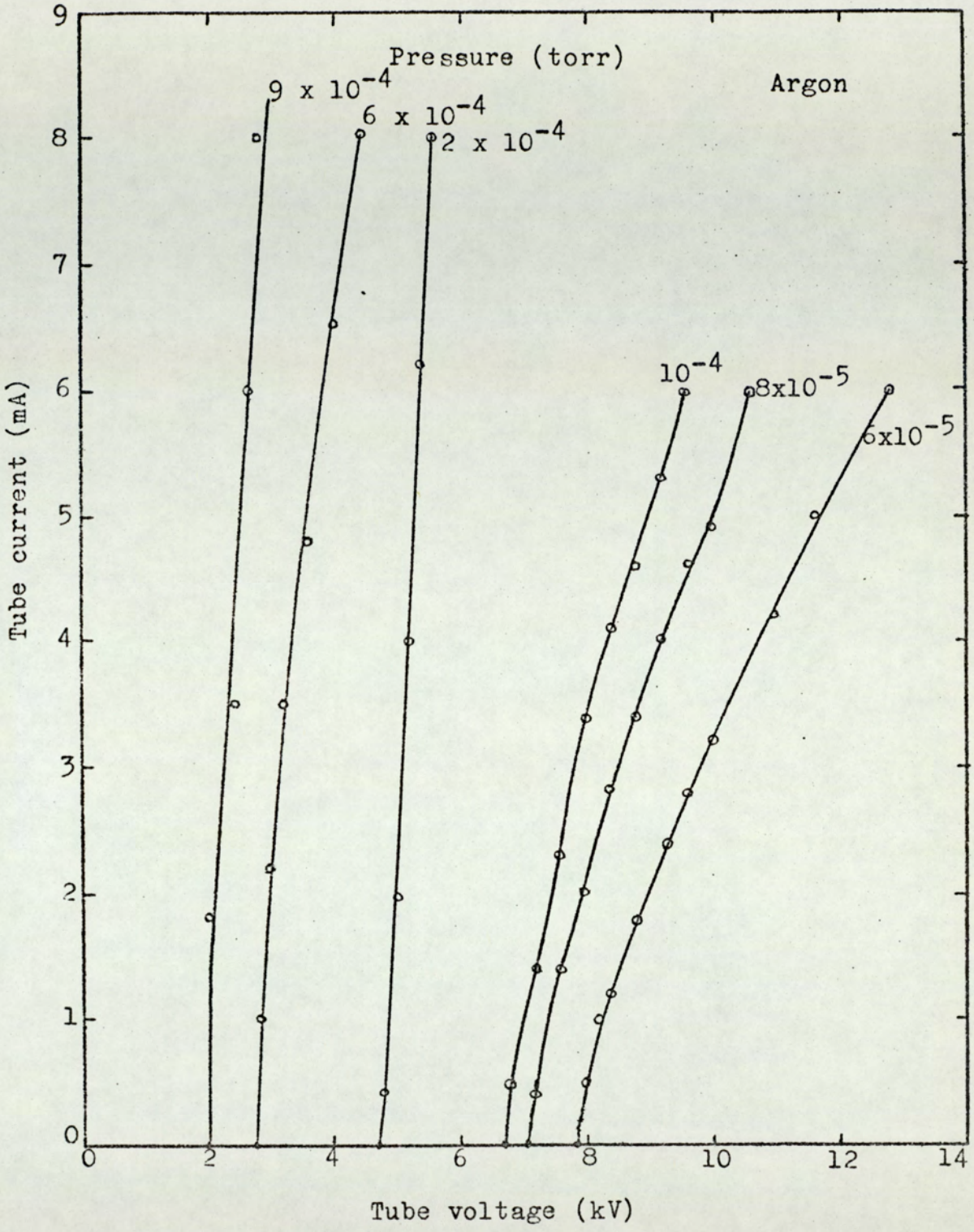

Figure 5.6 The discharge characteristics with a rectangular exit aperture of 3.2 x 10 mm.

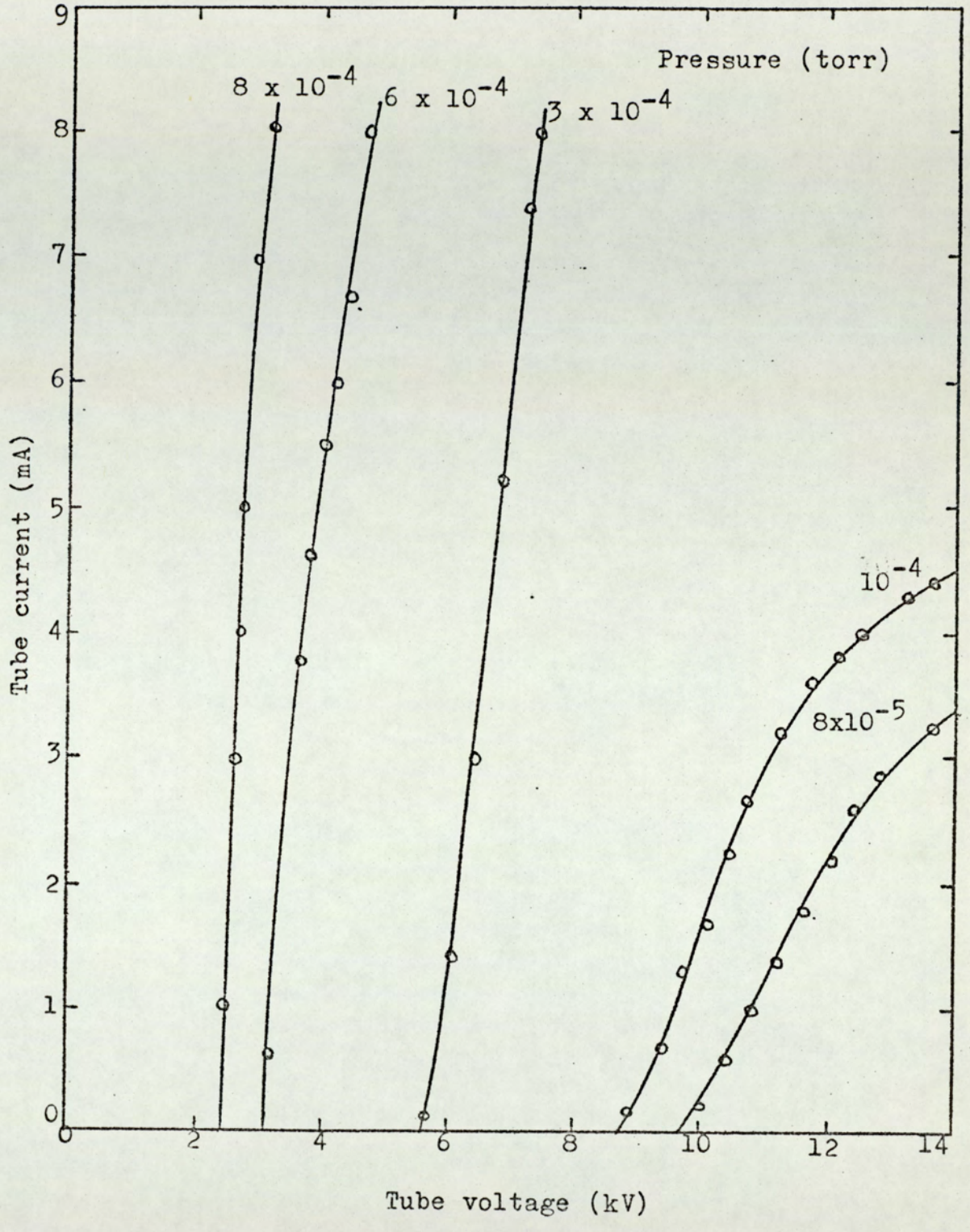

Figure 5.7 The discharge characteristics of the double-beam ion source.

5.7. Investigation of the ion current output.

The density of the ion beam current emerging from the source depends on three characteristic parameters - tube voltage, V_T, tube current, I_T, and the gas pressure in the source. For example, if the pressure is varied, I_T and V_T vary accordingly and thus it is only possible to keep one of these parameters constant.

However, the ion density in the discharge is a function of the input power to the discharge, $I_T V_T$, and the gas pressure. It is thus appropriate to express the ion current as a function of the input power to the source. A family of such curves at various pressures for a source with 5 mm. diameter ion exit aperture is given in Fig. (5.8). It can be seen that for a given input power, there is an optimum pressure for the greatest ion current. For example with the input power equal to 40 watts, I_B is equal to 80 μA at a pressure of 10^{-4} torr, whereas at a pressure of 5×10^{-5} torr I_B is only 22 μA. The beam current of 80 μA is equivalent to an ion density of 0.4 mA/cm^2 at the ion exit aperture.

Another family of such curves of the same source but with a 10 x 3.2 mm. ion exit aperture is shown in Fig. (5.9). As is expected the ion current is higher than the previous case because the area of the ion exit aperture is larger, and an ion current density of 1 - 1.5 mA/cm^2 at the ion exit aperture was achieved. Although, higher ion currents could be obtained by using an ion exit aperture of bigger area, it is not possible to increase that indefinitely because of the gas loading

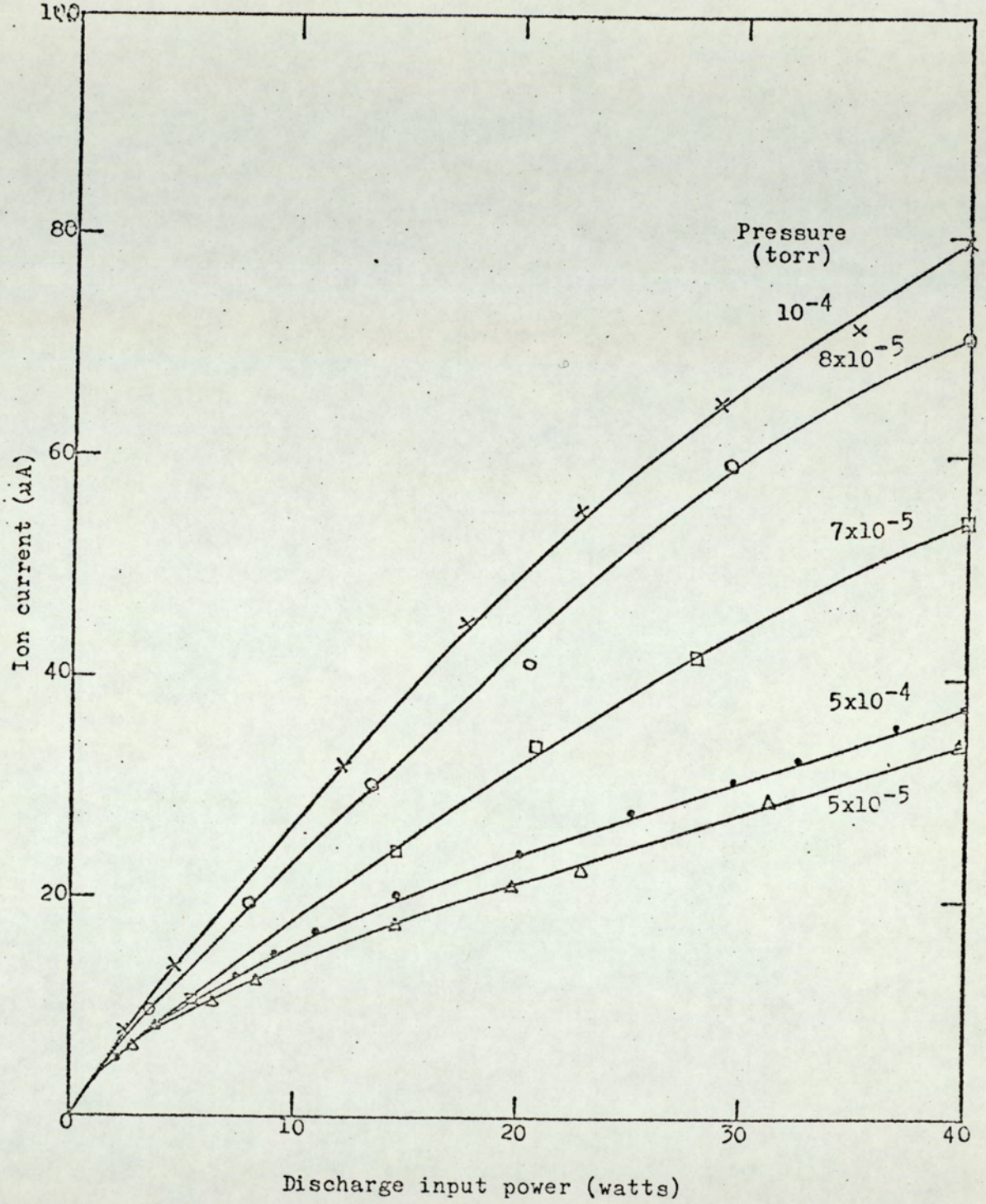

Figure 5.8 The relation between the discharge input power and the output ion current with ion exit aperture of 5 mm. diameter.

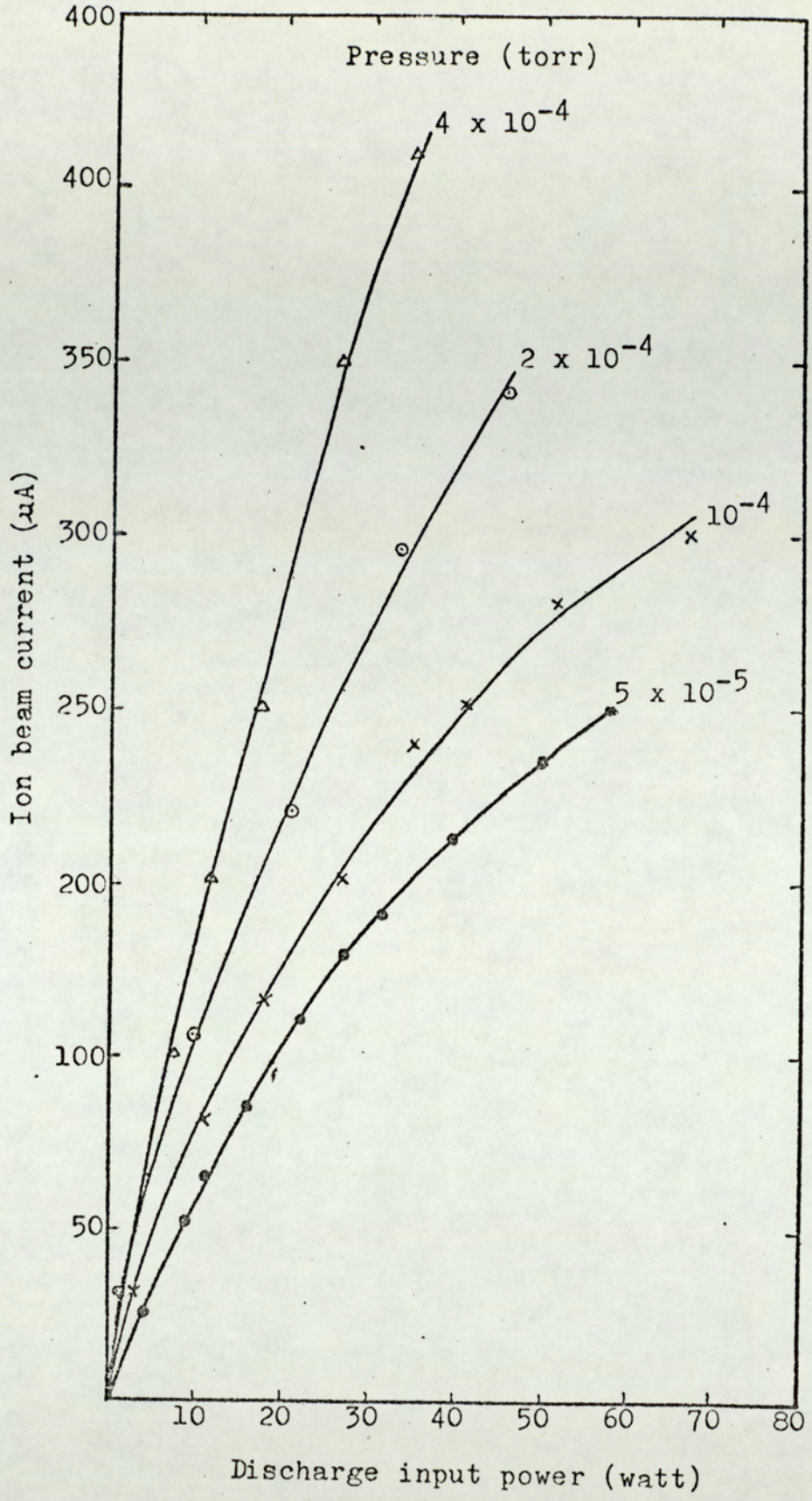

Figure 5.9 The relation between the discharge input power and the ion beam current with an ion exit aperture of 3.2x10 mm. 3.2 x 10 mm.

into the vacuum system. However, the reported ion currents are much higher than those published earlier by Fitch and Rushton (1972).

5.8. The double beam ion source.

The manner in which the double beam ion source is functioning may be explained with the aid of Fig. (5.10). The shape of the discharge is shown in Fig. (5.10.a), and the two regions etched on the inside of the cathode are shown in Fig. (5.10.b). The ions are accelerated towards two opposite directions, thus two apertures at diametrically opposite positions in the cathode should allow self extraction of the ions in the form of two energetic ion beams as explained previously (4.4).

A schematic diagram of the double beam ion source and its associated electrical circuit is shown in Fig. (5.11). The cathode is of stainless steel, length 7.5 cm. and diameter 2.5 cm. and the anodes were made from tungsten rod, 1.5 mm. in diameter at a surface separation of 5 mm. Two rectangular slots, 3.2 x 10 mm., milled at opposite positions in the cathode were used as the ion beam apertures. The ion currents were measured with 2 conical Faraday cups placed 3 cm. from the cathode.

Fig. (5.12) shows a photograph of the two ion beams emerging from the source. The ion currents for each beam as a function of the discharge input power at two pressures of 8×10^{-5} and 5×10^{-4} torr are shown in Fig. (5.13). It can be seen from the figure that, within the experimental error, the ion currents are the same in

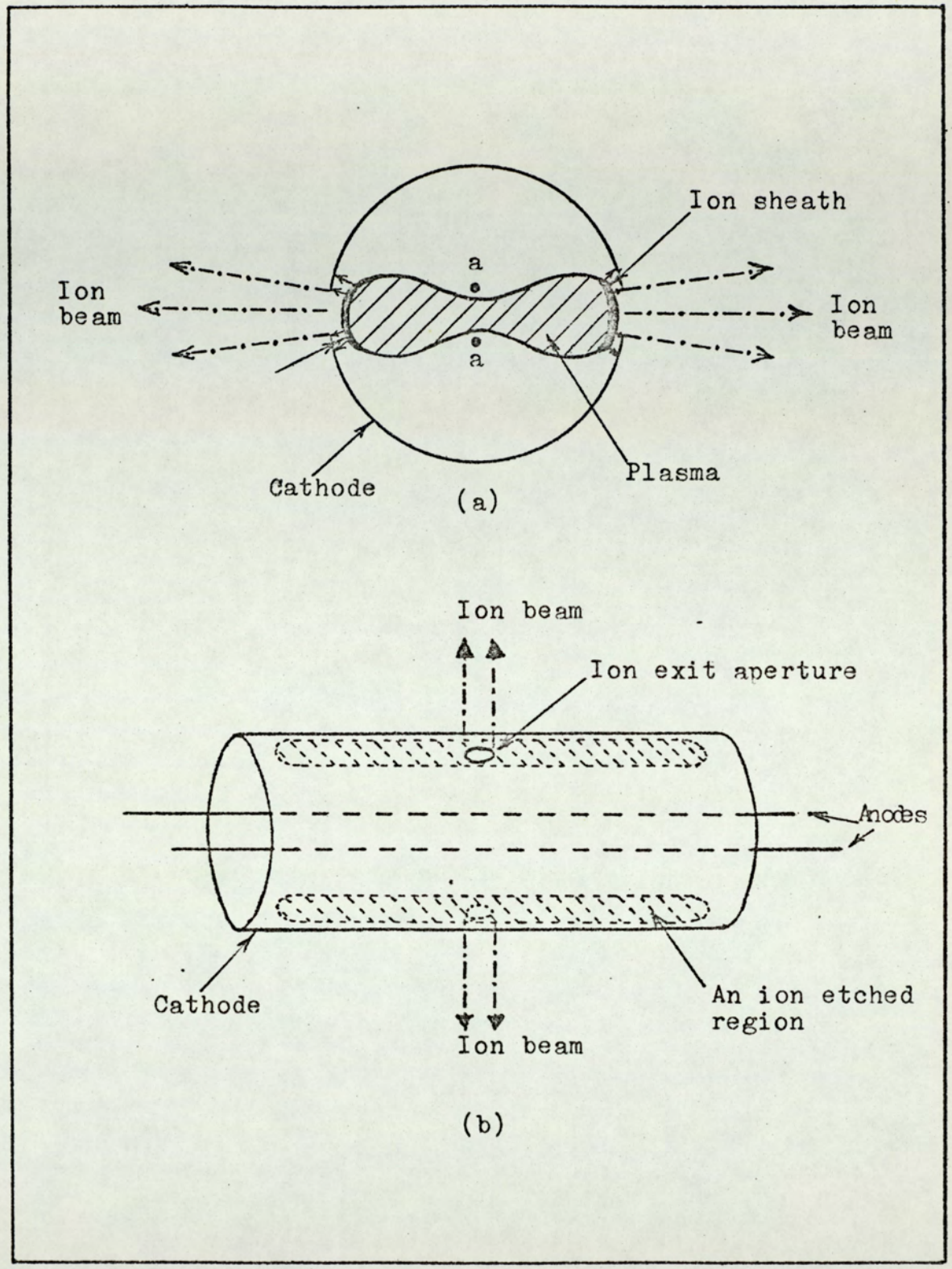

Figure 5.10 Schematic diagram of the double-beam ion source.

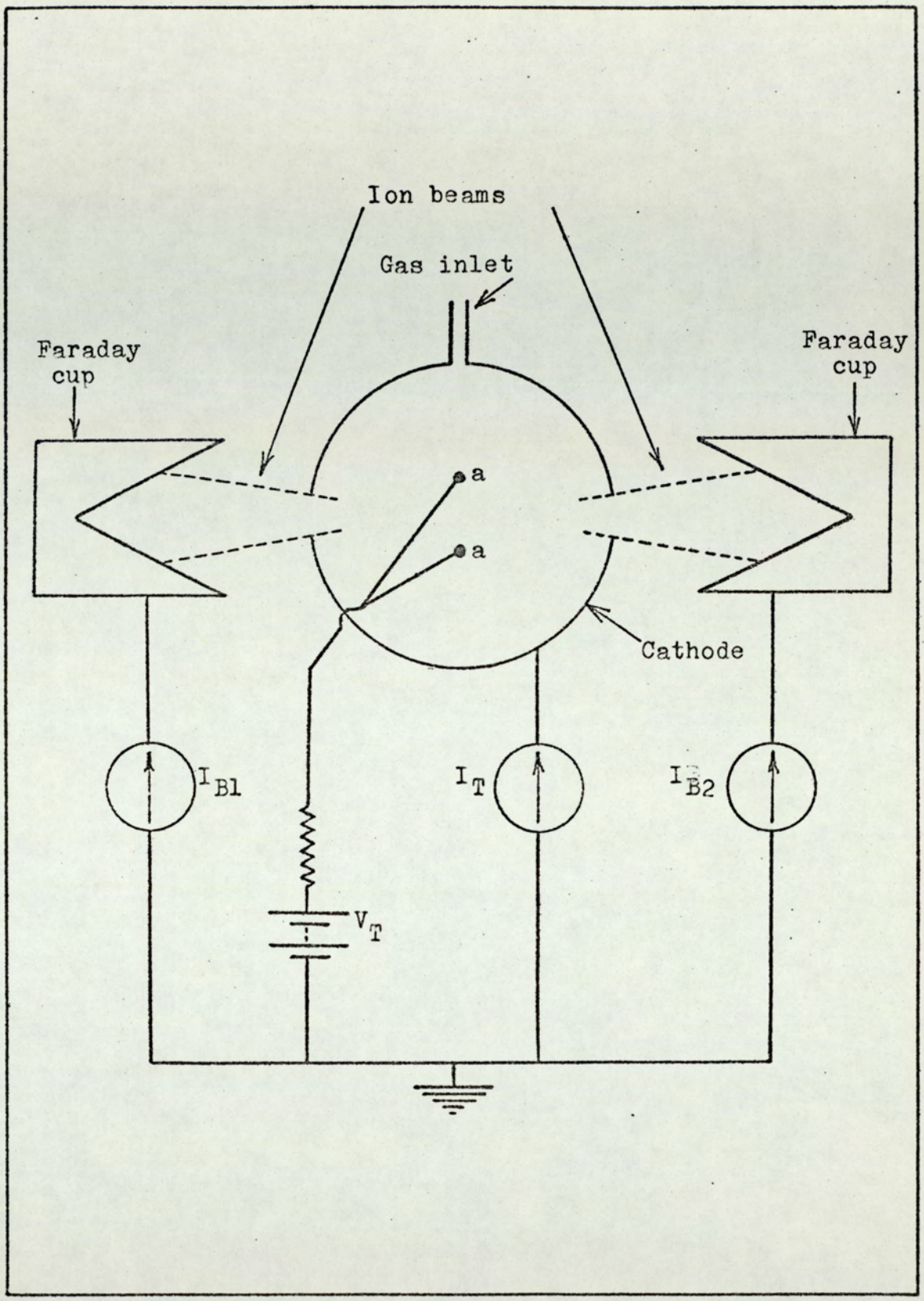

Figure 5.11 The electrical circuit of the double-beam ion source.

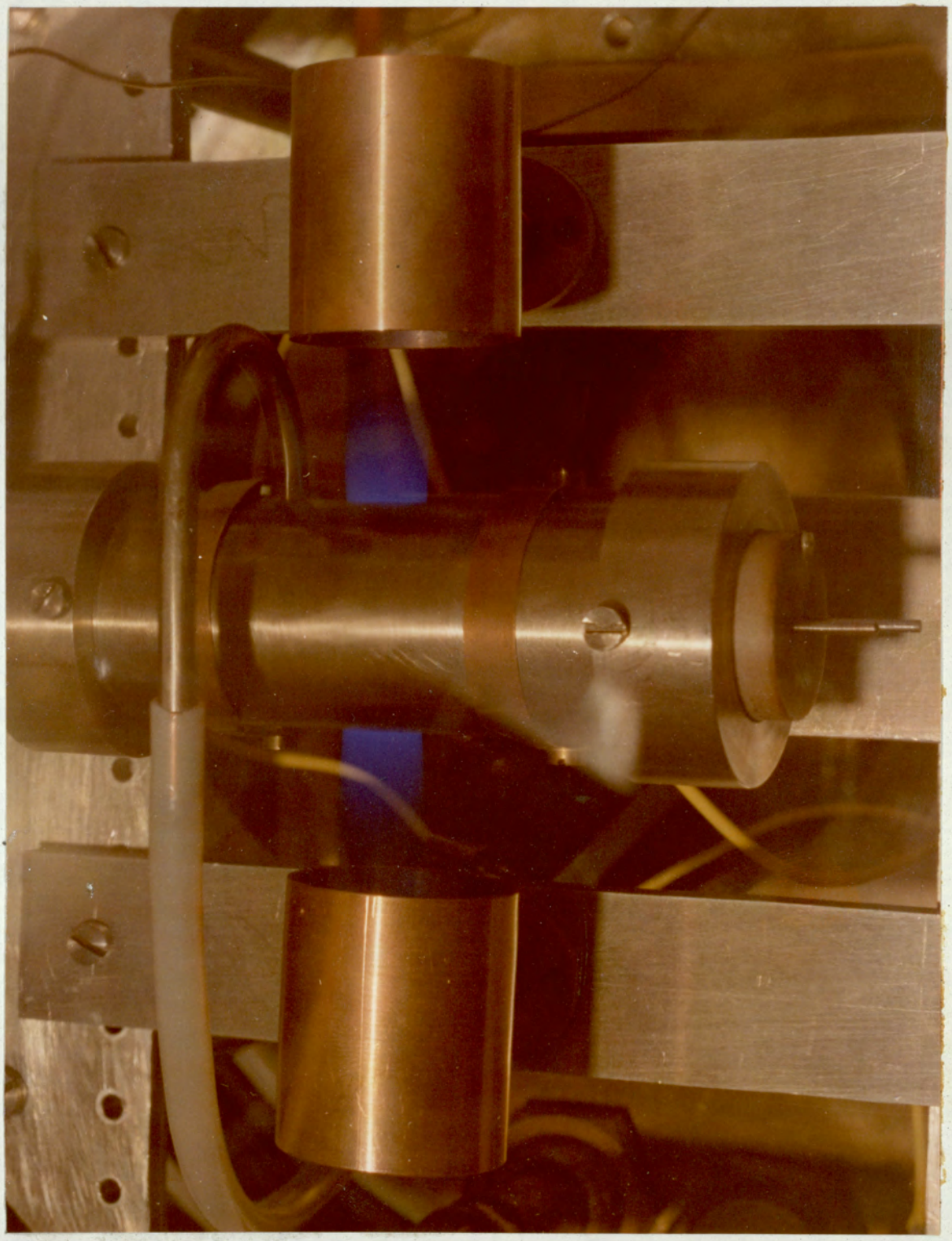

Figure 5.12 A photograph showing two beams of the double-beam ion source.

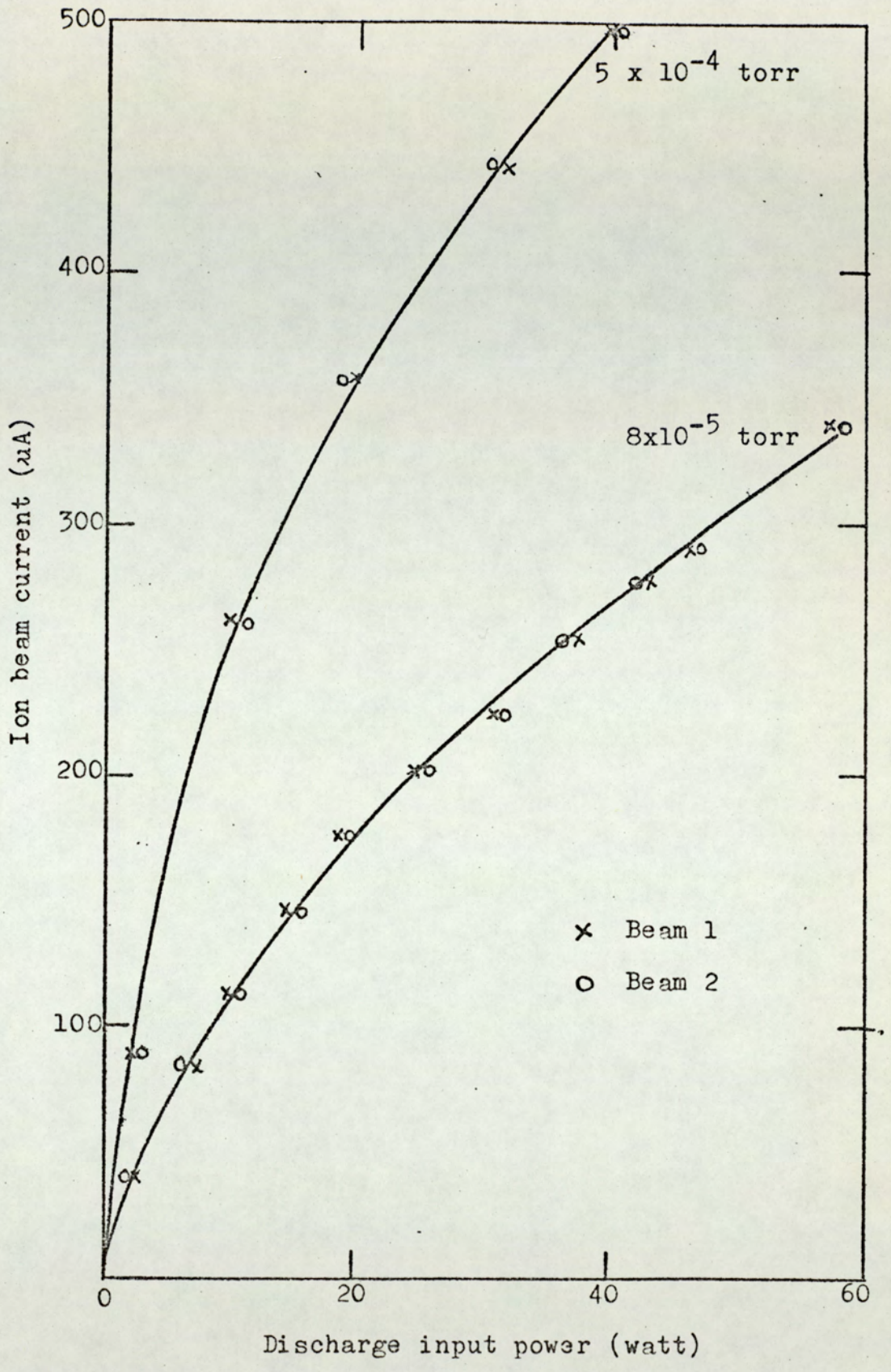

Figure 5.13 The relation between the discharge input power and the ion beam current of the double-beam ion source.

each beam. The ion beam density at a pressure of 5×10^{-4} torr and an input power of 40 watt is approximately $1.5 mA/cm^2$ at the ion exit aperture.

5.9. The operational modes.

In this section investigations of the pressure dependent operational modes and the tube current operational modes are described.

5.9.1. Pressure dependent operational modes.

In order to investigate the changes in the operation of the electrostatic oscillator as a function of the pressure, the tube current and the beam current were recorded over a wide range of the pressure. Fig. (5.14) shows the relation between I_B, V_T and the pressure for I_T equal to 4 mA when a 5 mm. circular ion exit aperture was used.

The curves of I_B and V_T show some well defined regions. In the region, ab, the ion current remains constant while V_T drops rapidly. In the region, bed, I_B increases rapidly and eventually a peak is reached at, cd, while V_T drops rapidly but stays nearly constant at the peak of I_B. This is the most efficient operating region. After the peak, cd, is reached, I_B and V_T decrease rapidly in the region, de, and then remain nearly constant in the region, ef. In the region, fgh, I_B and V_T drop quickly before they stay almost constant and the colour of the discharge changes to a pinkish colour. In the region, fgh, the source is the least efficient and the discharge is characterized by a very

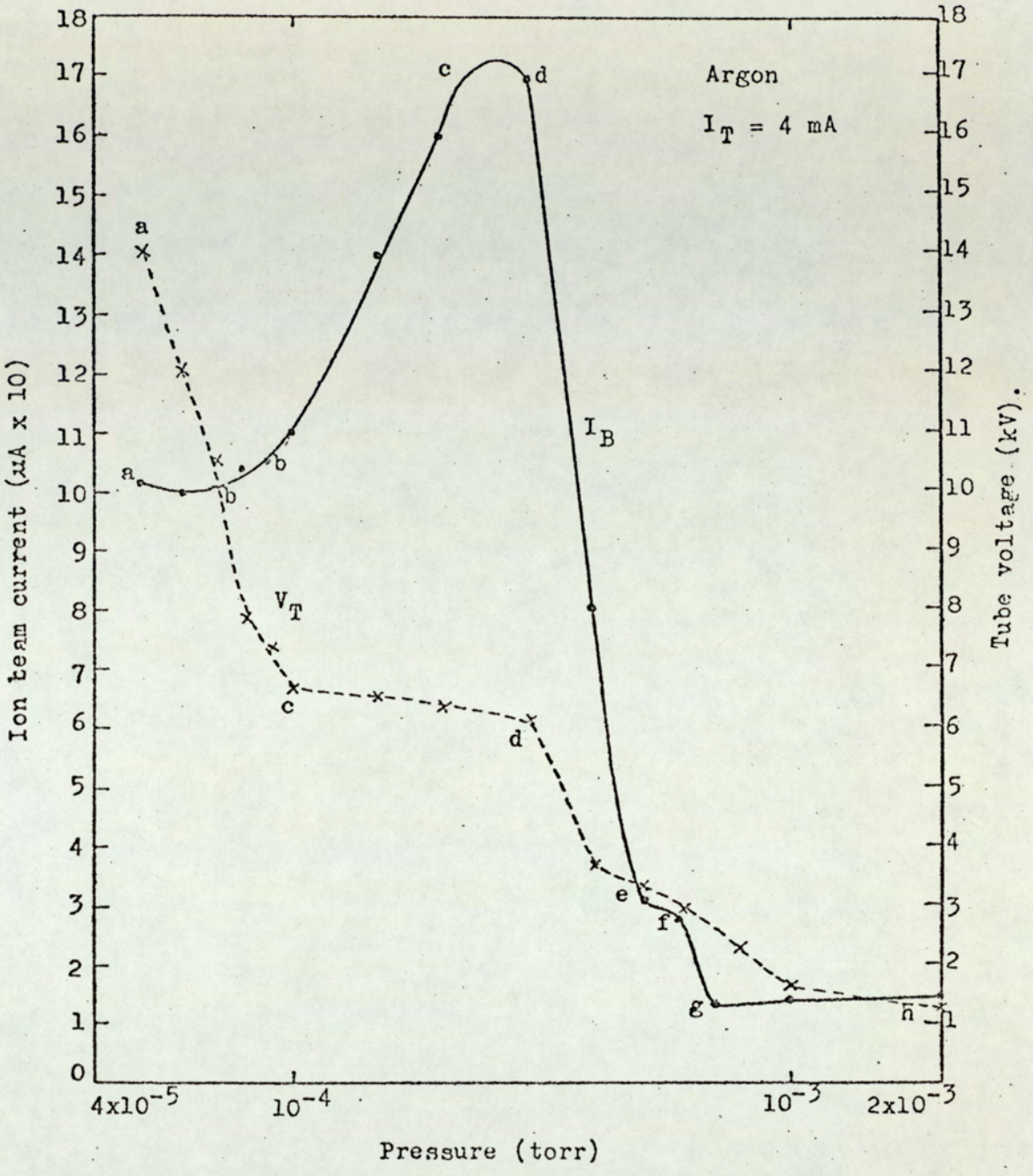

Figure 5.14 The relation between the pressure, the ion beam current and the tube voltage for an ion exit aperture of 5 mm diameter and a tube current of 4 mA.

low operating voltage and high tube current.

Figs. (5.15), (5.16) and (5.17) show the relation between I_B, V_T, and the pressure for a source with 3.2 x 10 mm. ion exit aperture for tube currents of 2, 4 and 6 mA respectively. They show the same trends as in the previous case. The different regions of the curves occur at different pressure because the pressure inside the source is different.

To get some understanding of the above curves, etching of thin copper films evaporated on glass slides was carried out at the different regions shown in Fig. (5.14). Fig. (5.18) shows the etched patterns when the source was operating in the different regions of the curves in Fig. (5.14). Copper films of the same thickness were used but the etching time was prolonged in the case of Figs. (5.18 b and c) to get reasonable etching in order to distinguish the different etched region.

Fig. (5.18.a) shows the etched patterns of the ion beam when the source was operating in the pressure range 4×10^{-5} to 3×10^{-4} torr, i.e. in the region, a b c d. Two distinct regions were observed; a central line in the Y-direction which is completely etched and a partially etched region of elliptical shape. The elliptical shape of the beam spot shows that the beam is divergent in the X-direction to a higher extent than in the Y-direction. The central line in the beam has small divergence (about 4°) comparing with that of the outer part of the beam. Since the etching is not uniform, the

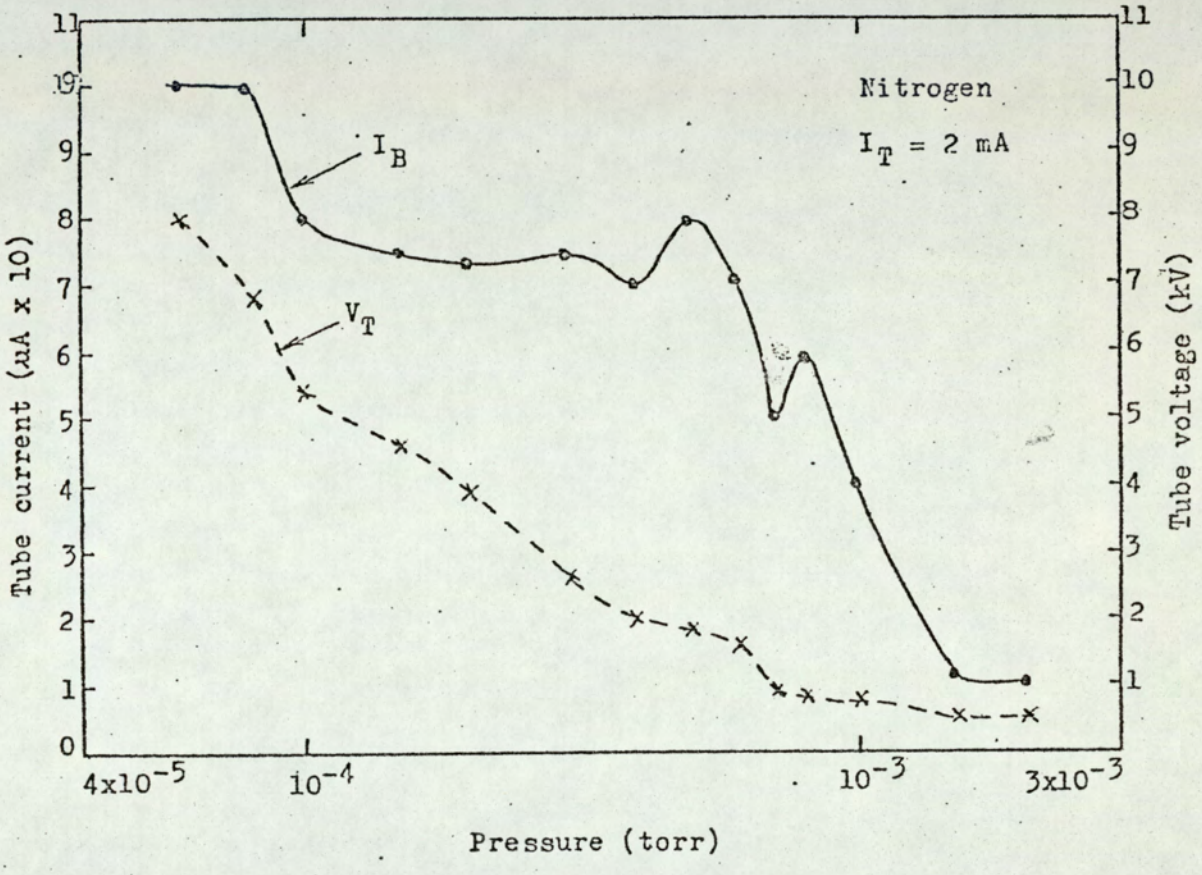

Figure 5.15 The relation between the pressure, the ion beam current and the tube voltage of an ion exit aperture of 3.2 x 10 mm.

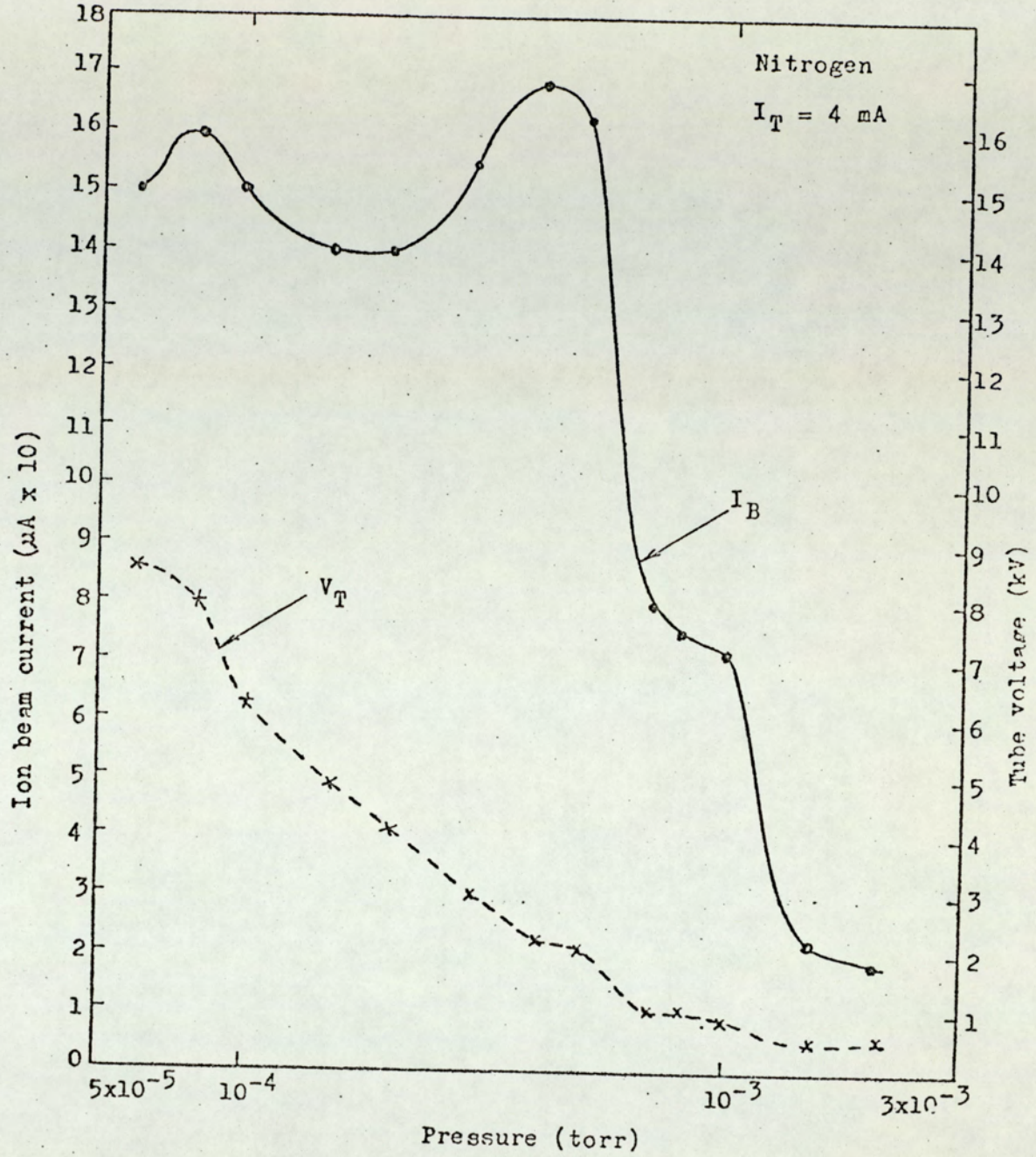

Figure 5.16 The relation between the pressure, the ion beam current and the tube voltage for an ion exit aperture of 3.2 x 10 mm.

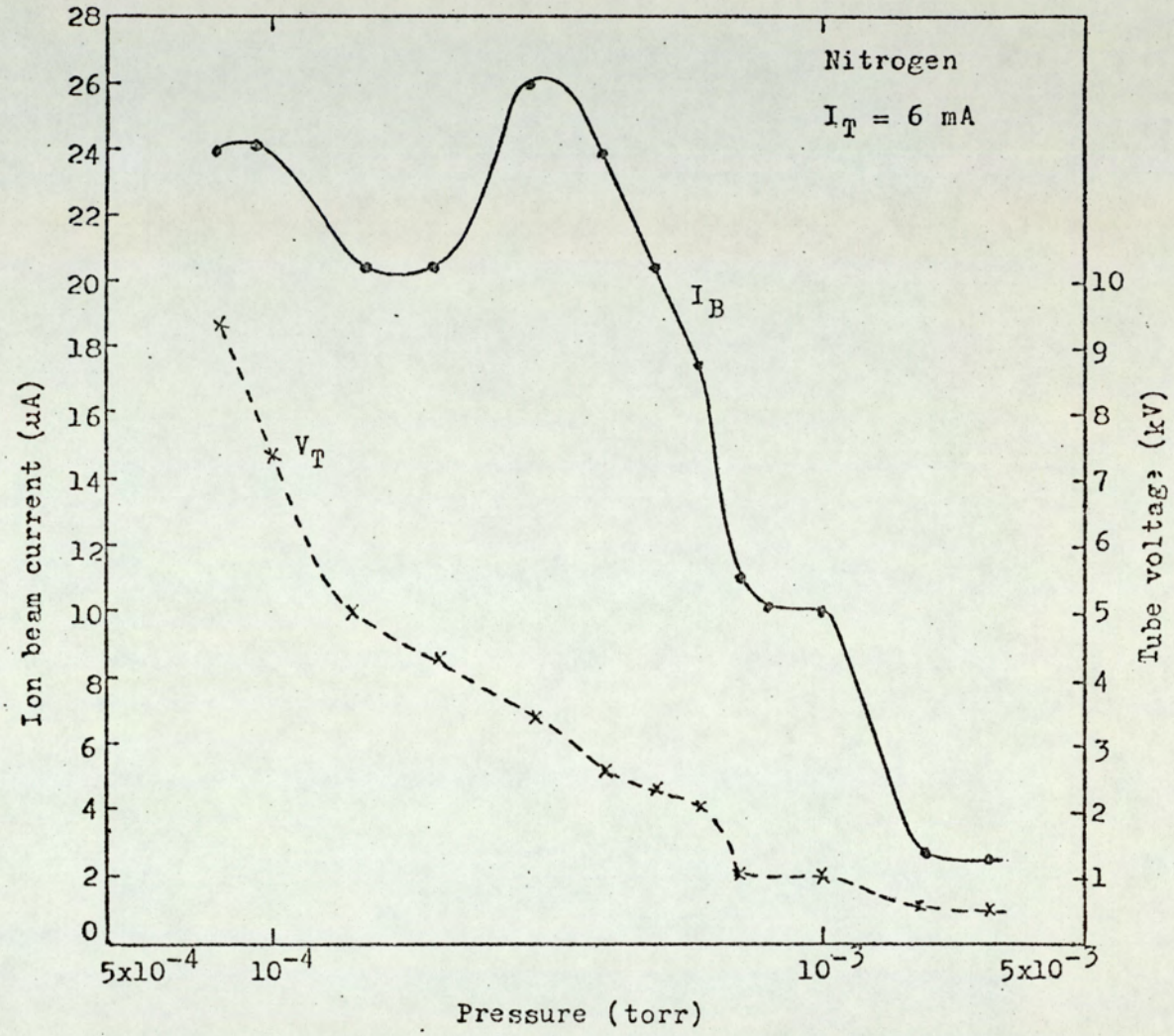

Figure 5.17 The relation between the pressure, the ion beam current and the tube voltage for an ion exit aperture of 3.2 x 10 mm.

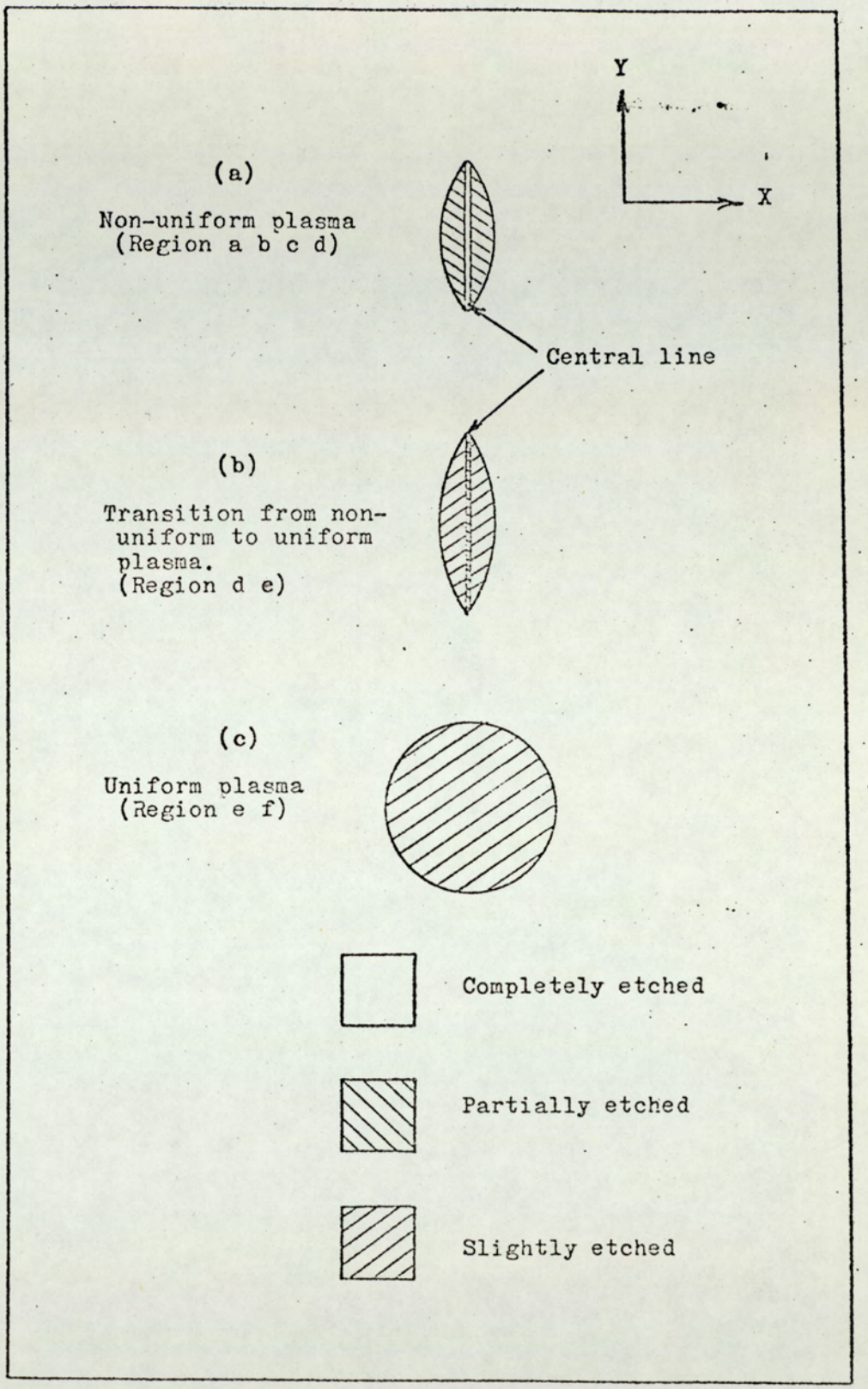

Figure 5.18 Diagrammatic representation of a copper film etched by ions for different operational modes of the oscillator.

plasma is also non-uniform and thus this mode of operation is called, "the non-uniform plasma mode".

Fig. (5.18.b) shows the etched patterns in the pressure range 3.4×10^{-4} torr (region de). It was noticed the shape of the beam is the same as in the non-uniform plasma mode, except that it was slightly elongated in the Y-direction and more elongated in the X-direction. The central line became thinner and fainter and a more uniform etching was obtained. Therefore this mode of operation is called "the transition mode" from "the non-uniform plasma mode" to the next mode. This mode is also characterized by lower ion density and operating tube voltage than those of "the non-uniform plasma mode".

Fig. (5.18.c) shows the etched pattern when the source was operating in the pressure range of 4×10^{-4} to 6×10^{-4} torr (region ef). Only one uniform etched pattern was obtained of a circular shape of bigger radius than the radii of the ellipse in Fig. (5.18.a and b). This means that the beam was equally divergent in the X and Y directions. When the etching time was increased a well uniformly etched circular spot was obtained and for this reason this mode of operation is called "the uniform plasma mode". This mode is also characterized by constant V_T and lower current density than the two modes previously discussed.

In the region, fgh, i.e. the high pressure region, I_B and V_T are very low and remain almost constant and the discharge colour changes to pink. It was also noticed

that the discharge fills the whole tube. This operational mode is a normal glow discharge mode. The figure suggests also that there is another transition mode from the uniform plasma mode to the glow discharge mode.

5.9.2. Current Dependent Modes.

From the previous figures (5.15, 5.16 and 5.17), it can be noticed that the transition mode and the uniform plasma mode depend also on the tube current. Therefore, another experiment was carried out in which the pressure was kept constant, while the tube current was varied and the ion current was recorded. The results are shown in Fig. (5.19) for three different pressures using an ion exit aperture of 3.2 x 10 mm. The ion current starts to increase with the tube current until it reaches the point b where there is a sharp decrease in the ion current. However, after it reaches the point c it starts to increase again with the tube current, but slower than in the region ab.

It can be seen that there are three operational modes. The above technique of etching copper films was used to distinguish these modes. In the region ab the etched pattern was identical to that shown in Fig. (5.18.a), i.e. the source was operating in "the non-uniform plasma mode", while in the region, cd, the etched pattern was similar to that shown in Fig. (5.18.c), i.e. the source was operating in "the uniform plasma mode". In the region bc, the discharge was hard to control, i.e. it was switching backward and forward from "the non-uniform plasma mode" to "the uniform plasma mode" and an

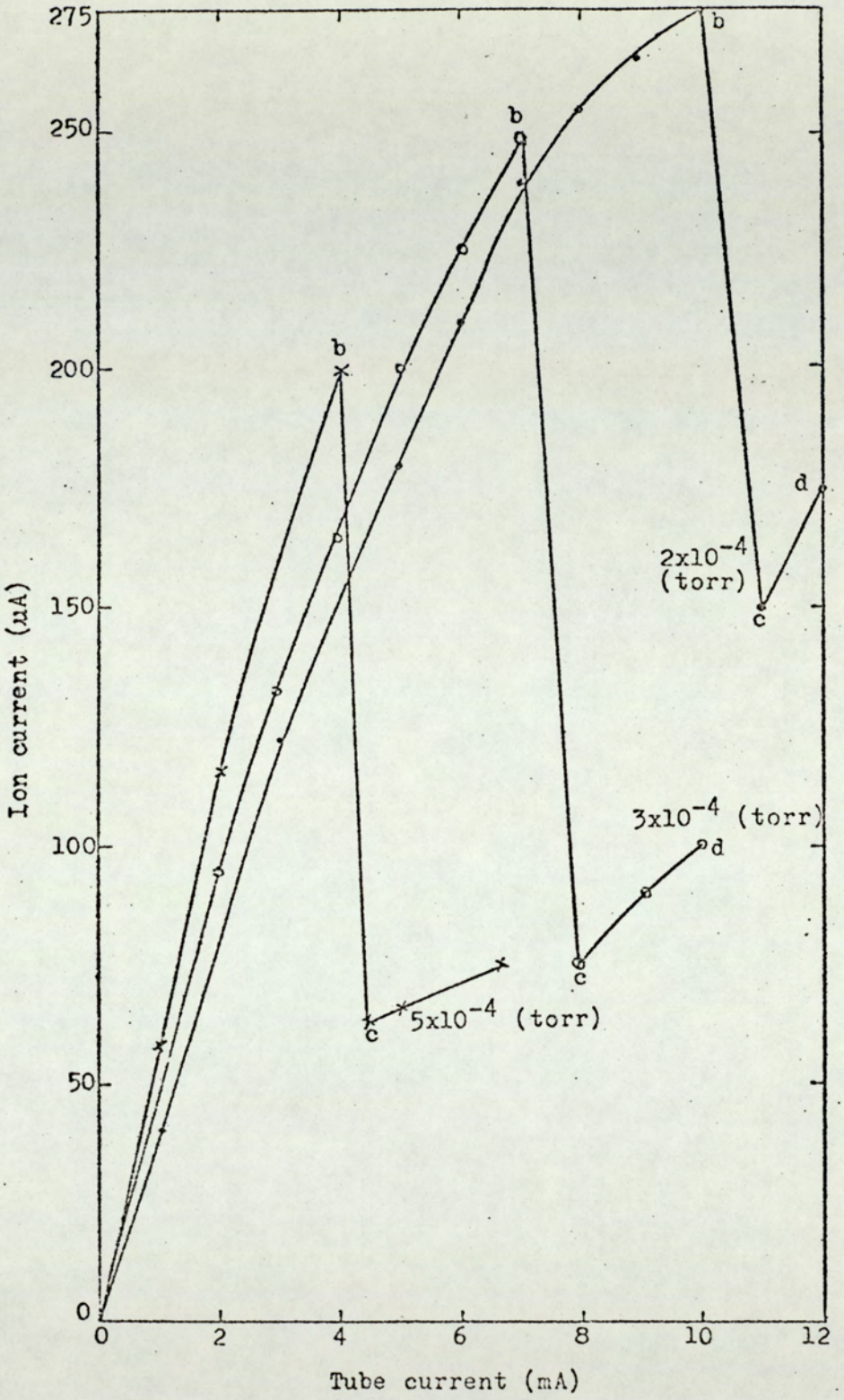

Figure 5.19 The relation between the ion beam current and the tube current at different pressures showing the tube-current dependent modes.

etched pattern could not be obtained. However, it is assumed that it is a transition mode.

5.10. Discussions.

It seems that the ion exit aperture disturbs the electric field as shown by the fact that the ratio I_T/V_T for constant pressure was lower when using a bigger aperture or two apertures. This is probably due to the distortion of the electric field in the vicinity of the aperture Fitch and Rushton (1972), and Piggs and McIlraith (1973) such that the equipotentials bulge through the aperture and deflect the electrons from their stable trajectories. The magnitude of this effect depends upon the shape and the size of the aperture. Some means of correcting this distortion are described in the next Chapter.

The deterioration of the source performance as a function of time has been investigated by Singh (1973) and Fitch et al (1974) and it is believed to be due to carbon deposit on the anode which perturbs the field near the anodes. One way of achieving stable operation is by water cooling of the anode. A new development of the source with water cooled anodes and cathode is described in Chapter 8.

Previous work on the single beam ion source by Fitch and Rushton (1972) had shown that with a 5.0 cm. diameter cathode a discharge could not be obtained if the ion exit aperture was greater than 4 mm. in diameter. This effect was not observed in the present work in spite of using a bigger aperture or even two bigger apertures

for the production of a double beam. It is thought that this is because in the present work the gas is admitted directly into the source which produces a pressure differential between the source and the experimental chamber. This was not the case in the original device where the source and the chamber were at the same gas pressure. This will also account for the fact that higher tube currents at lower tube voltages than those reported by Thatcher (1971) and Rushton (1972).

The fact that higher ion current density was obtained than that reported earlier by Rushton and Fitch (1971) when they used 5.0 cm. diameter cathode may be explained with the aid of Fig. (5.20). It can be seen from the figure that keeping the anode separation constant using a cathode with small diameter seems to confine the discharge and hence produces higher ion densities.

In the present ion source, the cathode is used as the ion collector and thus the change in the operational mode of the discharge may be explained with the help of the probe theories at low and high pressures as discussed by Swift and Schwar (1970). Fig. (5.21) gives a representation of the shapes of the discharge as observed in the present investigation and also by observing the various etched patterns produced in the cathode, using the source in different operating modes.

In the non-uniform plasma mode, the electron mean free path, λ_e, is much greater than both the cathode radius, R, and the cathode length, that is:

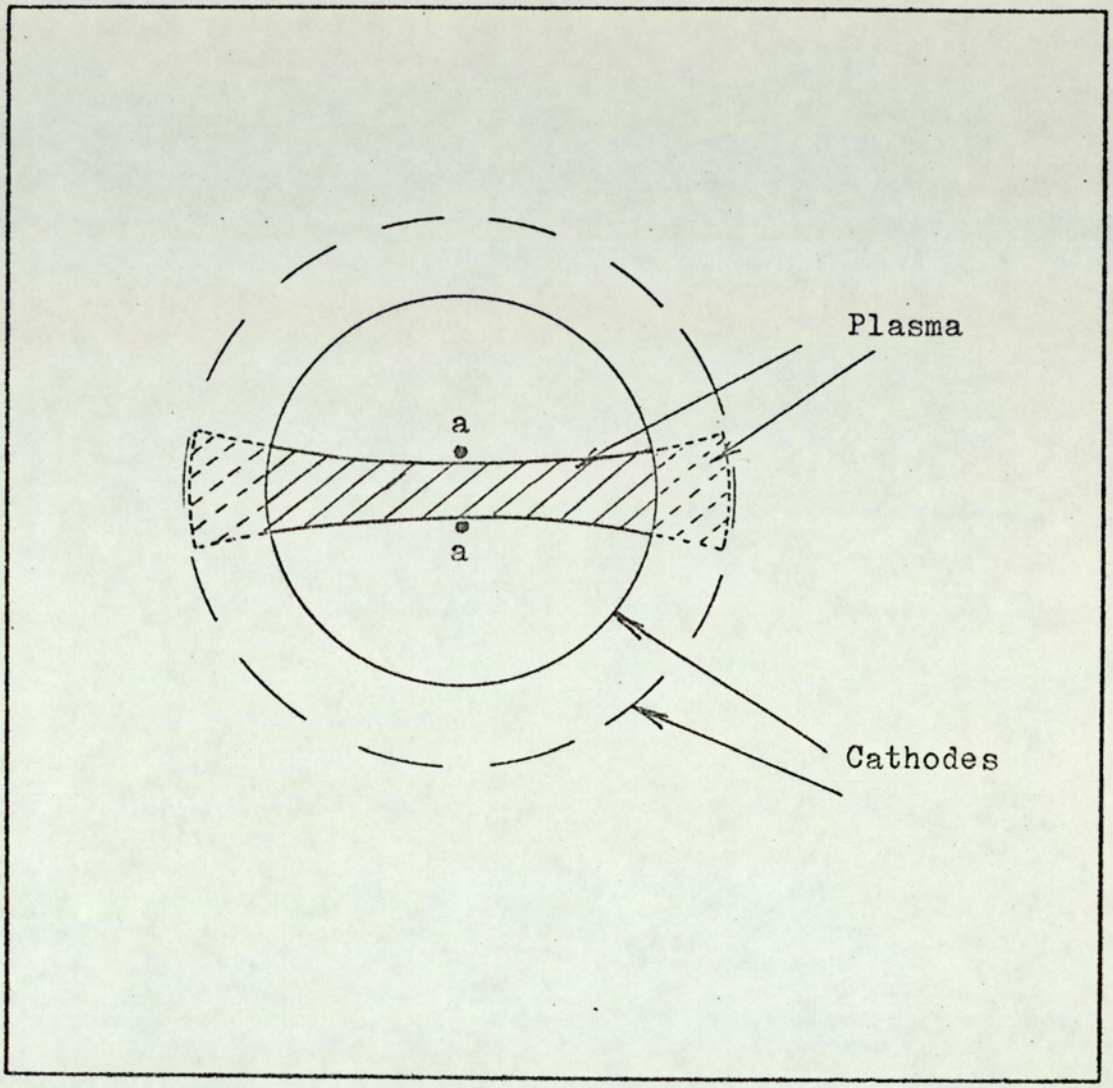

Figure 5.20 Schematic representation showing the confinement of the discharge for a smaller diameter cathode tube.

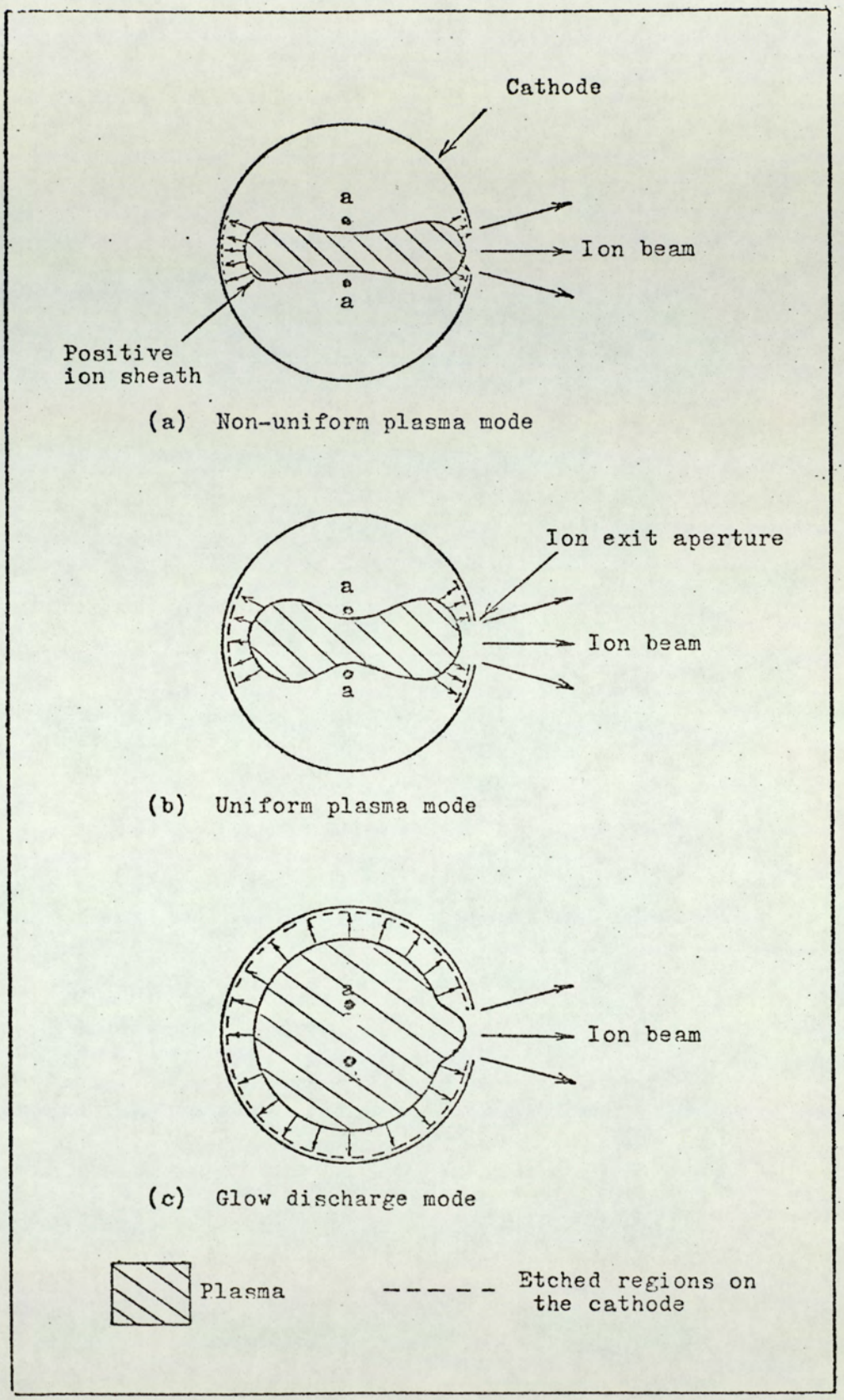

Figure 5.21 The shape of the discharge in various operational modes.

$$R \ll \lambda_e \gg L$$

Thus a confined collisionless plasma is formed between the two anodes and a thin ion sheath is created close to the cathode. The ions leave the sheath with free fall to the cathode according to Langmuir's space-charge theory producing an etched band parallel to the anode, Fig. (5.21.a). The intense central line is probably due to the high stability of the electron trajectories in that region.

In the non-uniform plasma mode when,

$$R \lesssim \lambda_e \lesssim L$$

some ion-neutral collisions occur and the diffusion laws may be applied, which results in a change of the charged particle density distribution. Consequently, there will be plasma depletion and the etched region on the cathode broadens out as can be seen in Fig. (5.21.b). The change in the mode from the non-uniform to the uniform plasma takes place through a transition region.

In the glow discharge mode, λ_e is much less than any characteristic length of the plasma,

$$R \gg \lambda_e \ll L$$

and ion neutral collisions will be dominant giving more plasma depletion. The motion of charged particles is then described by the collision dominant process of diffusion and mobility (von Pahl, 1957). As a result of this the charged particle density starts to fill the

whole tube as shown in Fig. (5.21.c). It seems that the discharge goes through a transition region before it changes from the uniform plasma mode to the glow discharge mode takes place through another transition mode.

The tube current, I_T, is equal to the ion current I_i, reaching the cathode plus the secondary electrons emitted, that is (assuming mono-energetic ions):

$$I_T = I_i + \gamma I_i$$

where γ is the secondary electron coefficient of ions when they bombard the cathode. In order to calculate the current density, then I_T must be divided by the etched area on the cathode. Now, since this area is less when the discharge is in the non-uniform plasma mode, this explains why the current efficiency I_B/I_T is a maximum in this mode and that of the uniform plasma mode is higher than that of the glow discharge mode.

The peaks in the pressure - ion current curves are probably due to multicharged ions as observed by Boumann et al (1972) in a Penning ion source. This has been investigated and the results are reported in Chapter 8.

The change in the modes with the tube current (and tube voltage) is not clearly understood.

The uniform plasma mode and probably the transition mode should be useful when uniform etching of a specimen is required.

Since the double beam ion source produces two identical beams, it should be particularly useful for

studying comparative etching rates of different materials when it is essential to ion bombard both specimens under identical conditions. Furthermore, there should be no problem of sputtering material from one specimen onto the other as they are virtually shielded from each other on either side of the cathode. The source also can be used for thinning of two specimens at the same time. One other advantage is that one beam can be continuously monitored, while the other beam is being used. It is evident that more beams can be produced from one source by milling more apertures in the cathode. However, this will increase the field distortion and a higher tube voltage is required to sustain the discharge and also will increase the gas loading into the experimental chamber. The latter problem can be overcome by using high speed vacuum system.

6. PRODUCTION OF FOCUSED HIGH CURRENT ION BEAMS

6.1. Introduction.

It has been shown in the previous Chapter that the emerging ion beam from the electrostatic ion source is divergent with an angle of half-width of about 25^{o} (Rushton, 1972). This is undesirable in many applications as this forces the user to place his specimen very close to the source, which may cause damage to the specimen due to the thermal radiation from the source. In ion thinning of specimens for electron microscopy, a well directed beam of high intensity is required. In particle accelerator applications, it is necessary to use an ion beam with low divergence, so that the beam emittance is lower than the accelerator acceptance, otherwise the accelerator tends to reject some part of the beam. Therefore, production of high current with low divergence should have many advantages for various applications.

One of the other problems discussed earlier is the field distortion due to the ion exit aperture which tends to reduce the ratio I_T/V_T (mA/kV) as the aperture is increased to allow higher ion current to emerge from the source.

Therefore, it is logical to look for some means of correcting the field distortion from the ion exit aperture and to produce focussed ion beams of higher current density. In this Chapter, two systems to achieve these aims are described. The technique is based on

adding a focus electrode in front of the ion exit aperture and is biased negatively with respect to the cathode.

6.2. The first system.

6.2.1. Description of the system.

The ion source is the same as described before with 5 mm. diameter ion exit aperture. The focus electrode is 3.8 cm. long, 2.5 cm. in diameter and with a 5 mm. diameter limiting hole. The distance between the cathode and the focus electrode is 2 mm. A photograph which shows the arrangement is shown in Fig. (6.1) and the electrical circuit used is shown in Fig. (6.2).

6.2.2. The effect of the focus electrode voltage on the tube characteristics.

The effect of the focus electrode voltage, V_f, on the tube characteristics is shown in Fig. (6.3). These are the characteristics at chamber pressure of 2×10^{-5} and 6×10^{-5} torr and at V_f of 0, 0.5 and 1 kV. It can be seen that the discharge starts at lower values of V_T and this depends on V_f and the pressure. The higher the focus voltage, the lower is the starting voltage and this is more noticeable at lower pressure. Also, higher values of I_T were obtained for a constant value of V_T and this again was more effective at lower pressures. For example, at a pressure of 2×10^{-5} torr and V_T = 10 kV, I_T was equal to 0.5, 1 and 2 mA, when V_f was equal to 0, 0.5 and 1 kV respectively, i.e. I_T was increased to four times when V_f was increased from 0 to 1 kV at this particular pressure.

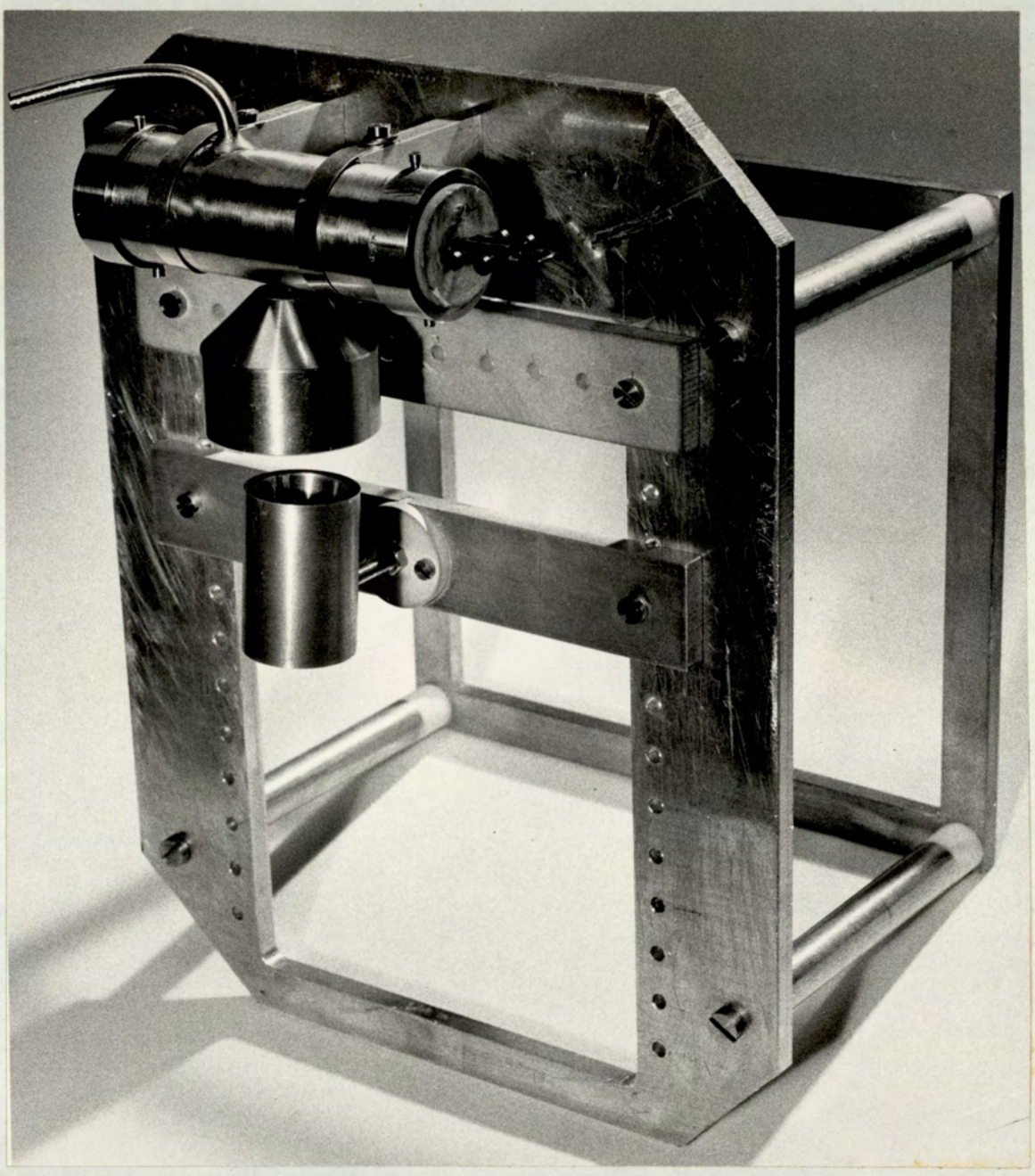

Figure 6.1 Photograph of the electrostatic ion source and the focusing electrode.

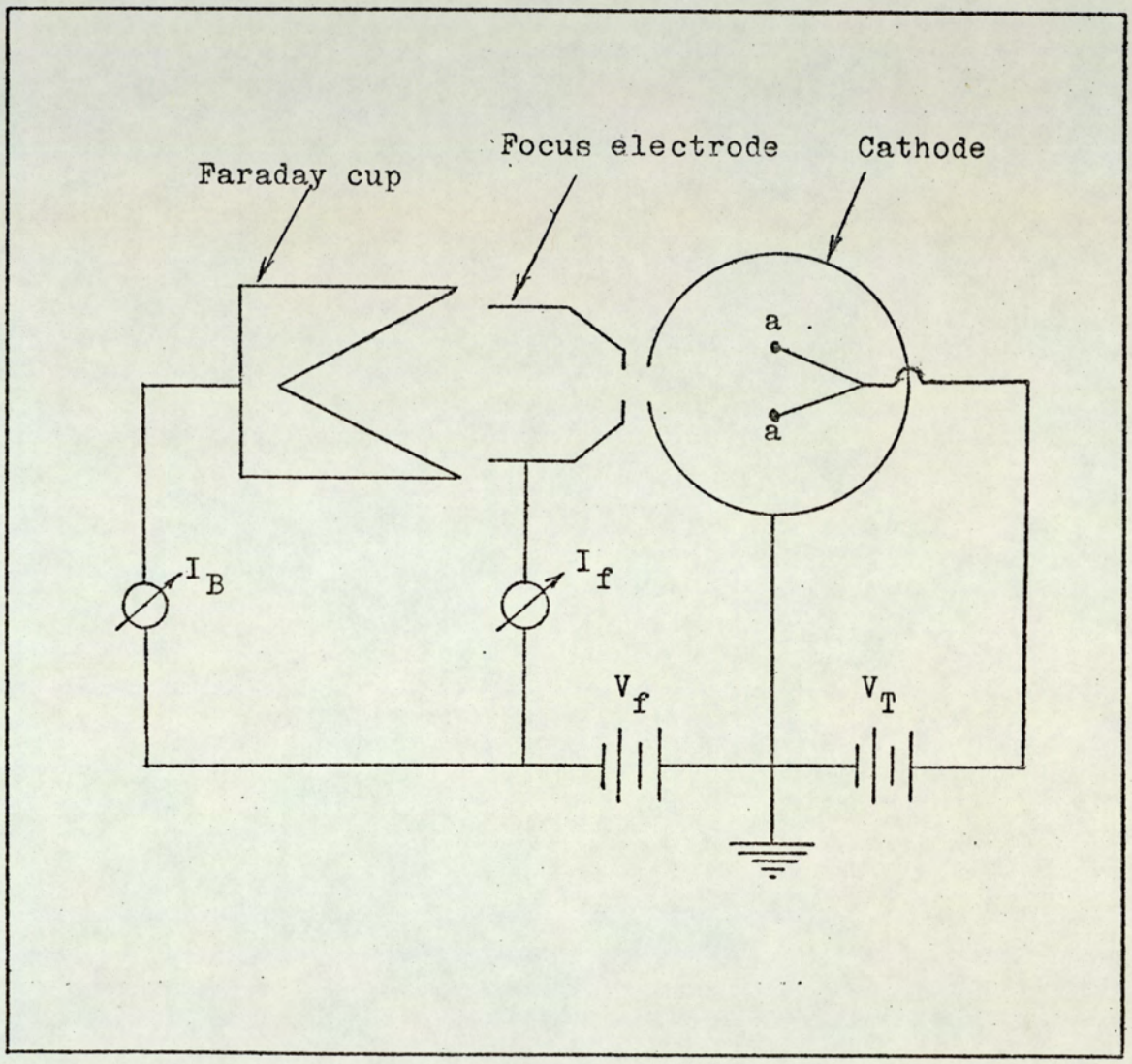

Figure 6.2 The electrical circuit of the focus electrode system.

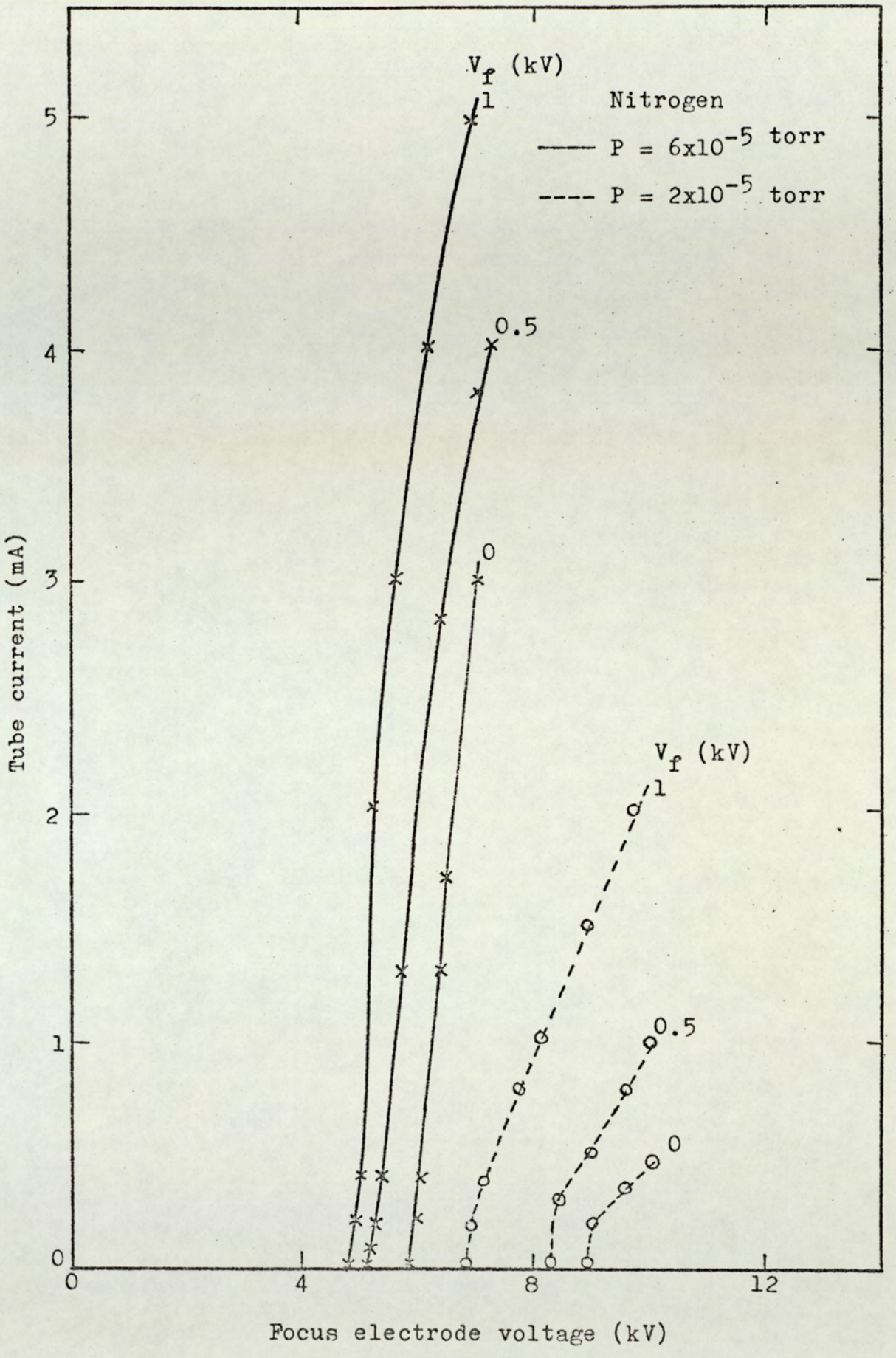

Figure 6.3 The tube characteristics at different focus-electrode voltage and pressures.

On the other hand at a pressure of 6×10^{-5} torr and $V_T = 6.8$ kV, I_T was equal to 3.4 and 5 mA, when V_f was equal to 0, 0.5 and 1 kV respectively, i.e. I_T was increased only by 70% when V_f was increased from 0 to 1 kV at this particular pressure. Moreover, it was noticed that the discharge was much more stable at low pressure than in the conventional source when $V_f = 0$.

The effect of higher values of V_f on I_T and V_T was also investigated. Fig. (6.4) shows the relation between V_f, I_T and V_T, when the pressure was 8×10^{-5} torr for helium. It can be seen that V_T dropped rapidly from 3.3 kV to 2.8 kV when V_f was increased from 0 to 0.2 kV and then it remained constant until V_f reached 1.2 kV. Also I_T was increased from 2 mA to 3.2 mA, by increasing V_T from 0 to 0.75 kV, then it remained constant until V_f reached 1.2 kV. When V_f was increased beyond 1.2 kV, I_T started to decrease and V_T increased. Eventually the discharge ceased at $V_F = 3.2$ kV.

However, it was possible to start the discharge again by raising V_T as shown in Fig. (6.5), which shows the tube characteristics for V_f equal to 3.5 and 5 kV. It can be seen that higher values of V_T were needed to start and sustain the discharge as V_f was increased. This is undesirable because of the increasing thermal load of the source.

6.2.3. The effect of the focus electrode voltage on the output ion beam current.

The variation of I_B and the ion current hitting the focus electrode, I_f with V_f is shown in Fig. (6.6). The

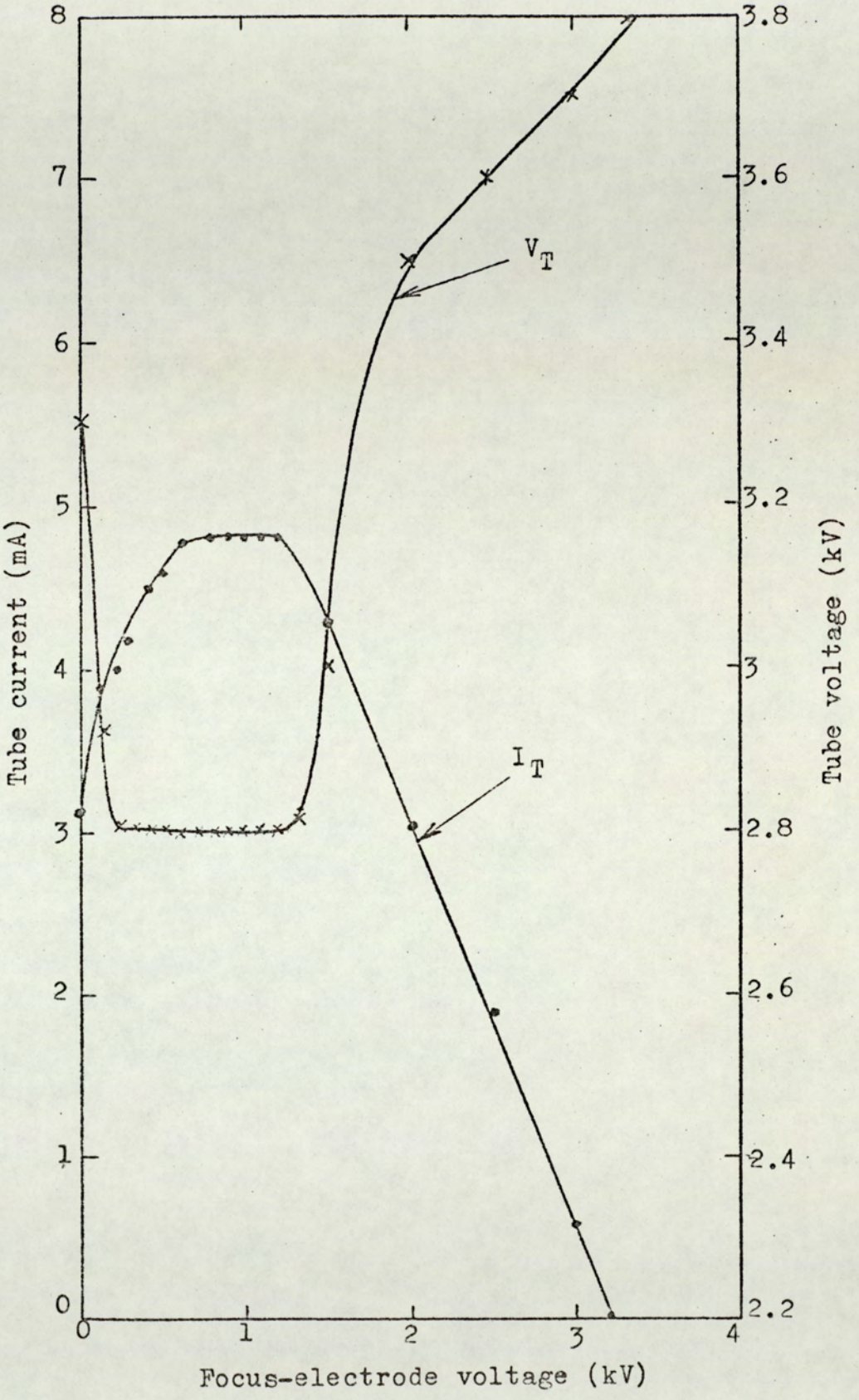

Figure 6.4 The effect of high focus electrode voltage on the tube current and voltage.

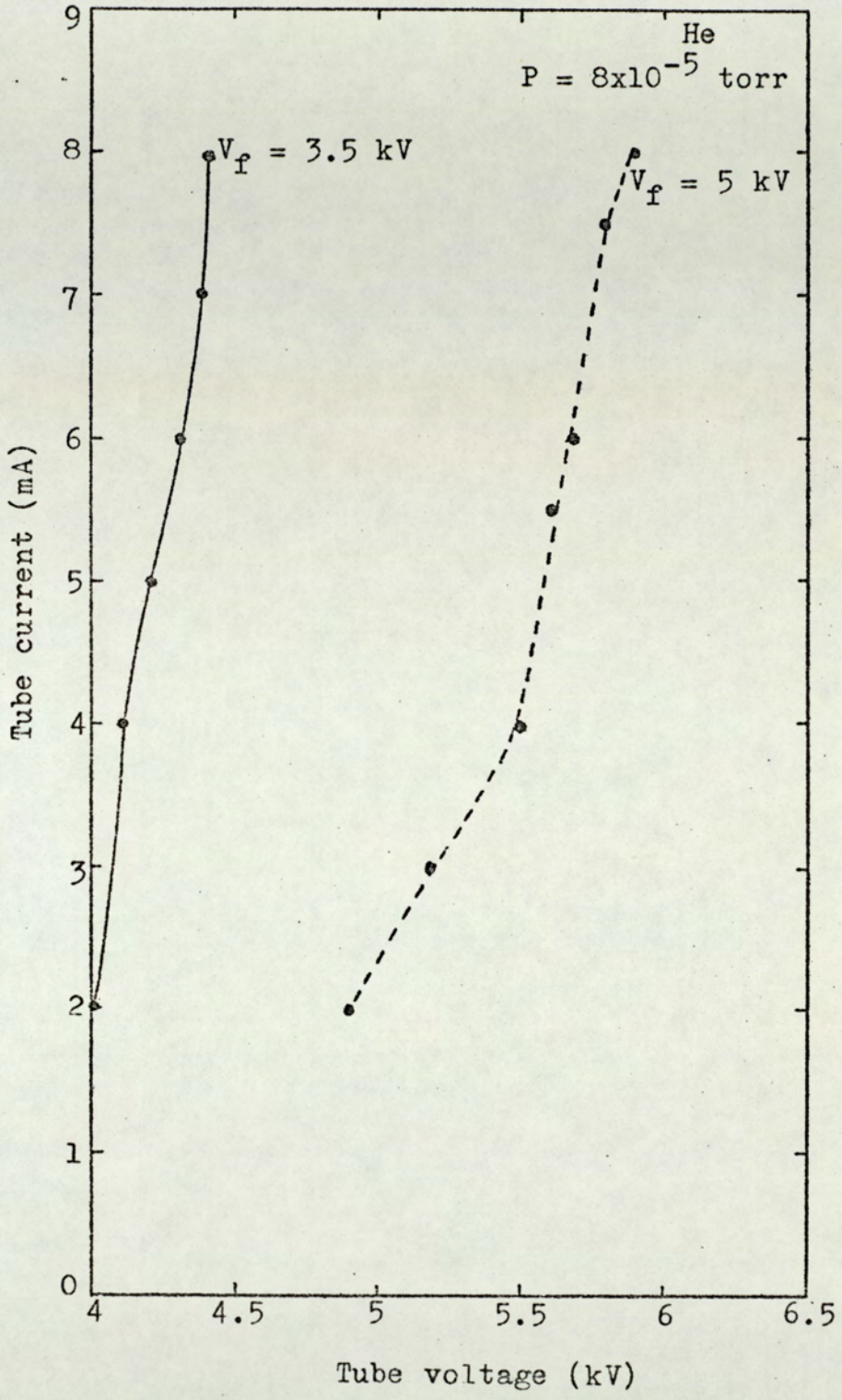

Figure 6.5 The tube characteristics at high focus-electrode voltages.

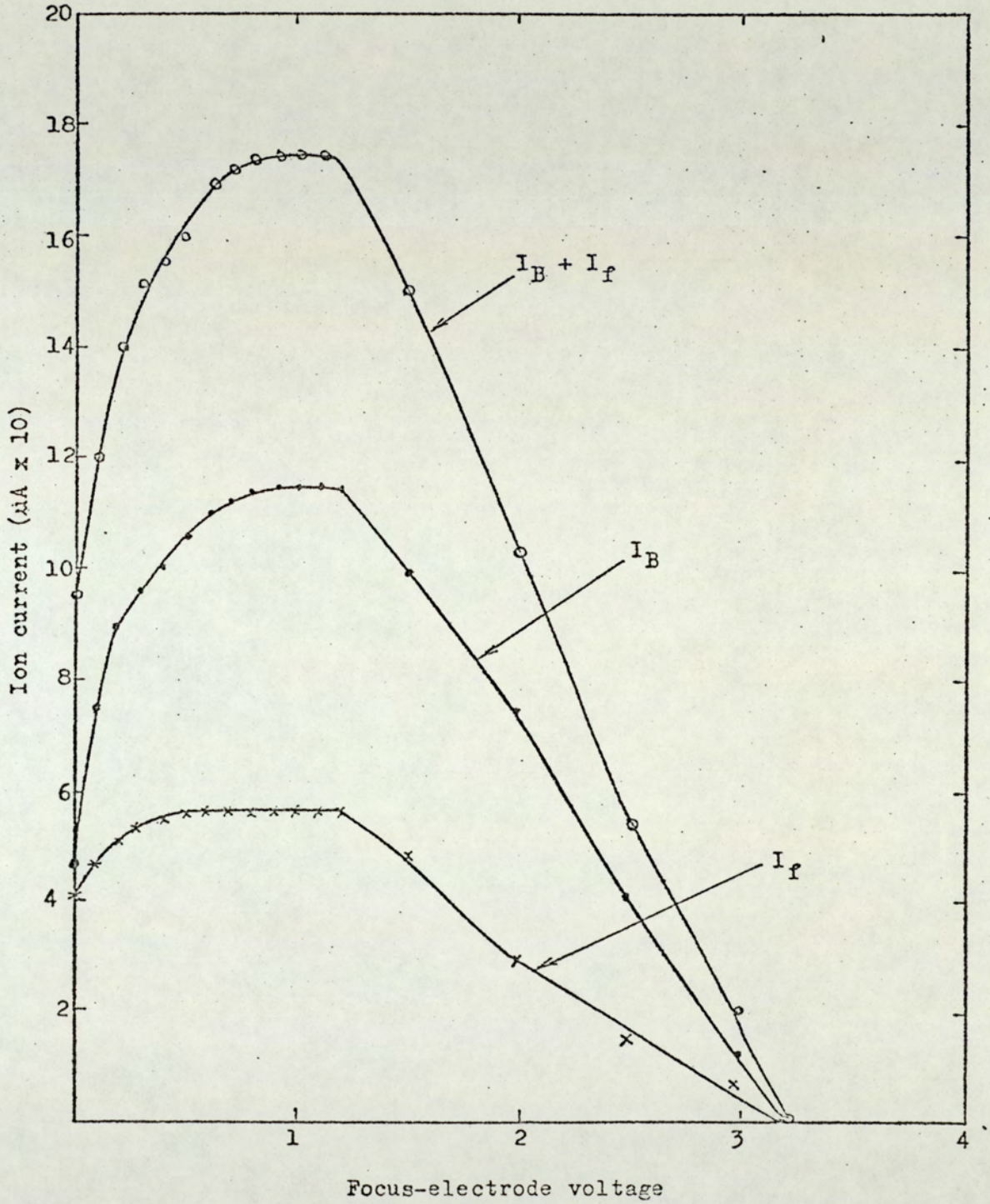

Figure 6.6. The effect of high focus-electrode voltage on the ion beam current and the focus electrode current.

corresponding changes in I_T and V_T were shown in Fig. (6.4). Since the beam was divergent, the outer part of the beam was hitting the focus electrode and therefore the total current emerging out of the source is the sum of I_B and I_F. The total current is also shown in Fig. (6.6). It can be seen that I_B and I_f were increased rapidly as V_f was increased from 0 to about 0.5 kV and then remained constant until V_f was equal to 1.2 kV before eventually decreasing to zero when the discharge ceased. It is then essential that when using this sytem that the value of V_f should not exceed 1.2 kV and that the focus electrode hole has to be increased to allow most of the ions to escape. The source current efficiency, defined as I_B/I_T was increased from 15 to 23 μA/mA when V_f was increased from 0 to 1.2 kV respectively and then it decreased as V_f was increased more and went to zero when V_f was equal to 3.2 kV. I_f was not taken into consideration.

The variation of I_B with I_T for values V_f = 0, 0.5 and 1 kV at a pressure of 8×10^{-5} torr is given in Fig. (6.7). I_B tends to increase more rapidly with I_T as V_f was changed from 0 to .5 kV and to 1 kV. It is clear that the source current efficiency was higher in the new source. Fig. (6.8) shows a photograph of four etched copper films at the same tube current of 5 mA, in which (A) and (B) were taken at a pressure of 6×10^{-5} torr (non-uniform plasma mode) and (C) and (D) at a pressure of 5×10^{-4} torr (uniform plasma mode). A and B are for a conventional source, and C and D are for the new source

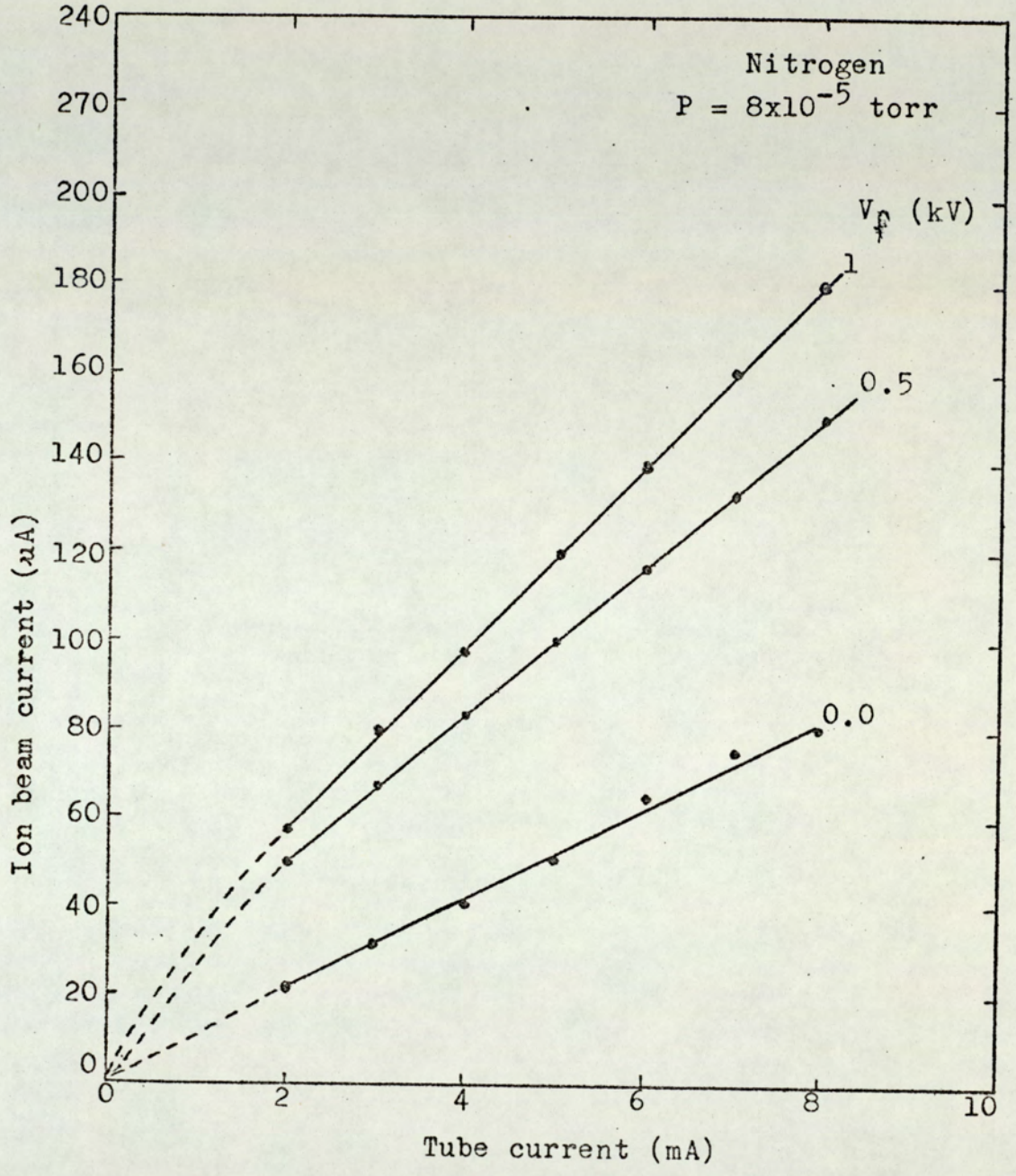

Figure 6.7 Relation between the tube current and ion beam current at different low focus-electrode voltages.

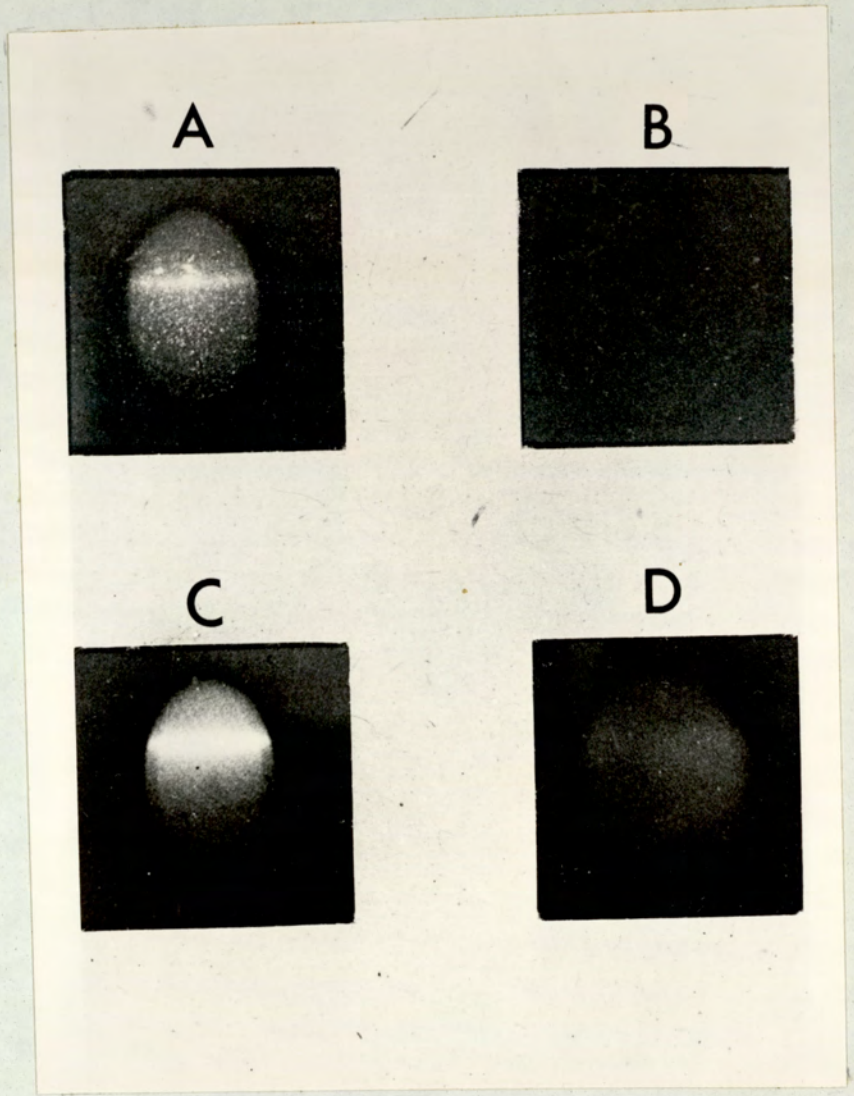

Figure 6.8 The etched pattern with and without focus-electrode in two operational modes of the discharge.

with V_f = 1 kV. The etching time was kept constant. It is clear that the etching rate was higher using the focusing electrode.

The variation of I_B and I_f with I_T for V_f values of 3.5 and 5 kV - i.e. in the region the discharge was ceased - is shown in Fig. (6.9). The corresponding values of V_T were shown in Fig. (6.5). It can be seen that much higher currents were obtained. It was also observed that the beam was well collimated which resulted in higher ion density beam and the ratio $\frac{I_f}{I_B}$ was reduced. The current efficiency was 37 and 46 μA/mA for V_f equal to 3.5 and 5 kV respectively, which is higher than when lower V_f values (0 to 1.2 KV) were used. However, V_T was much higher.

6.3. The second system.

6.3.1. Description of the system.

This sytem was designed to overcome the problem of the discharge disturbance caused by the field from the focus electrode when it was at high voltage. The tube dimensions were the same but the ion exit aperture of 5 mm. diameter was surrounded by a chimney welded into the cathode. The focus electrode was coupled to the chimney by an insulator to obtain a good alignment of the ion exit aperture and the hole in the focus electrode. The distance, d, between the ion exit aperture and the focus electrode was changed by changing the length of the insulator. A drawing of the new source and a photograph of it are shown in Figs. (6.10) and (6.11) respectively.

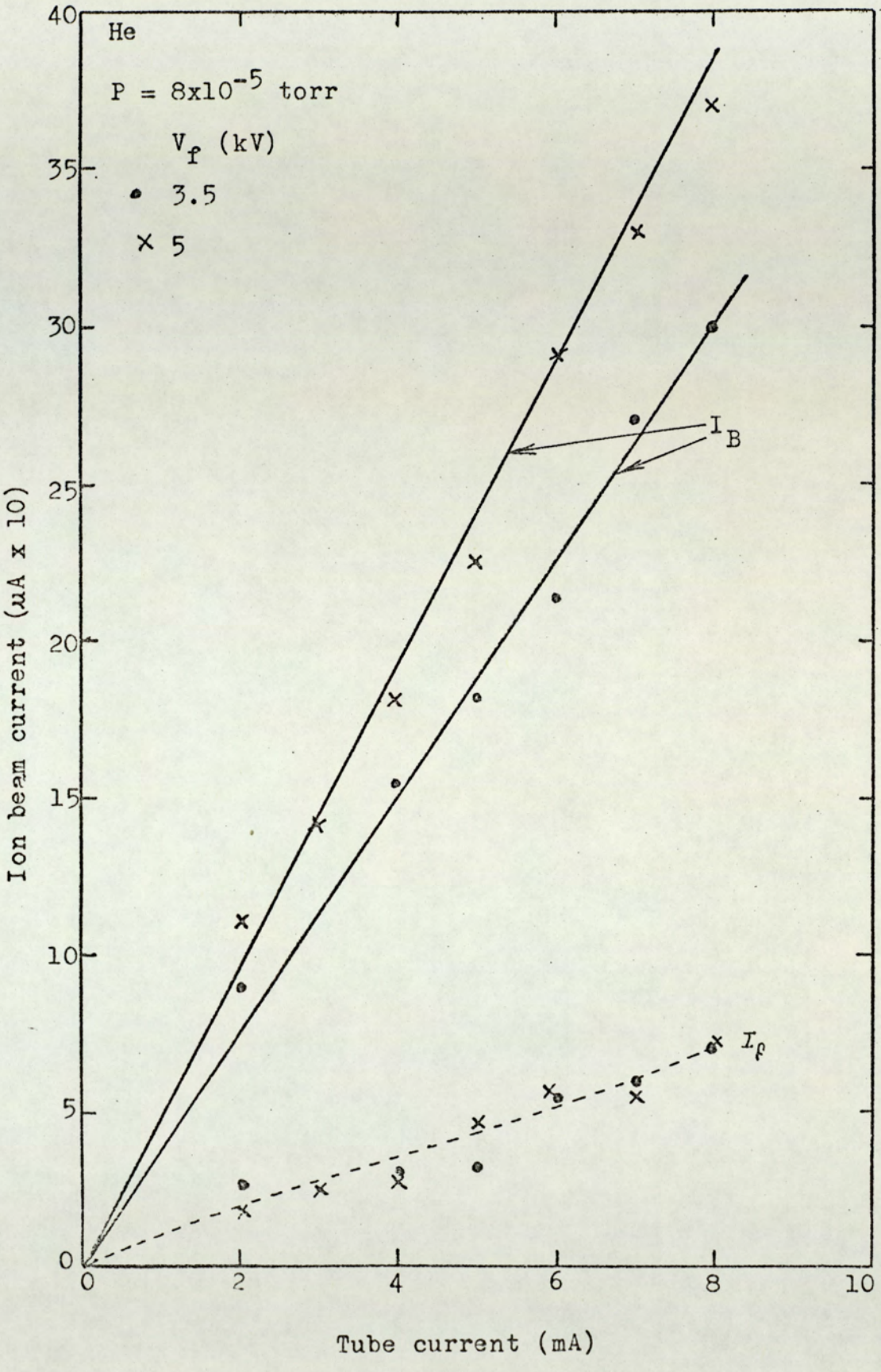

Figure 6.9 Relation between the tube current and ion beam current at high focus-electrode voltages.

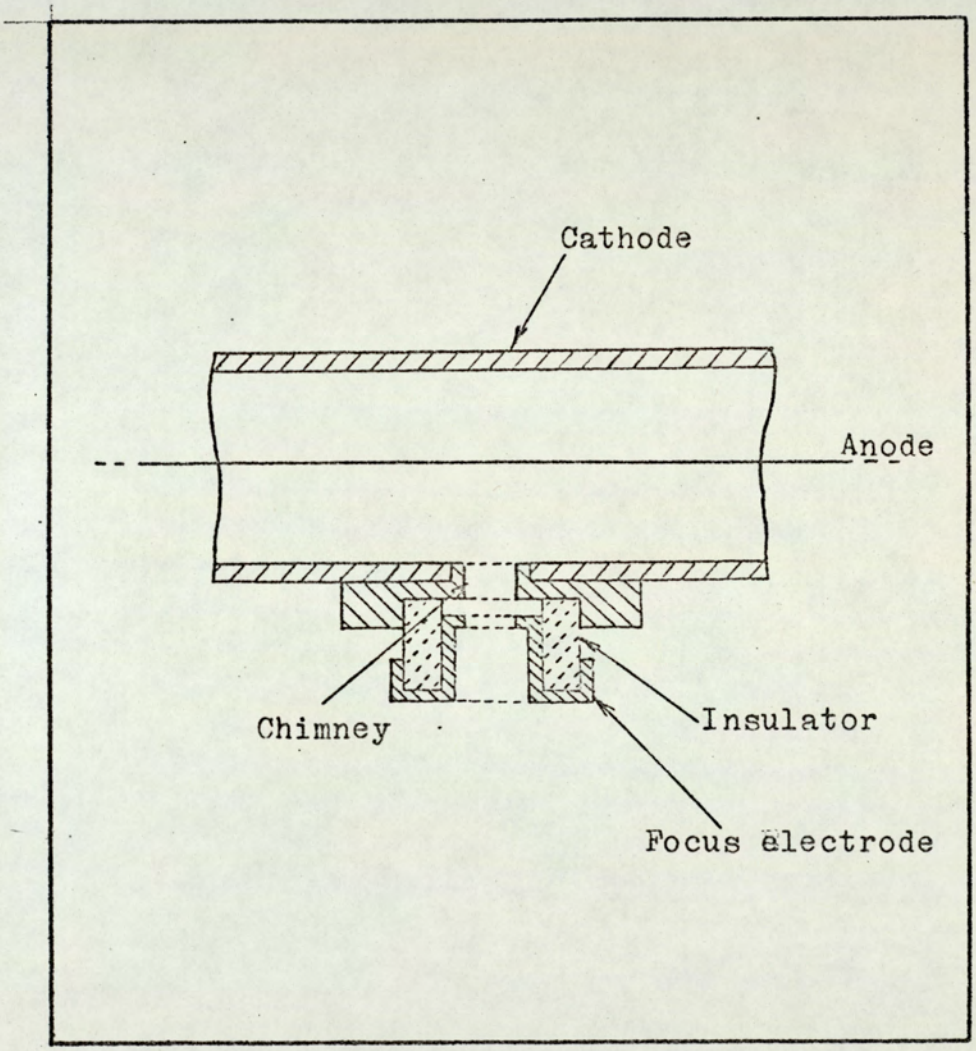

Figure 6.10 The electrostatic ion source with a modified focus-electrode.

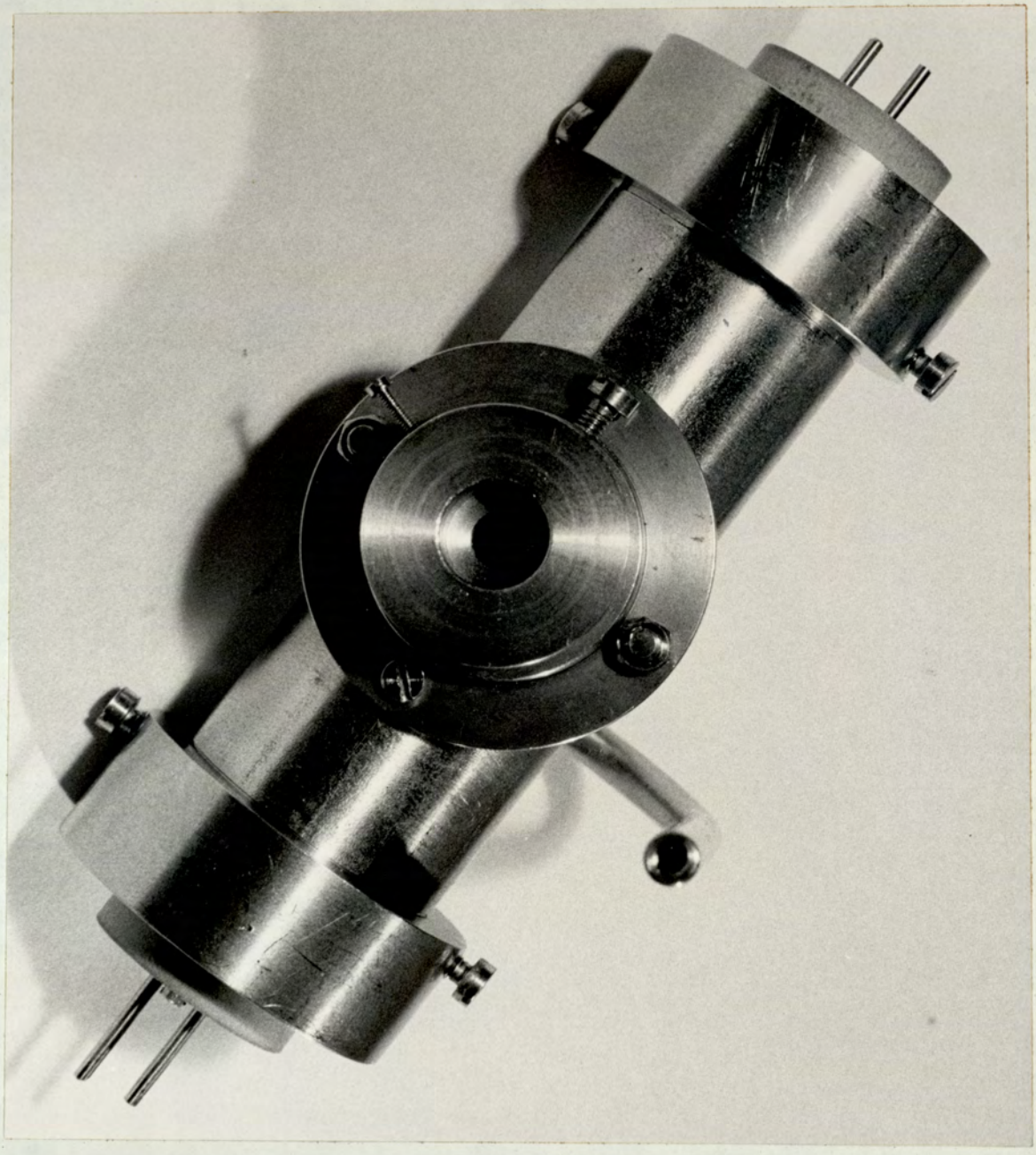

Figure 6.11 Ion source with a modified focus-electrode.

6.3.2. The effect of the new system on the tube characteristics.

It was noticed that the focus electrode voltage has only a slight effect on V_T and I_T, and the effect was only noticed at a very low pressure and high value of V_f (above 8 KV). However, there was a noticeable effect on the tube characteristics with the introduction of the chimney. Fig. (6.12) shows the tube characteristics of the conventional source and a source with a chimney ($V_f = 0$), at a pressure of 10^{-4} torr for argon. It can be seen that higher I_T values were obtained with the new system. For example, at V_T equal to 5 KV, I_T was equal to 3.5 and 7 mA for the conventional source and the new source respectively.

6.3.3. The ion current-focus electrode voltage characteristics.

These characteristics are the variation of I_B and I_f with V_f. A family of such curves for I_T of 2, 3, 4 and 5 mA at a pressure of 2×10^{-4} torr is shown in Fig. (6.13). The focus electrode had 5 mm. diameter hole and was placed 3.5 mm. away from the ion exit aperture. Another family of curves at the same experimental conditions, but at a pressure of 6×10^{-5} torr is shown in Fig. (6.14). As V_f was increased from 0 to 100 V, there was a sharp increase in both of I_B and I_f. After that I_f decreases with increasing V_f (due to focusing action) until it reached a constant value. On the other hand I_B increases continuously with increasing V_f. It can also be seen that I_f at a pressure of 6×10^{-5} torr is

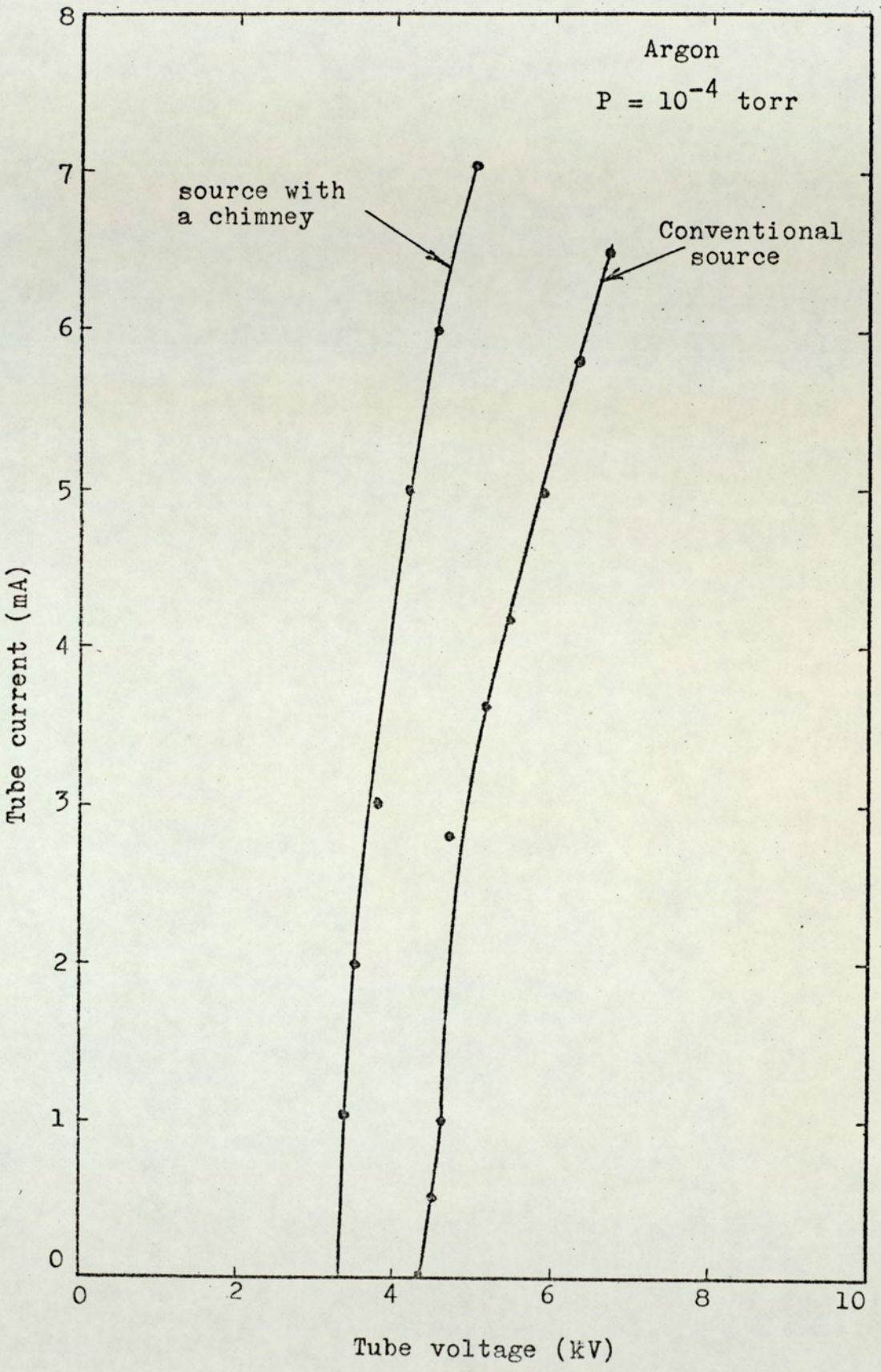

Figure 6.12 The tube characteristics of a conventional source and a source with a chimney.

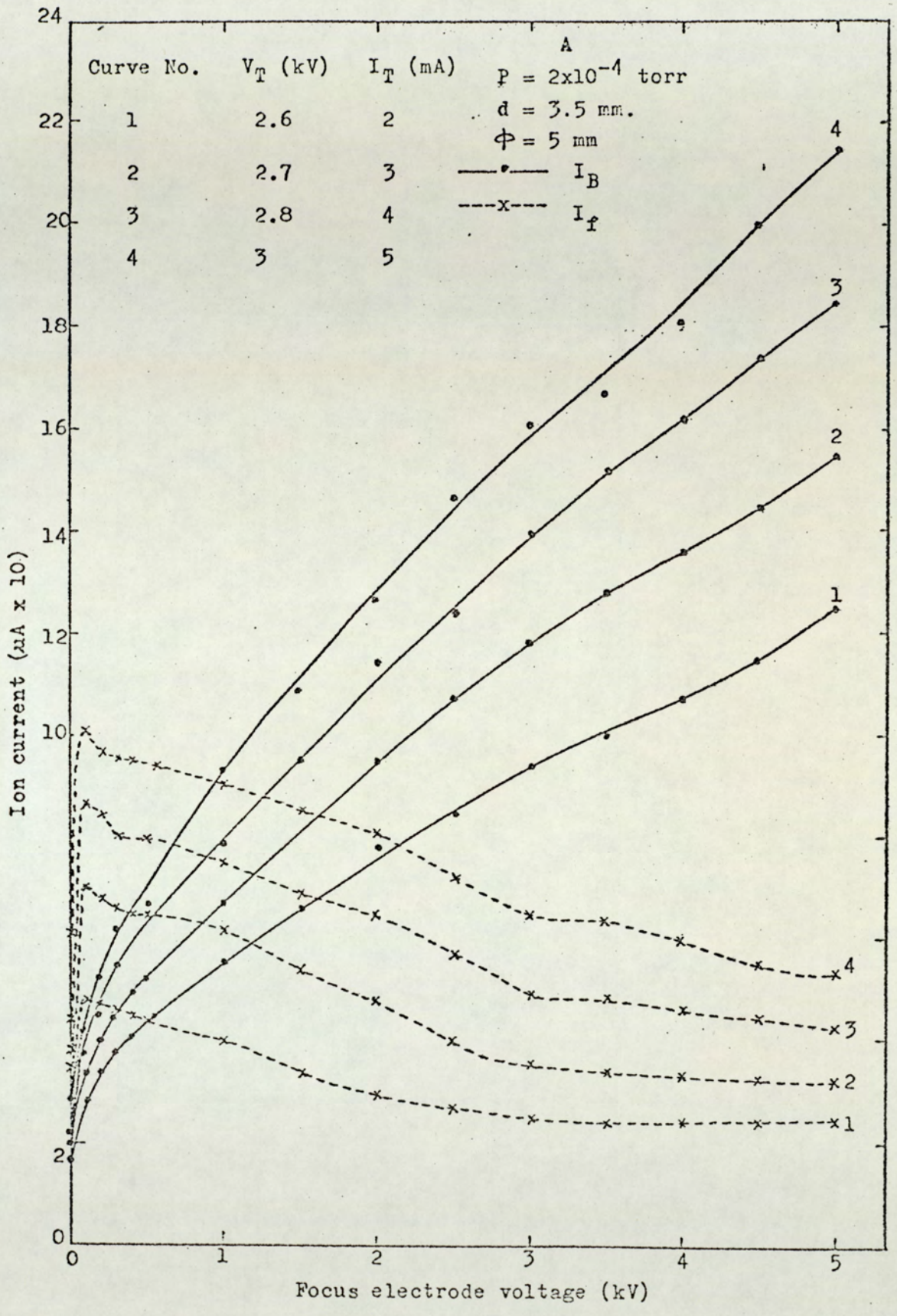

Figure 6.13 Variation of the ion current with the focus electrode - voltage.

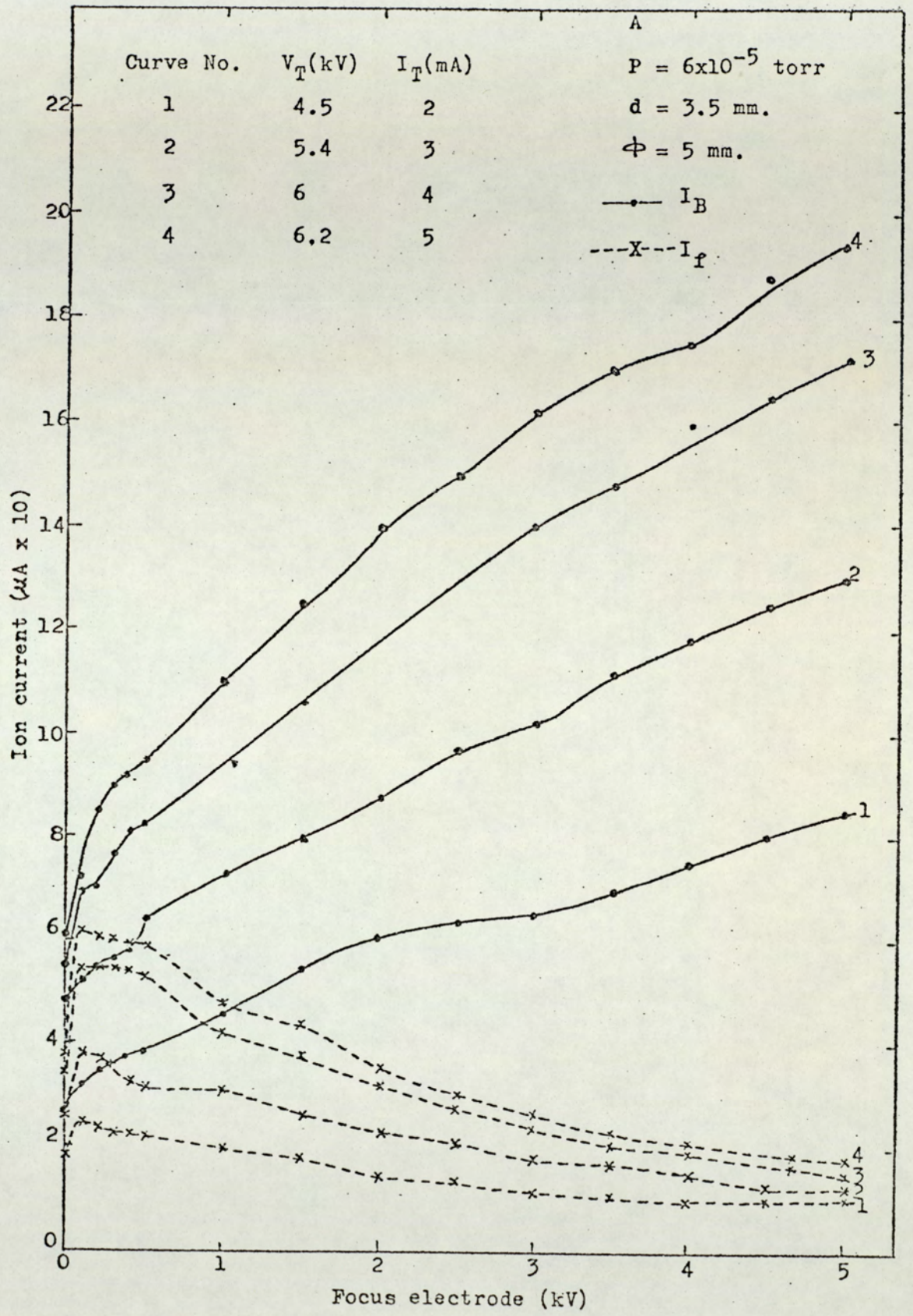

Figure 6.14 Variation of the ion current and the focus electrode voltage.

about one third of that at a pressure 2×10^{-4} torr. This is due to the divergence of the beam at high pressure, which suggested that d has to be smaller at high pressures.

Fig. (6.15) shows the relation between I_B, I_f and I_T, for different pressures and for $V_f = 5$ kV, d = 2 mm. and ion exit aperture diameter, ϕ, of 5 mm. An ion current as high as 0.43 mA was obtained which is much higher than that obtained with any conventional source. By shortening d, higher ion currents could be obtained. For example, at a pressure of 2×10^{-4} torr and d = 2 mm, $I_T = 5$ mA, $I_B = 290$ μA (Fig. 6.15) and at the same conditions, but with d = 3.5 mm, $I_B = 215$ μA (Fig. 6.13).

Figs. (5.16) and (5.17) show photographs of the beam (in the Y-direction), from the conventional source and the new source respectively using the same exposure time. It is clear that the beam from the new source is collimated and has a much higher intensity.

5.3.4. The focus electrode self biasing.

In the previous investigations two power supplies were used and the Faraday cup (or the specimen) was at the same potential of the focus electrode which is not convenient in many applications. Fig. (6.18) shows a new circuit where the discharge power supply was only used and the focus electrode was self-biased through a resistor R = 1.33 MΩ and the Faraday cup was at earth potential. A variable resistor could, of course, be used to control V_f.

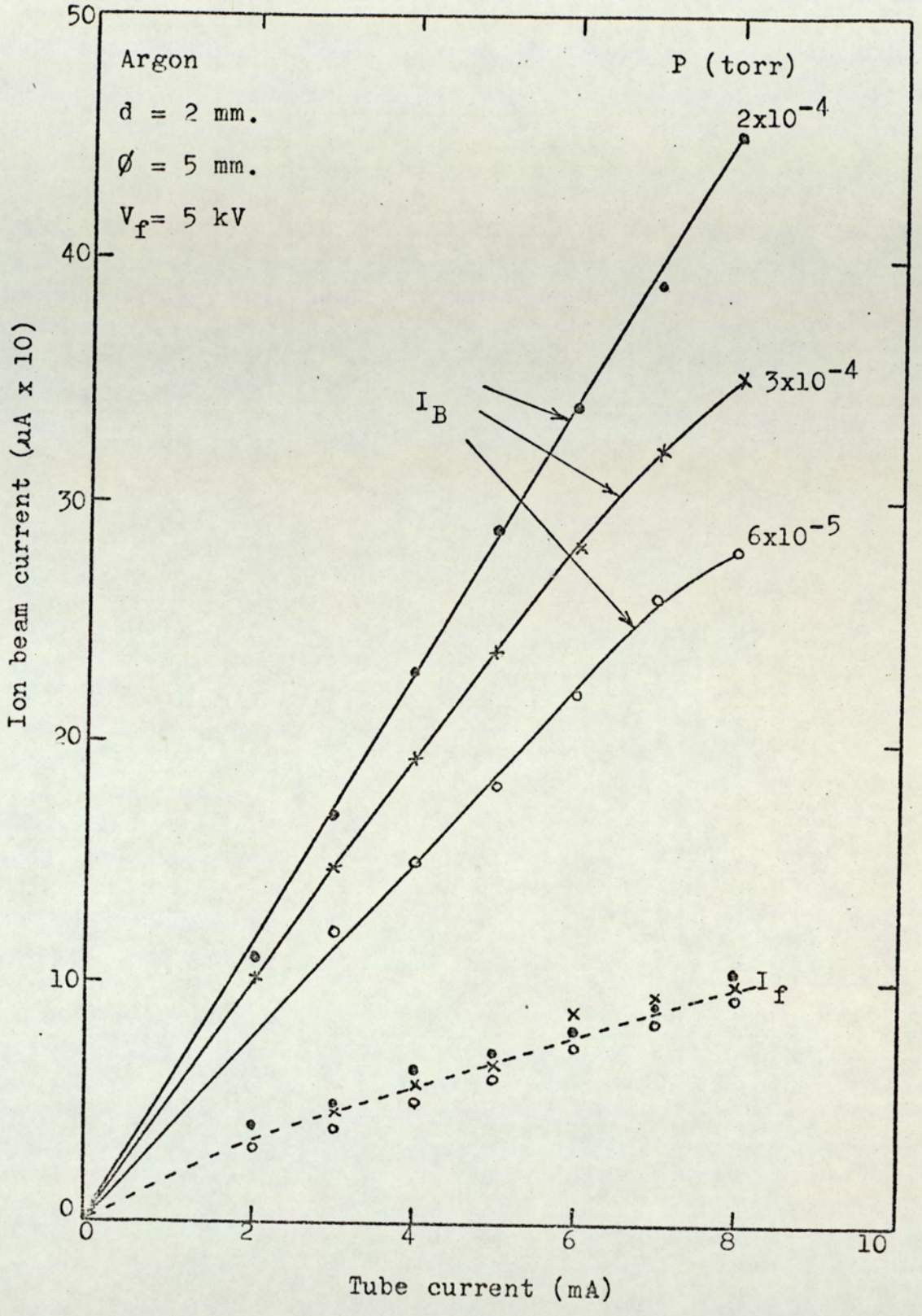

Figure 6.15 Relation between the tube current and the ion beam current at different pressures.

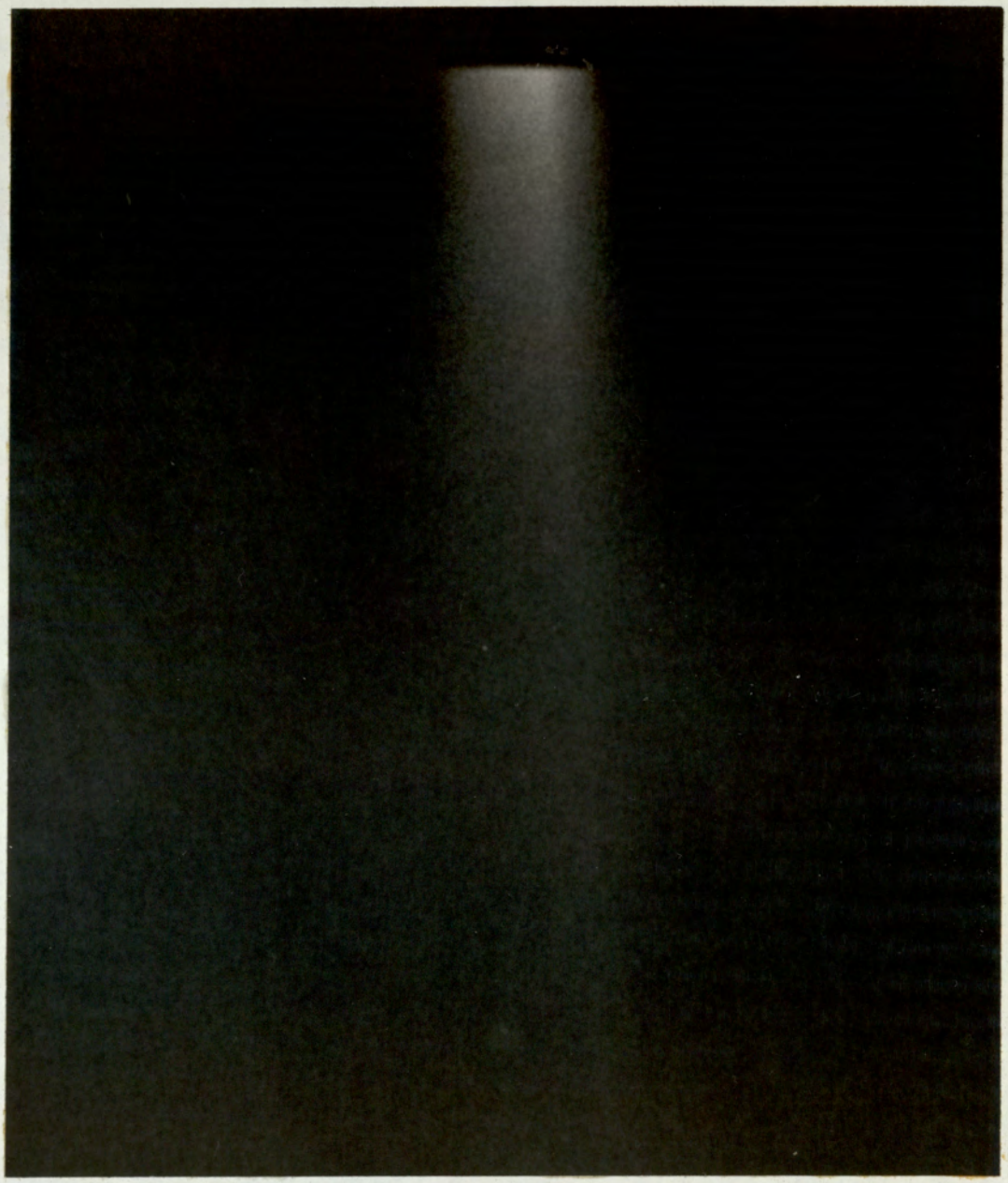

Figure 6.16 Ion beam emerging from the conventional source.

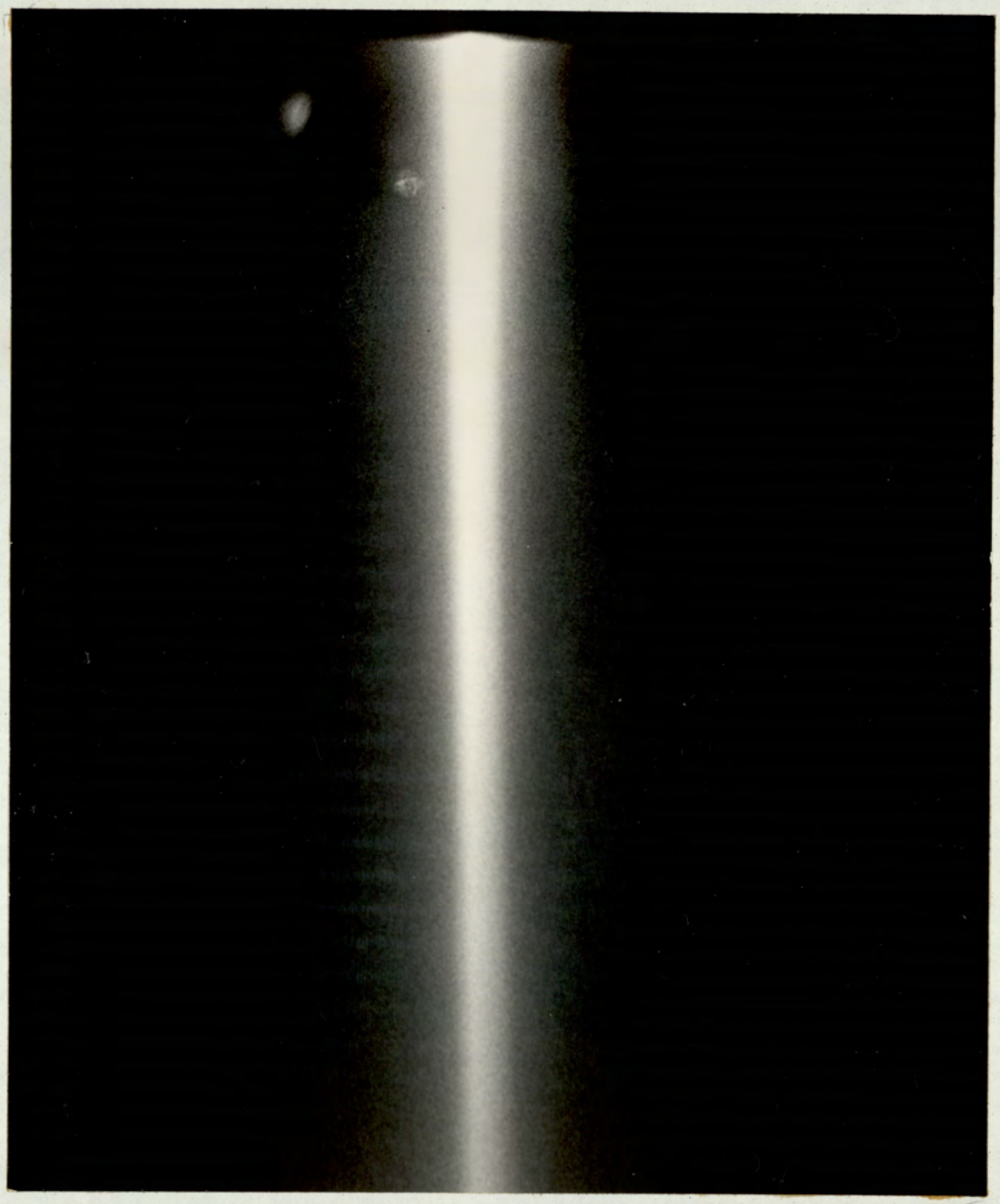

Figure 6.17 Ion beam emerging from the modified source.

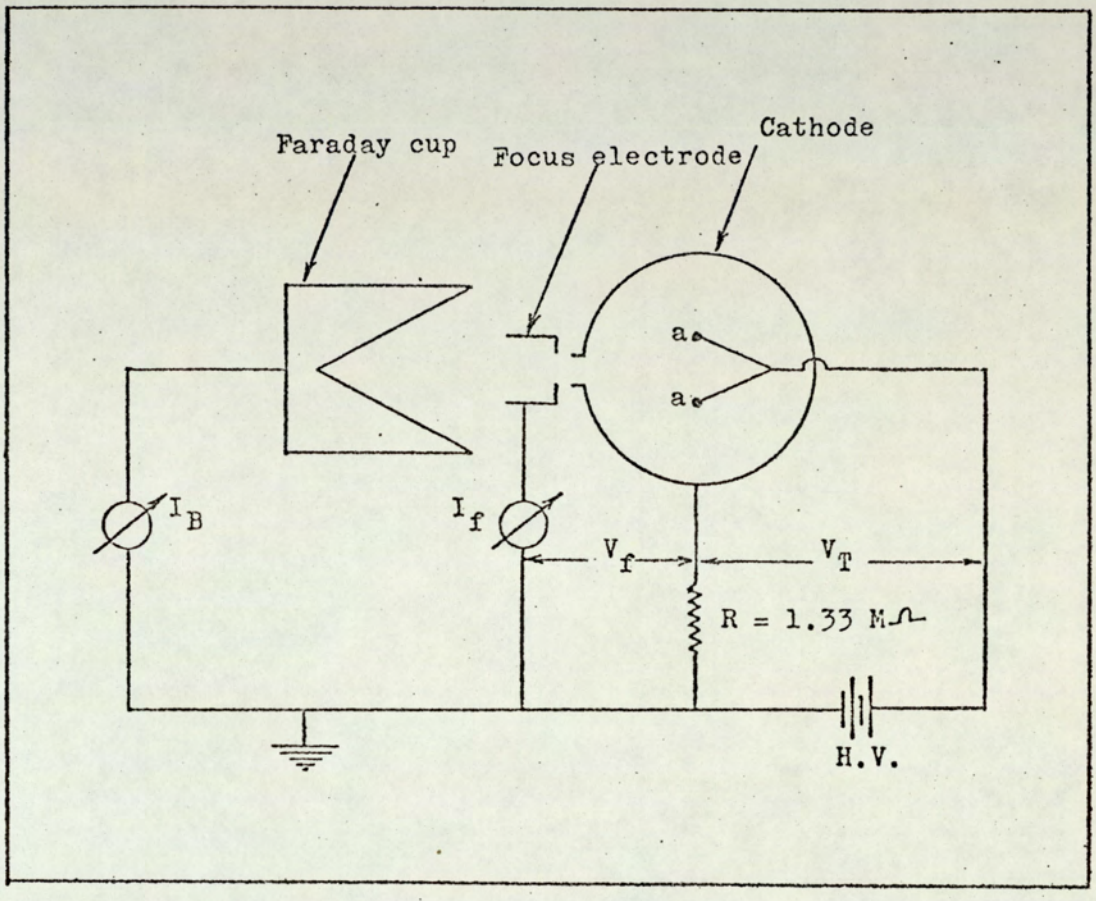

Figure 6.18 Electrical circuit of the self-biasing focus-electrode.

The following tables gives data of I_B, I_T, I_f, V_T and V_f at different pressures using the new circuit.

P (Torr)	8×10^{-5}		10^{-4}		1.5×10^{-4}	
I_T (mA)	5	7	5	7	5	7
V_T (kV)	2.9	3.1	2.1	2.3	1.8	2.2
V_f (kV)	6.7	9.3	6.7	9.3	6.7	9.3
I_B (μA)	410	660	320	600	380	600
I_f (μA)	35	65	40	60	30	70

It can be seen that I_B was still increasing with increasing V_f. An ion current as high as 650 uA was obtained at a pressure of 8×10^{-5} torr, $I_T = 7$ mA, $V_T = 3.1$ kV and $V_F = 9.3$ kV. This corresponds to an ion density of 16 mA/cm^2 at 7 cm away from the source. This is the highest yet to be achieved. At this high V_f V_T was now decreased, for example, V_T was equal to 2.3, and 4.8 kV when $I_T = 7$ mA, for $V_f = 9.3$ kV and using the chimney only respectively.

5.4. Discussions.

It seems that the ion exit aperture causes serious distortion to the field, which in turn gives a low source performance. To prove that such field distortions affect on the I_T - V_T characteristics, the following experiment

was carried out. The tube characteristics of a conventional source were investigated when the anodes were at 0^{o}, and 90^{o} with the ion exit aperture. In the latter case the field distortion should not effect the discharge. The result is shown in Fig. (6.19). It can be seen that when the anodes were at 90^{o} with respect to the ion exit aperture, I_T was about four times higher than the first case. This is presumably due to the distortion electric field such that the equipotentials bulge out through the aperture and deflect the electrons from their stable trajectories as described by Fitch and Rushton (1972) and Peggs and McIlraith (1973). The magnitude of this effect depends upon the shape and the size of the aperture.

The field due to the focus electrode compensates the field distortion due to the ion exit aperture by forcing the equipotential back into the aperture. It has also been shown that the field distortion can also be partially corrected by welding a chimney into the cathode around the ion exit aperture. This prevents the equipotential bulging out through the aperture to any large extent. It is important to prevent the field due to the focus electrode penetrating too far into the discharge otherwise the discharge is disturbed as shown in Fig. (6.4). This could be prevented by changing the distance between the ion exit aperture and the focus electrode or preferably by adding a chimney around the aperture.

The distortion of the equipotential line due to

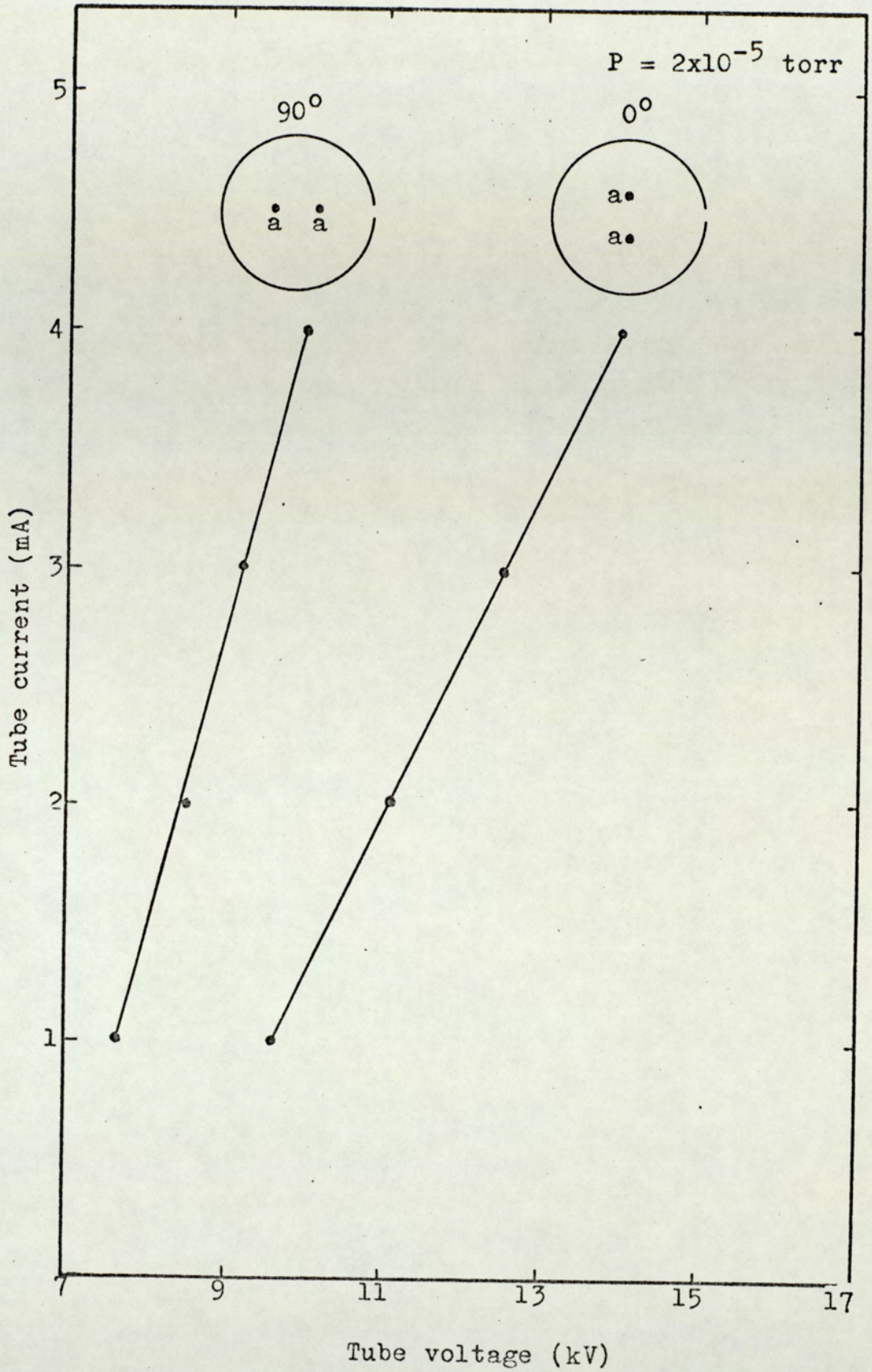

Figure 6.19 The discharge characteristics with the ion exit aperture at 0° and 90° with respect to the plane of the anodes.

the aperture has serious effects on the quantity and the quality of the ion beam (Septier, 1967), such as;

(a) The emission density from the source will not be uniform over its surface which results in a decrease in the source current efficiency below that which would be obtained neglecting the aperture effect.

(b) The distortion in the equipotential lines results in a transverse electric field that cause the ion trajectories to bend outward even near the source in such a way that a large fraction of the ions are not allowed to get out of the source and even those passing through the aperture are in the form of a divergent beam. This situation is highly undesirable because it prevents the formation of a beam that can be focussed and some ions are not allowed to get out of the source. It is therefore of great importance to design the focus electrode properly to create a laminar flow condition through the cathode aperture.

In the present ion source as the ions pass through the aperture in the cathode, they experience an outward (divergent) force due to the transverse component of the field lines which terminate in this aperture. If the diameter of this aperture is small compared with the cathode-plasma boundary spacing, the deflected trajectory can be treated as if it resulted from a thin electric lens with a focal length obeying the Davisson-Colbick

equation (1931) and (1932). This thin lens will exhibit a focal length (for a cylindrical aperture) given by:

$$F = \frac{4 V_1}{E_1 - E} \qquad \ldots\ldots (6.1)$$

Where V_1 is the voltage corresponding to the ion energy, E_1 and E the electric field values outside and inside the cathode. This analysis is for plane electrode system. Since the beam is injected into an electric-field-free region, $E_1 = 0$ and it can be seen from Eq. (6.1) that the lens effect of the aperture is always divergent. By assuming that the current flowing through the aperture is space-charge limited, the ions leave the cylindrical aperture of the plannar gun with a slope:

$$\tan \eta = -\frac{r_o}{f} = \frac{r_o E}{4V_1} = \frac{r_o}{3g} \qquad \ldots\ldots (6.2)$$

Where r_o is the ion-beam radius at the ion exit aperture and g is the cathode-plasma boundary spacing.

It should be noticed that the above analysis is based on the thin lens approximation which depends on Davisson-Colbick equation. These data are, therefore, useful only to show the qualitative physical behaviour of the ion beam. However, Harris (1960) has estimated corrections to the Davisson-Colbick lens equation for conditions where the aperture diameter is not negligible compared with the electrode spacing. He has shown that an increase in the lens strength of the order of 10 to 20% is appropriate. From this and the Davisson-Colbick equation a somewhat more accurate picture can be obtained.

The plasma boundary near the cathode is an equipotential and therefore it is also disturbed and has a somewhat convex shape. The ions leave the plasma boundary to the cathode at normal line, which in the case of a convex plasma boundary results in a divergent beam. A concave plasma boundary is an ideal ion emitting surface to form a high current and a focused ion beam (Echardt, 1964). This was achieved by using a focus electrode, the field due to this electrode is responsible for such a shape. In the Davisson-Colbick equation, $E_1 = \frac{V_f}{d}$ in this case where d is the spacing between the focus electrode and the cathode, and when V_f is high enough so that $E_1 > E$, the lens is convergent. This is what actually occurs to produce high current focussed ion beams.

The sharp increase in I_B and I_f at low values of V_f ($\sim$100 V) may be attributed to three reasons. The fact that I_T was also increased, the partial correction of the electric field in the ion exit aperture which allowed more ions to get out and the removal of negatively charged particles from the beam. The electron in the ion beam was observed by deflecting them on a quartz plate.

Therefore, the advantages of adding a focusing electrode to the electrostatic twin anode ion source can be summarised as follows:

(a) Improved source performance (high I_T values at the same V_T).

(b) More stable discharge.

(c) Lower operating pressures.

(d) Lower values of V_T and thus the thermal load was decreased.

(e) Production of higher ion beam current.

(f) Production of parallel or focused beams of much higher densities, so that higher etching and thinning rates can be achieved. Also the specimen can be placed far away from the source and thus the thermal damage can be minimized.

(g) The new development of the source can be an attractive possibility to be used in small accelerators, like the Van de Graf accelerator.

(h) The source can be used to produce ion beams with few keV energy required for certain applications, such as ion-electron interaction.

7. THE SPHERICAL SYMMETRY ELECTROSTATIC ION SOURCE

7.1. Introduction.

It has recently been shown by Franks (1973) that the saddle configuration can be achieved by using spherical geometry. This can be done with two hemispherical cathodes and an annular anode in place of a cylindrical cathode and the anode rods. The beam emerges through a hole in the cathode normal to the plane of the annulus and displays axial symmetry. Investigations of the characteristics of this new source and the beam characteristics emerging from it are described in this chapter. The design of the ion source is based on the design described by Franks (1973).

7.2. Description of the source.

A drawing of the source is shown in Fig. (7.1). The anode was made from stainless steel, of thickness 2 mm., and contains a central hole of 5 mm. diameter. Two hemispherical aluminium cathodes of radius 11 mm. were used. Each cathode has an aluminium insert so that ion exit apertures of different sizes can be used. This also allows these inserts to be changed when they get damaged by continuous ion bombardment. The anode was placed between a stainless steel screen, diameter 10 mm, at earth potential. The anode was isolated from the screen by four ceramic insulators. A schematic diagram of the source and its associated circuit is shown in Fig. (7.2). It has

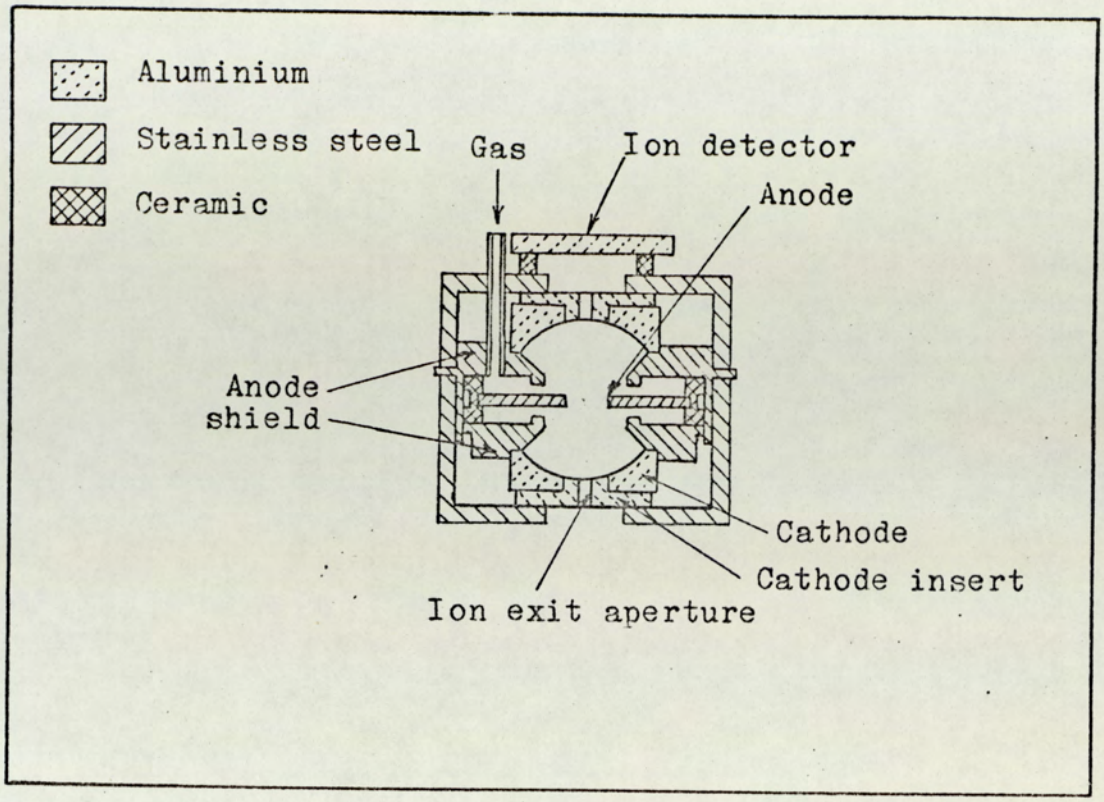

Figure 7.1 The spherical source.

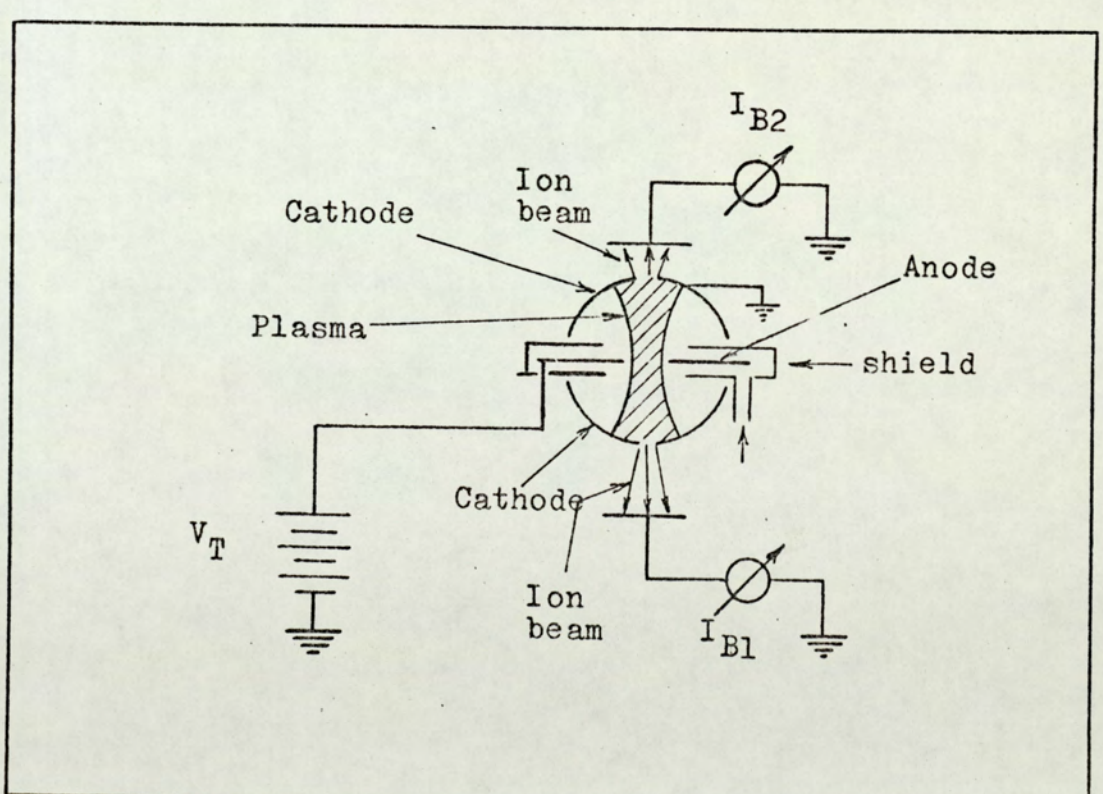

Figure 7.2 The electrical circuit.

been shown in section (5.8) that the cylindrical source could produce two or more ion beams, but in the case of the spherical source it can be seen from Fig. (7.2) that only two ion beams can emerge. One of these two beams was monitored continuously by an ion collector while the other beam was used for various applications. A photograph of the spherical source is shown in Fig. (7.3) and shows that the source is relatively small.

7.3. The tube voltage - tube current characteristics.

The variation of the tube current with the tube voltage is shown in Fig. (7.4). This was done at chamber pressures of 7×10^{-5}, 8×10^{-5} and 2×10^{-4} torr. The ion exit aperture was 1.5 mm. diameter, the anode hole was 5 mm. and the screen hole diameter was 10 mm. The general form of the curves are the same as those of the cylindrical source.

7.4. The effect of the variation of anode hole diameter.

At a pressure of 10^{-4} torr and with a screen hole diameter of 10 mm, the tube current and the ion beam current were measured at different anode hole diameters. Thus the current efficiency (I_B/I_T) was obtained for different anode hole diameters. Fig. (7.5) shows the relation between $\frac{I_B}{I_T}$ % and the anode hole diameter at a pressure of 10^{-4} torr with V_T equal to 5 kV, the diameter of the ion exit aperture 6 mm. and the diameter of the screen hole diameter equal to 10 mm.

Figure 7.3 The spherical source photograph.

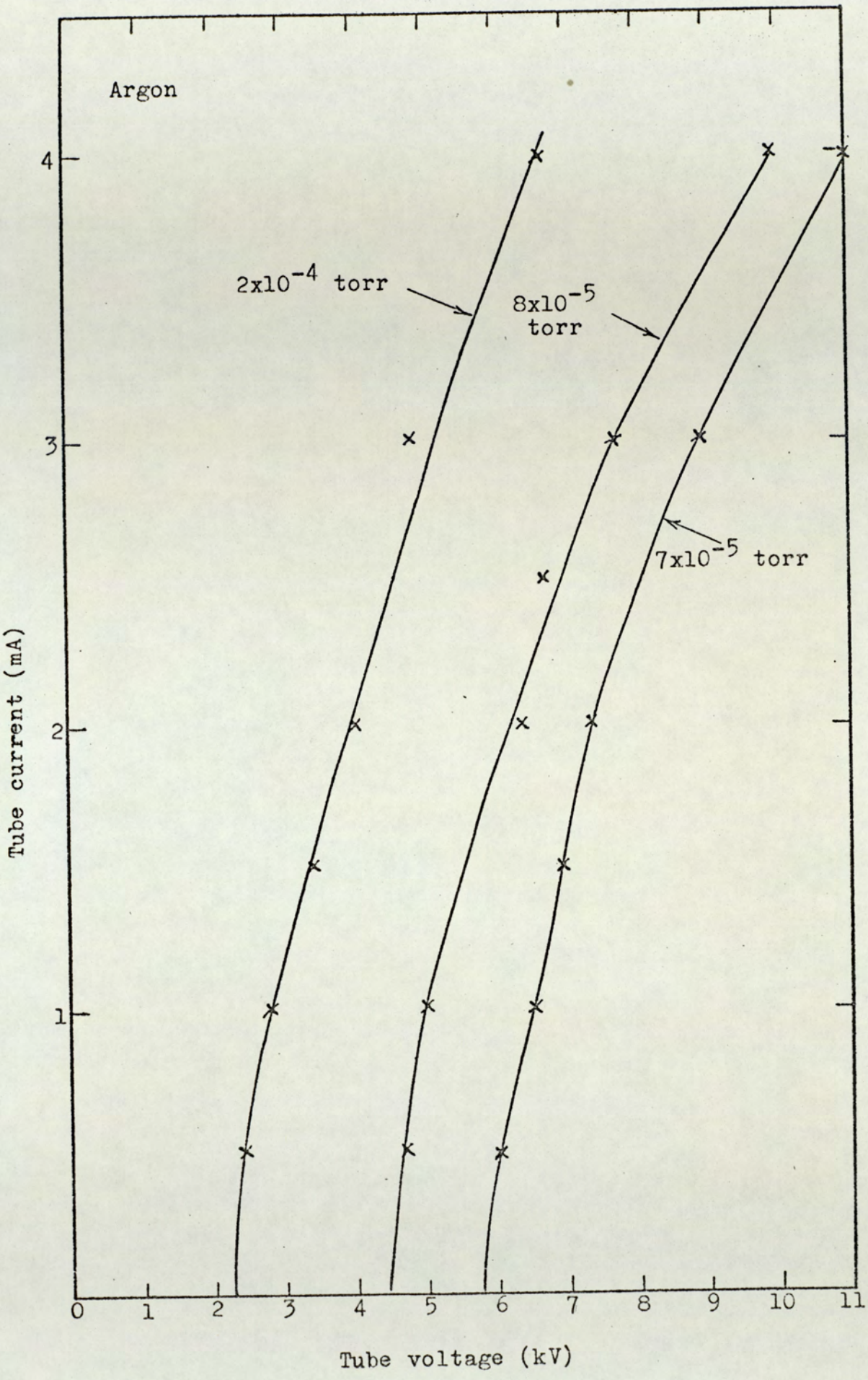

Figure 7.4 The discharge characteristics.

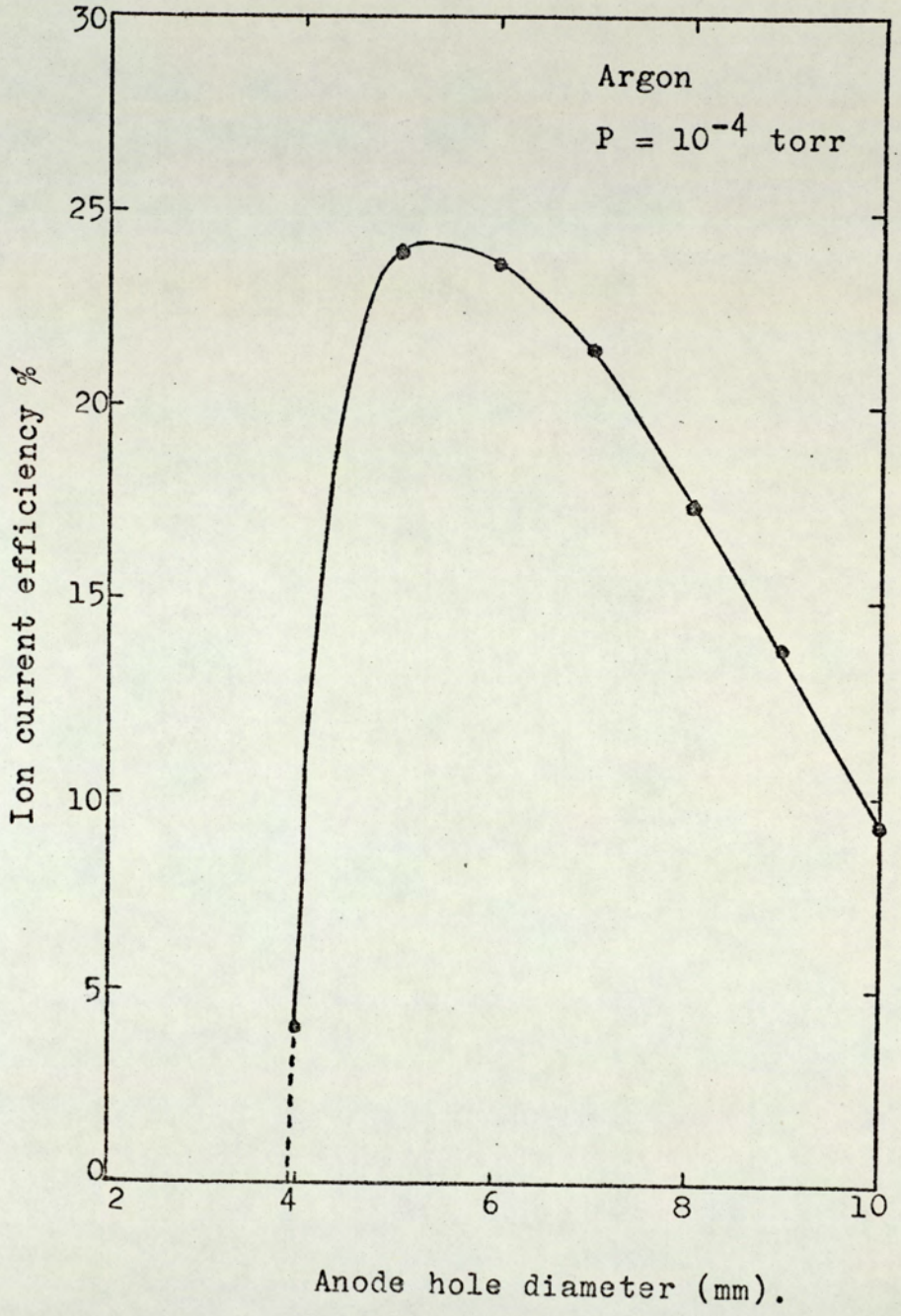

Figure 7.5 Relation between the current efficiency and the anode hole diameter.

It can be seen that when the anode hole diameter was less than 4 mm. the discharge ceased and that the current efficiency increased rapidly as the anode hole diameter was increased beyond 4 mm. The current efficiency reached an optimum at anode hole diameter of approximately 5 mm. When the anode hole diameter was increased beyond 5 mm, the current efficiency started to fall down.

7.5. The effect of the screen hole diameter.

The effect of the screen hole diameter on the current efficiency was carried out at a chamber pressure of 10^{-4} torr, anode hole diameter of 5 mm. and ion exit hole diameter of 6 mm. Fig. (7.6) shows the relation between the anode hole diameter and the current efficiency.

It can be seen that when the screen hole diameter was decreased below 6 mm, the discharge ceased but the current efficiency increased as the anode hole diameter was increased (although not so rapidly as in the case of the screen hole diameter-current efficiency). The current efficiency reached an optimum at an anode hole diameter of 10 mm, then it decreased as the anode hole diameter was increased beyond 10 mm.

7.6. The ion current density.

A shielded ion detector was used to measure the ion current density. A plate with a hole 0.1 mm. in diameter was placed in front of the ion detector and was positioned 2.5 cm. away from the source so that the

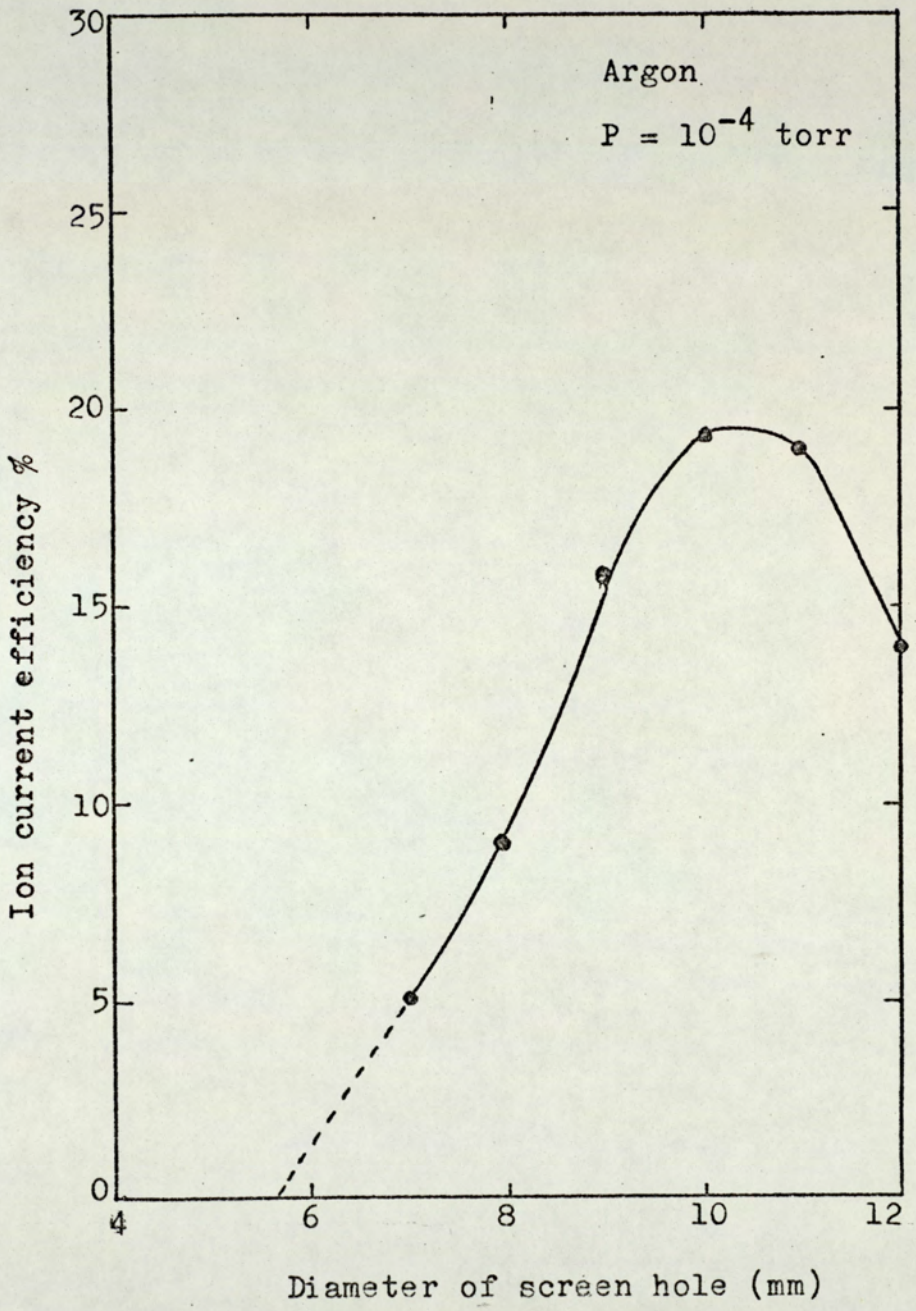

Figure 7.6 Relation between the current efficiency and the screen hole diameter.

centre of the hole coincided with the centre of the beam.

Fig. (7.7) shows the relation between the ion current density (central part of the beam) and the discharge input power at a chamber pressure of 7×10^{-5}, 9×10^{-5} torr (non-uniform plasma mode) and 2×10^{-4} torr (uniform plasma mode). It is, as expected, much higher in the non-uniform plasma mode than in the uniform plasma mode. The shape of the curves appear the same as those of the cylindrical source except that the ion current density is much higher. For example, at an input discharge power of 20 watts and at a chamber pressure of 7×10^{-5} torr, an ion current density as high as 2 mA/cm^2 was obtained at a distance of 2.5 cm. away from the source.

7.7. The current density distribution.

The ion current density distribution was measured with the Faraday cup arrangement used previously. After the Faraday cup was positioned in the centre of the beam, it was moved forward and backward by a small motor situated inside the vacuum chamber. The ion current was measured by a nA meter. The source was of the same dimensions as described before and the ion exit aperture was 1.5 mm. diameter.

Figures (7.8, 7.9, 7.10 and 7.11) show the current density distribution at chamber pressures of 7×10^{-5}, 9×10^{-5}, 2×10^{-5} and 2.5×10^{-4} torr respectively. It can be seen that the beam is symmetrical and is characterized by a dense central region. In fact

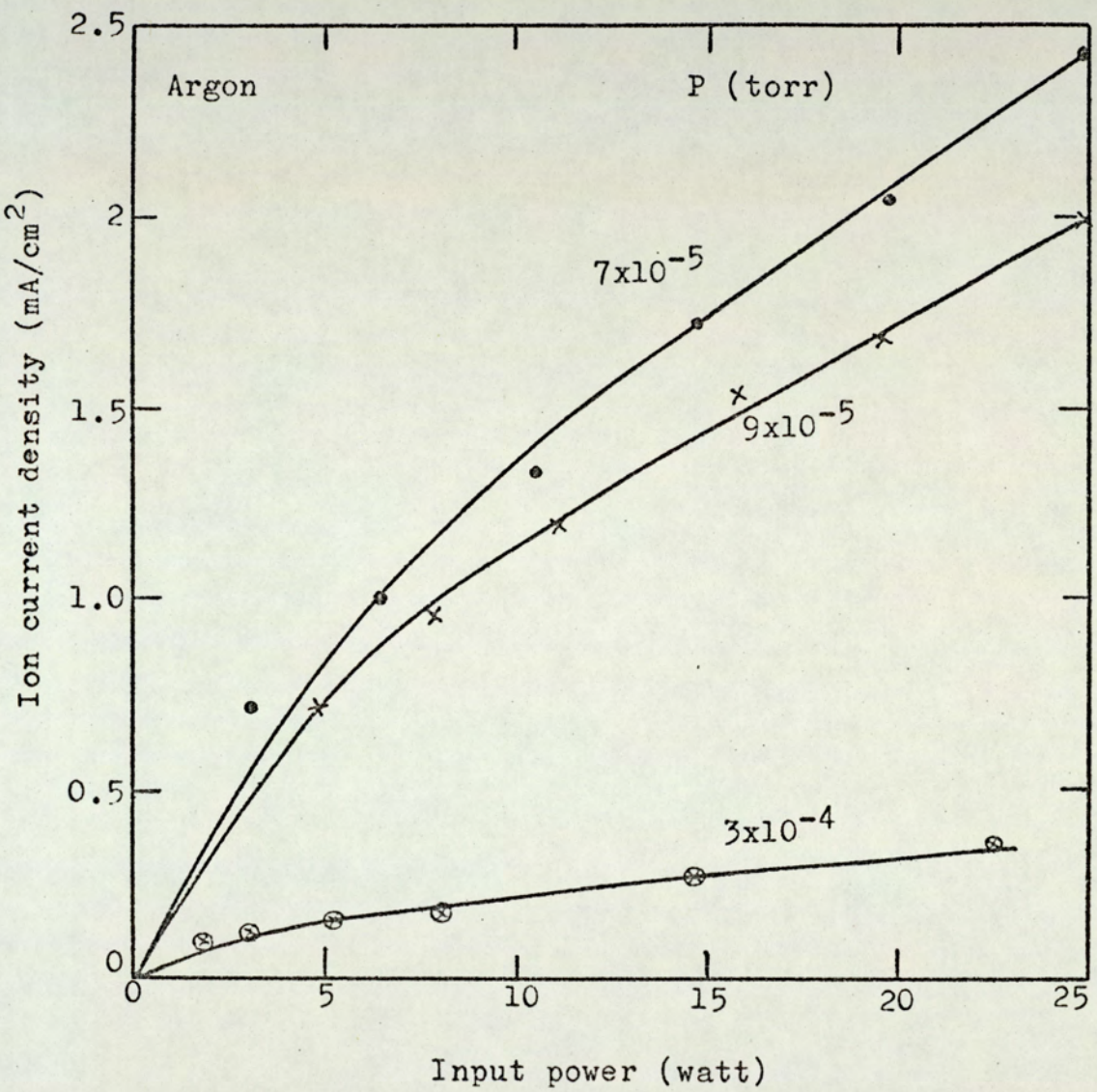

Figure 7.7 Relation between the ion current density and the discharge input power.

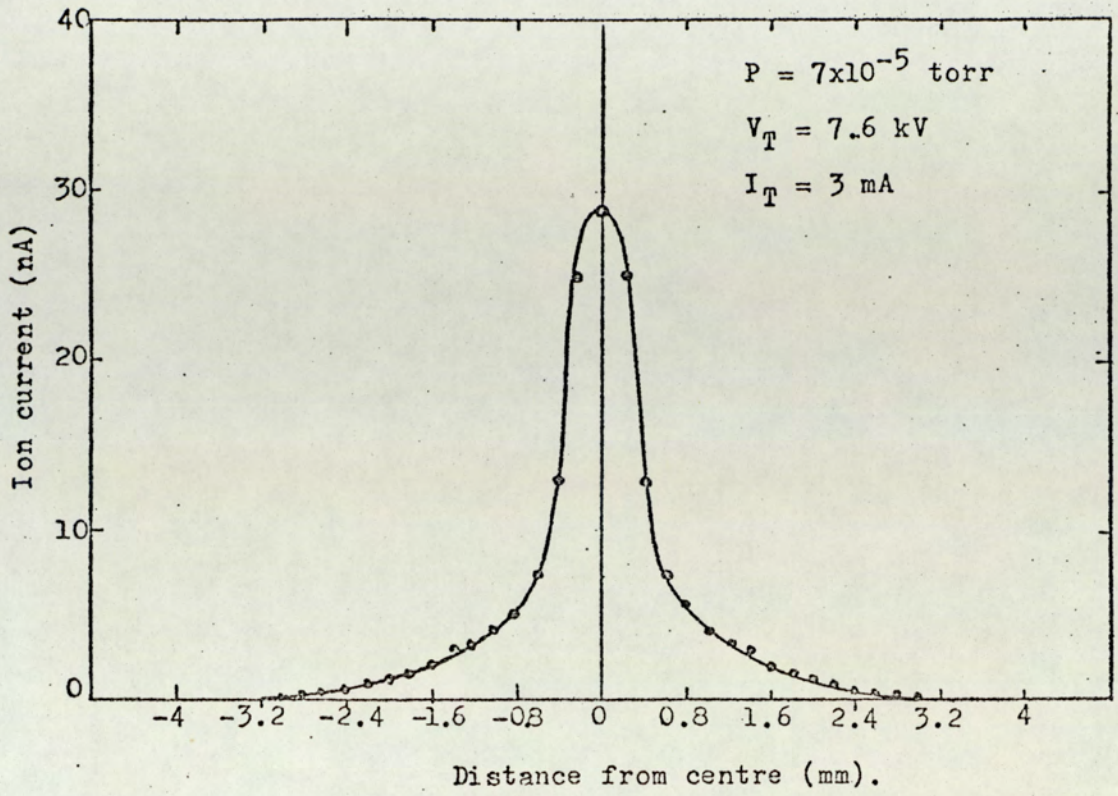

Figure 7.8 The current density distribution.

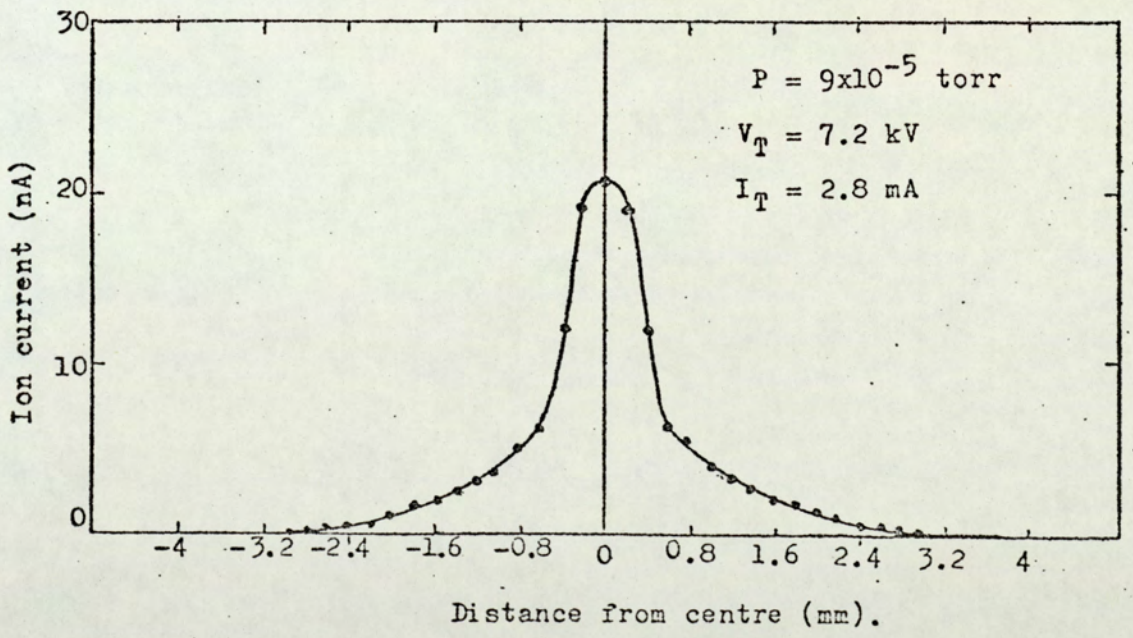

Figure 7.9 The current density distribution.

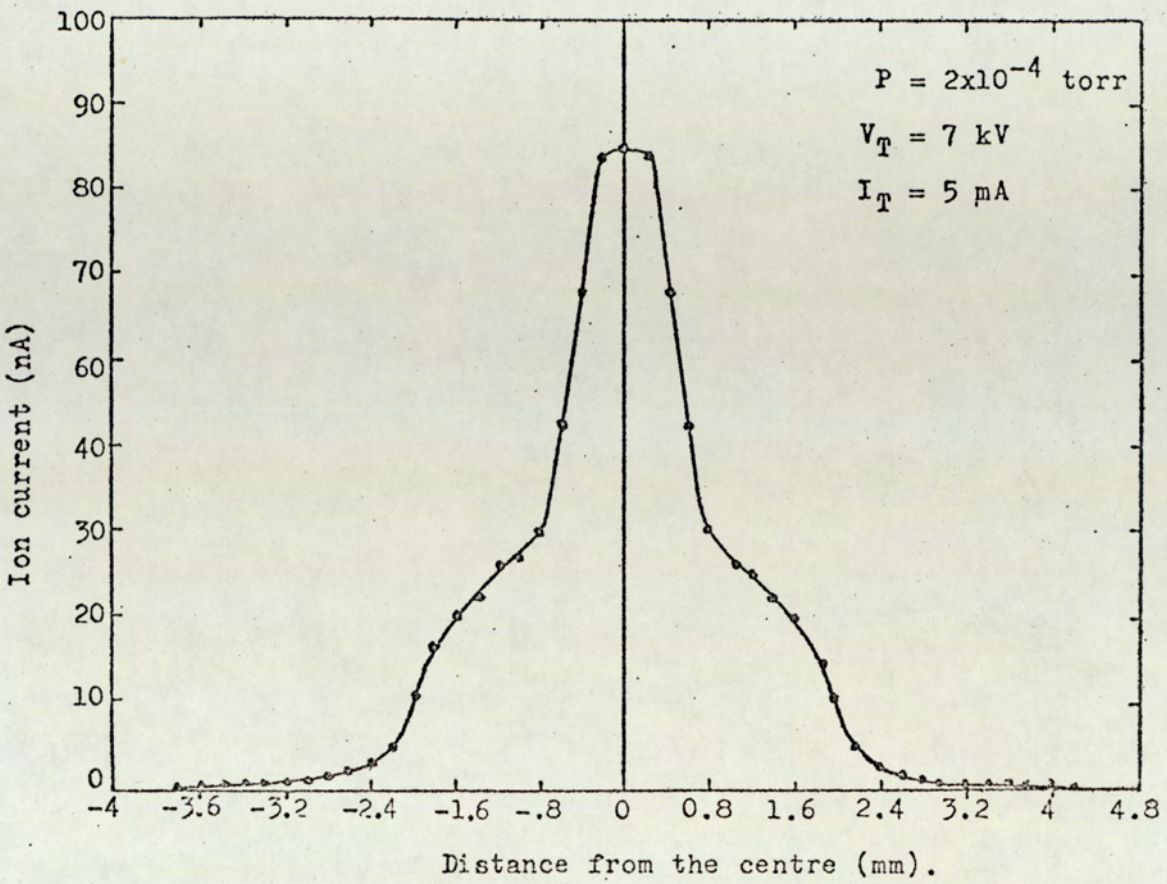

Figure 7.10 The current density distribution.

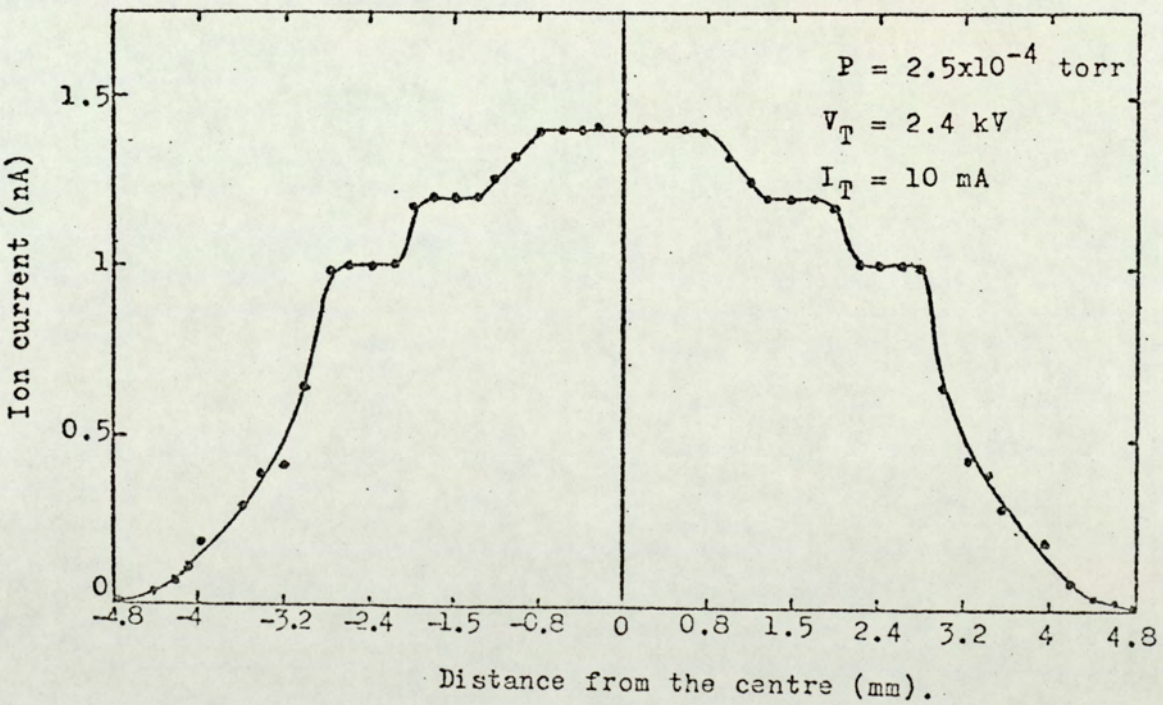

Figure 7.11 The current density distribution.

this dense central region of the beam could be seen by eye. It was found that the diameter of the central region as well as the whole beam diameter of the ion beam were increased as the pressure was increased. When the source was operating in the transition mode Fig. (7.11) the diameter of the beam was larger with better ion uniformity. However, the beam intensity was much less than when the source was operating in the non-uniform plasma mode. This agrees quite well with the investigations in Chapter 5 for the cylindrical source.

7.8. The ion beam profile.

The ion beam profile was measured by ion etching copper films of the same thickness at different distances away from the source. Three well defined etched regions were well observed, a central region which was completely etched corresponding to the dense central region of the beam. This region was surrounded by a partially etched region which was itself surrounded by an outer slightly etched region. These results are consistent with the ion current density distribution measurements of the previous section.

Fig. (7.12.a) shows the beam profile which was obtained by measuring the diameters of these three marked regions at different points away from the source. The central dense part of the beam has the lowest divergence (4.5^{o}) and the second part has a divergence of 11.5^{o}, while the outer part has a divergence as high as 17^{o}.

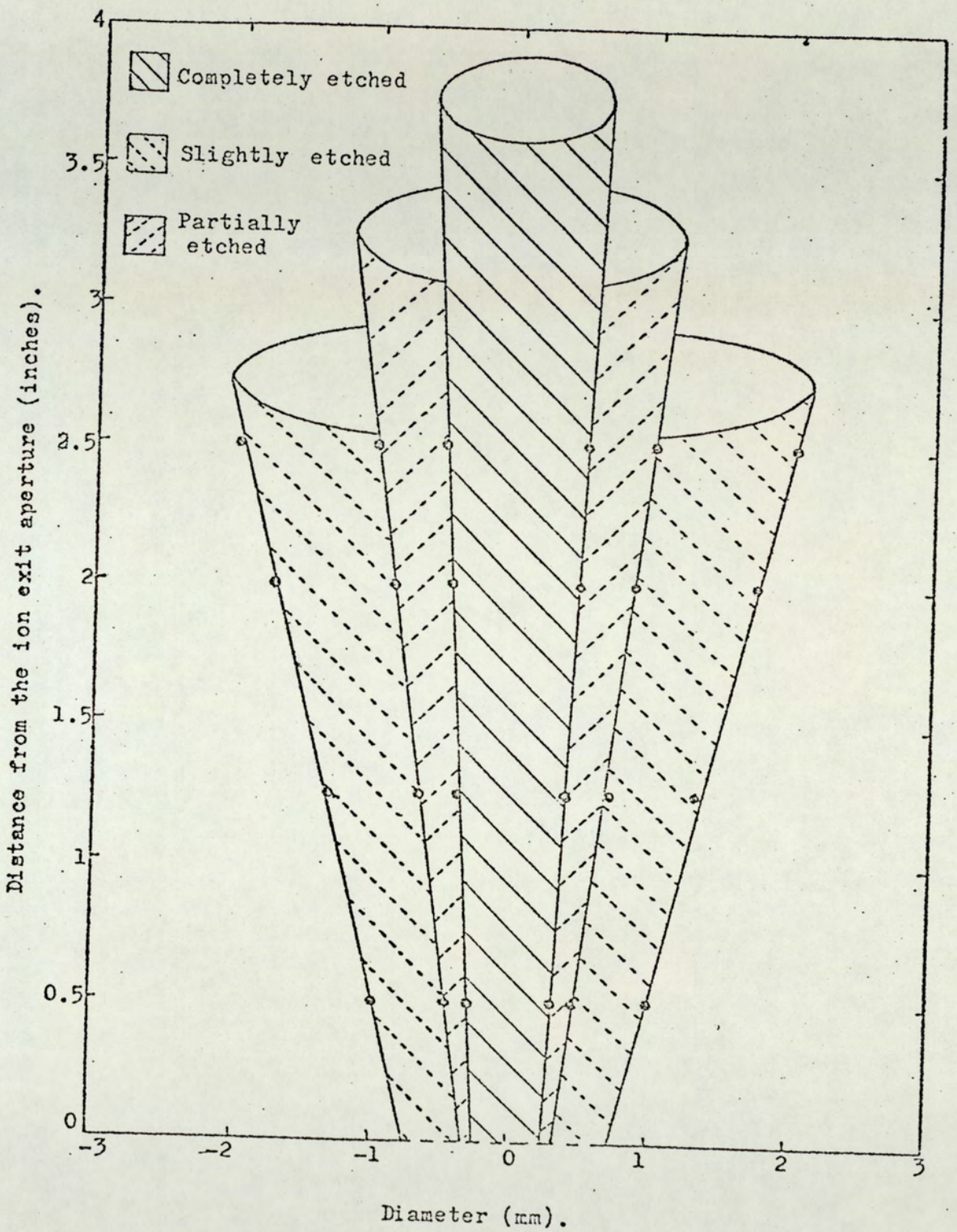

Figure 7.12.a The ion beam profile.

Fig. (7.12.b) shows a photograph of the emerging ion beam from the spherical source.

7.9. Production of energetic neutrals.

It has been shown that the ion beam produced by the spherical source with 1.5 mm. diameter ion exit aperture, has a high ion density and relatively low divergence. This makes it a very suitable source to be used for ion thinning of small specimens. During an attempt to scan this relatively narrow beam using deflection plates so that it can be used for etching larger specimens. It was found that a part of the beam was not deflected.

To investigate if this undeflected part of the beam was high energy ions or energetic neutrals, two deflection plates with applied d.c. voltage were placed in front of the ion exit aperture and the Faraday cup arrangement used to measure the ion current density and the ion density distribution was used to scan the beam. The result is shown in Fig. (7.13). It can be seen that there are no charged ions left at the centre after the beam was deflected. This concludes that this undeflected part of the beam consists of neutrals.

An approximate estimation of the neutral content of the beam was done by comparing the time required to etch through a copper film by the charged ion and by the neutrals. These experiments showed that the ion beam contains approximately 30% neutrals. Also since the

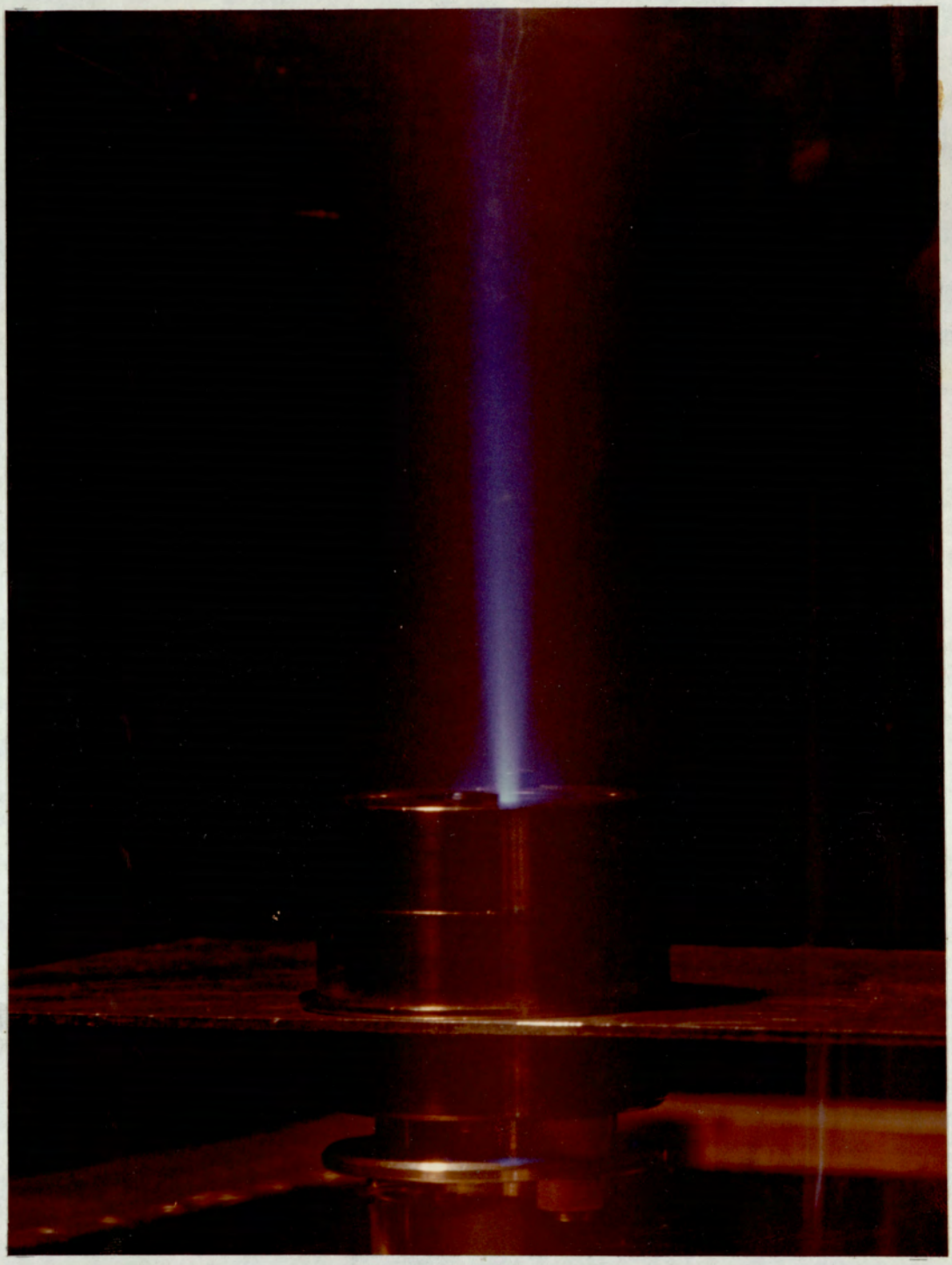

Figure 7.12.b. A photograph showing the ion beam from the spherical source.

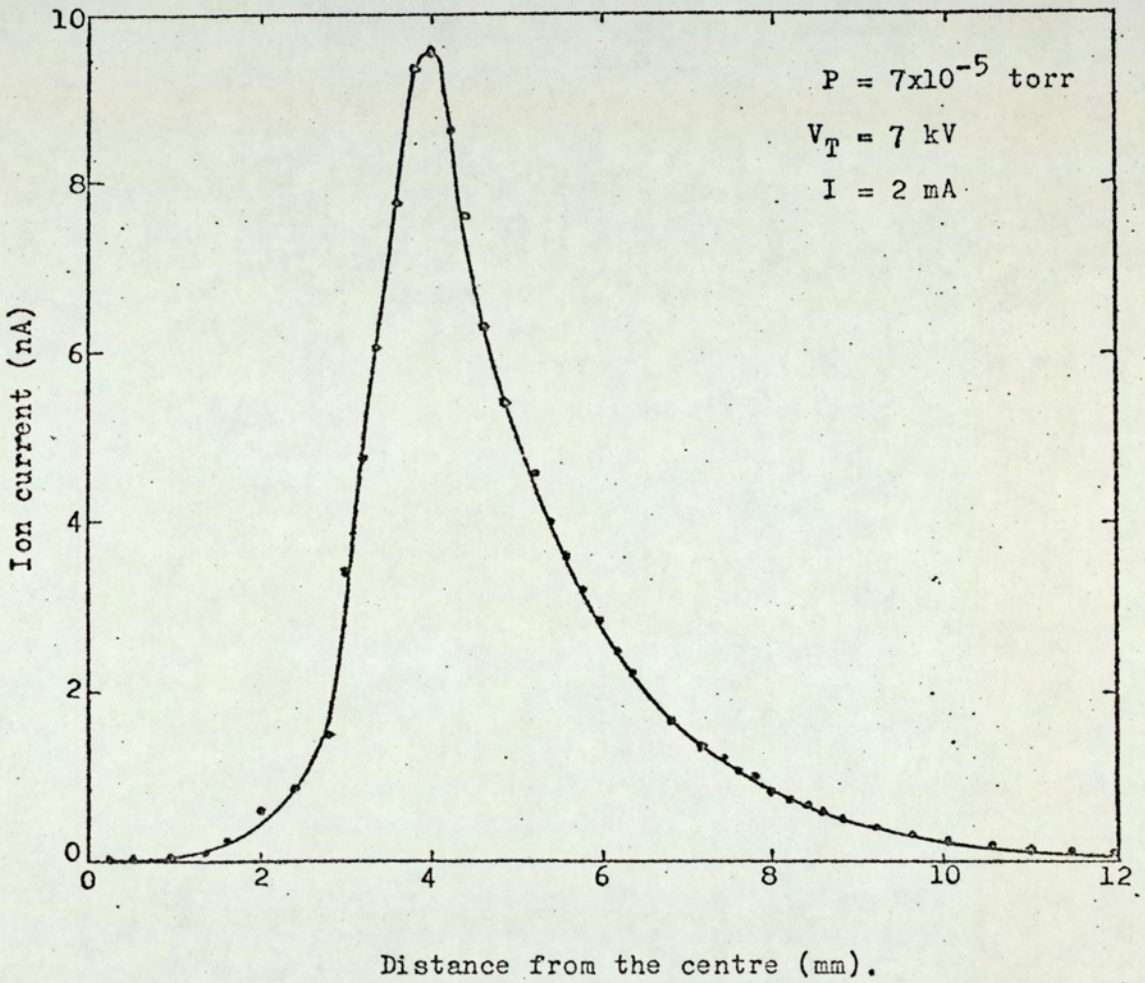

Figure 7.13 Scanning of the ion beam.

neutrals etched the copper film they must have been energetic.

7.10. The spherical source with a focus electrode.

A focus electrode in the form of a canal, diameter 2 mm. and length 5 mm., was placed 2 mm. away from the ion exit aperture (1.5 mm. diameter). A self-biased focus electrode electrical circuit was used. The spherical source, the focus electrode and the electrical circuit are illustrated in Fig. (7.14). Since the ion current detector was at earth potential, it served as a focus electrode for the second beam. The two ion beam currents I_{B1} and I_{B2} were found to be equal (the focus electrode and the ion current detector were at equal distances from the ion exit apertures).

The effect of the focus electrode voltage on the ion current efficiency is shown in Fig. (7.15) at a pressure of 9.5×10^{-5} torr. It can be seen that the ion current efficiency could be increased from 2.2% to 6% when V_f was raised from 0 to 3 kV.

The focus electrode was replaced with a flat plate placed 3 cm. away from the ion exit aperture. The ion current to this plate (I_{B1}) as a function of the tube current is shown in Fig. (7.16). The values of the focus electrode voltages are also shown in the figure. Fig. (7.16) also shows the relation between the ion current to the ion detector and the ion current from the conventional source, and the tube current. It can be seen that the ion

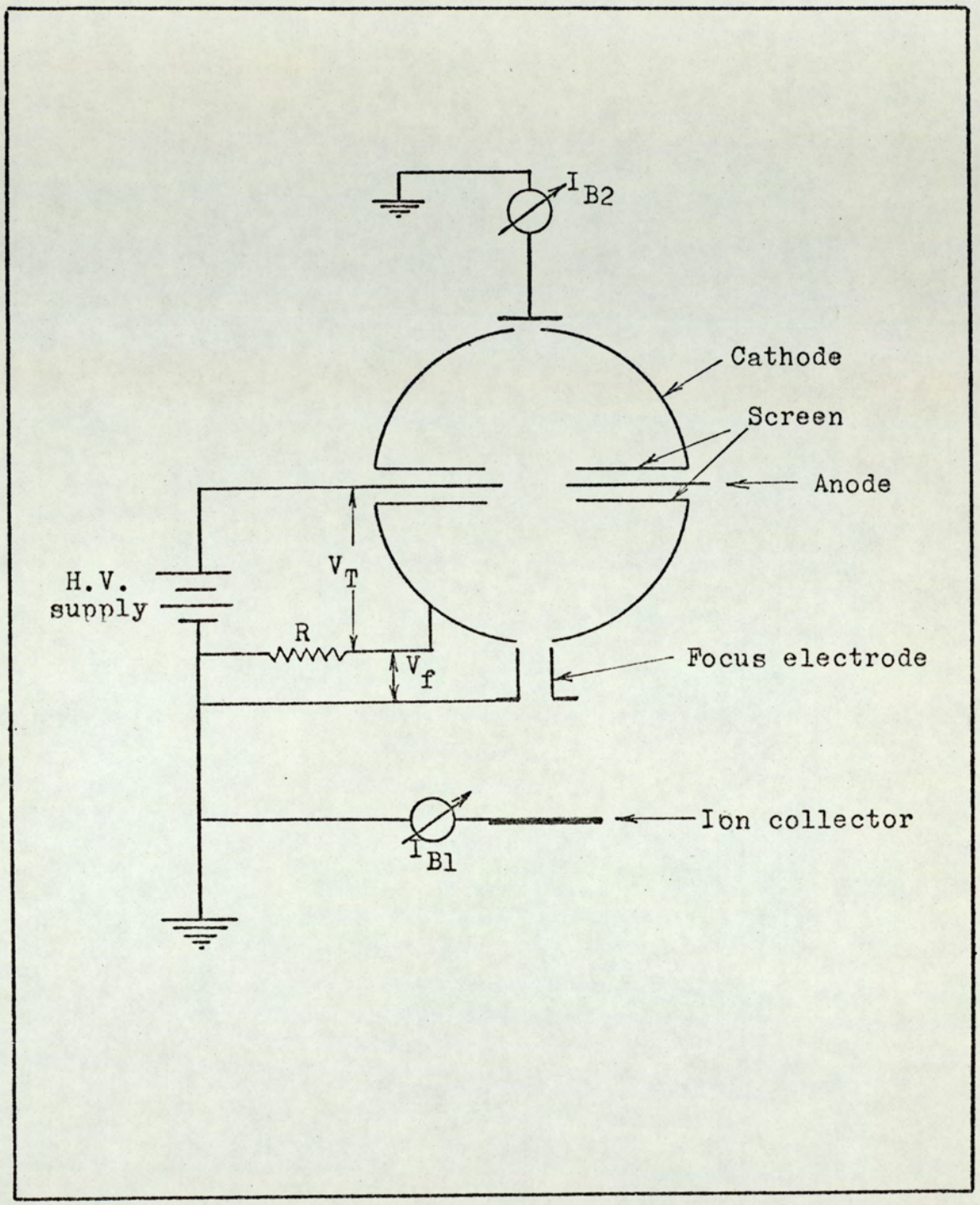

Figure 7.14 Schematic drawing of the spherical source with a focus-electrode.

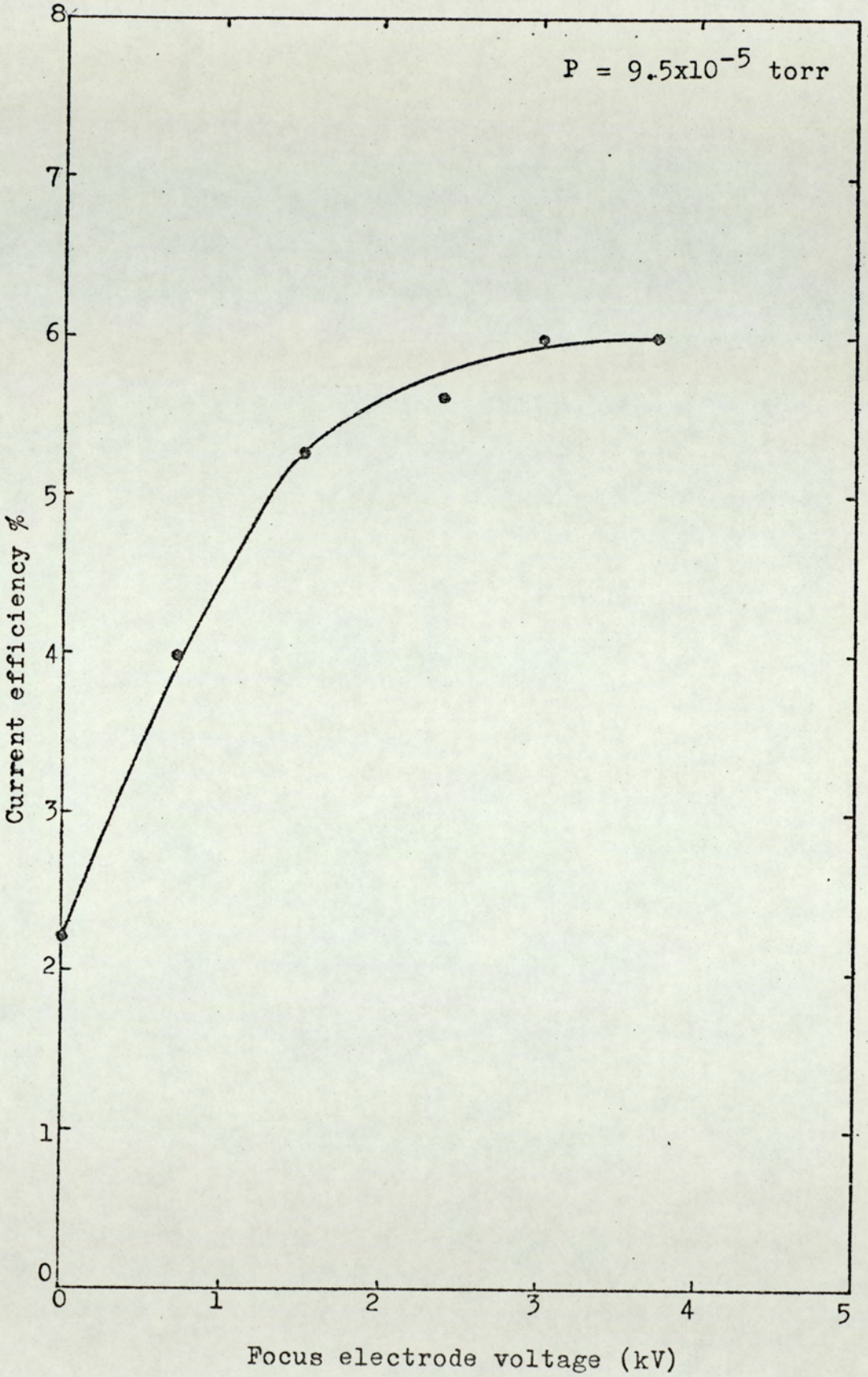

Figure 7.15 Relation between the focus-electrode voltage and the current efficiency.

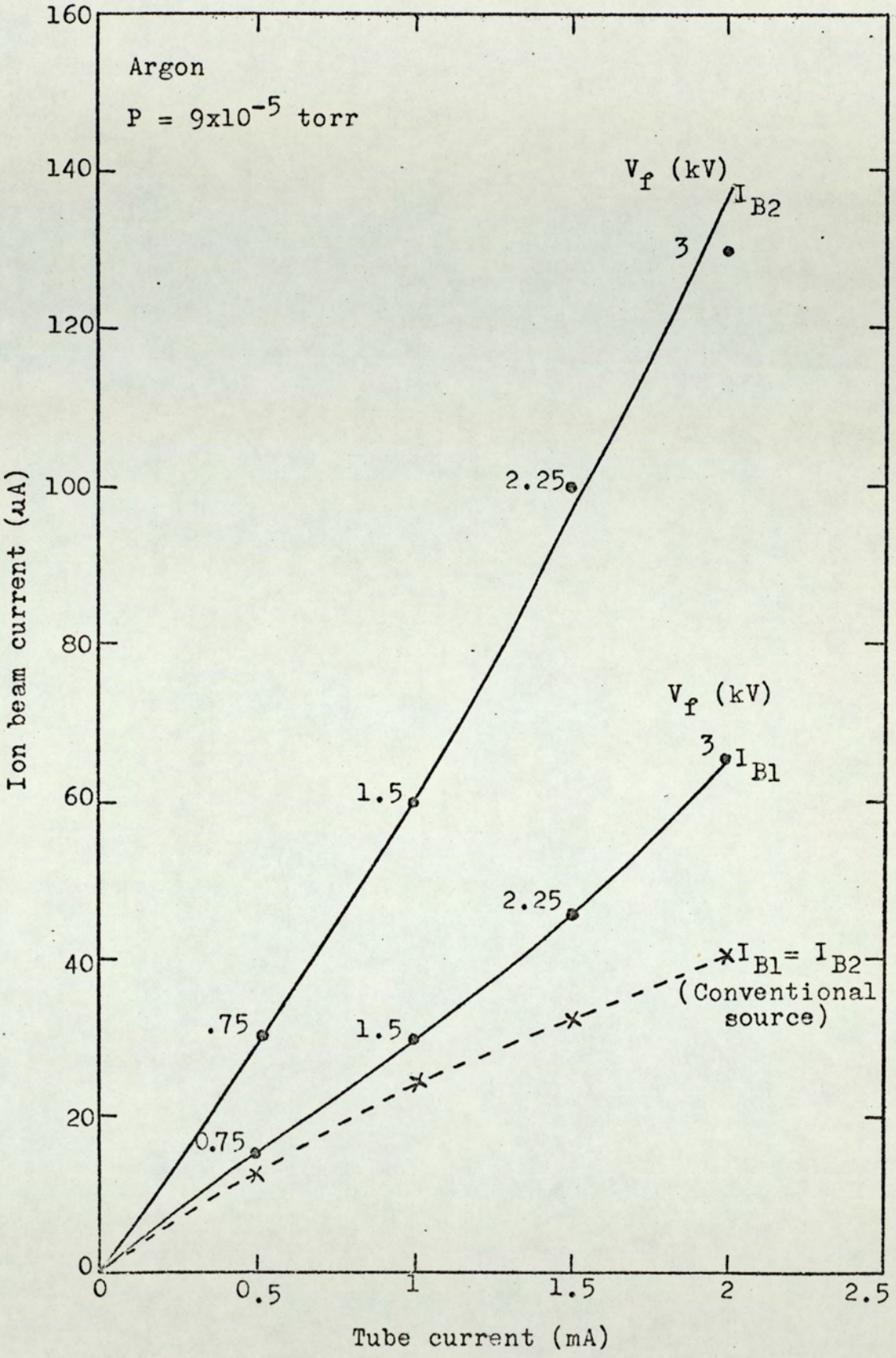

Figure 7.16 Relation between the tube current and the ion beam current.

beam current depends on the electric field strength between the focus electrode and the cathode. At a pressure of 9.5×10^{-5} torr and a tube current of 2 mA, the ion current from the conventional source, I_{B1} and I_{B2} is 40, 63, 130 μA respectively.

7.11. Discussion.

The spherical source is smaller than the cylindrical source which tends to confine the discharge and hence the emerging ion beam has a much higher ion density. One other advantage is that the anode rods used in the cylindrical tend to distort after they get hot, which is not the case with the anode disc.

Rushton and Fitch (1971) noticed a similar effect to that equivalent to the anode hole diameter when they plotted the separation of the two anode rods of a cylindrical source versus the tube current. When the anode hole diameter is large, the potential of the saddle point will be low and the anode exerts a torque on the electrons. This results in a relatively short average total electron path length and thus the source efficiency drops. As the anode hole diameter is decreased, the saddle-point potential increases, so making the electrostatic field appear to be more like a central force field (Rushton, 1972). Hence, the total electron path length tends to increase and so the discharge will build up and would continue to increase as the anode hole diameter is decreased further. This will continue if it

was not that electrons ejected from the cathode by positive ion bombardment, are ejected in random directions with initial energies of up to several electron volts (Hagstrum, 1953).

It seems then that there exists an optimum anode hole diameter so that the electrons ejected from the cathode are of low velocity and hence the electron oscillate in the electrostatic field with a large path length giving rise to a high source efficiency. However, by decreasing the anode hole diameter further, it seems that the radial electron velocity ejected from the cathode is high enough for the electrons to be captured by the anode before they make useful ionising collision. This would continue until an anode hole diameter is reached where there is a discharge cut-off.

The effect of the variation of the screen hole diameter on the source efficiency may be explained as follows. When the screen hole diameter is small, the electrostatic field would be distorted and hence the required saddle-field configuration is not achieved in which the electrons can oscillate. Experiments have shown that there is an optimum screen hole diameter to produce the field configuration for electrons to have a long total path length to make useful ionising collision before these are captured by the anode.

The figures of the ion density distribution and the beam profile show that the ion beam is constituted from different ion intensities. When using an ion exit

aperture of 1.5 mm. diameter, these beams are, a central dense beam which contains most of the ions, a less intense hollow beam surrounding the dense central beam and another outer hollow beam of much lower ion intensity than the other two beams. Additional outer hollow beams of lower ion intensity were observed when an ion exit aperture of 5 mm. diameter was used. This means that the discharge itself is not uniform and is formed of plasmas of different ion intensities. This may be due to the stability of the electron trajectory at different regions inside the source, very stable in the centre and weaker at points away from the centre. Moreover, it will be demonstrated in the next chapter that these ion beams have different energies. The central beam has the highest energy and the outer beam has the lowest energy. However, since the central beam contains most of the ions it has a big advantage in ion thinning of specimens for examination by electron microscopy.

When a positive ion collides with a gas molecule or atom, two processes can occur. The ion and the molecule exchange momentum and energy and the directions of their motion are changed. Secondly, an exchange of charge can take place. For example, if fast ions are moving through a gas, a collision can result in an ion extracting an electron from a gas atom, resulting in it becoming a fast neutral atom while the slow atom becomes a slow positive ion. The process does not change the number of ions in the system. Charge exchange can also

change the ion energy significantly; an energetic neutral and a thermal ion result from charge exchange between an energetic ion and a thermal neutral. This process is one potential source of energetic neutral atoms.

Another source of neutrals formation is electron recombination. Electrons in a gas may have energies corresponding to that of thermal equilibrium with the gas atoms. When an electron approaches a positive ion, it describes a path that does not necessarily close but may be a hyperbola. To form a neutral system the excess energy of the electron must be lost in some way so that a closed orbit, such as an ellipse, can be formed. The excess energy may be given up to a third body in the immediate vicinity at that incident. As a special case the third body necessary to absorb the surplus energy may be a solid wall.

Since, in the electrostatic ion sources, the ions which are accelerated towards the cathode are continuously met by secondary electrons emitted from the cathode under positive ion bombardment. The result would be that some energetic neutral ions are formed at the cathode wall. These neutrals are reflected back into the discharge and get reionized. The neutral ions which are formed close to or in the vicinity of the ion exit aperture are able to escape with the positive ions.

It may also be that some neutrals are being formed by charge-exchange process, but since when a bigger ion

exit aperture was used, the number of neutral ions decreased. Therefore, it is assumed that the neutral ions component in the beam is due to electron recombination to positive ions at the cathode wall, and charge exchange process.

When a source with a focus-electrode was used, it was found that the ion beam current is a function of the field strength between the focus-electrode and the cathode. This is one proof that more ions are allowed to emerge from the source under the influence of the focus-electrode voltage.

8. ENERGY DISTRIBUTION MEASUREMENTS AND MASS ANALYSIS

8.1. Introduction.

An important parameter of ion sources is the energy distribution of the ions extracted from the source. For example, in order to effect mass separation, which is needed, for example, for ion implantation, or beam focusing when dispersion ion-optical element is used, the distribution of initial energies of the ions created in the source should be minimum. Also, in order to obtain uniform ion etching or thinning, the ion beam should have a uniform current density as well as a small energy spread as possible.

One other important parameter of an ion source that must be considered for a given use is the type of ion species it is capable of producing. For example, many semiconductors are sensitive to very small concentrations of impurity atoms and in ion implantation, which is a process of doping impurities, restrictions must be placed on the purity of the ion beam. The ion beam should not contain species, other than the one desired, of nature and concentration that should cause undesired electrical activity in the substrate. Also in particle accelerators some need a high percentage of protons beams and others need beams of multicharged ions.

It is therefore clear that it is important to know the energy distribution measurement and mass analysis

of ion beams emergent from the electrostatic oscillators ion sources are realized. In this chapter investigations of the energy distribution measurement and the mass analysis are reported.

8.2. The energy distribution measurement.

8.2.1. The energy analyzer.

The energy distribution of the emergent ion beam was investigated using a simple retarding field energy analyzer which is illustrated in Fig. (8.1). This energy analyzer was made from two stainless steel meshes that were 40% transmission. A positive potential, $V_R^{\backprime}$, was applied to the retarding grid and the screening grid was at earth potential. The purpose of the screening grid was to screen the Faraday cup from the high field produced by the retarding grid, so that the secondary electrons from the Faraday cup were not accelerated towards the retarding grid.

The reason a grid construction electrostatic energy analyzer was used is that the cross section of the ion beam from the electrostatic oscillators is large and hence grids, which give localized electric field of any area, can be used to accommodate all the beam.

8.3. Measurement of energy distribution.

8.3.1. The twin anode source.

The variation of the ion current collected by the Faraday cup with $V_R^{\backprime}$ was studied. This is shown for nitrogen at a pressure of 5×10^{-4} torr in Fig. (8.2).

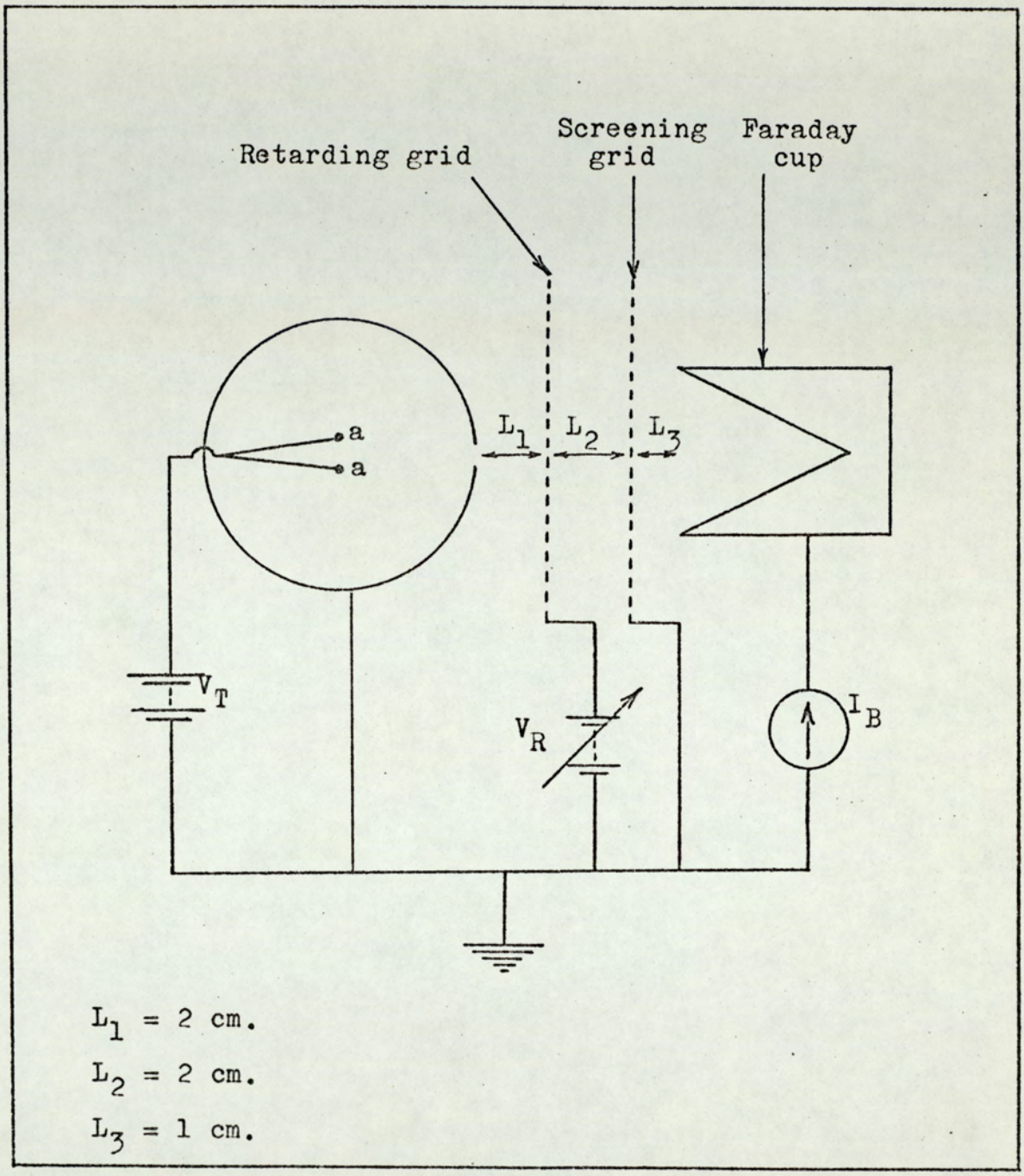

Figure 8.1 Schematic diagram of the energy analiser.

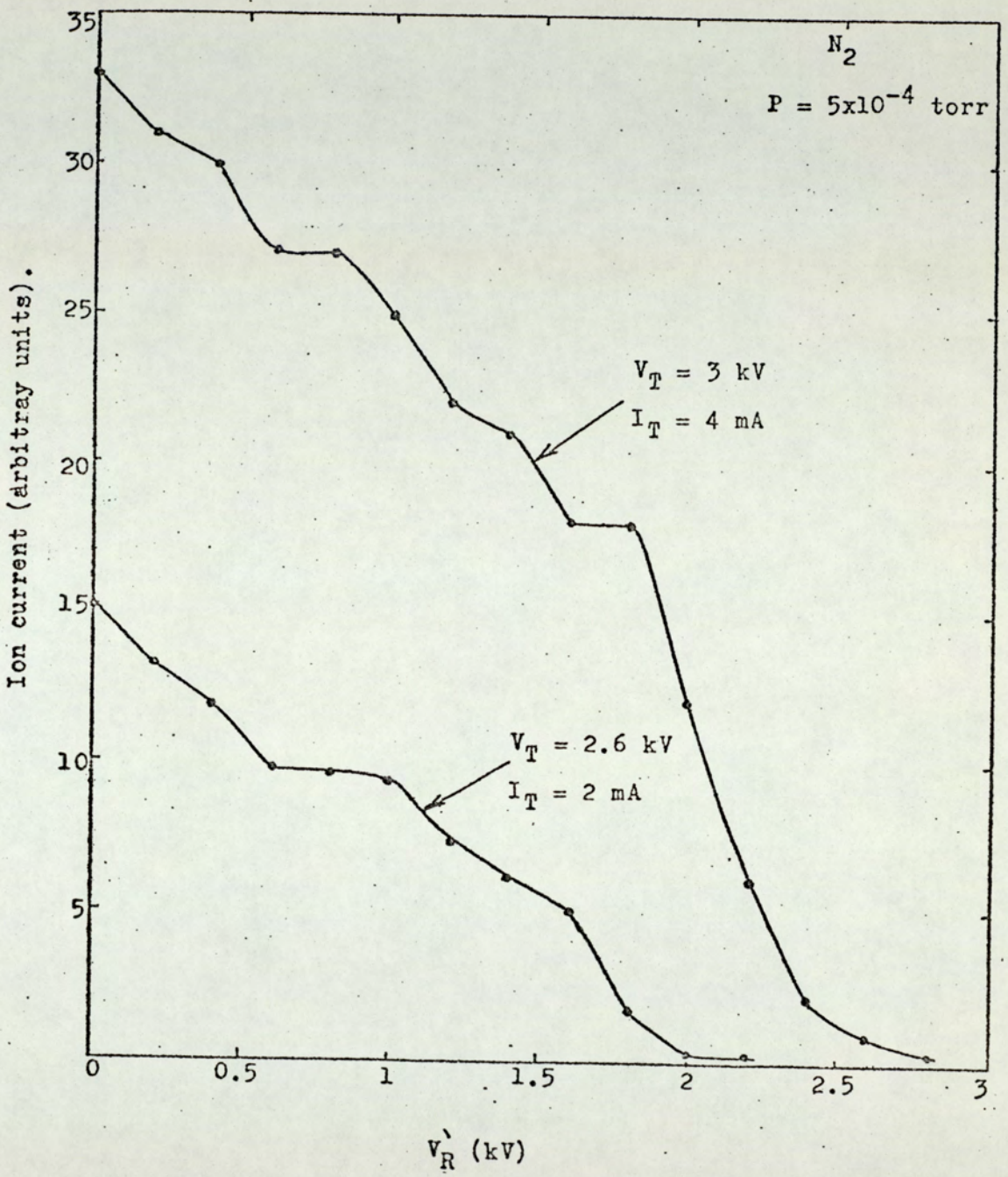

Figure 8.2 The energy distribution for nitrogen.

The energy distribution curves were obtained from such curves shown in Fig. (8.2) by subtracting the ion current at V_R' from that at $V_R' + \Delta V_R'$ and then the resultant ion current was plotted against $(2V_R' + \Delta V_R')/2 = V_R$. A large number of energy distribution diagrams were obtained for different gases and at different experimental conditions. It was found that nitrogen and argon behave in a very similar way but not helium.

The energy distribution for nitrogen at a pressure of 5×10^{-4} torr and at tube current of 2 and 4 mA and tube voltage of 2.6 and 3 kV, as obtained from Fig. (8.2) are shown in Figs. (8.3) and (8.4) respectively. Fig. (8.5) also shows the energy distribution for nitrogen at a pressure of 7×10^{-4} torr, a tube current of 6 mA and a tube voltage of 2.5 kV. These curves were for nitrogen emerging from the cylindrical source described in Chapter 4 and with an ion exit aperture of 3.2 x 10 mm.

It can be seen that the energy of the ions is broad and exhibit different peaks of different ion intensities. The energy of the ions ranges from a few eV to about 0.8 eV_T. The shape of the energy distribution curves and the intensity of the different peaks are affected by the pressure and the discharge conditions, tube voltage and tube current. It was noticed that the highest energy peak which is also the more intense one, had maximum intensity at a pressure corresponding to that showed in Figs. (5.14), (5.15), (5.16) and (5.18) when the total ion current was maximum. At a higher pressure

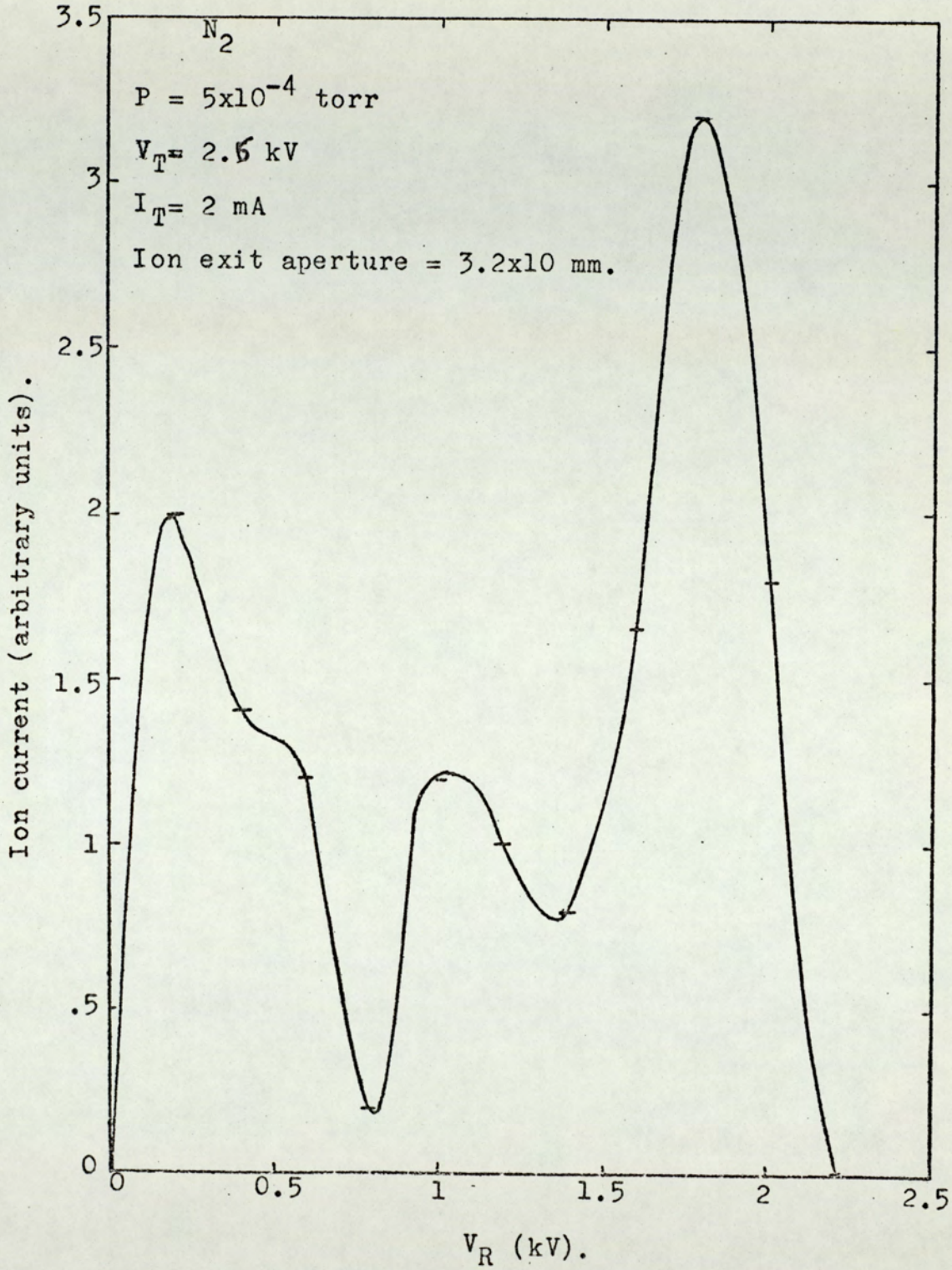

Figure 8.3 The energy distribution for nitrogen.

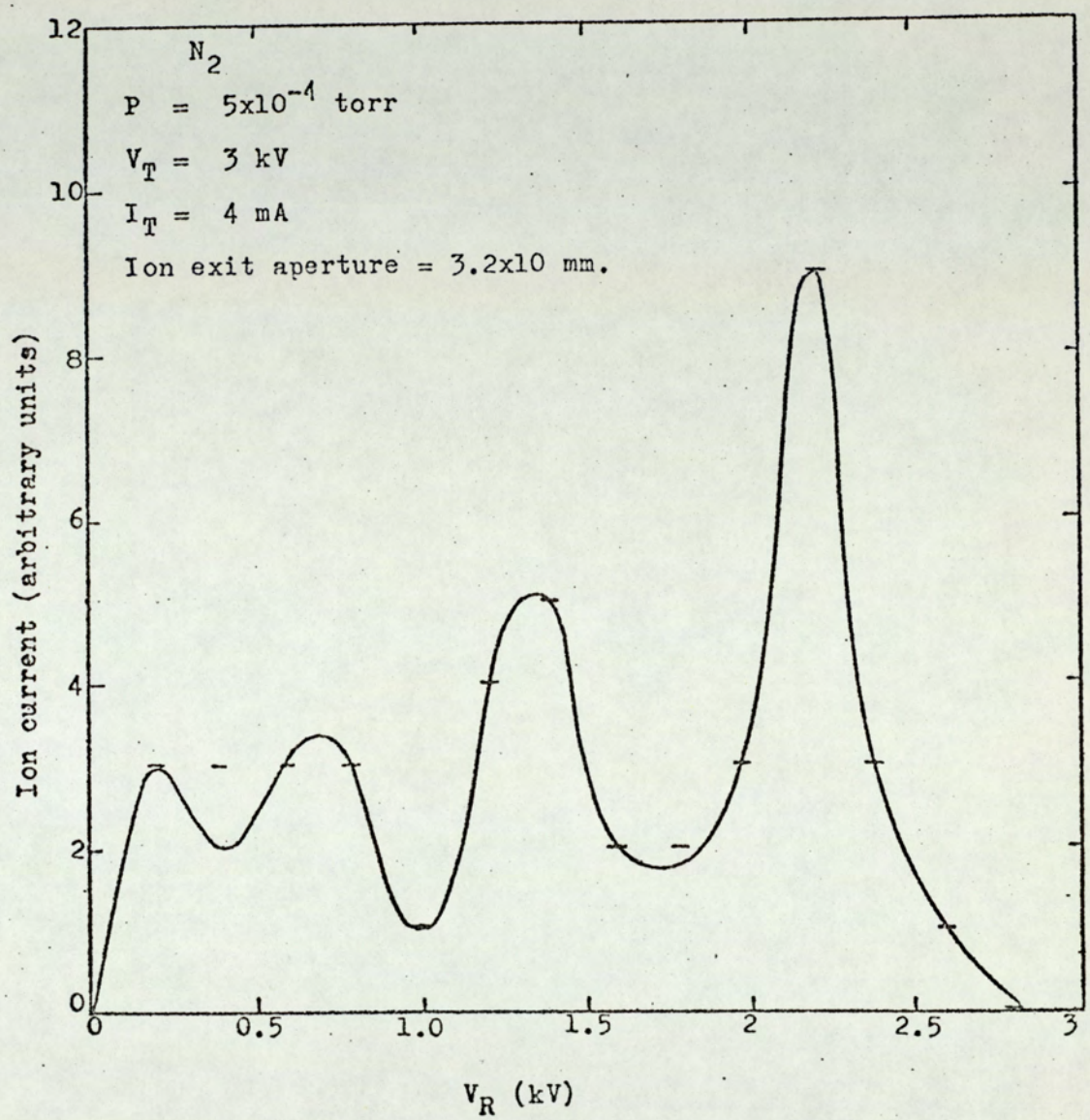

Figure 8.4 Energy distribution for nitrogen.

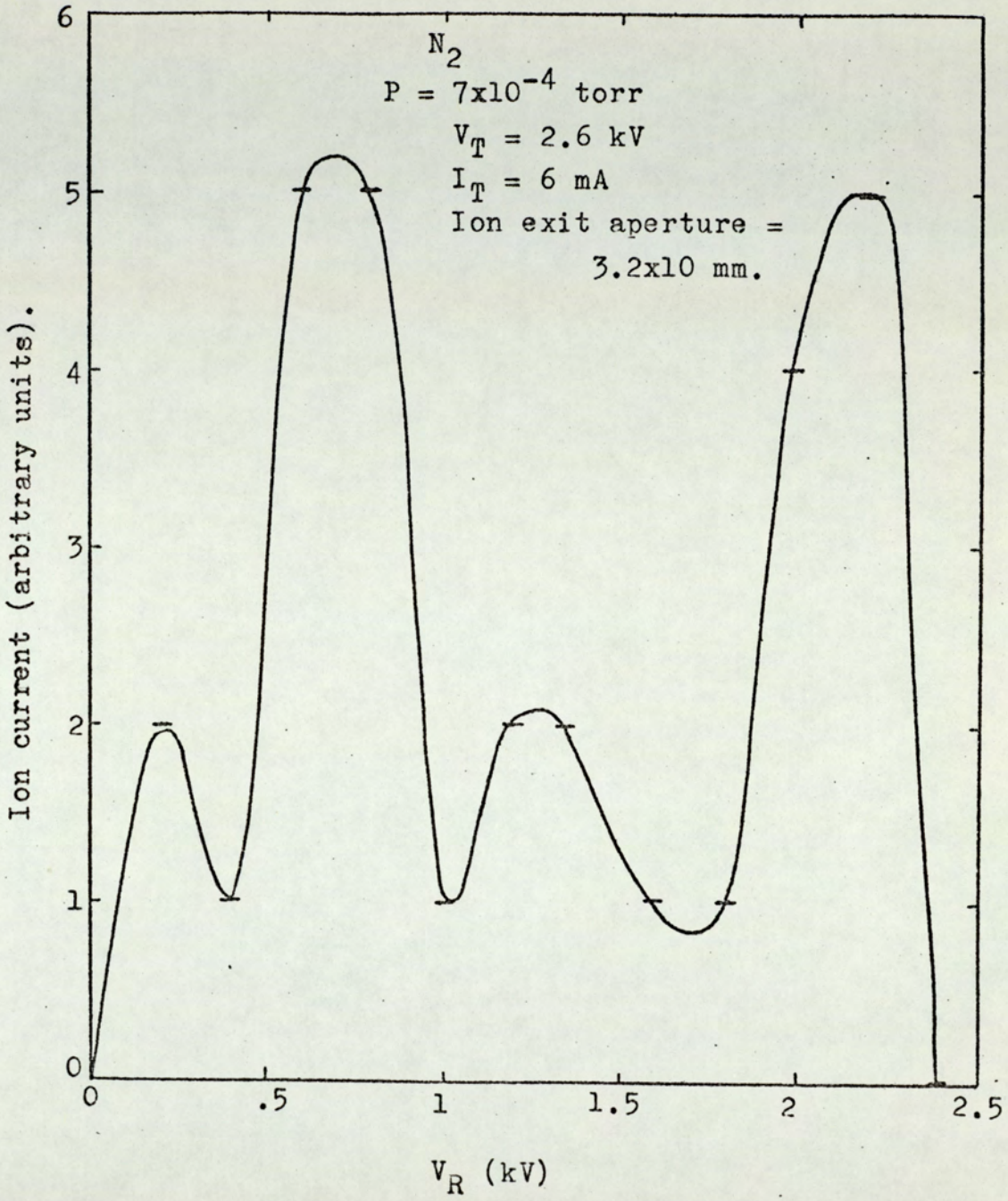

Figure 8.5 The energy distribution for nitrogen.

the intensity of this high energy peak was found to be minimum and those of lower energies contribute more to the ion beam.

When using an ion exit aperture of 5 mm. diameter another peak appeared in the energy distribution as shown in Fig. (8.6). It can also be seen that the lower energy peaks contribute more to the ion beam than when a rectangular ion exit aperture of 3.2 x 10 mm. was used.

Although nitrogen and argon were found to behave very similarly, helium behaved differently. Fig. (8.7) shows the energy distribution for helium at a pressure of 7×10^{-5} torr, tube current 4 mA, tube voltage 2.4 kV with an ion exit aperture of 3.2 x 10 mm. It can be seen that the highest energy peak is no longer the most intense and instead a lower energy peak at 0.4 kV is the most intense one. It was noticed that the central intense discharge line which was observed in the case of argon and nitrogen discharges, was hardly seen. This was confirmed by ion etching of a copper film.

It was thought that the peaks in the energy distribution are due to ions coming from different positions from inside the source. A source of the same dimensions as used before, with three ion exit apertures of 1 mm. diameter each was used. The three apertures were equally spaced at 1 mm. apart. The first one was at the centre, the second and the third were at 2 mm. and 3 mm. from the centre. The energy distribution of each individual ion beam was investigated. Fig. (8.8) shows

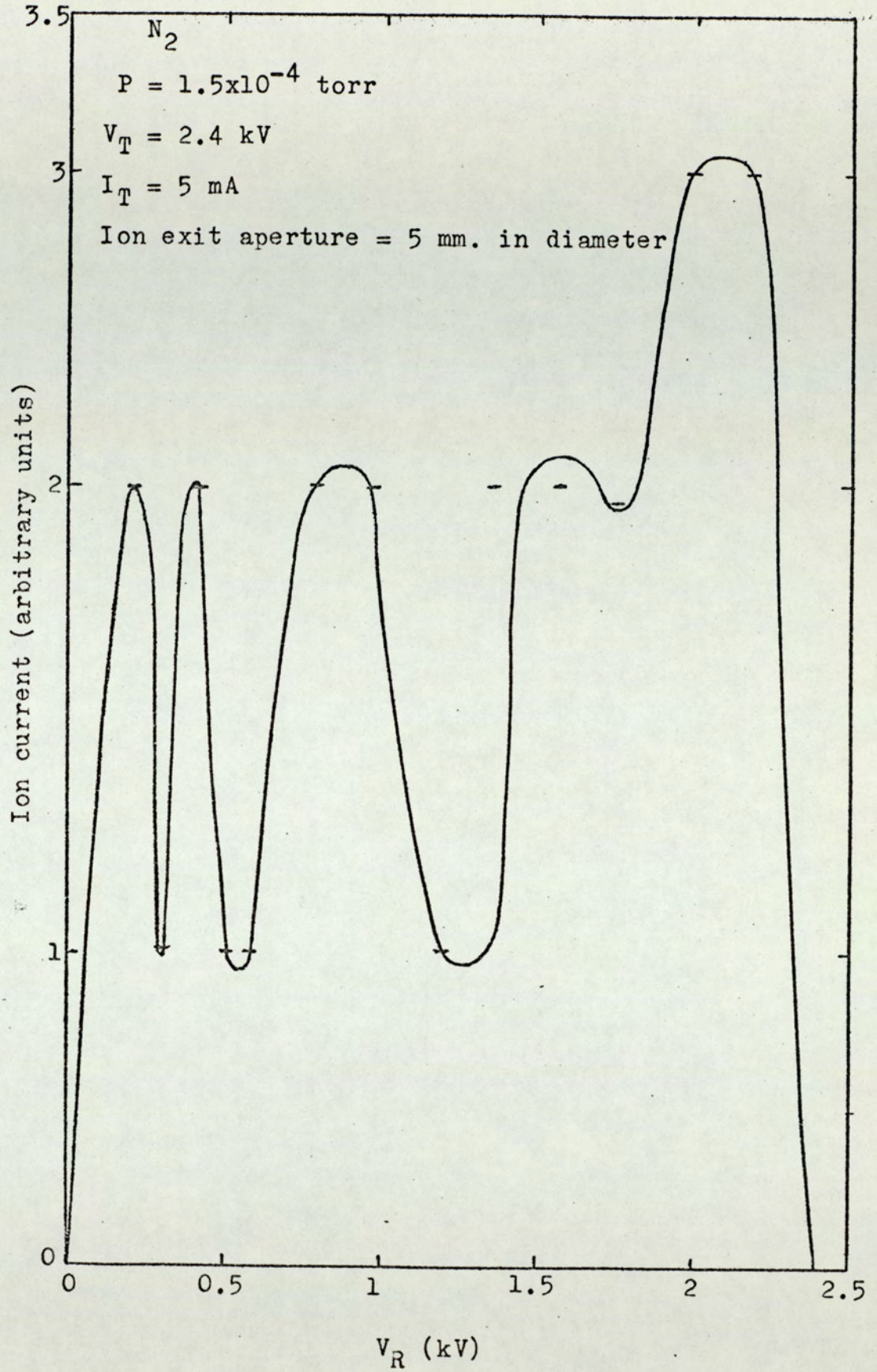

Figure 8.6 Energy distribution for nitrogen.

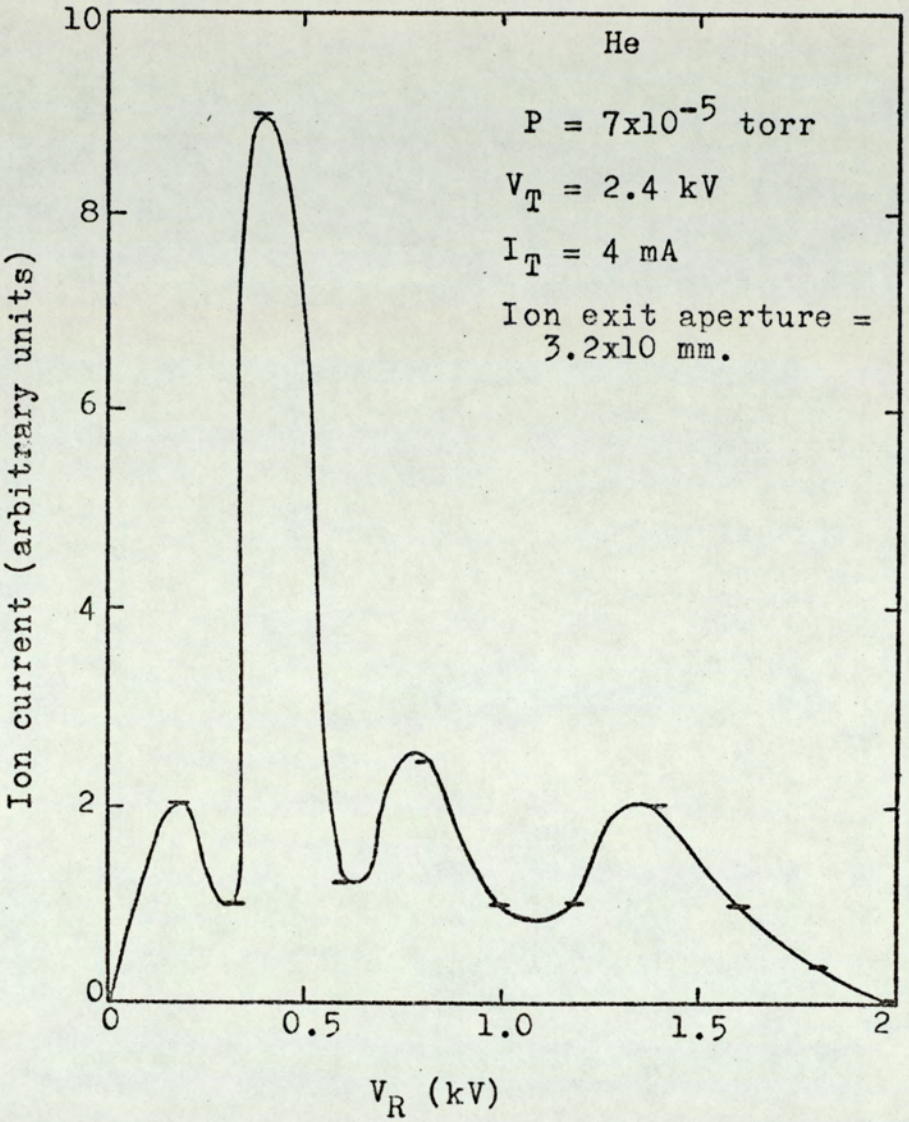

Figure 8.7 Energy distribution for helium.

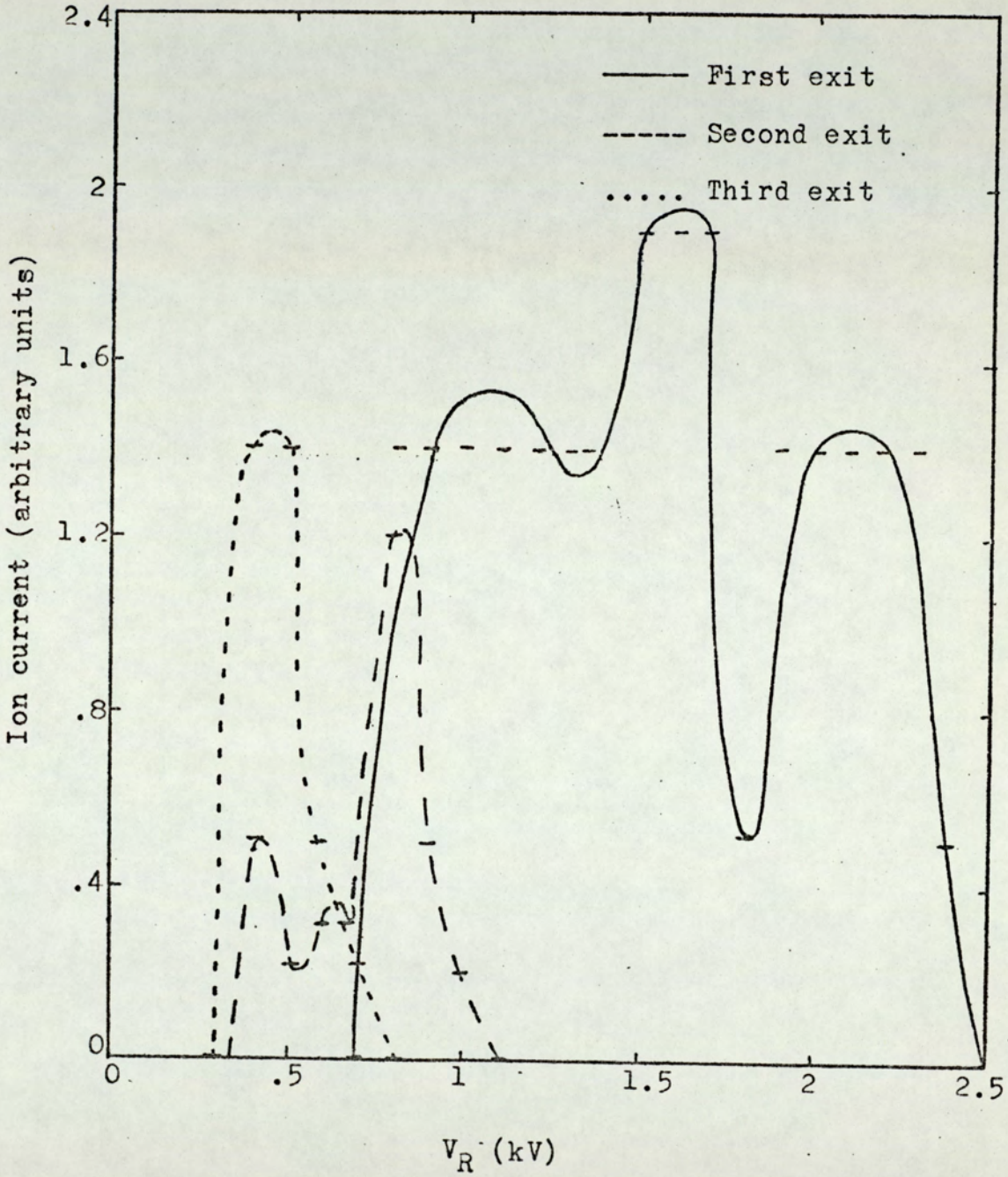

Figure 8.8 Energy distribution for ions emerging from different aperture in different position of the ion source.

the energy distributions of the three beams. It can be seen that the highest energy ions are coming from the centre and that the ion energy decreases in the X-direction. One other result of this experiment is that the lowest energy peak in Figs. (8.3), (8.4), (8.5), (8.6) and (8.7) was not observed.

8.3.2. The spherical source.

The energy distribution of the emergent ions from the spherical source was investigated when an ion exit aperture of 1.5 mm. was used. Figs. (8.9) and (8.10) show the energy distribution for argon. Fig. (8.9) was taken at a pressure of 8×10^{-5} torr, tube current 2 mA and tube voltage 6.4 kV, while Fig. (8.10) was taken at a pressure of 2×10^{-4} torr, tube current 4 mA and tube voltage 6 kV.

It can be seen that the ion beam from the spherical source has only a high intensity energy peak with a low energy tail. It seems that the low energy tail has two low intensity peaks which cannot be clearly resolved. However, this does not contribute much to the total ion current. The high energy peak has an energy equivalent to about 0.83 of the anode voltage and its half-width is about 250 volts.

However, when a bigger ion exit aperture was used some more low energy peaks were observed, the number of which depends on the size of the ion exit aperture.

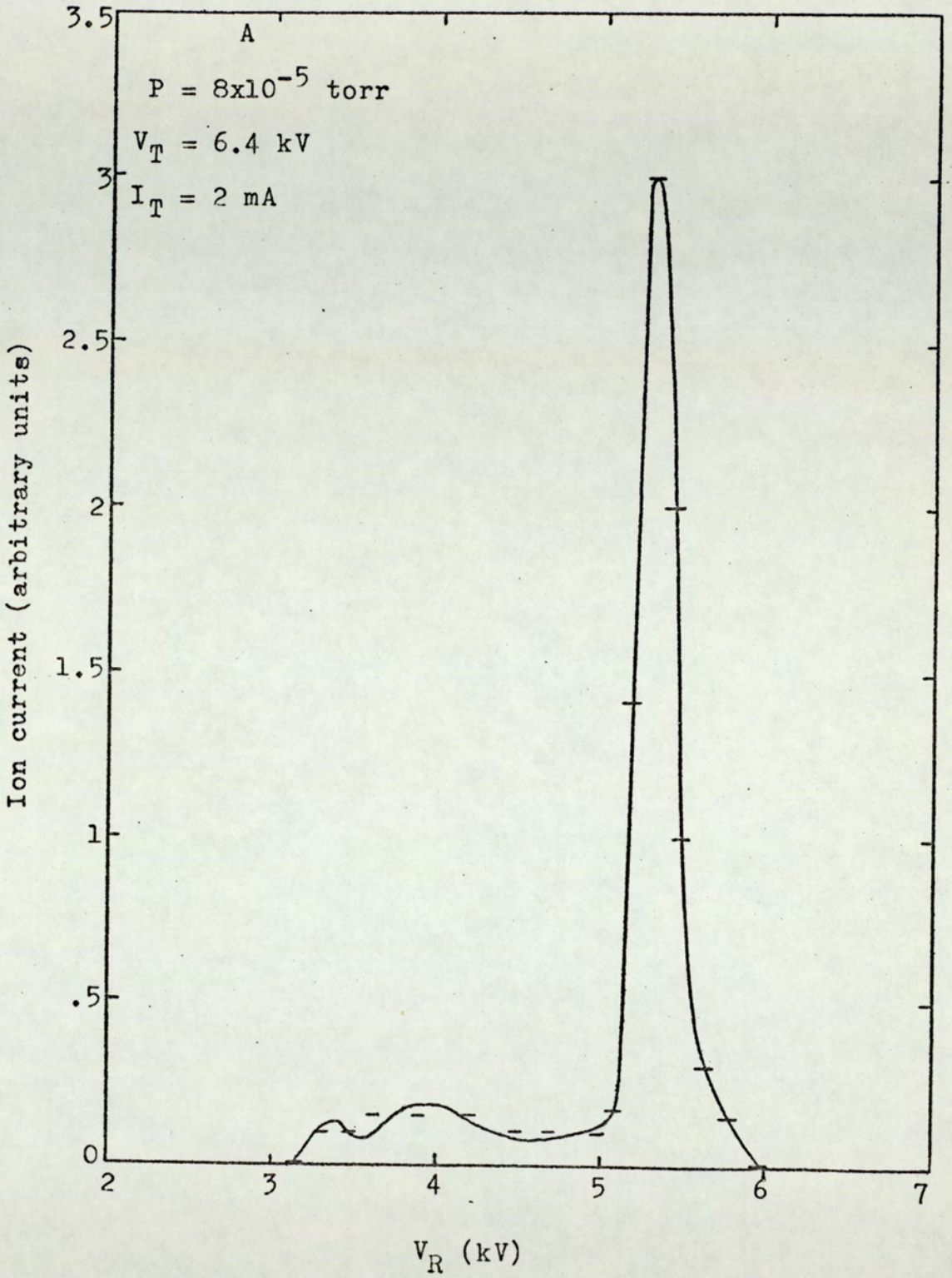

Figure 8.9 Energy distribution of ions from the spherical source.

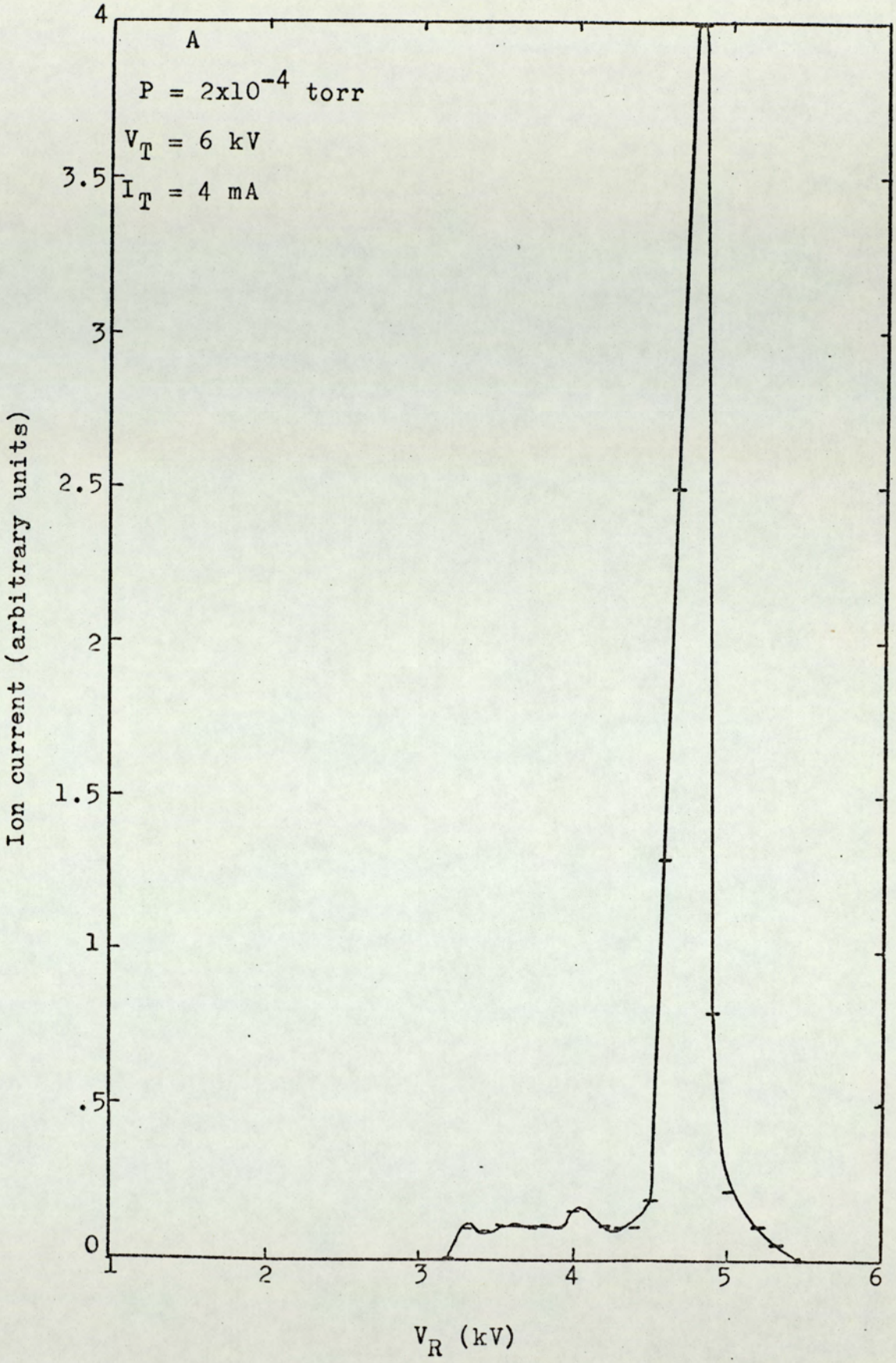

Figure 8.10 Energy distribution of ions from the spherical source.

8.3.3. Sources with focus electrodes.

The energy distribution of ions emerging from the cylindrical and spherical source with focus electrodes was also investigated. Fig. (8.11) shows the energy distribution of ions from a cylindrical source with an ion exit aperture of 5 mm. diameter and at V_T = 3.2 kV, I_T = 2 mA and V_F = 4 kV. It can be seen that the whole energy spectrum was shifted by the focus electrode voltage on 4 kV as should be expected. There is another energy peak below 4 kV which is probably due to ions formed between the focus electrode and the cathode. It is obvious from Fig. (8.11) that the low energy ions contribute much more to the ion beam than in the case of the conventional source.

Fig. (8.12) shows the energy distribution of ions emerging from the spherical source with an ion exit aperture of 1.5 mm. diameter and with a focus electrode. It can be seen that there are two distinct energy peaks in the low energy tail, beside the main high energy peak.

8.4. Mass analysis.

8.4.1. The ion source.

Drawings of two views of the cylindrical ion source used for mass anlysis is shown in Fig. (8.13). The source was mounted on a flange as shown in Fig. (8.13). The cathode was made from stainless steel of internal diameter 5 cm. and length 10 cm. enclosing two stainless steel tubular anodes of outside diameter 2.5 mm. at a separation of 10 mm. An ion exit aperture of 18 x 3mm was

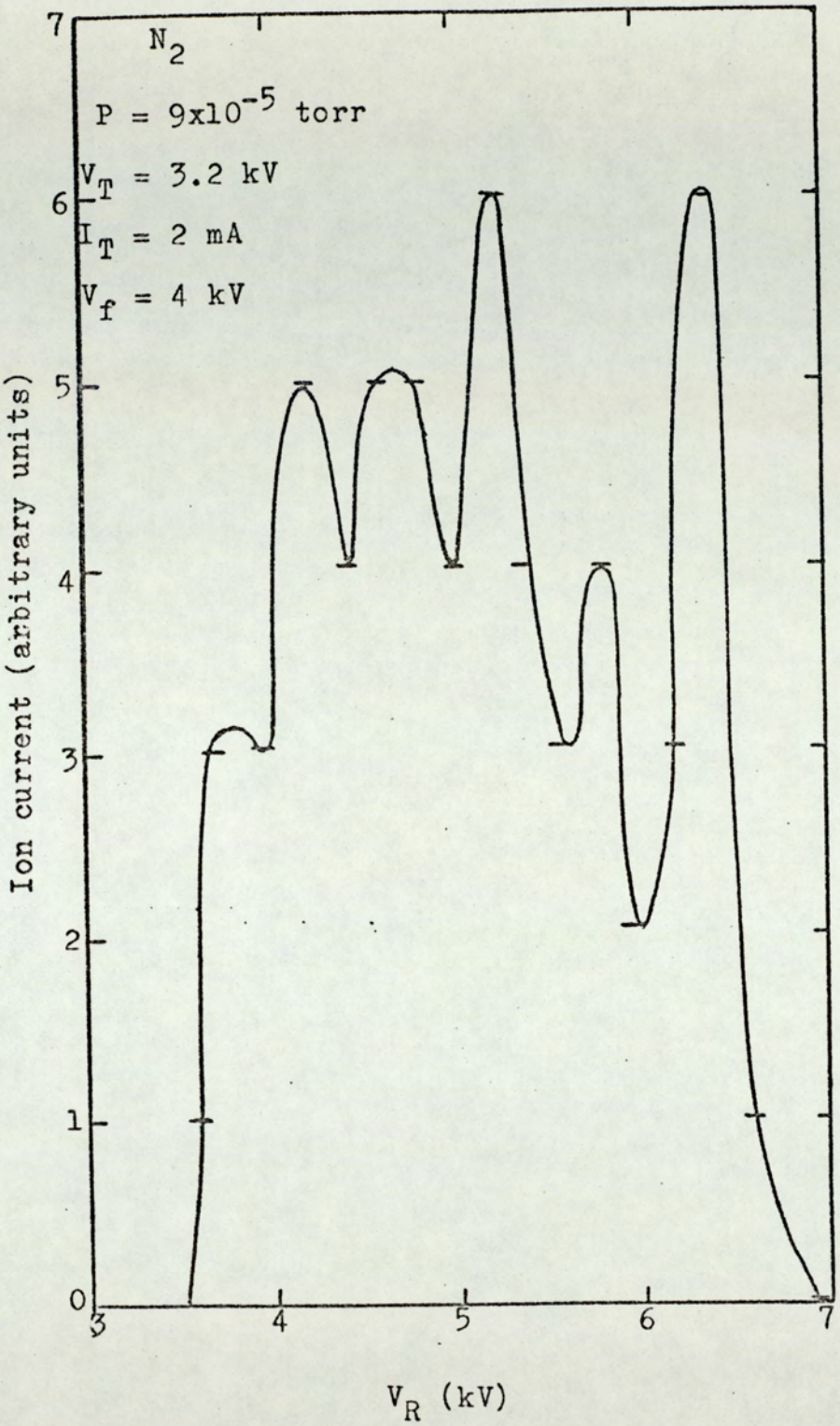

Figure 8.11 Energy distribution for ions from the cylindrical source with a focus-electrode.

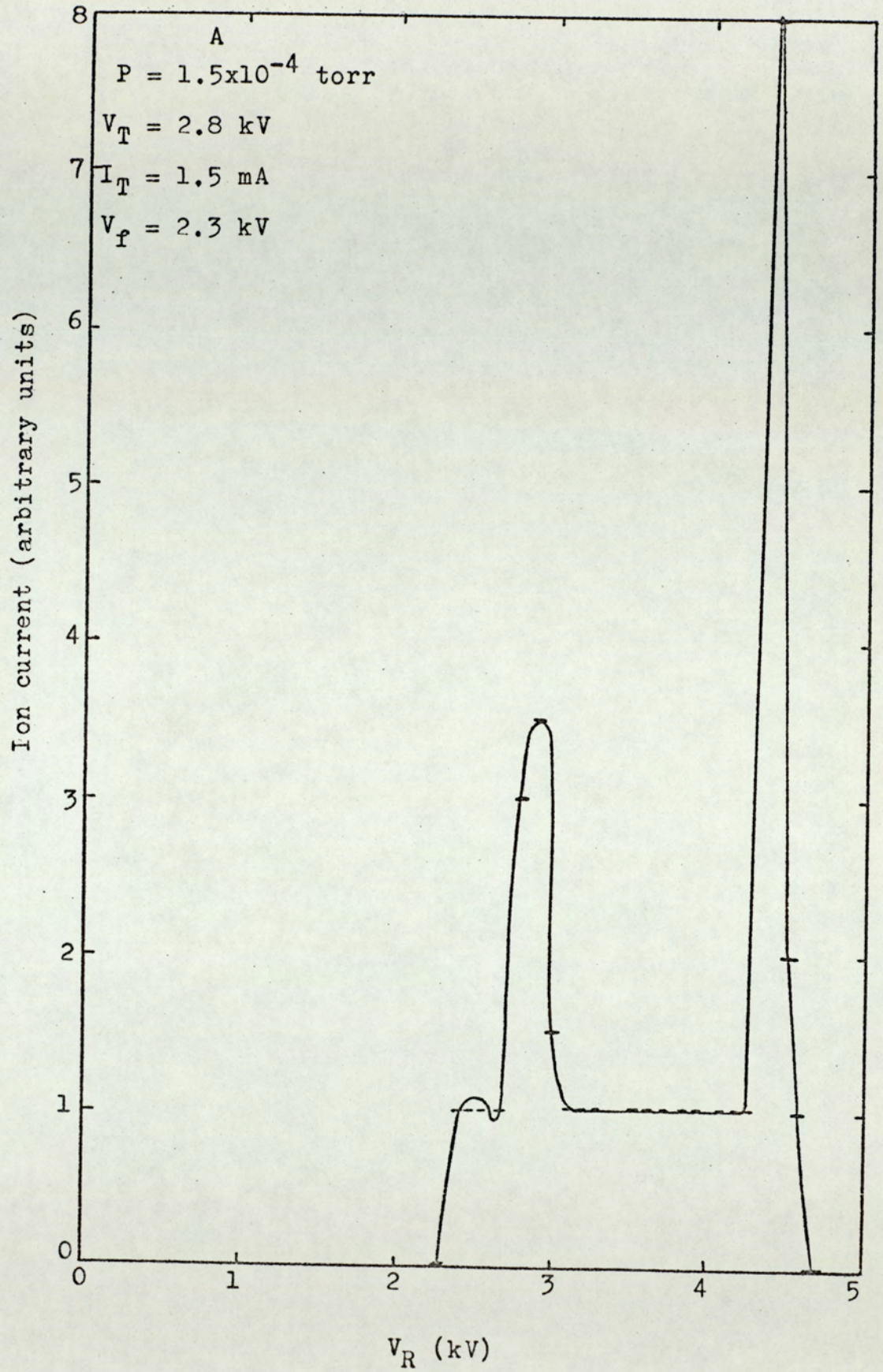

Figure 8.12 Energy distribution for ion from the spherical source with a focus electrode.

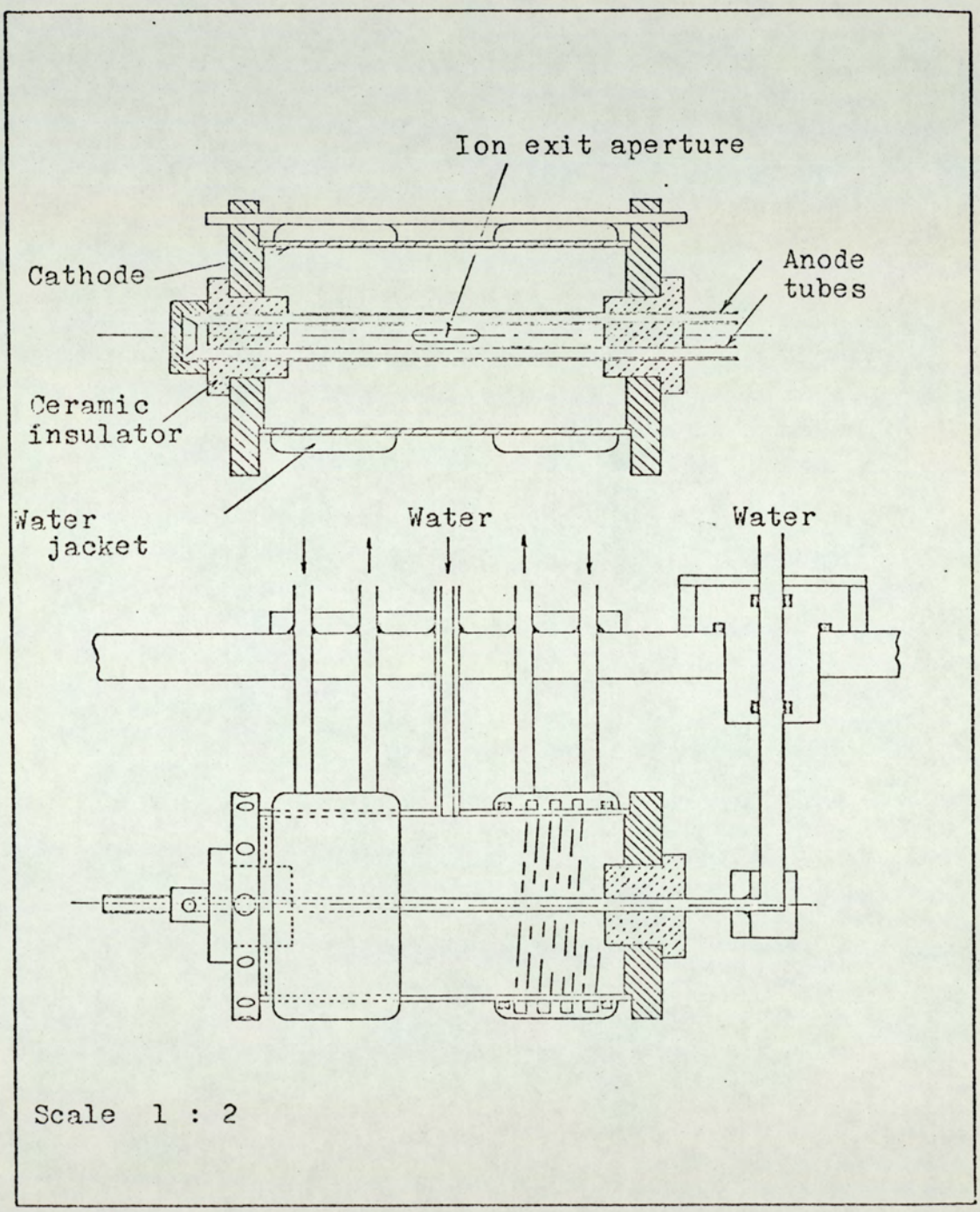

Figure 8.13 Drawing of the water-cooled source.

used. The anodes and the cathode were water cooled as it has been found that a cooled source is much more stable and higher ion currents can be obtained (Fitch et al, 1974). The anodes were water cooled by running water through these and 'O' rings were used to seal them. The water tubes for the anode were isolated from the mounting flange by a teflon insulator. The cathode was water cooled by two jackets surrounding the cathode at the two sides of the ion exit aperture. Photographs of two views of the water-cooled ion source are shown in Fig. (8.14).

8.4.2. The experimental arrangement.

A schematic diagram of the apparatus which is situated in the Linear Accelerator Laboratory of the University of Manchester is shown in Fig. (8.15). The complete system is evacuated by a conventional liquid nitrogen trapped oil diffusion pump and rotary pump.

The emergent ion beam is passed through an Einzel lens to reduce its divergence. It has been shown that the energy of the ions emerging from the cylindrical source range from a few electron volts up to about 80% of the source anode voltage, hence it was necessary to accelerate the ions up to 50 kV in order to increase the resolution of the analysing system. After the ions are accelerated, the ion beam is collimated with two 1.5 mm. diameter apertures 15 cm. apart before it enters the analyzer. The analyzer consists of an electromagnet providing a uniform field of 0 to 5 kG and a Faraday cup set at an angle of 10^{o} to the axis of the collimator. The cup

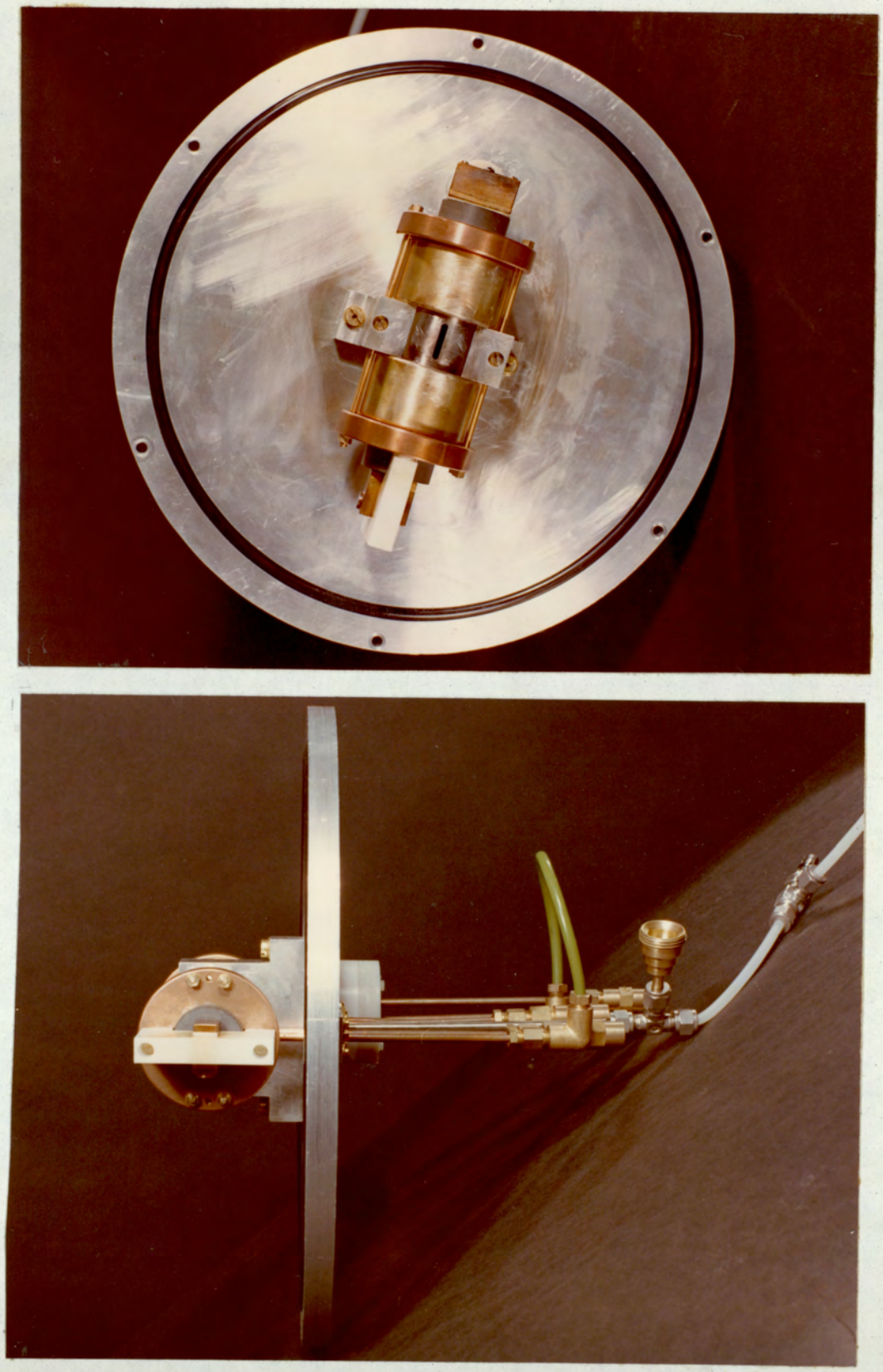

Figure 8.14 Photographs of the water-cooled source.

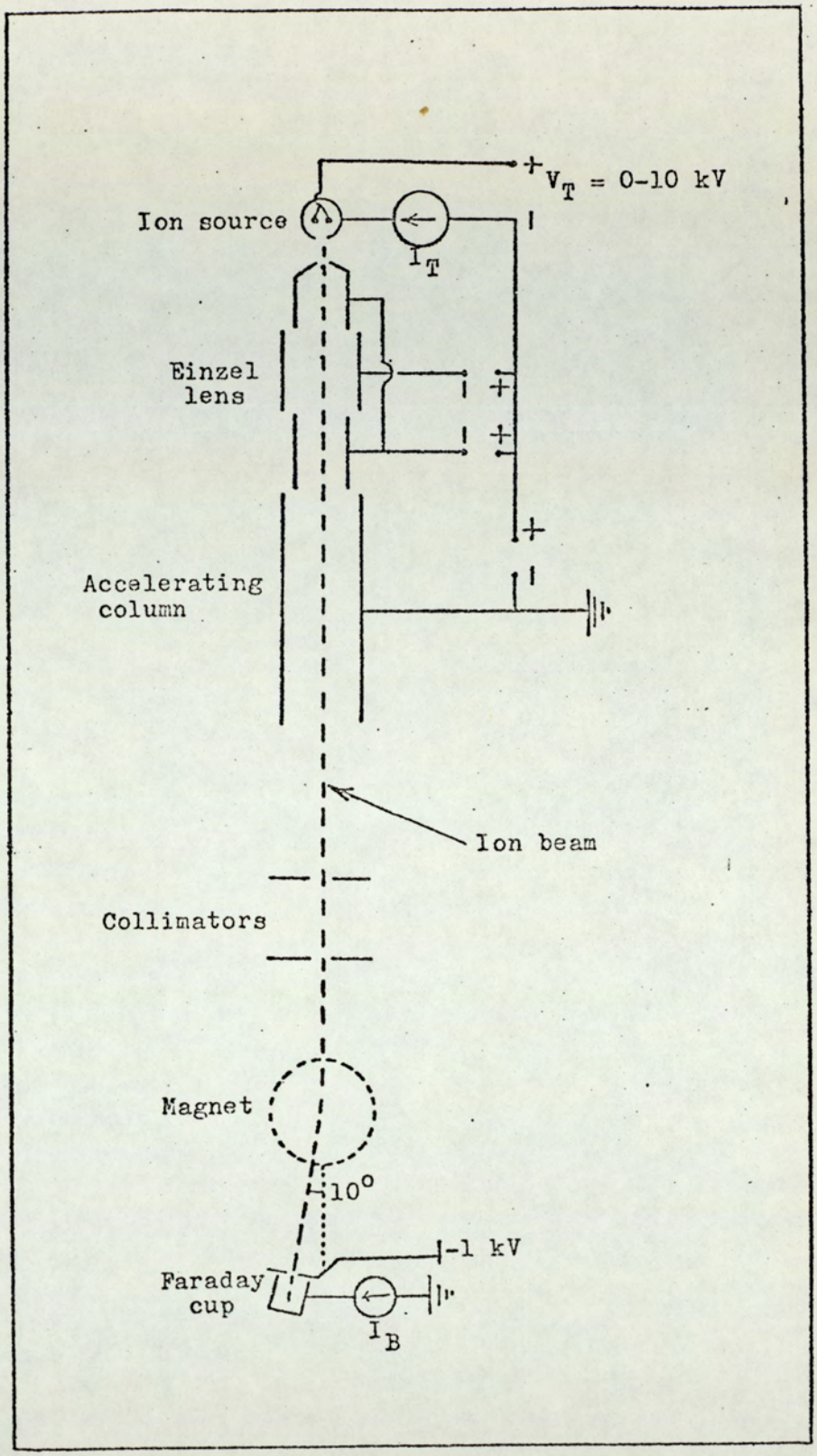

Figure 8.15 Experimental arrangement for the mass analysis.

includes a secondary electron suppressor electrode which is held at a potential of 1 kV negative with respect to the ion collector. The distance between the ion exit aperture and the Faraday cup was about 2 m.

8.4.3. The magnet calibration.

The variation of the magnetic field with the magnet current is shown in Fig. (8.16). It can be seen that the hysteresis effect is small in the order of 100 G between increasing and decreasing the field.

The variation of the magnetic field with the axial distance from the centre of the magnet is shown in Fig. (8.17). It can be seen that the magnetic field remains constant in the centre of the field in a region of radius of about 6 cm. The field falls off very rapidly before the Faraday cup and is therefore negligible.

8.4.3. Experimental results.

The mass spectra for nitrogen, argon, helium, and hydrogen were investigated by studying the variation of the Faraday cup ion current with the magnetic field. The different peaks in the spectra could be identified, since the motion of the ions in the magnetic field is governed by:

$$m_i v_i^2/R_c = H Z e v_i \quad \ldots\ldots (8.1)$$

Where H is the magnetic field strength, Z is the charge number, R_c is the radius of curvature and v_i is the ion velocity which is given by:

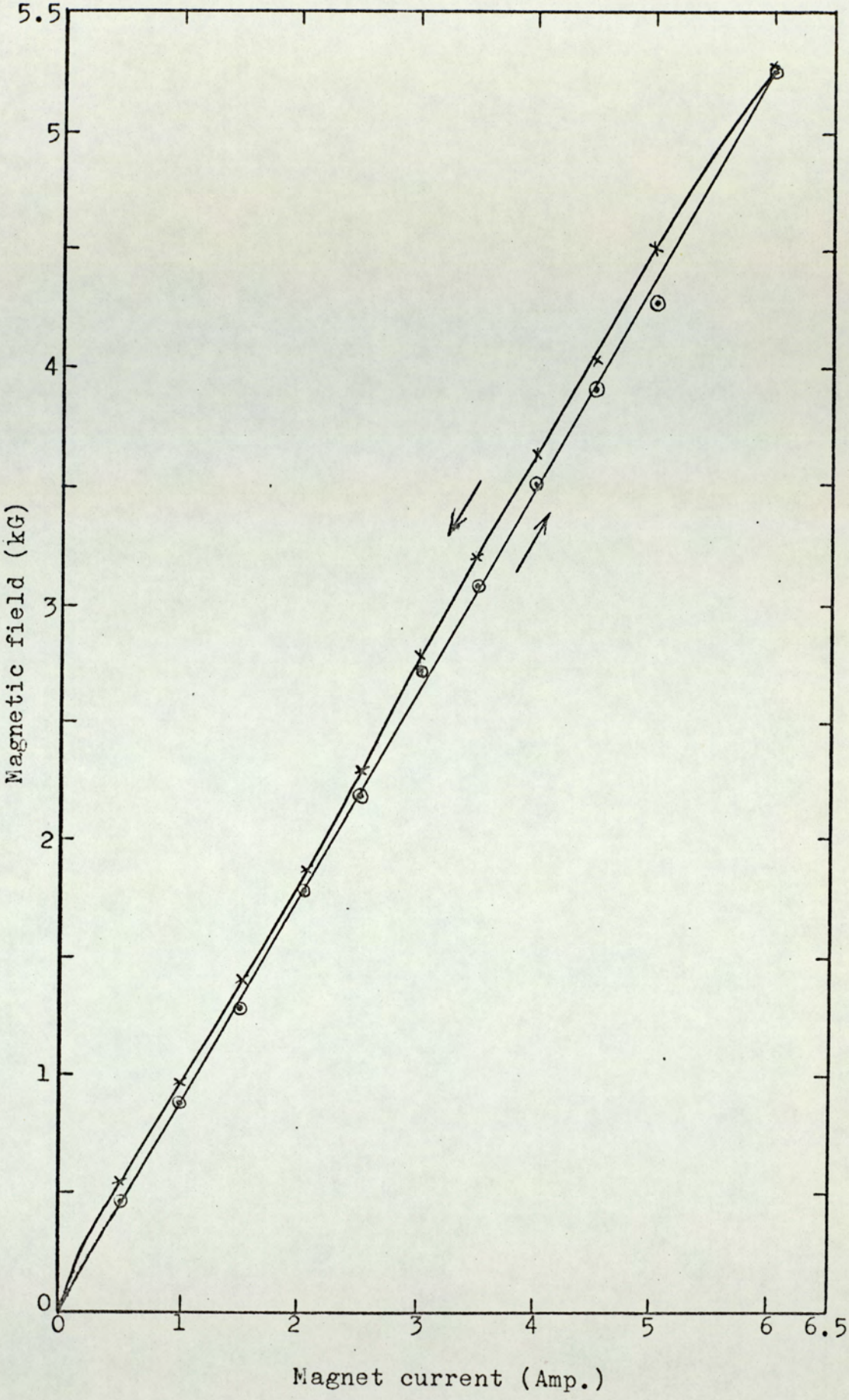

Figure 8.16 The magnet calibration.

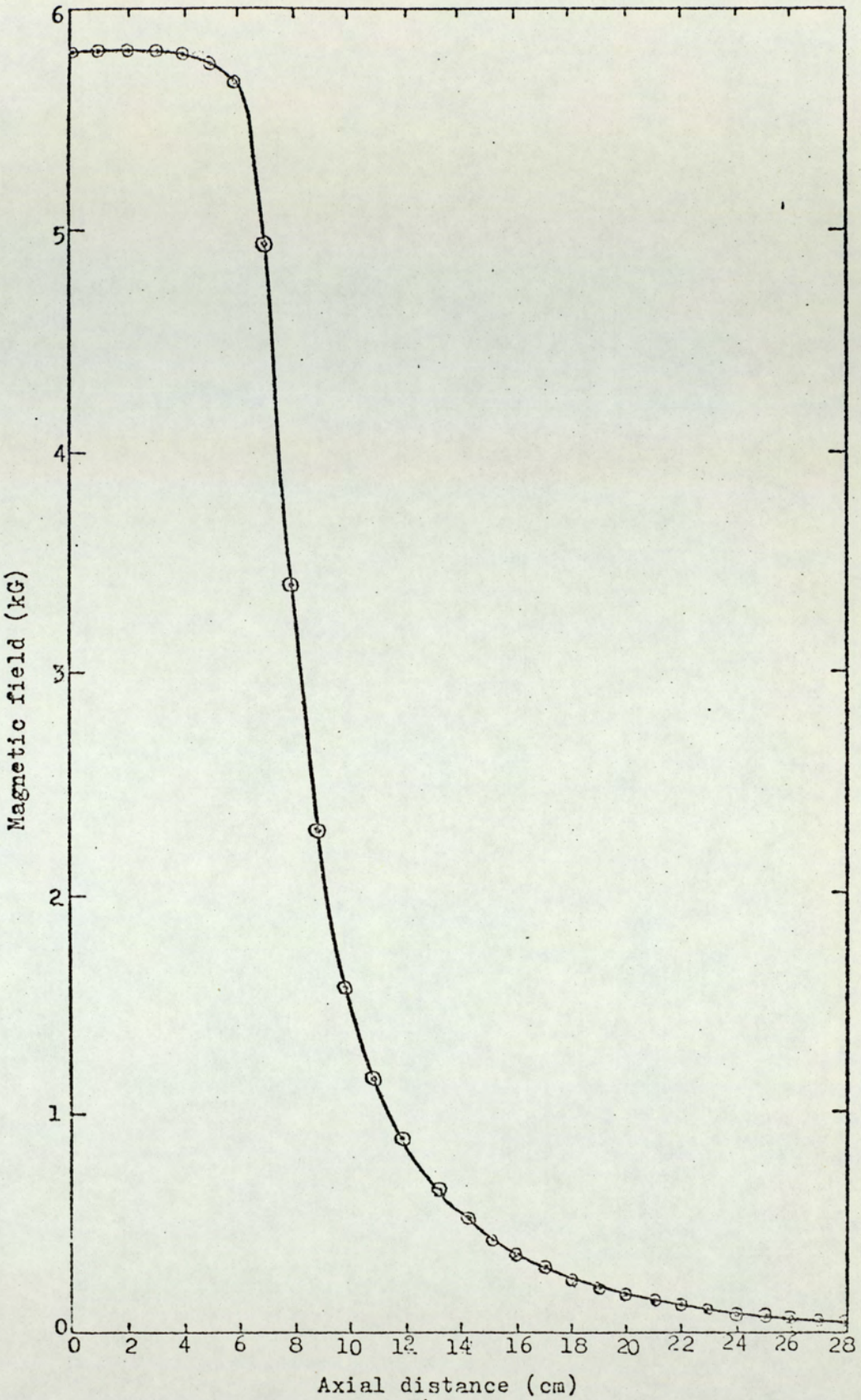

Figure 8.17 The variation of the magnetic field with the axial distance.

$$\frac{1}{2} m_i v_i^2 = Z e V_{as} \quad \ldots\ldots (8.2)$$

Where V_{as} is the voltage with which the ions are emerging from the source plus the accelerating voltage. R_c was constant because the Faraday cup was kept at a fixed position, and therefore for a constant ion energy,

$$H \propto \frac{m_i^{\frac{1}{2}}}{Ze} \quad \ldots\ldots (8.3)$$

Therefore, the different peaks in the spectra could be identified using Eq. (8.3).

The spectra for nitrogen at a chamber pressure of 3.5×10^{-5} torr and at tube voltages V_T of 5 and 5.5 kV and tube current I_T of 20 and 25 mA respectively are shown in Figs. (8.18) and (8.19). There are four well defined peaks in the spectra in both figures; these correspond to the molecular ion N_2^+ and the atomic ions N^+, N^{2+} and N^{3+}. The percentage of N^+ is higher than N^{2+} but, as can be seen from the two figures, increasing the input power of the source increases the abundance of N^{2+} and N^{3+} with respect of N^+.

The spectra for argon is given in Fig. (8.20) in which Ar^{2+} is the dominant ion and Ar^+ and Ar^{3+} are present in only small proportions. The spectra for helium and hydrogen are given in Figs. (8.21) and (8.22) respectively. It can be seen that with the two gases the source produces mainly He^+ and H_2^+ and that He^{2+} and H^+ are only present in small proportions.

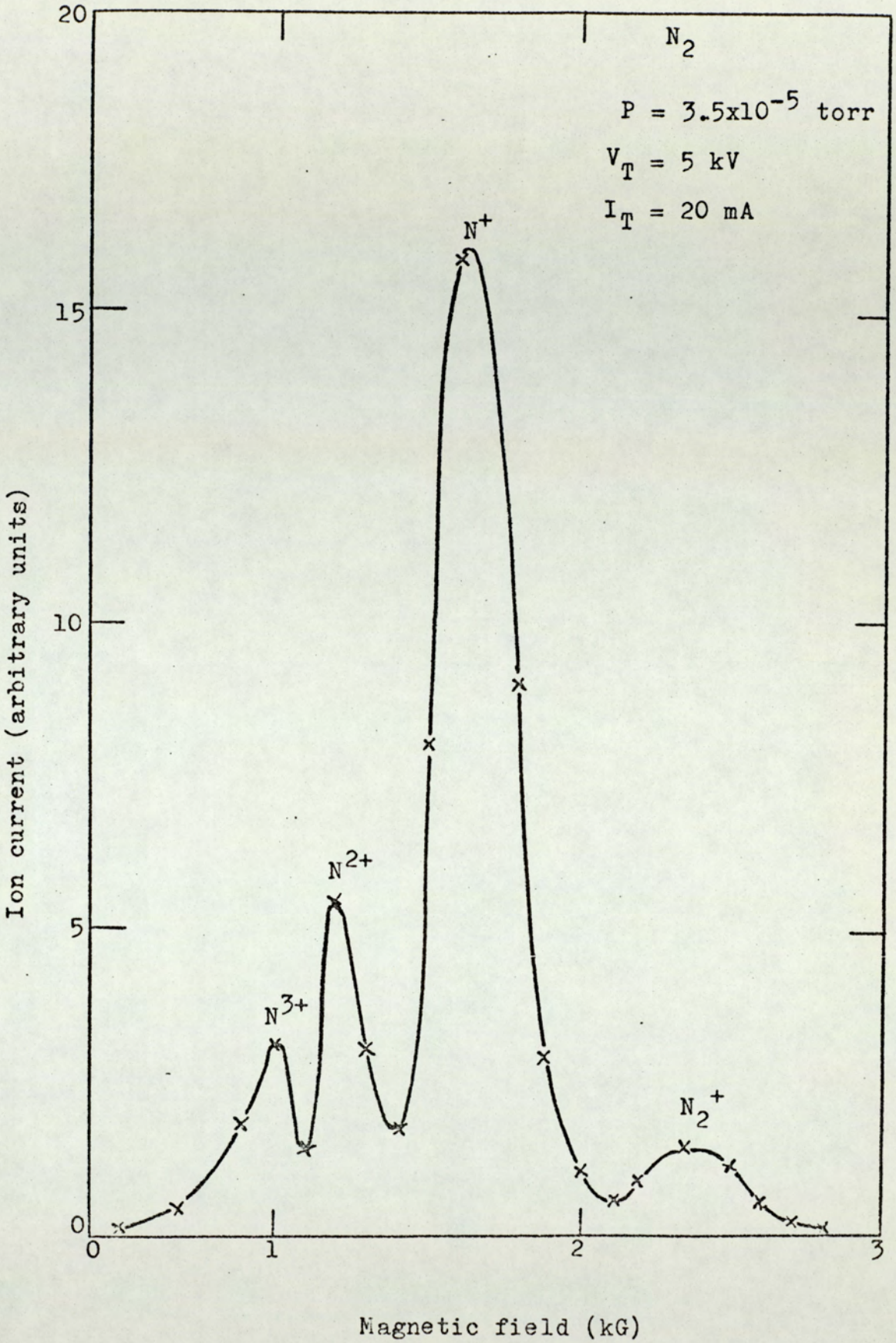

Figure 8.18 Mass spectrum for nitrogen.

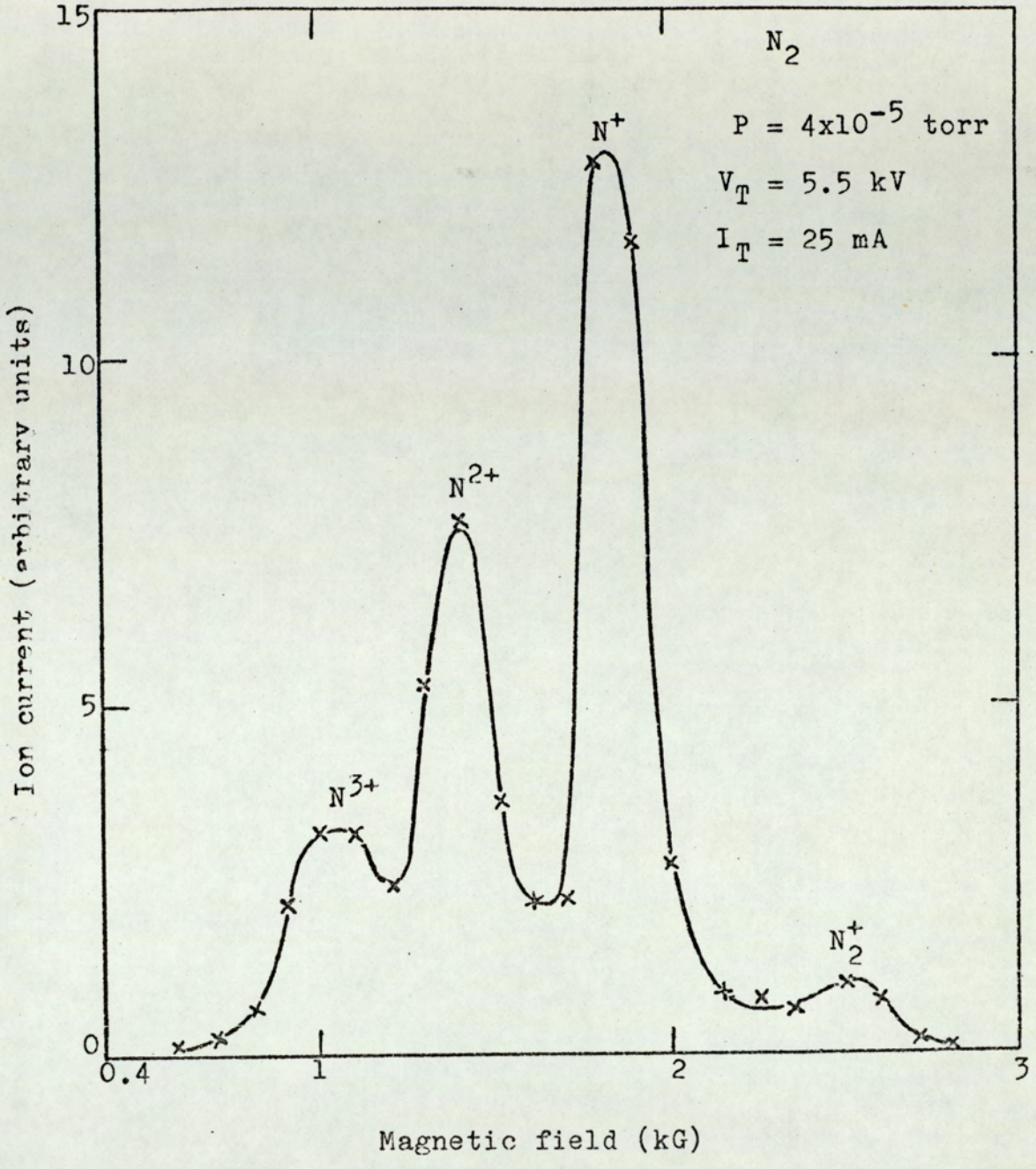

Figure 8.19 Mass spectrum for nitrogen.

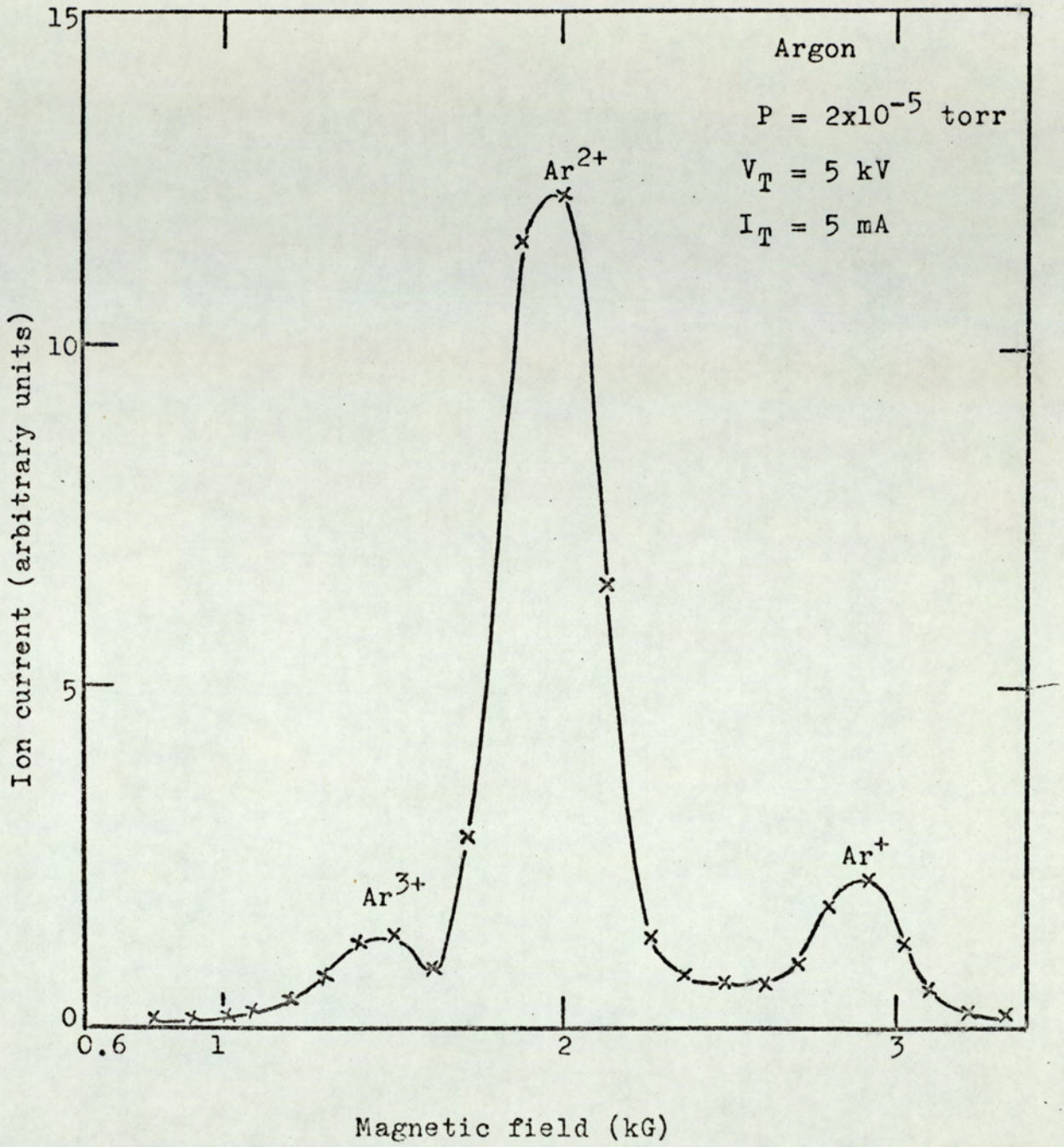

Figure 8.20 Mass spectrum for argon.

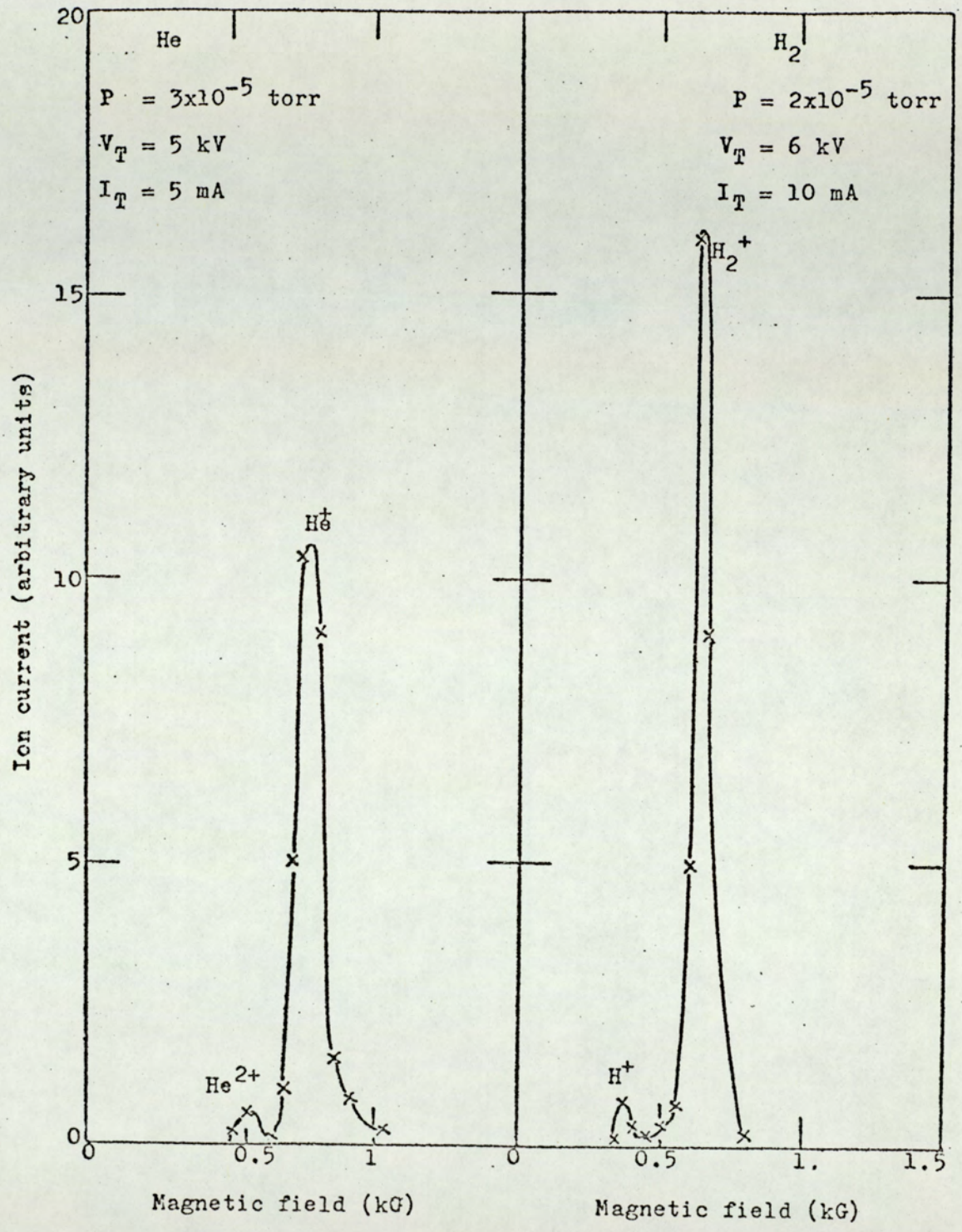

Figure 8.21 Mass spectrum for helium

Figure 8.22 Mass spectrum for hydrogen.

Fig. (8.23) shows the variation of $(m_i/Ze)^{\frac{1}{2}}$ with H as taken from the experimental figures. As it is expected from Eq. (8.3) this relation is a straight line which indicates that the identification of the charge states for each gas investigated are correct.

8.5. Discussion.

A distribution in an ion energy can result from a number of causes (Wilson and Brewer, 1973), for example, a spatial variation in the potential of the point in the source where an ion was created. Ions may be created at different locations in a discharge across which a potential difference exists. Another source of energy spread can be the thermal energy that is characteristic of the temperature of the ions in an ion source, which is frequently, if not always, equal to the atomic gas temperatures. Energy spread may also be attributed to collision of ions with atoms and molecules in the gas phase (Forst, 1972; Lob and Peyerimhoff, 196), and collision at solid surfaces within the extraction region (Lob, 1961). Generally speaking, in ion sources, both of these effects can contribute to the energy spread.

It has been shown that the energy distribution contains peaks and that ions contributing to these peaks are coming from different points inside the discharge. The highest energy ions are coming from the centre and the ion energy decreases in the X-direction. Hence, it seems that it is not only the plasma inside the source that is formed from the plasmas with different ion

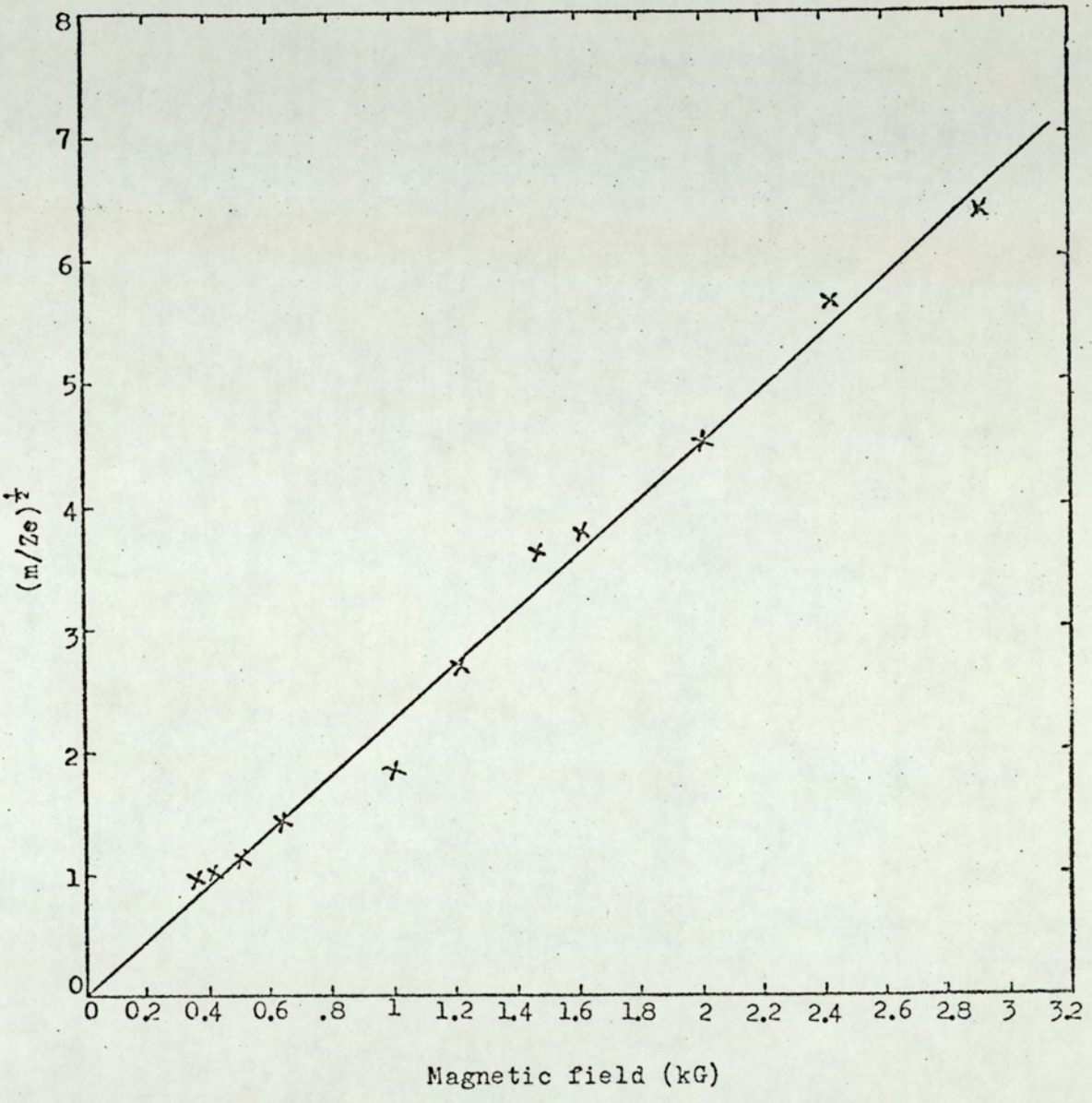

Figure 8.23 : Mass spectrum calibration.

intensities as discussed in Chapter 7, but these plasmas have also different voltages across them.

Moreover, since the central line in the beam, which contains the highest energy ions, is very intense in the case of argon and nitrogen gases, while it is much less intense in the case of helium, it is believed that this central line contains multicharged ions. This is because the ionization cross-section for argon and nitrogen are much higher than that of helium.

The lowest energy peak in Figs. (8.2), (8.3), (8.4), (8.5), (8.6) and (8.7) is probably due to ionization by electrons in the beam, or charge exchange process (Hurely and Holland, 1972), or both. Evidence for these effects is that the beam was found to contain electrons as well as energetic neutral ions. The electrons have a maximum energy of about 100 eV, which is enough to ionize an argon or nitrogen atom. Evidence for charge exchange process is the formation of energetic neutrals when energetic ions collide with gas atoms or molecules which results also in the formation of slow ions.

It is thus possible to obtain ion beams from the electrostatic oscillator ion source with energies ranging from a few tens of eV to about $0.8eV_T$ (the saddle point potential), by carefully milling small ion exit aperture at the appropriate place in the cathode so that ions with energy corresponding to one of the peaks appears in the energy distribution curves, is allowed to emerge from the source. Such low energy ions should be useful for some

applications such as utilization in the final thinning stages to reduce the damage induced into the samples from energetic ion bombardment (Meckel, 1972).

The energy distribution of ions emerging from the spherical source using an ion exit aperture of 1.5 mm. diameter is constituted mainly of a high peak with a spread of about 250 V. Therefore this source is much better than other sources used for large etching rates over a small area, e.g. the glow discharge ion gun (Crockett, 1973).

It has shown that more lower energy ions are contributing more to the beam than in the conventional source when focusing electrodes were used. This is an evidence that more low energy ions are extracted due to the influence of the focus electrode field.

There are three kinds of ion sources where electron-atom collisions are used to produce multicharge ions (Septier, 1972). These are; sources where the ions are produced by successive ionization by a simple ionization and since a long time is required to obtain the wanted charge state, the ions have to be trapped in an appropriate magneto-electric system during times of the order of 10^{-3} to 1 second, and sources in which both processes occur at the same time.

If an electron collides with a heavy atom, having for example K, L and M-shells, electrons are ejected from the M-shell (direct ionization), or from an internal shell (L or K). This will depend on the electron

energy.

Ionization may take place by Auger process (Burhop, 1952). A valency in the inner shells (K) is filled by an electron coming from an external shell (L); If the energy given up by the ionization L→ K is greater than the binding energy of a second electron of the L-shell, this second electron is ejected. At this time, the ion which is doubly charged, possess two vacancies in its L-shell. Both L-vacancies can themselves be filled by Auger transition from M-shell, and hence four vacancies are produced and so on. The vacancies multiply as they proceed outward through the electronic structure.

In ion containment sources, the positive ions are trapped during a time long enough to obtain multiple ionization by successive collisions. It is therefore necessary to maintain an electric and magnetic field to form an ion trap for a period of time which is long compared to the time required to produce the wanted charge state.

Therefore, in order for an ion source to produce ions with high charge states, three conditions have to be satisfied. Namely, one must have a low source pressure to avoid charge exchange, large electron path length, and a high containment for the positive ions to increase the probability of multiple ionization by successive collisions. The electrostatic oscillator ion source satisfies the first two conditions but not the third as the ions are accelerated over a distance of only one or

two centimetres in a radial direction towards the cathode. This is presumably why, for example, with argon no charge state greater than A^{3+} was detected. It is assumed that the detected multicharge ions are formed in the centre of the discharge by successive collisions where the electron stability is high.

It is apparent from the figures of the mass analysis that the relative proportion of the doubly charged state is greater for argon than for the other gases which can be attributed to the higher ionization - crossection of argon (Pigarot and Morozov, 1961) and also argon has a lower ionization potential (Carlson et al, 1970).

9. CONCLUSION AND SUGGESTIONS FOR FURTHER WORK

It has been shown that the electrostatic oscillator ion sources can operate in either the non-uniform plasma mode or the uniform plasma mode depending on the source pressure and tube current. The uniform plasma mode should be useful for applications where beams of uniform ion density are required to obtain uniform etching.

It is advantageous to use cathode tubes of small radius so that the discharge is confined and thus high intensity ion beams can emerge from the source. Since the emerging ion current is proportional to the tube current, cooling the anodes and the cathode allow use of higher tube currents and consequently, higher ion beam currents can be obtained. For example, the normal operating tube current is about 5 mA, but when the anodes and the cathode were water cooled, it was possible to operate the source at a tube current of up to 30 mA.

Since the double beam ion source produces two identical beams, it should be particularly useful for studying comparative etching rates of different materials when it is essential to ion bombard both specimens under identical conditions. Furthermore, there should be no problem of sputtering material from one specimen onto the other as they are virtually shielded from each other on either side of the cathode. Alternatively, the source can also be used for thinning one specimen whilst the

other beam can be continuously monitored.

The addition of a chimney and a focus electrode to the source is advantageous. This corrects the field distortion caused by the ion exit aperture producing higher tube currents and more ions are extracted from the source. Moreover, with high voltages on the focus electrode, the beam can be focused at some distance from the source. This increases the ion density and hence higher etching rates can be obtained even with the specimen placed at some distance away from the source. This minimizes the damage caused by the thermal radiation from the source.

The spherical source is relatively small and produces an ion beam with an intense central line. The ion intensity of this line is 1-2 mA/cm^2, the beam divergence is relatively small and the energy spread is only about 250 volts. Also, since a small ion exit aperture diameter of 1.5 mm. is used, a high pressure differential is obtained and hence the chamber pressure is lower and the gas economy is higher than with the cylindrical source. This source should be ideal for ion thinning specimens for transmission electron microscopy.

The energetic neutral ion component of the beam should be useful for some applications. For example, the charged ions can be deflected and the remaining neutral ions can be used to etch dielectric materials to avoid charge build during positive ion bombardment.

The ion energy distribution is broad and

exhibits different peaks with equivalent ion energies ranges from a few electron volts to about 0.8 eV_T. The ions contributing to each peak are coming from different points in the source. Therefore, it will be possible to use the source as an energy selector by carefully milling small ion exit apertures into the cathode to obtain ions with energies up to 0.8 eV_T.

A new application of the electrostatic oscillator ion source that is feasible, is in small particle accelerators for the gaseous elements where the first charge state and currents of a few milliamperes are required.

It is felt that future developments can still be made. An attempt was made to measure the plasma characteristic (spatial potential, ion and electron density and electron temperature) by simple Langmuir probes. Unfortunately, it was found that even using small probes the discharge was disturbed to such an extent the discharge ceased at a small positive probe voltage. Other plasma diagnostic techniques which do not disturb the discharge such as R.F. probes (Swift and Schwar, 1970) may be employed to study the discharge. It is believed that in this case useful information may be obtained to give a better understanding of the characteristics of the source.

Cooling the anode and the cathode of the spherical source may be tried so that the source can operate with higher tube currents and thus higher ion beam currents.

External electron injection from a filament into the spherical source to lower the operating voltage and hence the ion energies should also be possible using similar techniques to that described by Rushton and Fitch (1974) for the cylindrical source.

Although the spherical source is relatively small, it is still possible to reduce its size. An electrolytic tank should be extremely useful in this respect for any future developments to obtain optimum electrode configuration. If a smaller spherical source can be developed, a group of them may be built in one unit so that the ion exit apertures are close to each other. The ion beams are then allowed to overlap to form one beam with a larger cross-section. This should be useful for etching large area specimens and for application in sputtering.

REFERENCES

BAUMANN, H., HEINICK, E., and BETHGE, K., (1972), Proceeding of the Second International Conference on Ion Sources, Vienna.

BIONDI, M.A., and BROWN, S.C., (1949), Phys.Rev., 75, 1700.

BOHM, J., (1949), The Characteristics of Electrical Discharge in Magnetic Field, Ed. Cuthrie and Wakerling, N.Y.

BURHOP, E.H.S., (1952), The Auger Effect, P.49, Cambridge Univ. Press.

BYERLY, W.E., (1873), Fourier Series and Spherical Harmonics, Ginn and Company, Boston.

CARLSON, A.C., NESTOR, C.W., WASSERMAN, N., and McDOWELL, (1970), ORNL 4562.

COBINE, J.D. (1958), Gaseous Conductors, p.240, Dover Publications Inc., N.Y.

COLLINS, L.E., and STROUDS, P.T., (1964), N.I.M., 26, 157.

CROCKETT, C.G., (1973), Vacuum, 23, 11.

DAVISSON, G.J., and CALBIC, C.J. (1931), Phys.Rev., 38, 585.

DAVISSON, G.J., and CALBIC, C.J., (1932), Phys.Rev. 42, 580.

ECKHARDT, W.O., HYMAN, J., HAGEN, G., BUCKK, C.R., and KNETCHIL, R.C., (1964), AIAA J., 2, 1738.

FITCH, R.K., MULVEY, T., THATCHER, W.J., McILRAITH, A.H., (1970), J.Phys.E, 3, 1399.

FITCH, R.K., and RUSHTON, G.J., (1970), Vacuum, 20, 445.

FITCH, R.K., and RUSHTON, G.J., (1972), J.Vac.Sci.Tech., 9, 379.

FITCH, R.K., GHANDER, A.M., RUSHTON, G.J., and SINGH, R., (1974), Paper Presented at the 6th International Conference on Vacuum.

FRANCKEN, J.C., (1967), Focusing of Charged Particles, Ed. A. Septier, V.1, Ch. 1.3, Academic Press, N.Y.

FRANKS, J., (1972), British Patent Application No. 54627/72.

FRANKS, J., (1973), British Patent Application No. 44718/73.

FORST, G., (1960), Z. Physik, 159, 7.

GABOVICH, M.D., and KUCHERENKO, E.T., (1956), Sov.Phys. Tech.Phys., 1, 975.

GABOVICH, M.D., KUCHARENKO, (1957), Sov.Phys., Tech. Phys., 2, 266.

GABOVICH, M.D., and PASECHNIK, L.I., (1961), Sov.Phys., Tech.Phys., 6, 166.

GABOVICH, M.D., and ROMANYUK, L.I., (1961), Sov.Phys., Tech.Phys., (1961), 6, 225.

GHANDER, A.M., and FITCH, R.K., (1973), Vacuum, 23, 269.

HAGSTRUM, H.D., (1953), Phys.Rev., 89, 244.

HARRIS, L.A., (1960), J.Electron, 8, 580.

HURLY, R.E., HOLLAND, L., (1972), Proceedings of the Second International Conference on Ion Sources, (1972), P.409, Vienna.

LANGMUIR, I., and BLADGETT, D., (1923), Phys.Rev. 22, 347.

LANGMUIR, I., and BLADGETT, D., (1924), Phys.Rev. 24, 49.

LOB, H., (1961), Z.Naturforsch, 16A, 67.

LOB, H., and PEYERIMHOFF, S., (1961), Z.Naturforsch, 16A, 621.

LOEB, L.B., (1934), The Kinetic Theory of Gases, McGraw-Hill Book Company Inc., N.Y.

McILRAITH, A.H., (1966), Nature, Lord, 212, 1422.

McILRAITH, A.H., (1967), Unpublished work.

McILRAITH, A.H., (1971), J.of Vacc.Sci. and Tech., 9, 209.

MECKEL, B.B., (1972), 11th Symposium on Electron Ion, and Laser Beam Technology, San Francisco, U.S.A.

PAPOULAR, R., (1965), Electrical Phenomena in Gases, Iliffe Books Ltd., London.

PENNING, F.M., and MOUBIS, J.H.A., (1937), Physica, 4, 119.

PIGAROV, Yu. D., and MOROZOV, P.M., (1961), Sov.Phys., Tech.Phys., 6, 336.

PIGAROV, Yu. D., and MOROZOV, (1961), Sov.Phys., Tech.Phys., 6, 342.

PIGGS, G.N., and McILRAITH, A.H., (1973), J.Phys.E., 6, 1139.

ROSE, P.H., (1964), N.I.M, 28, 146.

RUSHTON, G.J., and FITCH, R.K., (1971), Vacuum, 21, 449.

RUSHTON, G.J., (1972), Ph.D. Thesis, University of Aston in Birmingham.

RUSHTON, G.J., and FITCH, R.K., (1973), J.Phys.D., 6, 1167.

RUSHTON, G.J., and FITCH, R.K., (1974), J.Phys.E., 7, 315.

SEPTIER, A., (1967), Focusing of Charged Particle, Ed. A.Septier, Vol.2, Chap.3,4, Academic Press, N.Y.

SEPTIER, A., (1972), I.E.E.E. Transaction on Nuclear Science, NS.19, 22.

SCHOTTKY, W., (1924), Z.Phys., 25, 635.

SINGH, R., (1973), M.Sc. Thesis, University of Aston in Birmingham.

SOLNYSHKOV, A.I., (1963), High Energy Accelerators, Conf., Dubna.

SWIFT, and SCHWAR, M.J.R., (1970), Electrostatic Probes for Plasma Diagnostics, London, Iliffe.

THATCHER, W.J., (1971), Ph.D. Thesis, University of Aston in Birmingham.

THONEMANN, P.C., and HARRISON, E.R., (1953), Prog.Nucl. Phys., 3, 219.

THONEMANN, P.C., and HARRISON, E.R., (1954), AERE Rept. GP/R-1190.

Von ARDENNE, M., (1956), Tabellen Für Elektronen, Ionenphysik und Übermikroskopie, VEB, Berlin.

Von ENGEL, A., STEENBECK, M., (1932), Elektrische Gasentladungen, ihre Physik U. Tecknik, Vol. 1 and 2., Verlag Julius Springles, Berlin.

Von ENGEL, A., (1965), Ionized Gases, Oxford Press.

WILSON, R.G., and BREWER, G.R., (1973), Ion Beams P. 104, John Willey and Sons, N.Y.